

**Department of Biology**

144 Mudd Hall / 3400 N. Charles Street  
Baltimore MD 21218-2685  
410-516-7330 / Fax 410-516-5213

October 2, 2013

Dean William Eggington  
Acting Chair, Graduate Board  
The Johns Hopkins University  
Baltimore, MD 21218

Dear Dean Eggington:

The undersigned have read the dissertation submitted by Nazanin Ashourian entitled "ESTABLISHING THE FIDELITY OF START CODON RECOGNITION: ROLE OF EUKARYOTIC INITIATION FACTOR 2" and recommend its acceptance in partial fulfillment of the requirements for the Doctor of Philosophy degree.

I certify that this dissertation is a significant contribution to knowledge and worthy of publication in its present form.

Sincerely,

Alan G. Hinnebusch  
Senior Investigator  
Laboratory of Gene Regulation &  
Development  
National Institutes of Health

Joseph Gall  
Professor  
Carnegie Institution for Science



**ESTABLISHING THE FIDELITY OF START CODON  
RECOGNITION: ROLE OF EUKARYOTIC INITIATION FACTOR 2**

By  
Nazanin Ashourian

A dissertation submitted to Johns Hopkins University in conformity with the  
requirements for the degree of Doctor of Philosophy

Baltimore, Maryland  
October 2013

© 2013 Nazanin Ashourian  
All Rights Reserved



## ABSTRACT

In eukaryotes, start codon selection is governed by base pairing between the start codon and the anticodon of the initiator tRNA (Met-tRNA<sub>i</sub>) and is achieved via a complex machinery involving at least twelve initiation factors. eIF2 is a heterotrimeric G-protein that, in its active GTP-bound state, binds and delivers the Met-tRNA<sub>i</sub> to the P-site of the small (40S) subunit of the ribosome, in a process facilitated by multiple other initiation factors forming a pre-initiation complex (PIC). The process of initiation is composed of two phases with distinct conformations of the PIC. First, the PIC in an *open* conformation scans the mRNA 5' UTR in a manner allowing for the Met-tRNA<sub>i</sub> to sample the nucleotides for complementarity. Upon a cognate codon:anticodon interaction, the PIC then adopts a *closed* conformation accompanied by the irreversible hydrolysis of eIF2-bound GTP and P<sub>i</sub> release. The molecular mechanisms by which cognate codon:anticodon base pairing is linked to the hydrolysis of eIF2-bound GTP and P<sub>i</sub> release, formation of the closed conformation, and start codon selection are not well understood.

In this study, we provide genetic and biochemical evidence that suggests a new function for domain-III of eIF2 $\gamma$  in coordinating these processes and maintaining the equilibrium between the two conformations of the PIC. In order to identify the structural elements in eIF2 essential for start codon selection, we isolated novel mutations in the yeast  $\gamma$  subunit that alter the accuracy of this process. We identified two classes of mutations with opposing effects: mutations that reduce the stringency of start codon recognition and those that, conversely, restore initiation fidelity. The isolated mutations localize to distinct regions on the surface of domain-III in close proximity of the

proposed binding interface between eIF2 and the 40S subunit. We propose a model in which eIF2( $\gamma$ ) maintains a dynamic interaction with the 40S subunit during the scanning of the mRNA 5' UTR. Upon cognate codon:anticodon base pairing, however, new contact points between eIF2 $\gamma$  domain-III and the 40S subunit are created that stabilize the closed conformation, hence stabilizing the accommodation of the Met-tRNA<sub>i</sub> in the P-site and allowing for the progress of translation initiation.

Thesis advisor and primary reader: Dr. Alan G. Hinnebusch (Senior Investigator, Eunice K. Shriver National Institute of Child Health and Human Development, National Institutes of Health)

Thesis committee member and secondary reader: Dr. Joseph G. Gall (Professor, Department of Biology, Johns Hopkins University; Staff member, Carnegie Institution of Washington)

## **DEDICATION**

*To my dear family:*

*Arash, baba, and maman*

## ACKNOWLEDGEMENTS

I would like to thank my thesis advisor Dr. Alan Hinnebusch. I am grateful to Dr. Tom Dever for scientific discussions and his intellectual contributions to my project. Many thanks to all my colleagues in the Hinnebusch and Dever labs. I would like to thank Dr. Jon Lorsch for serving on my annual review committee and for scientific contributions to my project. I would also like to thank members of the Lorsch lab for discussions and technical assistance. I am most grateful to Dr. Joe Gall, who served on my Graduate Board Oral Exam committee and also as the chair of my thesis committee, for providing me with great support and ensuring my progress from the beginning to the end. I am thankful to Dr. Dan Masison for serving on my annual review committee and providing guidance for the progress of my thesis project. Many thanks to Dr. Nick Ingolia for serving on my thesis defense committee. I would like to thank Drs. Orna Cohen-Fix and Michael Lichten, co-directors of the National Institutes of Health Graduate Partnership Program (GPP) with the Johns Hopkins University, for their support and enthusiasm in mentoring graduate students. I am most grateful for the unconditional support, guidance, and the care provided by Dr. Sharon Milgram, Director of National Institutes of Health Office of Intramural Training and Education, and Dr. Philip Wang, Deputy director of Graduate Partnership Programs, throughout my entire graduate experience. My deepest gratitude to Miss. Joan Miller who has been a constant support from the very first day to the very last and for the friendship, kindness, and care she has always provided me.

## TABLE OF CONTENTS

<b>ABSTRACT</b> .....	<b>ii</b>
<b>DEDICATION</b> .....	<b>iv</b>
<b>ACKNOWLEDGEMENTS</b> .....	<b>v</b>
<b>TABLE OF CONTENTS</b> .....	<b>vi</b>
<b>LIST OF FIGURES</b> .....	<b>viii</b>
<b>LIST OF TABLES</b> .....	<b>xi</b>
<b>LIST OF ABBREVIATIONS</b> .....	<b>xii</b>
<b>CHAPTER 1: INTRODUCTION</b> .....	<b>1</b>
<b>1.1 Translation Initiation</b> .....	<b>5</b>
1.1.1 <i>Initiation of Protein Synthesis in Bacteria</i> .....	5
1.1.2 <i>Initiation of Protein Synthesis in Eukaryotes</i> .....	7
<b>1.2 The eIF2 Complex</b> .....	<b>15</b>
1.2.1 <i>eIF2: The <math>\alpha</math>, The <math>\beta</math>, and The <math>\gamma</math></i> .....	15
1.2.2 <i>Ternary Complex Formation</i> .....	22
1.2.3 <i>Translational Control Through the eIF2 Complex</i> .....	26
<b>1.3 Figures and Tables</b> .....	<b>29</b>
<b>CHAPTER 2: IDENTIFICATION OF NOVEL MUTATIONS IN <i>GCD11</i> THAT ALTER THE FIDELITY OF START CODON RECOGNITION</b> .....	<b>35</b>
<b>2.1 Introduction</b> .....	<b>36</b>
<b>2.2 Materials and Methods</b> .....	<b>39</b>
2.2.1 <i>Yeast Strain Constructions</i> .....	39
2.2.2 <i>Plasmid Constructions</i> .....	41
2.2.3 <i>Biochemical Assays with Yeast Extracts</i> .....	42
<b>2.3 Results</b> .....	<b>43</b>
2.3.1 <i>Generation of Libraries of Randomly Mutated <i>GCD11</i> alleles</i> .....	43
2.3.2 <i>Identification of <i>GCD11</i> Mutants that Suppress the Recessive Lethality of <i>SUI5</i></i> .....	44
2.3.3 <i>Isolation of Mutations in <i>GCD11</i> that Reduce Initiation Fidelity</i> .....	53
2.3.4 <i>Identification of Mutations in <i>GCD11</i> that Alter Initiation Fidelity by Site-Directed Mutagenesis</i> .....	57
<b>2.4 Discussion</b> .....	<b>66</b>
<b>2.5 Figures and Tables</b> .....	<b>73</b>
<b>CHAPTER 3: CHARACTERICATION OF THE MUTANT ALLELES OF <i>GCD11</i> THAT REDUCE THE STRINGENCY OF START CODON RECOGNITION ...</b>	<b>132</b>
<b>3.1 Introduction</b> .....	<b>133</b>
<b>3.2 Materials and Methods</b> .....	<b>135</b>
3.2.1 <i>Yeast Strain Constructions</i> .....	135
3.2.2 <i>Plasmid Constructions</i> .....	136
3.2.3 <i>Biochemical Assays with Yeast Extracts</i> .....	137
3.2.4 <i>In Vitro Reconstitution Assays</i> .....	137
<b>3.3 Results</b> .....	<b>141</b>
3.3.1 <i>Novel Mutations in <i>GCD11</i> Reduce the Fidelity of Start Codon Recognition</i> .....	141
3.3.2 <i>The E460A Mutant Promotes Formation of the Closed Conformation at a UUG Codon</i> .....	145

3.3.3 Biochemical Analysis of the G418C <i>Ssu</i> Mutant .....	149
<b>3.4 Discussion .....</b>	<b>152</b>
<b>3.5 Figures and Tables .....</b>	<b>159</b>
<b>CHAPTER 4: CHARACTERIZATION OF THE MUTANT ALLELES OF <i>GCD11</i></b>	
<b>THAT RESTORE INITIATION FIDELITY .....</b>	<b>177</b>
<b>4.1 Introduction .....</b>	<b>178</b>
<b>4.2 Materials and Methods .....</b>	<b>180</b>
4.2.1 Yeast Strain Constructions .....	180
4.2.2. Plasmid Constructions .....	181
4.2.3. Biochemical Assays with Yeast Extracts .....	181
4.2.4. <i>In Vitro</i> Reconstitution Assays .....	181
<b>4.3 Results.....</b>	<b>182</b>
4.3.1 The <i>Ssu</i> Mutants of <i>GCD11</i> Restore Initiation Fidelity in Cells Harboring the <i>SUI3-2</i> Allele <i>in Vivo</i> .....	182
4.3.2 <i>SUI3-2</i> Stabilizes the Closed Conformation of the PIC .....	183
4.3.3. The <i>Ssu</i> Mutants of <i>GCD11</i> Reduce the Stability of the Closed Conformation of the PIC.....	187
<b>4.4 Discussion .....</b>	<b>191</b>
<b>4.5 Figures and Tables .....</b>	<b>199</b>
<b>CHAPTER 5: CONCLUDING REMARKS .....</b>	<b>210</b>
<b>REFERENCES.....</b>	<b>215</b>
<b>CURRICULUM VITAE.....</b>	<b>231</b>

## LIST OF FIGURES

Figure 1.1 Translation initiation is heavily regulated .....	29
Figure 1.2 Ribosome challenge: where shall I begin? .....	30
Figure 1.3 The scanning mechanism of translation initiation in eukaryotes .....	31
Figure 1.4 Crystal structure of aIF2 .....	32
Figure 1.5 Structures of eIF2 $\alpha$ , $\beta$ , and $\gamma$ subunits .....	33
Figure 2.1 Genetic reporter for monitoring the accuracy of translation initiation in vivo .....	73
Figure 2.2 <i>SUI5</i> displays dominant Sui <sup>-</sup> and recessive lethal phenotypes .....	74
Figure 2.3 Graphical illustration of the plasmid used for the generation of randomly mutated <i>GCD11</i> alleles .....	75
Figure 2.4 Selection scheme for identification of mutations in <i>GCD11</i> that suppress the recessive lethality of <i>SUI5</i> .....	76
Figure 2.5 Novel mutations identified in <i>GCD11</i> that suppress the recessive lethality of <i>SUI5</i> .....	77
Figure 2.6 Suppression of <i>SUI5</i> recessive lethality by the <i>GCD11</i> mutants .....	79
Figure 2.7 Suppression of <i>SUI5</i> His <sup>+</sup> phenotype by the <i>GCD11</i> mutants .....	80
Figure 2.8 Suppression of <i>SUI3-2</i> His <sup>+</sup> phenotype by the <i>GCD11</i> mutants .....	81
Figure 2.9 Isolated mutations in <i>GCD11</i> restore initiation fidelity in cells harboring the <i>SUI3-2</i> mutation .....	82
Figure 2.10 Suppression of <i>SUI5</i> and <i>SUI3-2</i> Gcd <sup>-</sup> phenotypes by the <i>GCD11</i> mutants .....	84
Figure 2.11 The Ssu <sup>-</sup> mutants of <i>GCD11</i> display a weak Gcn <sup>-</sup> phenotype .....	86
Figure 2.12 The Ssu <sup>-</sup> mutants of <i>GCD11</i> exhibit a modest leaky scanning phenotype .....	87
Figure 2.13 Growth phenotypes and protein levels of the Ssu <sup>-</sup> substitutions in eIF2 $\gamma$ .....	89
Figure 2.14 The isolated Ssu <sup>-</sup> substitutions in eIF2 $\gamma$ localize to a discrete region on the surface of domain-III close to h44 of the 40S subunit .....	90
Figure 2.15 Outline of the selection scheme for isolation of Sui <sup>-</sup> mutations in <i>GCD11</i> ..	92
Figure 2.16 The <i>G418C</i> and <i>R510H</i> mutants display a His <sup>+</sup> /Sui <sup>-</sup> phenotype .....	93
Figure 2.17 R510 is a highly conserved residue in domain-III of eIF2 $\gamma$ .....	94
Figure 2.18 R510 is located on the surface of eIF2 $\gamma$ at the interphase of domain-III and the G-domain .....	95
Figure 2.19 G418 is a highly conserved residue in domain-III of eIF2 $\gamma$ .....	96
Figure 2.20 G418 is located in the first $\beta$ -strand of eIF2 $\gamma$ domain-III .....	97
Figure 2.21 The <i>G418C</i> mutant is slow growing, cold sensitive, and displays a strong His <sup>+</sup> phenotype .....	98
Figure 2.22 G418 is positioned distant from the proposed interface of eIF2 with the 40S subunit .....	99
Figure 2.23 Multiple sequence alignment of eIF2 $\gamma$ domain-III displaying the conserved surface-exposed residues selected for site-directed mutagenesis .....	100
Figure 2.24 Positions of the eIF2 $\gamma$ residues selected for site-directed mutagenesis on the crystal structure of aIF2 .....	101
Figure 2.25 Growth phenotypes and protein levels of <i>GCD11</i> mutations created by site- directed mutagenesis .....	102
Figure 2.26 Spot assays for His <sup>+</sup> phenotype of site-directed domain-III mutants .....	104
Figure 2.27 The <i>E460A</i> allele confers a Gcd <sup>-</sup> phenotype .....	105

Figure 2.28 E460 is located on the surface of domain-III in proximity of the interface between eIF2 the 40S subunit .....	107
Figure 2.29 E460 side chain interacts with the side chain of R503 .....	108
Figure 2.30 <i>E460A/K</i> , <i>R503A/E</i> , and <i>R504A/E</i> do not display dominant growth defects, Gcd <sup>-</sup> , or His <sup>+</sup> phenotypes. ....	109
Figure 2.31 Overexpression of eIF1, Met-tRNA <sub>i</sub> , or TC containing the R503A or R504A mutant variants of eIF2 $\gamma$ do not suppress the recessive lethality conferred by the <i>R503A</i> or <i>R504A</i> alleles .....	111
Figure 2.32 Overexpression of TC containing the R503A or R504A mutant variants of eIF2 $\gamma$ does not create growth defects or a His <sup>+</sup> phenotype .....	113
Figure 2.33 Overexpression of TC containing the E460K substitution in eIF2 $\gamma$ rescues the severe growth defect conferred by the <i>E460K</i> allele .....	115
Figure 2.34 Suppression of <i>SUI3-2</i> His <sup>+</sup> phenotype by site-directed mutations in <i>GCD11</i> .....	116
Figure 2.35 Suppression of <i>SUI3-2</i> His <sup>+</sup> , Sui <sup>-</sup> , and Gcd <sup>-</sup> phenotypes by the <i>GCD11</i> mutants created by site-directed mutagenesis .....	117
Figure 2.36 Suppression of <i>SUI5</i> Slg <sup>-</sup> , His <sup>+</sup> , and Gcd <sup>-</sup> phenotypes by the <i>GCD11</i> mutants created by site-directed mutagenesis .....	119
Figure 2.37 Suppression of <i>tif11-SE1*SE2*F131</i> Slg <sup>-</sup> , His <sup>+</sup> , and Gcd <sup>-</sup> phenotypes by the <i>GCD11</i> mutants .....	121
Figure 2.38 The Ssu <sup>-</sup> substitutions in eIF2 $\gamma$ localize to a discrete region on the surface of domain-III .....	123
Figure 3.1 The Sui <sup>-</sup> mutants of <i>GCD11</i> display a His <sup>+</sup> phenotype and an increased UUG to AUG ratio .....	159
Figure 3.2 The Gcd <sup>-</sup> phenotype and the elevated UUG/AUG initiation ratio of the <i>GCD11</i> Sui <sup>-</sup> mutants are partially suppressed by overexpression of the eIF1 protein.....	161
Figure 3.3 eIF1 overexpression partially suppresses the His <sup>+</sup> phenotype of the <i>GCD11</i> Sui <sup>-</sup> mutants but does not alter their growth phenotypes .....	163
Figure 3.4 Binding of the Met-tRNA <sub>i</sub> reduces the spontaneous rate of GTP hydrolysis in eIF2 .....	164
Figure 3.5 E460A substitution in eIF2 $\gamma$ does not alter the affinity of Met-tRNA <sub>i</sub> binding to the eIF2 complex .....	165
Figure 3.6 E460A does not alter the affinity of TC binding to the 43S•mRNA PIC .....	166
Figure 3.7 The E460A substitution in eIF2 $\gamma$ increases the rate of TC binding to the 43S•mRNA PIC exclusively with a UUG start codon .....	167
Figure 3.8 The eIF1A dissociation kinetics from the 43S•mRNA complex serves as a proxy for partitioning between the open and closed conformations of the PIC .....	168
Figure 3.9 Principles of fluorescence anisotropy.....	169
Figure 3.10 The E460A substitution in eIF2 $\gamma$ does not alter the dissociation kinetics of eIF1A from reconstituted PIC.....	170
Figure 3.11 The G418C substitution in eIF2 $\gamma$ does not alter the affinity of Met-tRNA <sub>i</sub> binding to the eIF2 complex .....	171
Figure 3.12 The G418C substitution in eIF2 $\gamma$ does not alter the intrinsic rate of GTP hydrolysis in the eIF2 complex.....	172
Figure 3.13 G418C does not alter the affinity or the rate of TC binding to the 43S•mRNA PIC .....	173



Figure 3.14 The G418C variant of eIF2 $\gamma$ does not affect the dissociation kinetics of eIF1A from reconstituted PIC.....	174
Figure 4.1 The Ssu $^-$ mutants of <i>GCD11</i> suppress the His $^+$ phenotype and the elevated ratio of UUG to AUG initiation conferred by the <i>SUI3-2</i> allele.....	199
Figure 4.2 GTP hydrolysis in the mutant eIF2 complexes .....	201
Figure 4.3 Kinetic of eIF1A dissociation from reconstituted PIC containing the WT or the mutant variants of the eIF2 complex .....	202
Figure 4.4 Dissociation kinetics of TC from reconstituted PIC with WT and mutant eIF2 .....	204
Figure 4.5 Affinity of TC binding to reconstituted PIC assembled with WT and mutant eIF2 .....	205
Figure 4.6 Kinetics of TC binding to reconstituted PIC assembled with WT and mutant eIF2 .....	206
Figure 4.7 Positions of the isolated Sui $^-$ and Ssu $^-$ mutations on the structure of eIF2....	207

## LIST OF TABLES

Table 1.1 Various pathways for translation initiation.....	34
Table 2.1 List of <i>S. cerevisiae</i> Strains.....	125
Table 2.2 List of Plasmids .....	126
Table 2.3 List of Primers .....	128
Table 2.4 Frequency and type of mutations in the libraries of randomly mutated <i>GCD11</i> alleles .....	130
Table 2.5 List of isolated mutant alleles of <i>GCD11</i> that suppressed the recessive lethality of <i>SUI5</i> .....	130
Table 2.6 List of site-directed mutations created in domain-III of <i>GCD11</i> .....	131
Table 2.7 Suppression of the <i>Sui</i> <sup>-</sup> , <i>His</i> <sup>+</sup> , <i>Gcd</i> <sup>-</sup> , <i>Slg</i> <sup>-</sup> , and <i>TS</i> <sup>-</sup> phenotypes of different <i>Sui</i> <sup>-</sup> mutants by the <i>GCD11</i> <i>Ssu</i> <sup>-</sup> alleles.....	131
Table 3.1 List of <i>S. cerevisiae</i> Strains.....	175
Table 3.2 List of Plasmids .....	176
Table 4.1 List of <i>S. cerevisiae</i> Strains.....	208
Table 4.2 List of Plasmids .....	209

## LIST OF ABBREVIATIONS

CTD	<b>C-Terminal Domain</b>
CTT	<b>C-Terminal Tail</b>
EF	<b>Elongation Factor</b>
eIF	<b>eukaryotic Initiation Factor</b>
Gal	<b>Galactose</b>
GAP	<b>GTPase Activating Protein</b>
Gcd <sup>-</sup>	<b>General Control Derepressed</b>
Gcn <sup>-</sup>	<b>General Control Non-Inducible</b>
GEF	<b>Guanidine nucleotide Exchange Factor</b>
Glc	<b>Glucose</b>
hc	<b>high copy (plasmid)</b>
IF	<b>Initiation Factor</b>
lc	<b>low copy (plasmid)</b>
NTD	<b>N-Terminal Domain</b>
NTT	<b>N-Terminal Tail</b>
ORF	<b>Open Reading Frame</b>
P <sub>i</sub>	<b>Inorganic Phosphate</b>
PIC	<b>Pre-Initiation Complex</b>
PABP	<b>Poly-A-Binding Protein</b>
PTC	<b>Peptidyl Transferase Center</b>
rRNA	<b>ribosomal RNA</b>
SC	<b>Synthetic Complete medium (with glucose as carbon source)</b>
sc	<b>single copy (plasmid)</b>
SCgal	<b>Synthetic Complete medium with galactose as carbon source</b>
SD	<b>Standard Deviation</b>
SEM	<b>Standard Errors of the Mean</b>
Slg <sup>-</sup>	<b>Slow Growing</b>
Ssu <sup>-</sup>	<b>Suppressor of Sui</b>
Sui <sup>-</sup>	<b>Suppressor of Initiation codon</b>
TC	<b>Ternary Complex</b>
TCA	<b>Trichloroacetic acid</b>
tRNA <sub>i</sub>	<b>Initiator tRNA</b>
TS <sup>-</sup>	<b>Temperature Sensitive</b>
uORF	<b>upstream Open Reading Frame</b>
UTR	<b>Untranslated Region (of an mRNA)</b>
WCE	<b>Whole Cell Extract</b>
WT	<b>Wild Type</b>
ZBD	<b>Zinc-Binding Domain</b>
5-FOA	<b>5-Fluorotic Acid</b>
<b>Gene Names in <i>Saccharomyces cerevisiae</i></b>	
<i>GCD11</i>	Gene encoding eIF2 $\gamma$
<i>SUI3</i>	Gene encoding eIF2 $\beta$
<i>SUI2</i>	Gene encoding eIF2 $\alpha$

<i>SUI1</i>	Gene encoding eIF1
<i>TIF5</i>	Gene encoding eIF5
<i>TIF11</i>	Gene encoding eIF1A
<i>IMT4</i>	One of the four genes encoding tRNA <sub>i</sub> <sup>Met</sup>

## **CHAPTER 1: INTRODUCTION**

As the name implies, translation is the process by which the genetic code, preserved by DNA and transmitted through messenger RNAs, is *translated* into functional proteins that run the metabolic processes of an organism. The translation machinery is comprised of a complex set of elements including the ribosome, mRNA, tRNA, and many additional protein factors. Sequence and structural similarities among the different kingdoms suggest a common origin for this machinery<sup>1</sup>. Ribosomes are ribonucleoprotein particles that form the platform for the assembly of translation apparatus and perform the catalytic function of peptide bond formation, which ultimately leads to the synthesis of polypeptide protein chains. They are made of two subunits. The small subunit decodes the mRNA sequence and the large subunit carries the peptidyl-transferase activity. These two fundamental activities are linked by tRNAs that serve as adapters for the coded information on the mRNA and the specific amino acids that constitute a protein.

The process of protein synthesis can conceptually be divided into four stages of initiation, elongation, termination, and ribosome recycling. Initiation assembles the ribosomes at the correct start position, elongation synthesizes the proteins by adding one amino acid at a time to the growing peptide chains based on the information coded in the sequence of mRNAs, termination ends the elongating peptide chains at the correct stop position, and recycling prepares the ribosomes for another round of this process<sup>1-3</sup>. Although each stage has its own specific set of factors that facilitate its progress, for example, the initiation factors are involved in the initiation stage while the elongation factors act during elongation, some of the protein factors have overlapping functions as the different stages of protein synthesis are not autonomous. For example, while EF-G

(elongation factor-G, eEF2 in eukaryotes) is involved in the translocation step during the elongation stage, it is also required for the dissociation of ribosomes after the termination and the release of the polypeptide chains<sup>4</sup>. Moreover, several of the initiation factors are thought to also play significant functions during the recycling stage of translation, which prepares the ribosomes for the next round of initiation and protein synthesis<sup>5-8</sup>.

Protein synthesis is the most energy-demanding cellular activity. It has been estimated that up to 13,000 protein molecules are synthesized per second per a haploid cell of yeast *Saccharomyces cerevisiae*<sup>9</sup>. Thus, to maintain fitness, the process of translation needs to be tightly controlled to ensure accuracy and speed without the unnecessary waste of cellular resources. Furthermore, translational regulation is required for many of the essential processes in a cell. For example, it is needed for the refinement of protein levels during cellular proliferation, division, differentiation, and apoptosis<sup>3,10-12</sup>, for the temporal and spatial regulation of protein synthesis during development<sup>13,14</sup>, for synaptic plasticity, learning, and memory formation<sup>15,16</sup>, and for cellular response to external stimuli such as nutrients and environmental stress<sup>17,18</sup>.

Considering the pivotal function of translational control in the broad spectrum of essential cellular activities, it comes as no surprise that any disturbance in this process can have pathological consequences. Translational misregulation has been implicated in such illnesses as cancer (chronic myeloid leukaemia, gastric cancer), neurological disorders (leukoencephalopathy, fragile-X syndrome, microcephaly, autism), viral infections (foot-and-mouth disease, influenza), and hereditary diseases (hyperferritinaemia-cataract and Wolcott–Rallison syndromes, familial thrombocytosis)<sup>19-29</sup>. Among the various stages of translation, initiation is the most

compromised in the aforementioned translational pathophysiologies since it is the most heavily regulated stage of protein synthesis (see Figure 1.1 for examples of translational regulation at the level of initiation)<sup>1,21,22,30</sup>.

Initiation is also the most divergent stage of protein synthesis, not only among the three kingdoms of life but also within a single organism, as multiple pathways for translation initiation can exist (see Table 1.1)<sup>31</sup>. Regardless of the specific mechanism, however, the ultimate goal of initiation is to assemble an elongation-competent ribosomal complex at the correct start codon for protein synthesis. In the next section, we briefly present the current understanding of the most common mode of initiation in bacteria (Shine-Dalgarno dependent) and eukaryotes (5' cap dependent). The other pathways of translation initiation (listed in Table 1.1) are out of the scope of this study and will not be discussed here.



## 1.1 Translation Initiation

### 1.1.1 Initiation of Protein Synthesis in Bacteria

The bacterial initiation machinery is composed of a relatively small number of factors. A 2.5 MDa 70S ribosomal complex is formed by the small (30S) and the large (50S) subunits. The 30S subunit is composed of the 16S ribosomal RNA (rRNA, ~1,500 nucleotides) and about 21 proteins whereas the 50S subunit consists of the 23S and 5S rRNA elements (~2,900 and ~120 nucleotides, respectively) and about 31 proteins<sup>31-33</sup>. The other components of the bacterial initiation apparatus are initiation factors (IF) 1, 2, and 3 as well as the initiator tRNA (tRNA<sub>i</sub>)<sup>1</sup>. The majority of proteins, both in prokaryotes and eukaryotes, start with a methionine amino acid. Unlike eukaryotes, however, the methionine moiety of tRNA<sub>i</sub> in bacteria is formylated (fMet-tRNA<sub>i</sub>) by methionyl-tRNA transformylase, which is important for its function and recognition by IF2<sup>34-37</sup>.

In all three kingdoms of life, the sequence of the majority of mRNAs are longer than the actual region that codes for the protein product as they generally contain 5' and 3' untranslated regions (UTR), which usually perform some regulatory functions. In bacteria, besides the 5' UTR, a great number of mRNAs are polycistronic and contain the coding sequences for multiple proteins<sup>38</sup>. Thus, the most imperative challenge for an initiating ribosomal complex is to identify the correct start codon. In order to place the elongation-competent ribosome at the correct start site and reading frame for protein synthesis, bacteria take advantage of a direct physical interaction between the mRNA and the 30S subunit of the ribosome. Base pairing between the Shine-Dalgarno (SD) sequence of the canonical mRNAs and the anti-SD sequence present at the 3' end of the

16S rRNA places the start codon in the vicinity of the P-site of the 30S subunit. The precise positioning of the start codon in the P-site is then adjusted by the actions of the three initiation factors and the binding of the fMet-tRNA<sub>i</sub><sup>31,35,39-43</sup>.

In bacteria, the initiation stage of protein synthesis is thought to be intimately linked to ribosome recycling as the binding of IF3 stimulates the release of the mRNA and the unacylated tRNA bound to the 30S subunit from the previous round of translation and prevents the rejoining of the 50S subunit<sup>8,44,45</sup>. IF1 stimulates the activities of IF3 and also directs the binding of the fMet-tRNA<sub>i</sub> to the P-site by binding to the A-site of the 30S subunit, and hence blocking the access of the fMet-tRNA<sub>i</sub><sup>46-48</sup>. The order by which IF2, fMet-tRNA<sub>i</sub>, and mRNA are recruited to the 30S•IF1•IF3 initiation complex is not clear. IF1 is thought to also stabilize the binding of IF2, which interacts with the fMet-tRNA<sub>i</sub> and supports the binding of the latter to the 30S subunit. The interaction between IF2 and fMet-tRNA<sub>i</sub>, however, is believed to be dependent on the 30S subunit<sup>35,37,42,46,49</sup>. Upon binding of the fMet-tRNA<sub>i</sub>, IF3 is then involved in adjusting the position of the start codon in the P-site of the 30S subunit so that it can base pair with the anticodon of fMet-tRNA<sub>i</sub>. Moreover, it is believed that IF3 also stabilizes the binding of the fMet-tRNA<sub>i</sub> in the P-site and confers proofreading capabilities by destabilizing mismatched codon:anticodon interactions<sup>35,43,45,46,50-55</sup>.

Upon accommodation of the mRNA, which leads to the formation of a cognate codon:anticodon interaction and the stabilization of the initiation complex, IF1 and IF3 are ejected and the joining of the 50S subunit is stimulated by IF2. During this process the IF2-bound GTP is hydrolyzed to GDP and inorganic phosphate (P<sub>i</sub>). With the release of P<sub>i</sub> and IF2, the fMet-tRNA<sub>i</sub> is then fully accommodated in the peptidyl-transferase

center (PTC). The newly formed 70S complex then proceeds to the elongation stage of protein synthesis where the next amino acid is delivered to the A-site by EF-Tu (EF for elongation factor)<sup>35,42,52,55</sup>.

### *1.1.2 Initiation of Protein Synthesis in Eukaryotes*

Translation initiation in eukaryotes is achieved via a complex machinery involving at least twelve initiation factors. A eukaryotic 80S ribosome is formed by the joining of the small (40S) and the large (60S) subunits. Because of expansions to the ribosomal RNA and proteins as well as the presence of many additional protein factors, eukaryotic ribosomes are generally ~40% larger than their bacterial equivalents<sup>56</sup>. The 40S subunit consists of the 18S rRNA and 33 proteins while the 60S subunit is composed of three rRNA elements (25S, 5.8S, and 5S) and 46 proteins<sup>56</sup>. Contrary to bacteria, the majority of mRNAs in eukaryotes are monocistronic. Moreover, a canonical eukaryotic mRNA contains a 7-methylguanosine cap at its 5' end and a poly-A tail at its 3' end both of which are important for efficient translation. Another significant feature of the eukaryotic mRNAs is their lack of the Shine-Dalgarno sequence<sup>1</sup>. Therefore, the translation initiation machinery in eukaryotes has to rely on other mechanisms to identify the correct start position for protein synthesis (Figure 1.2).

The most common mode of translation initiation in eukaryotes is through a 5' to 3' scanning mechanism<sup>57-59</sup>. The underlying principle of this model is that initiation in eukaryotes is governed by base pairing between the start codon of mRNA and the anticodon of Met-tRNA<sub>i</sub>. The scanning mechanism can be thought of as a series of steps that ultimately leads to the placement of the Met-tRNA<sub>i</sub> base-paired with the start codon in an elongation-competent 80S complex. A pre-initiation complex (PIC) conducive to

scanning is first formed near the 5' cap of the mRNA. The PIC then scans the 5' UTR in a manner allowing for the Met-tRNA<sub>i</sub> to sample each of the nucleotides on the mRNA for complementarity to the start codon. Upon a cognate codon:anticodon interaction and recognition of the correct start codon, a series of structural rearrangements in the PIC then allows for the joining of the 60S subunit, and the resulting 80S complex proceeds to the elongation stage of protein synthesis where the next amino acid is delivered to the A-site by EF1A (ortholog of bacterial EF-Tu) (Figure 1.3)<sup>30,60</sup>.

The process of initiation, as elucidated above, starts with the loading of the Met-tRNA<sub>i</sub> on the 40S subunit, which is delivered in the context of a ternary complex (TC) with a GTP molecule and eIF2 (eIF for eukaryotic initiation factor) (details of eIF2 and TC formation are discussed in Sections 1.2.1 and 1.2.2, respectively). This process is facilitated by initiation factors 1, 1A, 3, and 5 to form the 43S PIC<sup>60-66</sup>. Binding of the TC to the 40S subunit is thought to be a result of physical interactions and cooperative binding among these initiation factors as TC alone has a low binding affinity for the 40S subunit<sup>60</sup>.

Among the aforementioned factors involved in the loading of the Met-tRNA<sub>i</sub> and PIC formation, eIF5 is a GTPase activating protein (GAP) that stimulates the hydrolysis of eIF2-bound GTP<sup>67,68</sup>. Interestingly, eIF5 physically connects with two different subunits of the eIF2 complex ( $\beta$  and  $\gamma$ ) via two distinct domains (C-terminal and N-terminal domains, respectively)<sup>69-71</sup>. It is likely that eIF5 also functions in the structural assembly of the PIC since it interacts with multiple other initiation factors (including eIF1, 1A, and 3), and recent evidence has implicated it in start codon recognition by mechanisms independent of its GAP function<sup>61,69-75</sup>. eIF1 is a small ~12 kD protein

without an exact sequence or structural bacterial ortholog. Nevertheless, it shares some common functions with the bacterial IF3 in discriminating against non-cognate start codons<sup>1,76</sup>. eIF1 binds near the P-site of the 30S subunit<sup>77-79</sup> and forms physical interactions with eIF2, 3, and 5<sup>61,70,80-82</sup>. eIF1A is the ortholog of bacterial IF1 and similarly binds over the mRNA entry channel near the A-site on the body of the 40S subunit<sup>79,83</sup>. eIF1A, however, contains additional C-terminal and N-terminal tail (CTT and NTT, respectively) expansions that are projected toward the mRNA entry channel<sup>79,83</sup>. eIF1A NTT has been shown to interact with eIF2 and eIF3, which is thought to stabilize the binding of the TC to the 40S subunit<sup>84</sup>. Finally, eIF3 is a large multi-subunit complex that spans the entire 40S subunit on the solvent side interacting with both the entry and the exit channels of the mRNA<sup>85-88</sup>. eIF3 is thought to play a vital function in the structural assembly of the PIC as it forms a network of interactions among many of its components including the mRNA and the 40S subunit as well as the initiation factors 1, 1A, 2, and 5<sup>61,64,81,86,88,89</sup>. Besides its involvement in TC recruitment and the formation of the PIC, eIF3 also plays an important function in loading the 43S PIC at the 5' cap of the mRNA (see below).

In order for the process of scanning and initiation to continue, the 43S PIC has to assemble at the 5' end of the mRNA, forming a 48S PIC. The 43S PIC can inherently bind to the 5' end of mRNAs lacking any structures in their 5' UTRs<sup>76</sup>. The majority of the endogenous mRNAs, however, contain secondary structures such as stem-loops that require the actions of helicases and other protein factors to facilitate this process. The attachment of the 43S PIC to the 5' end of a canonical mRNA takes place through a complex network of interactions among the components of the eIF4F and eIF3 complexes

as well as eIF4B and the poly-A-binding protein (PABP)<sup>30,60</sup>. The eIF4F complex consists of a cap-binding protein (eIF4E), a DEAD-box RNA helicase (eIF4A), and a scaffolding protein (eIF4G) that physically links eIF4E, eIF4A, PABP and eIF3<sup>1,90</sup>. The ultimate result of the many interactions among all these factors is the resolution of the 5' UTR secondary structures by eIF4A, and potentially by other helicases, which then allows for the attachment of the 43S PIC via interactions with eIF3, and perhaps with other components of the PIC (see Hinnebusch 2011<sup>90</sup> for a review of the 43S PIC loading on the mRNA).

After the assembly of the 43S PIC near the 5' cap of the mRNA, it has to scan the downstream nucleotides for complementarity with the anticodon of the Met-tRNA<sub>i</sub> in order to locate the start codon. In the absence of any 5' UTR structures, the 43S PIC alone is capable of the 5' to 3' movement along the sequence of an mRNA, but the presence of any secondary structures necessitates the activities of the eIF4A helicase, eIF4B, and eIF4G of the 48S PIC<sup>76</sup>. Remarkably, the scanning capability of the 43S PIC heavily depends on the presence of eIF1A and almost completely on the eIF1 protein,<sup>76</sup> and PIC lacking eIF1 and eIF1A is unable to locate the initiator codon<sup>91</sup>. This observation suggests that the binding of the eIF1 and 1A proteins induces such structural rearrangements that make the 43S PIC competent for scanning the 5' UTR of mRNAs to search for the start codon. Indeed, recent biochemical and cryo-electron microscopy (cryo-EM) structural studies, using in vitro reconstituted PIC, have demonstrated that the binding of the eIF1 and 1A proteins to the 40S subunit is cooperative and induces an '*open*' conformation of the PIC that allows for the loading of the TC, recruitment of the mRNA, and presumably the scanning of the mRNA 5' UTR<sup>63</sup>.

Start codon selection depends on the irreversible hydrolysis of the eIF2-bound GTP and the release of the inorganic phosphate<sup>92</sup>. Another essential feature of the open conformation of the PIC is that the premature dissociation of P<sub>i</sub> is blocked. As indicated above, eIF5 is the GAP factor that stimulates the hydrolysis of eIF2-bound GTP. Hence, a fraction of eIF2•GTP is hydrolyzed to GDP and P<sub>i</sub> in the 43S PIC<sup>92</sup>. Structural arrangement of the open conformation, however, blocks the release of P<sub>i</sub> in the absence of a cognate codon:anticodon interaction between the mRNA and the Met-tRNA<sub>i</sub><sup>72,92</sup>. This allows for the PIC to remain in the open conformation and to continue scanning the 5' UTR of the mRNA until cognate codon:anticodon base pairing is reached.

Moreover, another significant feature of the open conformation is that the Met-tRNA<sub>i</sub> may not be fully accommodated in the P-site during the scanning process. Based on structural studies, it has been proposed that the presence of the eIF1 and 1A proteins in the open conformation is likely to prevent the full insertion of the Met-tRNA<sub>i</sub> in the P-site. eIF1 binds in the vicinity of the P-site and is predicated to have a slight steric clash with the Met-tRNA<sub>i</sub>. Furthermore, while the body of eIF1A binds in the A-site, its CTT is inserted in the mRNA channel toward the P-site where the Met-tRNA<sub>i</sub> samples the mRNA codons for complementarity<sup>77-79,83,93,94</sup>. This destabilization of the Met-tRNA<sub>i</sub> in the P-site is important because it induces a certain dynamics and competition that ultimately prevents the stabilization of the Met-tRNA<sub>i</sub> binding to near-cognate codons and allows for only a stable cognate codon:anticodon interaction to signal start codon detection.

Upon recognition of the start codon through a cognate codon:anticodon interaction between the mRNA and the Met-tRNA<sub>i</sub>, a series of structural rearrangements

in the PIC then leads to the stabilization of the '*closed*' conformation that signals initiation. Cognate codon:anticodon base pairing stabilizes TC binding to the 40S subunit<sup>95</sup>. It also stabilizes the binding of the eIF1A protein by inducing an interaction between its CTT and the N-terminal domain (NTD) of the eIF5 protein<sup>72,75</sup>. Recent evidence suggests this interaction is coupled to the dissociation of eIF1 and P<sub>i</sub> release from the PIC, which are among the events essential for start codon recognition<sup>72,96</sup> as they contribute to the accommodation of the Met-tRNA<sub>i</sub> in the P-site and its dissociation from the eIF2 complex, respectively. As explained above, the CTT of eIF1A extends toward the P-site of the 40S subunit<sup>79,83</sup>; therefore, interactions with the NTD of eIF5 may also lead to the displacement of eIF1A CTT that together with the dissociation of eIF1, which binds near the Met-tRNA<sub>i</sub> in the P-site<sup>77-79</sup>, would contribute to the accommodation of the Met-tRNA<sub>i</sub> in the P-site.

As elucidated earlier, eIF5 also physically interacts with both the eIF1 and eIF2 proteins<sup>61,69,71,73</sup>. Interestingly, recent evidence has suggested that eIF1 and eIF2 $\beta$  compete for binding to eIF5 as the regions in the C-terminal domain (CTD) of eIF5 that bind to eIF1 overlap with its binding sites for eIF2 $\beta$ <sup>70</sup>. It was further proposed that start codon recognition strengthens the interactions between eIF5 and eIF2 $\beta$ , which contributes to the stabilization of the closed conformation as well as to the dissociation of eIF1<sup>70</sup>. Thus, multiple interactions seem to contribute to the dissociation of eIF1 upon start codon recognition. Genetic studies have also provided evidence for the importance of eIF1 release in the accuracy of start codon selection in vivo. Mutations that increase the dissociation rate of eIF1, by disrupting its contact points with the 40S subunit, have been shown to display a Sui<sup>-</sup> (suppressor of initiation codon) phenotype by reducing the



stringency of start codon recognition and allowing for translation initiation from a near-cognate UUG codon<sup>97,98</sup>. Conversely, mutations that reduce the dissociation rate of eIF1 have been reported to display an Ssu<sup>-</sup> (suppressor of Sui<sup>-</sup>) phenotype by restoring the accuracy of start codon selection and blocking translation initiation from a UUG codon (Martin-Marcos et al. 2013).

After start codon recognition, in order to assemble an elongation-competent 80S complex, the 60S subunit has to join the 40S with the Met-tRNA<sub>i</sub> fully accommodated in the P-site. 60S subunit joining and the dissociation of eIF2•GDP and eIF5 are mediated by eIF5B, a ribosome-dependent GTPase and an ortholog of bacterial IF2<sup>96,99</sup>. Efficient subunit joining and GTP hydrolysis, which is required for the dissociation of eIF5B itself, are dependent on the interactions of eIF5B with the CTT of eIF1A<sup>84,100-102</sup>. Thus, the CTT of eIF1A is involved in orchestrating multiple events during the entire process of translation initiation. During the scanning phase, it is positioned near the P-site and cooperates with eIF1 to prevent the full accommodation of the Met-tRNA<sub>i</sub>, which maintains the PIC in the open conformation and allows for the scanning to proceed. Upon cognate base pairing between the start codon and the anticodon of Met-tRNA<sub>i</sub>, eIF1A CTT is then repositioned from the P-site by interacting with the NTD of eIF5 that contributes to both the accommodation of the Met-tRNA<sub>i</sub> in the P-site and also to the dissociation of eIF1, which in turn further adds to the stabilization of Met-tRNA<sub>i</sub> binding to the P-site. Genetic evidence has also implicated eIF1A CTT and NTT in the initiation of protein synthesis. Mutations in the two tails of eIF1A have been shown to display opposing effects in the accuracy of start codon recognition. Whereas mutations in the scanning enhancer (SE) elements of its CTT lead to a reduction in the fidelity of initiation

and a Sui<sup>-</sup> phenotype, mutations in its NTT display an Ssu<sup>-</sup> phenotype and restore the stringency of start codon selection in vivo<sup>103-105</sup>.

Thus, start codon selection requires the coordinated actions of a number of events in the PIC that collectively commit the complex to begin translation. While thus far some of these essential interactions among the different factors have been determined, many more are yet to be identified. Understanding the full mechanistic details of translation initiation in eukaryotes requires mapping the entire network of interactions among its different components. In this study, we have identified a new function for the eIF2 complex essential for establishing the fidelity of protein synthesis. Our findings suggest a model in which domain-III of eIF2 $\gamma$  also contributes to the stabilization of the closed conformation and Met-tRNA<sub>i</sub> binding upon a cognate codon:anticodon interaction, which then signals starts codon recognition.

## 1.2 The eIF2 Complex

### 1.2.1 eIF2: The $\alpha$ , The $\beta$ , and The $\gamma$

eIF2 is a heterotrimeric G-protein complex that, in its active GTP-bound state, binds and delivers the Met-tRNA<sub>i</sub> to the P-site of the 40S subunit<sup>106,107</sup>. It is composed of the  $\alpha$ ,  $\beta$ , and  $\gamma$  subunits (encoded by *SUI2*<sup>108</sup>, *SUI3*<sup>109</sup>, and *GCD11*<sup>110</sup> in *S. cerevisiae*, respectively) that are well conserved between the archaeal and the eukaryotic domains of life<sup>111</sup>. There is no bacterial ortholog of eIF2. Although a crystal structure of a eukaryotic complex is not yet available, multiple structures of archaeal complexes (aIF2) in the apo form or with GDP or different non-hydrolysable analogues of GTP have been determined (Figure 1.4)<sup>112-116</sup>. The archaeal heterotrimeric complex is composed of a rigid core body (formed by the  $\gamma$  subunit, domain-III of the  $\alpha$  subunit, and the N-terminal  $\alpha$ -helix of the  $\beta$  subunit) and two flexible parts on each side (formed by domains -I and -II of  $\alpha$  and the central  $\alpha$ - $\beta$  fold and the C-terminal zinc-binding domain of  $\beta$ ). Due to high conservation between the eukaryotic and archaeal e/aIF2 complexes, the archaeal structures have been invaluable in analyzing the functions of the various elements in the eukaryotic complex.

eIF2 $\gamma$  is a ~57 kDa protein that forms the core of the eIF2 complex holding the  $\alpha$  and  $\beta$  subunits. No physical interaction between  $\alpha$  and  $\beta$  has been detected in yeast and archaea<sup>116-120</sup>. Interactions between recombinant human eIF2 $\alpha$  and  $\beta$  have, however, been reported<sup>121,122</sup>. Structural analysis of the archaeal proteins have revealed a close structural homology between  $\gamma$  and EF-Tu (EF1A in eukaryotes)<sup>114,119,123,124</sup>. This is consistent with the function of both proteins in binding tRNA in a GTP depended manner

and delivering it to the ribosome. The  $\gamma$  subunit consists of an N-terminal G-domain and  $\beta$ -barrel structured domains -II and -III (Figure 1.5C)<sup>119,124</sup>. Eukaryotic eIF2 $\gamma$  also contains an N-terminal tail, which varies in length among different species and is absent in archaea<sup>125</sup>. The G-domain is the largest of the three domains, and it binds to the guanine nucleotide and contains contact points for Met-tRNA<sub>i</sub> binding. Domain-II participates in binding the Met-tRNA<sub>i</sub> along with the G-domain and also binds to domain-III of the  $\alpha$  subunit. Domain-III interacts with both the G-domain and domain-II<sup>113,114,116,119,123,124,126</sup>. Comparison of different structures have suggested that domains -II and -III retain a fixed position with respect to one another but can move around the G-domain through a pivot point around the switch-I element<sup>115,119,124</sup>. Furthermore, using in vitro reconstituted yeast PIC and a directed hydroxyl radical probing approach, a recent study has mapped domain-III of the  $\gamma$  subunit as the binding interface between the eIF2 complex and the 40S subunit<sup>127</sup>. Moreover, our findings from this study suggests a novel function for the  $\gamma$  subunit in which domain-III is involved in establishing the accuracy of start codon recognition through adjusting the equilibrium between the open and closed conformations of the PIC.

The G-domain of eIF2 $\gamma$  harbors features highly conserved among all GTP-binding proteins, including the switch-I, switch-II, and P-loop elements. In all G-proteins known so far, GTP hydrolysis is achieved mainly through the conformational rearrangements of the two mobile switch-I and switch-II regions<sup>128</sup>. Indeed, large structural reorganizations in the two switch elements as well as in the orientation of the G-domain with respect to domains -II and -III have been observed in the structures of EF-Tu in complex with GDP versus GTP analogues<sup>129-131</sup>. In the GTP-bound protein, the switch elements take the ‘on’

position, and EF-Tu is in a *closed* state where domain-II is packed against the G-domain. When in complex with GDP, however, the switch elements are in the ‘off’ position, and EF-Tu is in the *open* state with a hole between the two domains as domain-II has moved away from the G-domain<sup>129,131,133</sup>. Remarkably, the  $\gamma$  subunit assumes an orientation resembling the *closed* state of EF-Tu, which represents its active GTP-bound state, regardless of whether it is in the apo form or in complex with GDP or GDPNP (a non-hydrolysable analogue of GTP)<sup>114,116,119,123,124,126,132</sup>. Moreover, the switch elements of  $\gamma$  do not seem to follow the simple ‘on’ and ‘off’ scheme depending on the nucleotide bound. When the switch regions of all known aIF2 $\gamma$  structures<sup>114,116,119,123,124,126,132</sup> were superimposed, no obvious correlation between their conformation and the nucleotide state of the  $\gamma$  subunit was observed<sup>114</sup>.

It is important to note that unlike in eukaryotes, GTP hydrolysis and the exchange of GDP for GTP in aIF2 is thought to be spontaneous as archaea lack homologues of eIF2B $\epsilon$  (the catalytic subunit of eIF2B) and eIF5, which serve as the GEF (guanine nucleotide exchange factor) and GAP factors for the eIF2 complex, respectively<sup>1</sup>. Therefore, it is likely that the exact conformations of the elements in the G-domain involved in GTP hydrolysis, such as the switch-I and switch-II regions, may differ between the archaeal and eukaryotic complexes. Moreover, as elucidated above, unlike EF-Tu and many other GTPases, the domains of the  $\gamma$  subunit do not seem to undergo large conformational rearrangements upon GTP hydrolysis. This observation suggests other protein factors in contact with the G-domain may participate in regulating its nucleotide-binding activity. The eIF5 and eIF2 $\beta$  proteins are both logical candidates for this function. The NTD of eIF5 has been reported to directly interact with the G-domain

of eIF2 $\gamma$  in yeast<sup>69</sup>. Although the main stable contact point between the  $\beta$  and  $\gamma$  subunits is through the N-terminal domain of  $\beta$  and the G-domain of  $\gamma$ , the core  $\alpha$ - $\beta$  fold and the C-terminal domains of  $\beta$  may potentially have transient interactions with the switch-I region of the G-domain (see below). As discussed above, the irreversible hydrolysis of the eIF2-bound GTP and the release of P<sub>i</sub> is an essential step for the dissociation of Met-tRNA<sub>i</sub> and the initiation of protein synthesis. Moreover, as elucidated earlier, translation initiation in eukaryotes is a result of an orchestrated series of events that ultimately lead to the formation of an elongation-competent 80S complex at the start codon. Therefore, by involving other factors, such as eIF5 that forms a series of networks with other players in this process (see Section 1.1.2), GTP hydrolysis and P<sub>i</sub> release are physically linked and coordinated to other events that have to take place in order for initiation to proceed.

eIF2 $\alpha$  is a ~35 kDa protein with conserved sequence and structural organization among various organisms. It is composed of three domains: an N-terminal  $\beta$ -barrel domain-I, a helical domain-II, and a C-terminal  $\alpha$ - $\beta$  fold domain-III (Figure 1.5A)<sup>133-135</sup>. Domain-III forms a rigid body that interacts with loop-1 of eIF2 $\gamma$  domain-II. Domains -I and -II are connected via a flexible linker to domain-III and exhibit a high degree of conformational mobility<sup>114,133,136,137</sup>. Eukaryotic eIF2 $\alpha$  also contains an acidic extension at its C-terminus that is missing in archaea<sup>125</sup>. Recently, it has been reported that the C-terminal acidic tail of *S. cerevisiae* eIF2 $\alpha$  potentially antagonizes Met-tRNA<sub>i</sub> binding (see next section)<sup>138</sup>.

Multiple functions have been attributed to eIF2 $\alpha$ . Perhaps it is most widely studied for its global regulatory role in response to environmental factors (discussed in Section 1.2.3 below). eIF2 $\alpha$  has also been implicated in the recognition of the -3 context

position as well as in the accuracy of start codon selection. The importance of context sequence in the efficiency of translation initiation has been well documented<sup>139-145</sup> although the mechanisms by which the context of a start codon is *read* are not yet fully understood. mRNAs with *optimal* (or near-optimal) context are generally translated at a higher rate. It should, however, be noted that multiple reports have indicated that the effects of context on the efficiency of translation is less pronounced in *S. cerevisiae* than in mammalian organisms and plants<sup>146-149</sup>. Using in vitro reconstituted PIC, it was observed that human eIF2 $\alpha$  cross-links to the -3 purine nucleotide of the mRNA<sup>150</sup>. Furthermore, it was illustrated that the efficiency of eIF2 dissociation after an eIF5-induced GTP hydrolysis depends upon the nature of the -3 nucleotide and the  $\alpha$  subunit of eIF2<sup>150</sup>. Thus, it was proposed that the previously reported effect of mRNA on the dissociation of eIF2•GDP after start codon recognition<sup>96</sup> is likely to be via interactions between the -3 context position and the  $\alpha$  subunit<sup>150</sup>. Consistent with an interaction between eIF2 $\alpha$  and mRNA, a recent cryo-EM model of an in vitro reconstituted mammalian PIC positions the  $\alpha$  subunit near the Rps5e protein in the vicinity of the mRNA channel in the 40S subunit<sup>151</sup>. Furthermore, it has also been proposed that eIF2 $\alpha$  is involved in maintaining the fidelity of translation initiation as two substitutions have been isolated in its domain-I that reduce the stringency of start codon recognition and allow for initiation from a near-cognate UUG codon<sup>108,152</sup>. The underlying mechanism for these Sui<sup>-</sup> mutations has not yet been determined. Considering the conformational flexibility of domain-I and the precedent for an eIF2 $\alpha$  interaction with the mRNA, it is possible that its Sui<sup>-</sup> mutants reduce the accuracy of start codon selection by altering the network of physical interactions around the mRNA exit channel.

eIF2 $\beta$  is a ~32 kDa protein composed of three conserved domains and one eukaryotic-specific domain. The conserved domains consist of an unstructured N-terminal domain that contains the  $\alpha$ -helix-1 ( $\alpha_1$ ), a core  $\alpha$ - $\beta$  fold, and a C-terminal C<sub>2</sub>-C<sub>2</sub> zinc-binding domain (ZBD) (Figure 1.5B)<sup>116,125,126,153,154</sup>. Eukaryotic eIF2 $\beta$  also contains an N-terminal extension that harbors three poly-lysine boxes, which are implicated in binding to a common set of acidic- and aromatic-rich motifs present in the C-terminal domains of eIF2B $\epsilon$  and eIF5<sup>155-157</sup>. It should be noted that eIF5 and eIF2B $\epsilon$  were later shown to also directly interact with the G-domain of eIF2 $\gamma$  through their N-terminal and C-terminal domains, respectively<sup>69</sup>. Interestingly, the NTD of eIF5 is also composed of an  $\alpha$ - $\beta$  fold and a ZBD that bear structural homology to those of the eIF2 $\beta$  protein<sup>116,158</sup>. Moreover, it has been reported that the poly-lysine boxes in the N-terminal extension and the ZBD of eIF2 $\beta$  can also bind RNA<sup>159,160</sup>.

Three independent structures of the  $\beta$  subunit either in complex with  $\gamma$  or with an  $\alpha\gamma$  heterodimer in archaeon *Pyrococcus furiosus* or *Sulfolobus solfataricus* have been published so far<sup>114,116,126</sup>. While a high degree of flexibility is reported with respect to the positions of the central  $\alpha$ - $\beta$  fold and the C-terminal ZBD, the N-terminal domain of  $\beta$  is the main contact point with the  $\gamma$  subunit in all three structures as its  $\alpha_1$ -helix is inserted between two  $\alpha$ -helices of eIF2 $\gamma$  G-domain.  $\alpha_1$  is the most conserved region of eIF2 $\beta$  and, interestingly, is disordered in the solution structure of an isolated  $\beta$  subunit<sup>154</sup>. Moreover, studies in yeast have illustrated that substitutions in  $\alpha_1$  of eIF2 $\beta$  significantly reduce its association with eIF2 $\gamma$  and lead to the loss of initiation fidelity<sup>117</sup>. Thus,



interactions between  $\alpha_1$  of e/aIF2 $\beta$  and domain-III of e/aIF2 $\gamma$  are required and potentially sufficient to anchor the  $\beta$  subunit to the eIF2 complex.

The central  $\alpha$ - $\beta$  fold and the C-terminal ZBD of eIF2 $\beta$  exhibit a high degree of flexibility<sup>114,116,141</sup> that is also observed in the isolated  $\beta$  subunit in solution<sup>154</sup>. The two domains were detected in different orientations in the three aforementioned crystal structures. Interestingly, the domains assume diverse positions even in the different complexes formed in a single crystal, as the structures of four separate molecules were determined in the asymmetric unit of a crystal from *S. solfataricus* aIF2<sup>114</sup>. This observation suggests that the diverse orientations of aIF2 $\beta$  central and C-terminal domains are unlikely to be an artifact of crystal packing. In this structure, where a complete heterotrimer of aIF2 is resolved, only the N-terminal domain contacts the  $\gamma$  subunit, and the other two domains are mobile and solvent-exposed<sup>114</sup>. In the structure of the  $\beta\gamma$  heterodimer (with or without a GDP molecule) from *P. furiosus*, the core  $\alpha$ - $\beta$  domain is packed against the G-domain of aIF2 $\gamma$  while the ZBD does not contact the  $\gamma$  subunit and is solvent-exposed<sup>141</sup>. Finally, in the second structure of aIF2 from *S. solfataricus*, which contains the full  $\beta$  and  $\gamma$  subunits but only domain-III of aIF2 $\alpha$  ( $\alpha_3\beta\gamma$ ) and a GDP molecule, the ZBD is in close proximity to the nucleotide-binding site of the  $\gamma$  subunit but there is no contact between the central  $\alpha$ - $\beta$  fold and aIF2 $\gamma$ <sup>116</sup>.

It is interesting to note that the same region of the  $\gamma$  subunit is observed to interact with the two different domains of  $\beta$  reported above. In both the structure of *P. furiosus*  $\beta\gamma$  heterodimer and the *S. solfataricus*  $\alpha_3\beta\gamma$  complex, the switch-I region of aIF2 $\gamma$  G-domain interacts with the central  $\alpha$ - $\beta$  or the C-terminal ZBD of the  $\beta$  subunit,

respectively<sup>116,141</sup>. As elucidated above, the  $\alpha$ - $\beta$  fold and the ZBD of  $\beta$  exhibit a high degree of conformational mobility<sup>114,116,141</sup>. Therefore, it is feasible that they may interact with the G-domain of  $\gamma$  transiently during the different events of initiation to allow for their coordination. Indeed, eIF2 $\beta$  has been reported to contribute to Met-tRNA<sub>i</sub> binding in yeast<sup>161,162</sup>. Moreover, multiple Sui<sup>-</sup> mutations have been isolated in its ZBD that reduce the accuracy of start codon selection<sup>163</sup>. Our findings from this study also provide evidence for the involvement of eIF2 $\beta$  ZBD in the stabilization the closed conformation of the PIC (discussed in Chapter 4).

### 1.2.2. Ternary Complex Formation

Ternary complex is formed by the binding of Met-tRNA<sub>i</sub> to the active GTP-bound state of the eIF2 heterotrimer<sup>164-167</sup>. TC delivers the Met-tRNA<sub>i</sub> to the P-site of the 40S subunit and maintains it during the scanning phase of initiation while its anticodon searches the sequence of the mRNA for complementarity in order to identify the initiation site. Upon start codon recognition, GTP hydrolysis and P<sub>i</sub> release then allows for the dissociation of Met-tRNA<sub>i</sub> from the eIF2 complex. It has been reported that Met-tRNA<sub>i</sub> binds to the eIF2•GTP complex around 15- and 70-fold tighter than to the GDP-bound complex in *S. cerevisiae* and *S. solfataricus*, respectively<sup>132,165</sup>, which can explain the dissociation of Met-tRNA<sub>i</sub> after GTP hydrolysis and start codon recognition. It is interesting to note that the effect of GTP on Met-tRNA<sub>i</sub> binding to eIF2 does not seem as substantial as the effect of GTP on the binding of elongator tRNAs to EF-Tu. Due to the conformational arrangements of its domains and switch regions in the *open* state, EF-Tu•GDP does not contain a binding site for an aminoacylated tRNA. By contrast, it has been reported that the body of Met-tRNA<sub>i</sub> can still interact with eIF2•GDP and that the

GTP nucleotide is more involved in the recognition of the methionine moiety in yeast<sup>131,165</sup>. As discussed in Section 1.2.1, unlike EF-Tu, the  $\gamma$  subunit of eIF2 is always in the *closed* state and, based on the available structures, does not seem to undergo large conformational rearrangements. Moreover, no obvious correlation between the conformation of the two switch elements and the nucleotide state of eIF2 $\gamma$  has been observed<sup>114</sup>. Thus, it seems unlikely that the GTP nucleotide alone could confer the entire binding affinity and the specificity of Met-tRNA<sub>i</sub> for eIF2•GTP. In agreement with this expectation, many studies have implicated the participation of elements in the body of the initiator tRNA as well the  $\alpha$  and  $\beta$  subunits in Met-tRNA<sub>i</sub> binding to the eIF2 complex<sup>132,136,161,162,165,168-174</sup>.

The sequence of the initiator tRNA is the most conserved among all tRNA species throughout the three kingdoms of life<sup>175</sup>. It has been reported that conserved features of the Met-tRNA<sub>i</sub> itself contributes to its recognition by eIF2 $\gamma$ <sup>136,165,169,170,173,174</sup>. The methionine moiety of the bacterial initiator tRNA is formylated, which helps the initiation complex to distinguish it from the elongator methionyl tRNA<sup>176-178</sup>. Eukaryotic Met-tRNA<sub>i</sub>, however, lacks the formyl modification and needs to rely on other features to differentiate it from the elongator Met-tRNA for binding to eIF2. The A1:U72 base pair, which is specific to the Met-tRNA<sub>i</sub>, has been suggested to play an important role in its function and recognition by eIF2<sup>165,169,170,173,179</sup>. When the A1:U72 base pair of the yeast initiator tRNA was mutated to G1:C72, which is specific to elongator tRNAs, it could function as an elongator tRNA *in vivo*<sup>179</sup>. Moreover, it has been illustrated that the methionine moiety also contributes to the binding of the Met-tRNA<sub>i</sub> in a GTP dependent manner<sup>165,174</sup>. It was further proposed that A1:U72 could potentially position the

methionine moiety in its proper binding pocket in eIF2<sup>164</sup>. Furthermore, structural elements and modifications on base of the T-stem and loop of Met-tRNA<sub>i</sub> have been implicated in blocking its binding to EF1A<sup>180-184</sup>. Thus, Met-tRNA<sub>i</sub> is an active participant in determining the specificity and affinity of its binding to the eIF2 complex.

The extent of the  $\alpha$  and  $\beta$  subunits contributions to the binding of the Met-tRNA<sub>i</sub> to eIF2 has been the subject of much debate. Genetic and biochemical experiments have generated contradictory results for the effects of each subunit on the affinity of Met-tRNA<sub>i</sub> for eIF2 in eukaryotes in comparison with archaea. The archaeal  $\alpha$  subunit has been shown to substantially increase the binding of the Met-tRNA<sub>i</sub> to aIF2<sup>113,118,132,136,137,171</sup>. In eukaryotes, however, it is the  $\beta$  subunit that seem to increase the affinity of Met-tRNA<sub>i</sub> for eIF2 with minor or no contributions from the  $\alpha$  subunit<sup>161,162,168,172</sup>. Recently, this dispensability of eIF2 $\alpha$  was attributed to its eukaryotic-specific C-terminal extension, where progressive shortening of this acidic tail increased the contribution of the  $\alpha$  subunit to Met-tRNA<sub>i</sub> binding<sup>138</sup>. Interestingly, it has also been reported that in the primitive eukaryote *Encephalitozoon cuniculi*,  $\alpha$  and  $\beta$  each contribute equally to the affinity of Met-tRNA<sub>i</sub> for eIF2<sup>185</sup>. This species-specific contribution of the  $\alpha$  and  $\beta$  subunits suggests that there may potentially be subtle structural differences by which Met-tRNA<sub>i</sub> binds to the eIF2 complex in different organisms.

Based on the close structural homology between eIF2 $\gamma$  and EF-Tu and mutational analysis in yeast and archaea, it was originally thought that the two proteins bind tRNA in a similar manner<sup>119,124,130,136,164</sup>. A directed hydroxyl radical probing study, using an in vitro reconstituted yeast PIC, provided the first evidence that the mode of Met-tRNA<sub>i</sub>

binding to the eIF2 complex may in fact be different from EF-Tu<sup>127</sup>. EF-Tu interacts with both the amino acid and the body of the elongator tRNAs so that its domain-III binds to the T-stem of the tRNA<sup>186-189</sup>. In this recent study, however, it was reported that eIF2 $\gamma$  only interacts with the methionine moiety and the acceptor stem of the Met-tRNA<sub>i</sub> and contributions from the  $\beta$  subunit were also detected<sup>127</sup>. It was further observed that eIF2 $\gamma$  domain-III faces helix 44 of the 40S subunit and is potentially involved in the binding of the TC to the PIC<sup>127</sup>, which is in good agreement with our findings in this study.

While no crystal structure of a eukaryotic eIF2 in complex with Met-tRNA<sub>i</sub> is yet available, recently two independent structures of a partial *S. solfataricus* aIF2 in complex with GDPNP and *E. coli* fMet-tRNA<sub>i</sub> have been resolved<sup>113,115</sup>. Remarkably, the mode of fMet-tRNA<sub>i</sub> binding is drastically different between the two structures. The differences can be, at least partially, attributed to the different composition of the complexes used. In one study aIF2•GDPNP•fMet-tRNA<sub>i</sub> was assembled using aIF2 containing full length  $\alpha$ ,  $\beta$ , and  $\gamma$  subunits<sup>113</sup>. It should, however, be noted that the core  $\alpha$ - $\beta$  fold and the ZBD of the  $\beta$  subunit could not be resolved in this structure. In the second study, a partial aIF2 containing the full  $\gamma$  subunit and only domain-III of  $\alpha$  was used to assemble an incomplete aIF2•GDPNP•fMet-tRNA<sub>i</sub> complex<sup>115</sup>. Considering the conformational mobility of domains -I and -II of eIF2 $\alpha$  as well as the core  $\alpha$ - $\beta$  fold and the ZBD of eIF2 $\beta$ , it is feasible to assume that their presence would potentially affect the mode of Met-tRNA<sub>i</sub> binding to the  $\gamma$  subunit. It is also important to note that the Met-tRNA<sub>i</sub> may hold a different conformation in eIF2 alone as opposed to when in complex with the PIC.

Thus, more structures of both eukaryotic and archaeal TC alone and in complex with the PIC are needed to fully determine the structural arrangement of the Met-tRNA<sub>i</sub> on eIF2.

### *1.2.3. Translational Control Through the eIF2 Complex*

In the 5' scanning pathway for translation initiation, which is the most common mode of initiation in eukaryotes, the Met-tRNA<sub>i</sub> is delivered to the PIC via the ternary complex. As elucidated above, Met-tRNA<sub>i</sub> binds eIF2 only when in complex with GTP. After each round of initiation, the GTP of eIF2 is hydrolyzed to allow for the dissociation of Met-tRNA<sub>i</sub> so that the process of protein synthesis can proceed. eIF2•GDP has to then *recycle* in order to form the active form of the complex (eIF2•GTP) so that the Met-tRNA<sub>i</sub> can be delivered in the next round of initiation. Therefore, the conversion of eIF2•GDP to eIF2•GTP constitutes a rate-limiting step of translation initiation and has been used as an essential point of regulation in the cell.

eIF2B is the guanine exchange factor for eIF2 that catalyzes the exchange of GDP for GTP<sup>62</sup>. It is a heteropentamer with  $\alpha$ ,  $\beta$ ,  $\gamma$ ,  $\delta$ , and  $\epsilon$  subunits. eIF2B $\epsilon$  is the catalytic subunit that together with  $\gamma$  forms the 'catalytic' subcomplex.  $\alpha$ ,  $\beta$ , and  $\delta$ , on the other hand, form the 'regulatory' subcomplex<sup>190-192</sup>. As elucidated in the Section 1.2.1, eIF2B binds to the eIF2 complex through physical interactions between the C-terminal domain of the catalytic  $\epsilon$  subunit and the poly-lysine boxes present in the N-terminal extension of eIF2 $\beta$ <sup>155</sup>. An interaction between the C-terminal domain of eIF2B $\epsilon$  and the G-domain of eIF2 $\gamma$ , which is likely catalytic in nature, has also been reported<sup>69</sup>. Phosphorylation of the serine residue at position 51 (S51) of eIF2 $\alpha$  in eIF2•GDP transforms the complex to a poor substrate for eIF2B that prevents the exchange of GDP for GTP. It has been elucidated that the eIF2•GDP complex containing the phosphorylated eIF2 $\alpha$  binds with

higher affinity to eIF2B and forms a non-productive complex with the  $\alpha\beta\delta$  regulatory subcomplex that fails to associate productively with the catalytic subcomplex<sup>190,193-196</sup>. Consequently, the concentration of active eIF2•GTP, and hence TC, in the cell is reduced that then leads to a global reduction in protein synthesis. It is important to note that the concentration of eIF2B in the cell is lower than that of the eIF2 complex. Therefore, phosphorylation of even a small fraction of eIF2 $\alpha$  can lead to a large-scale inhibition of protein production.

S51 of eIF2 $\alpha$  is the target of phosphorylation by four different kinases that respond to different stimuli<sup>197,198</sup>. The kinase GCN2 is activated in response to depletion of nutrients<sup>199</sup>. As elucidated above, protein synthesis is the most energy-consuming process in the cells. Therefore, it can be expected that to maintain fitness, protein synthesis has to be down-regulated when amino acids and nutrients are scarce. PKR (for Protein Kinase RNA-dependent) is present in vertebrates and is activated by double stranded RNA<sup>200,201</sup>. By inhibiting protein synthesis, PKR is part of the cellular defense against viral infection<sup>202</sup>. PERK (PKR-like Endoplasmic Reticulum Kinase) is activated upon ER stress, for example upon activation of the unfolded protein response (UPR)<sup>203,204</sup>. This allows for the coupling of the rate of protein synthesis to the folding capacity of the protein chaperones to avoid the formation of, often toxic, misfolded proteins. Finally, HRI (Heme Regulated Inhibitor) is activated in response to heme deprivation in erythrocytes and other forms of oxidative stress in the cell<sup>203,205</sup>.

Interesting, phosphorylated eIF2 $\alpha$  can also act conversely as a positive regulator. It has been reported that a reduction in TC, which is a consequence of eIF2( $\alpha$ -P), leads to an increase in the translation of *GCN4* mRNA (*ATF4* in higher eukaryotes). Gcn4 is a

transcription factor that induces the expression of a set of amino acid biosynthetic enzymes and stress response genes (for a review see Hinnebusch 2005<sup>206</sup>). *GCN4* translation is under the regulatory control of four upstream ORFs (uORFs). The AUG codon of the first uORF is in an optimal context sequence. Therefore, nearly all of the PICs forming near the 5' cap of *GCN4* mRNA translate uORF1. After translating uORF1, about 50% of the ribosomes fail to be recycled at the stop codon of uORF1 and continue scanning the mRNA. When there are plenty of nutrients available, and hence the concentration of TC for delivering the Met-tRNA<sub>i</sub> is not limiting, the majority of the ribosomes reinitiate at uORF3 or uORF4. There is not enough distance between these uORFs and the AUG codon of *GCN4*. Consequently, the complexes that translate uORFs 3 or 4 fail to reinitiate again at the AUG codon of *GCN4*. Under nutrient-starved conditions, however, when eIF2 $\alpha$  is phosphorylated and TC is limiting, a greater proportion of reinitiating ribosomes bypass uORFs 3 and 4 and reinitiate at the AUG codon of *GCN4* increasing the translation of its mRNA<sup>206</sup>. Thus, the eIF2 complex plays an essential role in the translational control of cellular pathways. It provides a link between the external factors and the internal processes in the cell and allows for the adjustment of cellular resources in response to the environment.



### 1.3 Figures and Tables

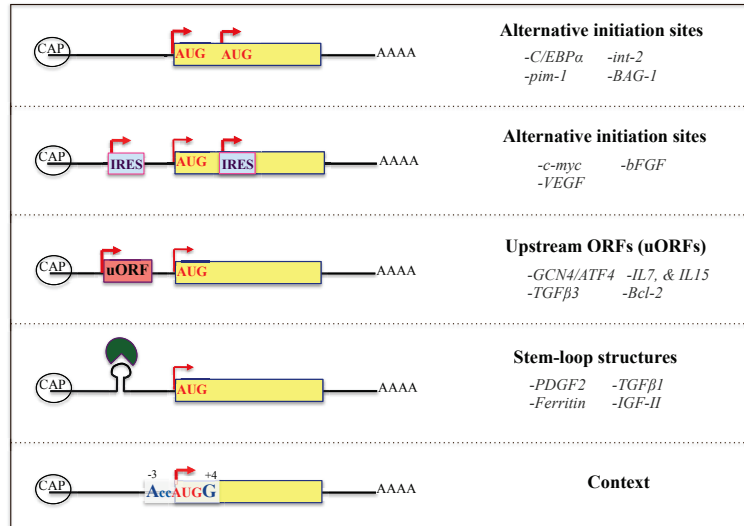


**Figure 1.1 Translation initiation is heavily regulated**

Protein synthesis is the most energy-consuming process in the cell. Therefore, multiple layers of regulation are put in place to prevent the waste of cellular resources. The majority of translational control takes place at the stage of initiation. Multiple examples of regulation at this stage are represented in this schematic (examples of genes employing each indicated type of regulation are listed on the right). A canonical eukaryotic mRNA contains an untranslated region (UTR) at its 5' end that often performs regulatory functions during initiation. For example, multiple initiation sites (either AUG codons or Internal Ribosome Entry Sites) are used to synthesize proteins that are targeted to cytoplasm or different cellular organelles based on the initiation site used. Short upstream ORFs (uORFs) and stem-loop structures in the 5' UTR generally exert negative effects and reduce initiation from the main ORF. The context of a start codon also impacts the amount of initiation. mRNAs that contain start codons in an optimal context are generally translated at higher levels. See Cazzola and Skoda 2000<sup>22</sup> for review.

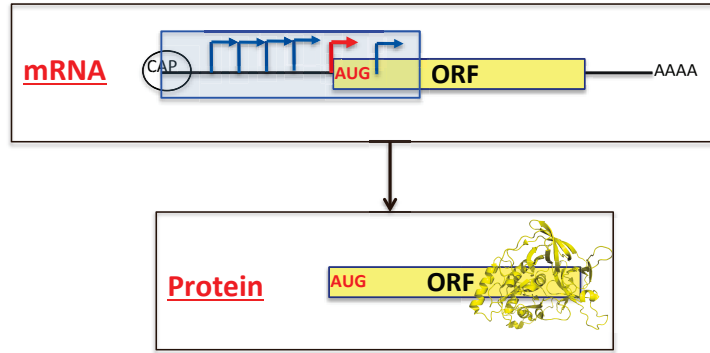


**Figure 1.2 Ribosome challenge: where shall I begin?**

The majority of mRNAs in all the three kingdoms of life are longer than the open reading frame that codes for the protein product as they contain sequences at their 5' and 3' regions that are not translated. This leaves the ribosome with the monumental task of finding the correct start codon for translation. A cartoon of a canonical eukaryotic mRNA with a 5' cap and a poly-A tail is represented.

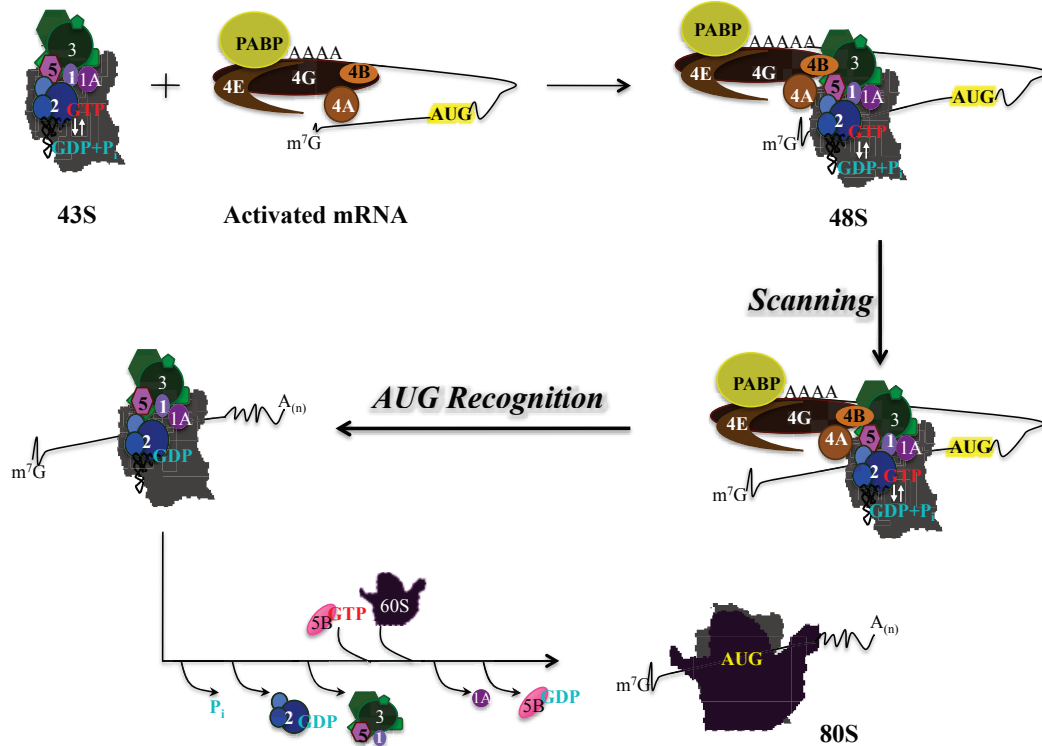


**Figure 1.3 The scanning mechanism of translation initiation in eukaryotes**

The Met-tRNA<sub>i</sub> is loaded on the 40S subunit in the context of a ternary complex with GTP-bound eIF2 in a process that is facilitated by eIF1, 1A, 3, and 5 to form the 43S pre-initiation complex. The mRNA is activated through the actions of PABP, eIF4B, and the eIF4F complex (consists of eIF4E, eIF4G, and eIF4A) and is loaded on the 43S complex to form the 48S PIC. The complex then scans the 5' UTR of the mRNA allowing the Met-tRNA<sub>i</sub> to sample each of the nucleotides for complimentary to locate the start codon. Upon a cognate codon:anticodon interaction, eIF2-bound GTP is irreversibly hydrolyzed and P<sub>i</sub> is release, which allows for the dissociation of Met-tRNA<sub>i</sub> from the eIF2 complex. Dissociation of eIF2•GDP, eIF5, and other initiation factors and the joining of the 60S subunit allows for the formation of an elongation-competent 80S complex that proceeds to the next stage of protein synthesis.

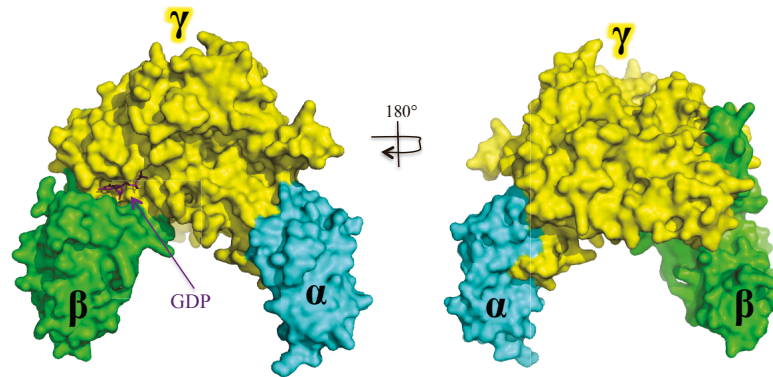


**Figure 1.4 Crystal structure of aIF2**

Two views of a surface-exposed representation of a partial aIF2 (full  $\gamma$  and  $\beta$  subunits with only domain-III of  $\alpha$ ) in complex with GDP from *S. solfataricus* (PDB 2QMU) are presented. The  $\gamma$  subunit forms the center of the complex that holds  $\alpha$  and  $\beta$ . The  $\gamma$  subunit, the N-terminal domain of  $\beta$ , and the C-terminal domain of  $\alpha$  (both of which bind to  $\gamma$ ) form a rigid body whereas the central and C-terminal domains of  $\beta$  and the N-terminal and central domains of  $\alpha$  (not depicted here) display high conformational mobility. Images were created using the PyMOL software<sup>207</sup>.

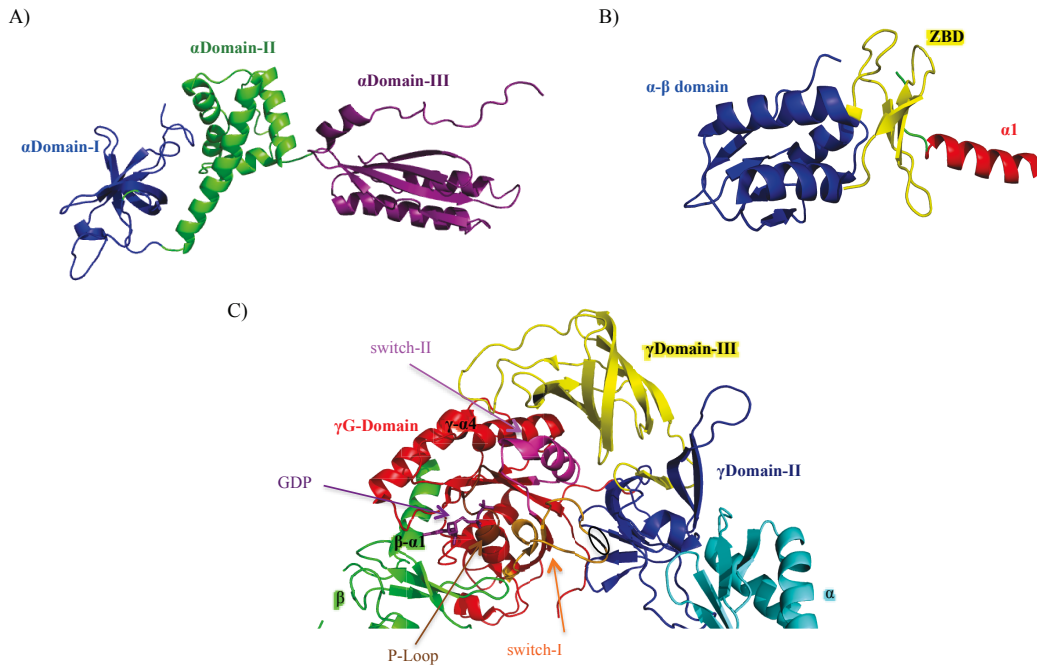


**Figure 1.5 Structures of eIF2 $\alpha$ ,  $\beta$ , and  $\gamma$  subunits**

(A) NMR structure of human eIF2 $\alpha$  (PDB 1Q8K). The  $\alpha$  subunit is composed of an N-terminal  $\beta$ -barrel structured domain-I, a helical domain-II, and an  $\alpha$ - $\beta$  fold domain-III.

(B) Crystal structure of aIF2 $\beta$  from archaeon *S. solfataricus* (PDB 2QMU). The  $\beta$  subunit consists of a helical N-terminal domain ( $\alpha_1$ ), a core  $\alpha$ - $\beta$  fold, and a C-terminal zinc-binding domain (ZBD).

(C) Crystal structure of aIF2 $\gamma$  in complex with GDP from archaeon *S. solfataricus* (PDB 2QMU). The  $\gamma$  subunit contains an N-terminal G-domain and  $\beta$ -barrel structured domains -II and -III. The essential features of the G-domain (switch-I, switch-II, and the P-loop) are marked. Regions of the  $\alpha$  (domain-III) and  $\beta$  (N-terminal  $\alpha_1$ ) subunits that contact eIF2 $\gamma$  are shown. Images were created using the PyMOL software<sup>207</sup>.

**Table 1.1 Various pathways for translation initiation**

<b>Mechanism</b>	<b>Organisms Employed</b>	<b>Key Principle</b>
Shine-Dalgarno Dependent	Bacteria and Archaea	Base pairing between SD <sup>a</sup> sequence of mRNA and anti-SD of 16S rRNA positions the ribosome at the start codon
5'-Cap Dependent	Eukaryotes	5' to 3' scanning of mRNA leader sequence until start codon is reached
Shine-Dalgarno Independent	Archaea and some Bacteria	Efficiency regulated by mRNA leader sequence
Leaderless	Archaea, some in Bacteria and Eukaryotes	Direct assembly of 70S and 80S ribosomes on the start codon
Internal Initiation	Eukaryotes (both viral and endogenous mRNAs)	IRES <sup>b</sup> directly recruits the 40S subunit to the start codon

<sup>a</sup>. Shine-Dalgarno

<sup>b</sup>. Internal Ribosome Entry Site

See Malys and McCarthy 2011<sup>31</sup> for review

**CHAPTER 2: IDENTIFICATION OF NOVEL MUTATIONS IN *GCD11* THAT  
ALTER THE FIDELITY OF START CODON RECOGNITION**

## 2.1 Introduction

As discussed in Chapter 1, eIF2 is a heterotrimeric GTP-binding protein complex at the center of the 5' cap dependent translation initiation pathway in eukaryotes. In its active GTP-bound state, eIF2 binds and delivers the Met-tRNA<sub>i</sub> to the P-site of the 40S subunit. During the scanning phase of initiation, eIF2 maintains the Met-tRNA<sub>i</sub> so that it can sample the nucleotides of the mRNA 5' UTR for complementarity in order to identify the start codon. Upon a cognate codon:anticodon interaction between the mRNA and Met-tRNA<sub>i</sub>, the irreversible hydrolysis of eIF2-bound GTP is needed for the dissociation of Met-tRNA<sub>i</sub> and the progress of the initiation pathway. Thus, the eIF2 complex is intimately involved in the events that lead to the selection of the start codon and initiation in eukaryotes. Furthermore, eIF2 plays vital regulatory functions and is involved in the translational control of many essential cellular processes (see Section 1.2.3).

Considering the pivotal role of eIF2 in translation initiation, we set out to closely examine this complex and identify features essential for start codon selection. The  $\gamma$  subunit of eIF2 forms the central part of the complex, which holds the other two subunits, and directly binds to GTP and Met-tRNA<sub>i</sub> (discussed in Sections 1.2.1 and 1.2.2). Therefore, we focused our study on the  $\gamma$  subunit. In order to identify new functional elements in eIF2 $\gamma$  that are involved in start codon selection, we employed three independent methods to isolate mutant variants of eIF2 $\gamma$  that either reduced the stringency of start codon recognition (Sui<sup>-</sup> class of mutants) or conversely restored initiation fidelity to cells harboring a Sui<sup>-</sup> mutation (Ssu<sup>-</sup> class of mutants).

To monitor the accuracy of translation initiation in vivo, we took advantage of a mutant allele of the *HIS4* gene (*his4-301*) that lacks a cognate AUG start codon<sup>208,209</sup>.



His4 is an essential protein in the histidine biosynthetic pathway. Thus, otherwise wild type (WT), yeast cells fail to translate the *his4-301* mRNA and consequently exhibit histidine auxotrophy. *Sui*<sup>-</sup> class of mutations, however, reduces the stringency of start codon recognition and allows for initiation from the third in-frame (UUG) codon of *his4-301*<sup>208,209</sup>. Thus, *Sui*<sup>-</sup> mutants display a *His*<sup>+</sup> phenotype by suppressing the histidine auxotrophy of cells harboring the *his4-301* allele and allowing them to grow on medium lacking histidine, or containing only 1% of the normal histidine supplement (-His medium). The *Ssu*<sup>-</sup> mutant alleles, on the other hand, reestablish the accuracy of start codon selection, block translation initiation from the UUG codon of *his4-301* mRNA, and hence suppress the *His*<sup>+</sup> phenotype restoring histidine auxotrophy in cells also expressing a *Sui*<sup>-</sup> allele (Figure 2.1).

In order to isolate novel *Ssu*<sup>-</sup> mutations in eIF2 $\gamma$ , we took advantage of the recessive lethality of a known *Sui*<sup>-</sup> allele. A glycine to arginine substitution at position 31 (G31R) of the eIF5 protein (encoded by the *SUI5* allele) is recessive lethal and displays a dominant *Sui*<sup>-</sup> phenotype (Figure 2.2)<sup>163</sup>. From a pool of randomly mutated *GCD11* alleles, we selected mutants that suppressed the inviability of cells expressing the *SUI5* allele as the sole source of eIF5. A selection scheme like this (rather than screening through mutants) allowed us to analyze a large pool of randomly mutated *GCD11* alleles. The majority of the mutations identified in this way localized to a discrete surface-exposed region in domain-III of eIF2 $\gamma$ . To further study this domain and to avoid isolating mutations in the G-domain that reduced initiation fidelity by merely altering the rate of GTP hydrolysis, we then used a library containing randomly mutated *GCD11* alleles corresponding to domains -II and -III to select for mutants that displayed a *His*<sup>+</sup>

phenotype by reducing the accuracy of start codon recognition and allowing for initiation of *his4-301* translation from a near-cognate UUG codon. Finally, we selectively mutated conserved surface-exposed residues in domain-III of eIF2 $\gamma$  by site-directed mutagenesis and screened for Sui<sup>-</sup> and Ssu<sup>-</sup> phenotypes.

This chapter explains how each class of mutations was isolated by employing the various strategies stated above. A genetic description of the isolated mutations is provided for each class. Since only three mutant alleles with a potential Sui<sup>-</sup> phenotype were identified by either the random selection procedure or by site-directed mutagenesis, this chapter only briefly describes some of the basic genetic characteristics of these mutants, and a more detailed genetic and biochemical analysis is presented in Chapter 3. Many mutations, however, with a potential Ssu<sup>-</sup> phenotype were identified either by selecting for the suppressors of *SUI5* recessive lethality from an array of randomly mutagenized *GCD11* alleles or by site-directed mutagenesis and screening for the same phenotype. Thus, it would not have been feasible to provide a comprehensive genetic and biochemical analysis of all the mutants. Therefore, a genetic characterization of these mutants is provided in this chapter, and the alleles with the most promising genetic phenotypes that were then selected for a thorough biochemical analysis are presented in Chapter 4.

## 2.2 Materials and Methods

Standard methods were used for culturing, transforming, plasmid shuffling, and construction of *S. cerevisiae* strains<sup>210-212</sup>. For yeast growth assays, cultures were grown to saturation, diluted to OD<sub>600</sub> of 1 or 0.5, and 5µl of 10X serial dilutions were spotted on the appropriate medium.

### 2.2.1 Yeast Strain Constructions

For a complete list of yeast strains see Table 2.1. Strain NAY13, lacking the chromosomal *GCD11* gene and harboring *GCD11* on a *URA3* plasmid, was constructed in multiple steps by deleting the *TRP1* gene in EY647 (note that *GCD11* is an essential gene in yeast. Thus, when the chromosomal copy of *GCD11* is deleted, an episomal WT allele is provided to the cell). Briefly, plasmid Ep293 was first replaced with Ep517 by transforming strain EY647 with Ep517 using the method of lithium acetate transformation<sup>210</sup>. NAY7 was then obtained by growing the resulting transformants on synthetic complete (SC) medium lacking leucine (SC-L), to select for the *LEU2*-containing plasmid Ep517, and 5-fluoroorotic acid (5-FOA), to select against the *URA3*-containing plasmid Ep293<sup>212</sup>. *TRP1* was then deleted by transforming NAY7 with the *trp1Δ::hisG::ura3* disruption fragment of plasmid pNJY1009 and growing the resulting transformants on 5-FOA-containing medium as described previously<sup>213</sup>. The resulting strain, NAY11, was then transformed with Ep293, and NAY13 was finally obtained by replacing the *LEU2*-containing plasmid Ep517 with Ep293, which carries the *URA3* marker. To achieve this plasmid replacement, NAY11 was transformed with Ep293 and a single colony transformant was grown in SC medium lacking uracil (SC-U), to select for Ep293, but containing leucine to allow for loss of the *LEU2*-containing plasmid

Ep517 across multiple generations. When the culture reached saturation, it was diluted in SC-U medium and grown to saturation again. Finally, it was diluted and spread on SC-U plates. Single colonies were isolated and the loss of Ep517 was established by confirming leucine auxotrophy. Deletion of the *TRP1* gene was confirmed by PCR analysis of genomic DNA and by confirming tryptophan auxotrophy in NAY13.

Strain NAY17 was generated by placing the *TIF5* gene, encoding the eIF5 protein, under the control of the GAL1 promoter in NAY13. This promoter replacement was achieved by the one-step PCR strategy<sup>214</sup> selecting for kanamycin resistance on SC medium containing galactose as carbon source (SCgal). Integration of the kanMX6- $P_{GAL1}$  cassette at the correct chromosomal locus was confirmed by PCR analysis of NAY17 genomic DNA using primers TIF5.F2 and TIF5.R2 (see Table 2.3 for the sequences of all primers used in this study). NAY17 was then transformed with a *TRP1* plasmid encoding the *SUI5* allele to generate NAY25, which was the final strain used in the selection process. NAY25 was confirmed to be inviable on glucose medium (where the expression of chromosomal  $P_{GAL1}$ -*TIF5* is shut off) and to display a His<sup>+</sup> phenotype (Figure 2.2).

Using a similar procedure explained above for NAY17, the *TIF11* gene (encoding the eIF1A protein) was placed under the control of the GAL1 promoter in NAY13 to create NAY74. Strains NAY115 and NAY117 were generated by transforming NAY13 with single copy (sc) *TRP1* plasmids containing the *SUI3-2* (p4280) and *SUI5* (p4281) alleles, respectively, using the standard lithium acetate procedure<sup>210</sup> and selecting for transformants on SC medium lacking uracil and tryptophan (SC-U-W).

To construct strain NAY66 with a myc-tagged *his4-301* allele, a fragment of *his4-301-myc<sub>10</sub>-kanMX6*, beginning from 207 bp upstream of the myc<sub>10</sub> coding sequence and ending 176 bp downstream of the *his4-301* stop codon, was amplified from strain JCY04 using primers CHA209 and CHA210. NAY13 was then transformed with the PCR product, and transformants were selected for resistance to kanamycin. The insertion of the fragment at the correct locus was confirmed by PCR analysis of NAY66 genomic DNA. To generate NAY64, a portion of the *HIS4* gene from 340 bp upstream to 437 bp downstream of the start ATG codon was amplified from the genomic DNA of WT strain H4 using primers PM-18 and PM-19. NAY66 was then transformed with the PCR product, and transformants were selected on SC-U medium lacking histidine (SC-U-H). The replacement of *his4-301-myc<sub>10</sub>-kanMX6* with *HIS4-myc<sub>10</sub>-kanMX6* was then verified by PCR analysis of NAY64 genomic DNA.

### 2.2.2 Plasmid Constructions

For a complete list of plasmids see Table 2.2. Plasmid pNA4 (encoding WT eIF2 $\gamma$  tagged with the His<sub>8</sub> epitope at its N-terminus) was generated in two steps by i) creating a NcoI restriction site at the 3' end of the *GCD11* coding sequence in pC2872, and ii) removing the first internal KpnI restriction site, both without altering the amino acid sequences and using the QuickChange Site-Directed Mutagenesis kit (Agilent Technologies) following the manufacturer's protocol and primer sets g\_NcoI.F1/g\_NcoI.R1 and g\_KpnI.F1/g\_KpnI.R1, respectively. pNA4 was verified by DNA sequence analysis of the region encompassing the *GCD11* coding sequence. pNA18 was created by ligating a 2kb *GCD11* HindIII fragment isolated from Ep293 at the HindIII site of YCplac22 to generate a sc *TRPI* plasmid encoding the WT *GCD11*

allele. Insertion was confirmed by DNA sequencing. To create a high copy (hc) *TRP1* plasmid encoding eIF1, a 1.6kb HindIII-SacI fragment containing *SUI1* isolated from pCFB04 was inserted between the HindIII and SacI sites of plasmid YEplac122 to create pNA19. The insertion was confirmed by DNA sequencing. pNA20 was created by first amplifying a 788 bp fragment surrounding the *IMT4* gene (encoding tRNA<sub>i</sub><sup>Met</sup>) from yeast genomic DNA using primers IMT4\_HindIII.F1 and IMT4-HindIII.R1. The PCR product was then digested and inserted at the HindIII site of YEplac122. Insertion was confirmed by sequencing the plasmid DNA surrounding the HindIII sites. To create a hc plasmid co-expressing all the four genes encoding the components of the WT TC (*GCD11-His<sub>8</sub>*, *SUI3*, *SUI2*, and *IMT4*), the SacI-SbfI fragment of pAV1732 was replaced by the 2.57 kb SacI-SbfI *GCD11-His<sub>8</sub>* fragment from pNA4 to generate plasmid pNA21. pNA23, pNA24, and pNA25 were made by replacing the 2.57 kb SacI-SbfI fragment of pNA21 (containing WT *GCD11-His<sub>8</sub>*) with the SacI-SbfI fragments from pNA4-E460K, pNA4-R503A, and pNA4-R504A that contain mutant *gcd11-His<sub>8</sub>* alleles. The plasmids were verified by DNA sequence analysis of the *GCD11*, *SUI2*, and *SUI3* genes.

### 2.2.3 Biochemical Assays with Yeast Extracts

For Western blot analysis, exponentially growing yeast cells (OD<sub>600</sub> of ~0.5) were harvested by centrifugation and whole cells extracts (WCEs) were prepared by trichloroacetic acid (TCA) extraction method as previously described<sup>215</sup>. Immunoblotting was performed using antibodies against the His<sub>6</sub> epitope (abcam), eIF2 $\alpha$ <sup>216</sup>, eIF2B $\epsilon$ /Gcd6<sup>217</sup>, eIF1<sup>81</sup>, and Myc epitope (Sigma) as described.  $\beta$ -galactosidase assays with yeast WCEs obtained from exponentially growing cells (OD<sub>600</sub> of ~0.5) were performed as described previously<sup>218</sup>.

## 2.3 Results

### 2.3.1 Generation of Libraries of Randomly Mutated *GCD11* alleles

We employed the error-prone PCR technique<sup>219</sup> to generate libraries of random mutations in the open reading frame (ORF) of *GCD11*. The mutant libraries were generated in a sc *LEU2* plasmid containing N-terminally His<sub>8</sub>-tagged *GCD11* under its endogenous promoter and terminator sequences (plasmid pNA4)(Figure 2.3). Due to the large size of the *GCD11* coding region, it was divided into two overlapping segments, and two pools of randomly mutated alleles were generated using the GeneMorph II Random Mutagenesis kit (Agilent Technologies) following the manufacturer's protocol. pNA4 plasmid DNA was used as template. The first library (L1), covering the first half of *GCD11* (codons 1-306, which encompass the G-domain), was generated using primers GCD11\_L1.F1 and GCD11\_L1.R1. The second library (L2), covering the second half of *GCD11* (codons 251 to 527, which encompass the last 59 amino acids in the G-domain and the entirety of domains -II and -III), was created using the GCD11\_L2.F1/GCD11\_L2.R1 primer set (Figure 2.3). The resulting PCR fragments were digested with BamHI and KpnI (for the L1 library) and KpnI and NcoI (for the L2 library) and inserted back into pNA4 to generate two pools of randomly mutated *GCD11* plasmids. DNA from 171,000 bacterial transformants was pooled. To analyze the quality of the libraries, a random sample of at least 30 plasmids from each library was selected and their respective *GCD11* coding region was subjected to DNA sequencing. The frequency of mutations in *GCD11* was 72.4% and 86.4% in L1 and L2, respectively. Table 2.4 displays the frequency and type of mutations generated in each library.

### 2.3.2 Identification of *GCD11* Mutants that Suppress the Recessive Lethality of *SUI5*

In order to identify substitutions in eIF2 $\gamma$  that suppress the recessive lethality of *SUI5*, libraries of yeast strains containing random *GCD11* mutant alleles were first generated by transforming strain NAY25 (*gcd11 $\Delta$* , *P<sub>GAL1</sub>-TIF5*, *sc TRP1 SUI5*) with the L1 and L2 libraries. Transformants were plated on SCgal medium lacking leucine, uracil, and tryptophan (SCgal-L-U-W) to allow for the expression of WT *TIF5* and to select for the *URA3*, *LEU2*, and *TRP1* plasmids harboring WT *GCD11*, mutant *GCD11* alleles, and *SUI5*, respectively. Around 1,000,000 transformants were then pooled, diluted, and spread on SC medium lacking leucine and tryptophan (SC-L-W) with glucose as carbon source, to shut off the expression of WT *TIF5*, and containing 5-FOA, to select for loss of the *URA3*-containing WT *GCD11* plasmid. The transformants that could survive with *SUI5* as the sole source of eIF5 being expressed were then isolated and streaked on SCgal-L-U-W medium to purify single colonies for further analysis. The resident plasmids were rescued and reintroduced back into NAY25 to verify that their ability to suppress the recessive lethality of *SUI5* is indeed linked to the *GCD11* mutant plasmids. The corresponding *GCD11* mutations were identified by sequencing the region of the plasmid DNA corresponding to the *GCD11* coding sequence. For a schematic description of the selection process see Figure 2.4.

Using the above selection scheme, numerous mutations were isolated in *GCD11* that suppressed the recessive lethality conferred by the *SUI5* allele (Table 2.5 and Figure 2.5). Although some of the mutant plasmids isolated contained multiple missense mutations in *GCD11*, many of the point mutations such as those generating substitutions at asparagine 433 to glutamic acid or lysine (N433D/K), methionine at position 482 to



lysine or isoleucine (M482K/I), aspartic acid at 481 to glutamic acid or histidine (D481E/H), and leucine at position 423 to methionine (L423M) were isolated from more than one independent colony (i.e. they were recovered from multiple independent mutant plasmids). Seven of the mutant alleles that contained the above substitutions and showed the strongest phenotype in suppressing the inviability of cells harboring *SUI5* as the sole source of eIF5 were selected for further analysis; these mutant alleles included *M482K*, *F297S/D481E*, *M482K/T488M*, *M482I*, *E341K*, *L423M/D481H*, and *N433D*. We further confirmed that single substitutions at positions 481 (D481A/E) and 423 (L423M) suppress the recessive lethality of *SUI5* by generating the indicated mutations in plasmid pNA4 using the QuickChange Site-Directed Mutagenesis kit (Agilent Technologies) following the manufacturer's protocol (Figure 2.5B). In order to examine the extent to which these alleles restore growth to cells harboring *SUI5* as the sole source of eIF5 being expressed, strains with the above *GCD11* mutant alleles and episomal *SUI5* were streaked on SC-L-W medium to monitor their colony sizes (note that the expression of *P<sub>GALI</sub>-TIF5* is shut off since glucose is the carbon source). Among these alleles, there is a range by which the mutations restore growth to cells harboring *SUI5* as the sole source of eIF5, with *M482K* and *L423M/D481H* displaying smaller colony sizes compared to the *F297S/D481E*, *M482K/T488M*, *M482I*, and *N433D* mutants (Figure 2.6)

To determine if the above mutants, which suppress the recessive lethality of *SUI5*, also suppress its slow growth (Slg<sup>-</sup>) phenotype, cells harboring the various *GCD11* alleles and episomal *SUI5* were spotted on SC-L-W medium to establish their growth phenotypes. In these strains, where the chromosomal *TIF5* gene is expressed in single copy from its endogenous promoter, the *SUI5* allele confers a dominant Slg<sup>-</sup> phenotype

(Figure 2.7, compare the first and second rows on the +His medium). Even though the isolated mutations in *GCD11* restore growth to cells harboring the *SUI5* allele as the sole source of eIF5 to different extents (Figure 2.6), they all suppress its dominant  $\text{Slg}^-$  phenotype. This is apparent as the transformants with the mutant alleles of *GCD11* and *SUI5* grow similarly to the strain harboring WT *GCD11* and lacking the episomal *SUI5* allele (Figure 2.7, compare the rows on the +His medium).

As these *GCD11* mutants suppressed the recessive lethality and  $\text{Slg}^-$  phenotypes of *SUI5*, we next assayed for their ability to suppress the  $\text{His}^+$  phenotype of *SUI5* by blocking initiation from the UUG codon of the *his4-301* allele. As elucidated earlier, *SUI5* reduces the fidelity of start codon recognition and allows for translation initiation from a near-cognate UUG codon of *his4-301*, consequently conferring a  $\text{His}^+$  phenotype<sup>163</sup> (Figure 2.7, compare the first and second rows on the -His medium). Strains harboring the WT or *GCD11* mutant alleles and expressing episomal *SUI5* were spotted on SC-L-W medium supplemented with either 0.3 mM (+His) or 0.003 mM (-His) histidine (note that in these strains the chromosomal copy of *TIF5* is expressed from its endogenous promoter, and hence cells carrying a sc *TRP1 SUI5* plasmid are viable on glucose medium). Isolated *GCD11* mutants exhibit various strengths in suppressing the dominant  $\text{His}^+$  phenotype of *SUI5*, with the *F297/D481E*, *M482K/T488M*, *M482I*, and *N433D* alleles fully suppressing, *M482K* partially suppressing, *E341K* very weakly suppressing, and the *L423/D481H* allele failing to suppress the  $\text{His}^+$  phenotype as indicated by the inability of the double mutants to grow on the -His medium (Figure 2.7).

In order to determine how universal the isolated *GCD11* mutations are in blocking the initiation of *his4-301* translation from a UUG codon, their ability to suppress the  $\text{His}^+$

phenotype of *Sui*<sup>-</sup> mutations in other initiation factors was assayed. A tyrosine substitution of the serine residue at position 264 of eIF2 $\beta$  (encoded by the *SUI3-2* allele) reduces the stringency of start codon recognition and suppresses the histidine auxotrophy of cells harboring the *his4-301* allele, hence conferring a His<sup>+</sup> phenotype<sup>163</sup> (Figure 2.8, compare the first and second rows on the -His medium). The *GCD11* mutants follow a similar pattern in suppressing the dominant His<sup>+</sup> phenotype of *SUI3-2*, with the *F297S/D481E*, *M482K/T488M*, *M482I*, and *N433D* alleles fully suppressing, *M482K* partially suppressing, *E341K* very weakly suppressing, and the *L423M/D481H* allele failing to suppress the His<sup>+</sup> phenotype as indicated by the inability of the double mutants to grow on the -His medium (Figure 2.8).

While the *GCD11* mutants display a similar behavior in suppressing the His<sup>+</sup> phenotypes of *SUI5* and *SUI3-2*, they fail to do so in the *tif11-SE1\*SE2\*F131* mutant (Figure 2.37A). *tif11-SE1\*SE2\*F131* is a *Sui*<sup>-</sup> allele of the gene encoding the eIF1A protein<sup>105</sup>. Since the phenotypes associated with *tif11-SE1\*SE2\*F131* are recessive, *M482I*, *E431K*, *N433D*, *M482I/E431K*, and *M482I/N433D* mutant alleles of *GCD11* where introduced into a strain where the chromosomal *TIF11* gene is under the control of the *GAL1* promoter (*P<sub>GAL1</sub>-TIF11*) and *tif11-SE1\*SE2\*F131* is expressed from a sc *TRP1* plasmid. *tif11-SE1\*SE2\*F131* allows for translation initiation from the UUG codon of *his4-301*, consequently conferring a His<sup>+</sup> phenotype<sup>105</sup> (Figure 2.37A compare the first and second rows on the -His medium). The *M482I*, *E431K*, *N433D*, *M482I/E431K*, and *M482I/N433D* mutants all fail to suppress this His<sup>+</sup> phenotype as double mutants harboring the indicated *GCD11* alleles and *tif11-SE1\*SE2\*F131* grow on the -His medium (Figure 2.37A, compare the first seven rows). The indicated *GCD11* mutants

also fail to suppress the Slg<sup>-</sup> and the temperature sensitivity (TS<sup>-</sup>) phenotypes associated with *tif11-SE1\*SE2\*F131* (Figure 2.37B, compare the first seven rows on the +His medium). Therefore, the isolated *GCD11* mutants do not *universally* suppress the phenotypes associated with Sui<sup>-</sup> mutations in different initiation factors. This finding suggests that the identified mutations suppress a specific defect (or a set of defects) in the process of translation initiation associated with particular Sui<sup>-</sup> mutations.

To confirm that the mutant alleles of *GCD11* suppress the His<sup>+</sup>/Sui<sup>-</sup> phenotypes of *SUI3-2* by restoring the fidelity of start codon recognition and blocking translation initiation from the UUG codon of *his4-301*, the ratio of initiation from a UUG codon to that from an AUG was assayed in vivo using the appropriate reporter genes. The WT *HIS4* and *his4-301* alleles were chromosomally tagged with the myc<sub>10</sub> epitope in isogenic strains. The expression level of *his4-301-myc<sub>10</sub>* (UUG) and His4-myc<sub>10</sub> (AUG) proteins in strains harboring episomal *SUI3-2* and the various *GCD11* mutants were then measured by Western blot analysis, and the ratios of the *his4-301-myc<sub>10</sub>* protein to that of the His4-myc<sub>10</sub> were calculated (UUG/AUG ratio). In WT yeast cells, there is very inefficient translation initiation from a UUG codon as indicated by the low expression level of the *his4-301-myc<sub>10</sub>* protein compared to His4-myc<sub>10</sub> (Figure 2.9B, compare lanes 1 and 2 in the top panel to that of the bottom). Therefore, the ratio of UUG to AUG initiation is very low in WT cells (Figure 2.9C). In cells harboring the *SUI3-2* allele, where the fidelity of start codon recognition is reduced, however, the amount of translation initiation from a UUG codon is increased significantly (Figure 2.9B, compare lanes 1 and 2 to lanes 3 and 4) leading to an elevated UUG/AUG ratio as compared to the WT cells (Figure 2.9C). Consistent with suppressing the His<sup>+</sup> phenotype of *SUI3-2*, the

*M482K*, *F297S/D481E*, *M482K/T488M*, *M482I*, *E341K*, *L423M/D481H*, and *N433D* mutant alleles of *GCD11* restore the fidelity of start codon recognition as indicated by their ability to lower the expression level of the his4-301-myc<sub>10</sub> protein in cells harboring the *SUI3-2* allele (Figure 2.9B) and to partially suppress the elevated ratio of UUG to AUG initiation (Figure 2.9C). Thus, the isolated mutations in *GCD11* display a bona fide Ssu<sup>-</sup> phenotype by restoring the fidelity of start codon recognition in vivo as indicated by their ability to lower the ratio of UUG to AUG initiation in cells expressing the *SUI3-2* allele.

It has been illustrated that *SUI3-2* confers a Gcd<sup>-</sup> phenotype in addition to its Sui<sup>-</sup> and His<sup>+</sup> phenotypes<sup>220</sup>. As elucidated in Section 1.2.3, translation of the *GCN4* mRNA can serve as a genetic reporter for monitoring the stability and the loading of the ternary complex to the PIC. In nutrient-replete conditions, translation of *GCN4* mRNA is repressed. A reduction in TC stability or binding to the 40S subunit, however, leads to the derepression of *GCN4* expression even in nutrient-replete conditions (this is called a Gcd<sup>-</sup>, General control derepressed, phenotype) (Figure 2.10A)<sup>206,220</sup>. To examine if the mutant alleles of *GCD11*, which suppress the His<sup>+</sup> and Sui<sup>-</sup> phenotypes of *SUI3-2*, can also suppress the Gcd<sup>-</sup> phenotype conferred by *SUI3-2*, the expression of a *GCN4-lacZ* reporter was measured in strains harboring the various *GCD11* alleles and episomal *SUI3-2*. In WT cells, when plenty of nutrients are available in the medium, there is low basal translation of the *GCN4-lacZ* reporter. Cells harboring the *SUI3-2* allele, however, confer a Gcd<sup>-</sup> phenotype, derepressing the expression of the *GCN4-lacZ* reporter by a factor of ~2.8-fold (Figure 2.10B). The *M482I*, *E431K*, *N344D*, *M482I/E431K*, and *M482I/N433D* alleles of *GCD11* partially suppress this elevated expression of the *GCN4-*

*lacZ* reporter in cells harboring *SUI3-2*, reducing the derepression ratio to values  $\leq 1.7$  (Figure 2.10B).

Similar to *SUI3-2*, the *SUI5* allele also confers a Gcd<sup>-</sup> phenotype. Thus, in order to determine if the *GCD11* mutants, which suppress the recessive lethality, Slg<sup>-</sup>, and His<sup>+</sup> phenotypes of *SUI5*, can also suppress its Gcd<sup>-</sup> phenotype, expression of the *GCN4-lacZ* reporter was measured in cells harboring the various *GCD11* alleles and episomal *SUI5* cultured in SCgal-L-W medium, where WT eIF5 is expressed from the chromosomal *P<sub>GALI</sub>-TIF5*. As in the case of *SUI3-2*, *GCD11* mutants partially suppress the Gcd<sup>-</sup> phenotype conferred by *SUI5* (Figure 2.10C). *SUI5* allele results in a ~2-fold derepression of the *GCN4-lacZ* expression under non-starvation conditions, and the *GCD11* mutants suppress the derepression ratio to values  $\leq 1.4$  (Figure 2.10C).

It has been reported that the *tif11-SE1\*SE2\*F131* Sui<sup>-</sup> allele also derepresses the expression of *GCN4-lacZ* under nutrient-replete conditions, conferring a Gcd<sup>-</sup> phenotype<sup>105</sup> (Figure 2.37C). To determine if the mutants of *GCD11* suppress the Gcd<sup>-</sup> phenotype conferred by *tif11-SE1\*SE2\*F131*, as they do that conferred by *SUI3-2* and *SUI5*, expression of the *GCN4-lacZ* reporter was measured in cells harboring the various *GCD11* alleles and episomal *tif11-SE1\*SE2\*F131* cultured in SC-L-W medium (note that in the glucose medium expression of the chromosomal *P<sub>GALI</sub>-TIF11* is shut off). Surprisingly, the isolated *GCD11* mutants not only do not suppress, but even seem to increase the Gcd<sup>-</sup> phenotype of the *tif11-SE1\*SE2\*F131* Sui<sup>-</sup> allele (Figure 2.37C). Whereas *E431K* and *E431K/M482I* have no effect, *M482I*, *N433D*, and *N433D/M484I* further increase expression of the *GCN4-lacZ* reporter by ~2.4-fold in cells harboring *tif11-SE1\*SE2\*F131* under non-starvation conditions (Figure 2.37C). This increase in

the Gcd<sup>-</sup> phenotype of *tif11-SE1\*SE2\*F131* is not due to an intrinsic Gcd<sup>-</sup> phenotype of the *GCD11* mutants, as shown next.

The isolated *GCD11* mutants do not derepress the expression of the *GCN4-lacZ* reporter in otherwise WT cells under nutrient-replete conditions (Figure 2.11A). This observation suggests that the indicated substitutions in eIF2 $\gamma$  do not alter the stability of the ternary complex, for example by causing the misfolding of the protein, since a defect in TC formation would generally manifest itself as a Gcd<sup>-</sup> phenotype<sup>206</sup>. In fact, *GCD11* mutants display a mild Gcn<sup>-</sup> (General control non-inducible) phenotype by failing to induce the expression of the *GCN4-lacZ* reporter even in nutrient-starvation conditions (Figure 2.11B). The Gcn<sup>-</sup> phenotype conferred by the *GCD11* mutant alleles is consistent with their suppression of the *SUI3-2* and *SUI5* Gcd<sup>-</sup> phenotypes. Multiple defects can lead to a Gcn<sup>-</sup> phenotype (see Hinnebusch 2005<sup>206</sup> for review). One such defect is reduced AUG recognition, which reveals itself as the leaky scanning phenotype<sup>221</sup>. A construct with an elongated upstream ORF1 (el-uORF1) in-frame with and overlapping the AUG start codon of the *GCN4-lacZ* allele is used as a genetic reporter for leaky scanning (Figure 2.12A). In WT cells, there is low basal translation of the *GCN4-lacZ* fusion reporter since most ribosomes translate exclusively from the AUG codon of el-uORF1. In mutants that have a defect in AUG recognition, however, a greater proportion of ribosomes bypasses the AUG codon of el-uORF1 and instead initiate downstream at the AUG codon of *GCN4-lacZ*. Thus, translation of *GCN4-lacZ* increases in a mutant that displays leaky scanning. The *GCD11* mutants exhibit a mild leaky scanning phenotype as they result in a weak, but significant, increase in the expression of the *GCN4-lacZ* fusion reporter (Figure 2.12A). The Gcn<sup>-</sup> phenotype of the *GCD11* mutant

alleles, however, cannot not be fully explained by reduced AUG recognition since the increase in leaky scanning is very mild, ~1.5-fold (Figure 2.12). Nonetheless, an increase in leaky scanning is expected if the *Ssu*<sup>-</sup> mutants restore initiation fidelity by destabilizing the closed conformation since by making the process of start codon recognition more stringent, AUG recognition would also decrease to some small extent.

To determine if the isolated *GCD11* mutants exhibit any growth defects or TS<sup>-</sup> phenotypes, cells harboring the various *GCD11* alleles were cultured in SC-L medium and the growth phenotypes were monitored by spot assays. None of the various *GCD11* alleles confer any growth defects or TS<sup>-</sup> phenotypes in otherwise WT cells (Figure 2.13A). Moreover, the mutations do not alter the level of the eIF2 $\gamma$  protein (Figure 2.13B). Thus, their phenotypes cannot be attributed to altered protein expression.

As discussed in Section 1.2.1, the  $\gamma$  subunit is the core of the eIF2 complex and provides the binding sites for GTP and Met-tRNA<sub>i</sub> (Figure 1.4). It is composed of three domains: G-domain, which binds to GTP and Met-tRNA<sub>i</sub> and contains the binding platform for the  $\beta$  subunit, domain-II, which is involved in Met-tRNA<sub>i</sub> binding and also provides the binding interface with the  $\alpha$  subunit, and domain-III, which remains mainly uncharacterized. Interestingly, the majority of mutations we isolated encode substitutions corresponding to residues in domain-III of eIF2 $\gamma$ . In order to determine the position of these mutations on the three-dimensional structure of the eIF2 complex, we took advantage of an X-ray crystal structure of the archeon *S. solfataricus* aIF2 in complex with GDP (PDB 2QMU)<sup>116</sup>. As elucidated in Section 1.2.1, this structure, which is used through the remainder of this study, contains the full  $\beta$  and  $\gamma$  but only domain-III of the  $\alpha$  subunit ( $\alpha 3\beta\gamma$ ). Remarkably, the *Ssu*<sup>-</sup> mutations localize to a discrete surface-exposed



area in domain-III of eIF2 $\gamma$  (Figure 2.14A). The area that contains the mutations is distant from the interface of domain-III with the other two domains (G-domain and domain-II) and from the interface between  $\gamma$  and the  $\alpha$  and  $\beta$  subunits. Moreover, it is located on the opposite surface of eIF2 $\gamma$  from that containing the GTP and Met-tRNA<sub>i</sub> binding sites (Figure 2.14A). Unfortunately, a crystal structure of the eukaryotic 40S subunit in complex with TC is not available. Recently, however, directed hydroxyl radical probing experiments were performed to map the binding of *S. cerevisiae* eIF2 on the 40S ribosomal subunit and on Met-tRNA<sub>i</sub><sup>127</sup>. As elucidated in Chapter 1, these experiments identified domain-III of eIF2 $\gamma$  and helix 44 (h44) of the 18S rRNA as a key binding interface between the eIF2 complex and the 40S subunit. Remarkably, the cluster of *GCD11* Ssu<sup>-</sup> mutants maps to a surface-exposed region of domain-III that is proposed to be in proximity of h44 of the 40S subunit (Figure 2.14B). This raises the intriguing possibility that our Ssu<sup>-</sup> mutations act by altering the physical interactions between the TC and the 40S subunit.

### 2.3.3 Isolation of Mutations in *GCD11* that Reduce Initiation Fidelity

In order to isolate mutations that lower the stringency of start codon recognition, we took advantage of the *his4-301* allele and selected for substitutions in eIF2 $\gamma$  that conferred a His<sup>+</sup> phenotype by allowing the initiation of *his4-301* translation from a UUG codon. To avoid isolating mutants that reduced the initiation fidelity by merely increasing the rate of GTP hydrolysis, we avoided the G-domain and only screened the L2 library that contains randomly generated mutations in domains -II and -III of *GCD11* on a *LEU2* plasmid. To isolate mutant alleles conferring a His<sup>+</sup> phenotype, a pool of yeast strains containing randomly mutated domains -II and -III was first created by

introducing the L2 library into strain NAY13 (*gcd11Δ, his4-301, sc URA3 GCD11*) and selecting for transformants on SC-L-U medium to maintain both plasmids. The transformants were then pooled, diluted, and spread on SC-L medium containing 5-FOA to select for loss of the *URA3*-containing WT *GCD11* plasmid. Around 250 million colonies were subsequently pooled, diluted, and spread on SC-L medium either lacking or supplemented with 0.006 mM or 0.015 mM histidine (0.2% and 0.5% of normal concentration of histidine in SC medium, respectively). The three different concentrations of histidine (0, 0.006 mM, and 0.015 mM) were chosen so that mutants with a range of His<sup>+</sup> phenotypes could be selected. Different Sui<sup>-</sup> mutants display various strengths in their His<sup>+</sup> phenotypes, and a Sui<sup>-</sup> mutation with a weak phenotype may be unable to grow on medium completely lacking histidine as compared to one supplemented with 0.2% or 0.5% of the normal histidine level. Transformants able to grow on medium lacking abundant histidine (His<sup>+</sup> phenotype) were isolated and streaked on SC-L medium to purify single colonies. The resident plasmids were rescued and reintroduced into NAY13 to verify that their His<sup>+</sup> phenotypes are conferred by the mutant *GCD11* plasmids. The corresponding *GCD11* mutations were subsequently identified by sequencing the plasmid DNA corresponding to the coding region of *GCD11*. For a schematic diagram of the selection procedure see Figure 2.15.

Two point mutations were identified through this selection process (Figure 2.16). 55% of the recovered mutant plasmids encoded a substitution in the arginine residue at position 510 (R510) and 7% encoded a glycine to cysteine change in residue 418 (G418C). The frequency of mutants with a His<sup>+</sup> phenotype in the initial screen was 0.002%. Both *gcd11-R510H* and *gcd11-G418C* alleles were recovered with similar

frequencies from media with the different concentrations of histidine (0, 0.006 mM, and 0.015 mM). Cells harboring the *G418C* allele are slow growing yet they exhibit a stronger His<sup>+</sup> phenotype compared to those expressing the *R510H* allele (Figure 2.16). Interestingly, *R510H* was previously identified as a Gcd<sup>-</sup> mutant in a screen for spontaneous revertants of the Gcn<sup>-</sup> phenotype of *gcn2-101 gcn3-101* double mutant<sup>222</sup> and was later shown to also display Sui<sup>-</sup> and His<sup>+</sup> phenotypes by elevating the ratio of UUG to AUG initiation<sup>223</sup>. This suggests that the selection procedure here worked well to isolate mutations with the desired phenotype.

Residue R510 is extremely well conserved in eIF2 $\gamma$  from various organisms. In a multiple sequence alignment of thirty nine different eukaryotic and archaeal e/aIF2 $\gamma$  proteins, the residue corresponding to R510 in yeast eIF2 $\gamma$  is always an arginine (Figure 2.17). In fact, the region surrounding residue R510, which contains the sequence motif W<sub>509</sub>R<sub>510</sub>L<sub>511</sub>I<sub>512</sub>G<sub>513</sub> encompassing the last  $\beta$ -strand of domain-III, is identical in all organisms analyzed (Figure 2.17). R510 is partially exposed on the surface of the  $\gamma$  subunit and is positioned at the interface of domain-III with the G-domain on the same face of the protein that binds to GTP and Met-tRNA<sub>i</sub> (Figure 2.18A). The side chain of R510, however, is pointing inside the protein toward the G-domain and is only 2.6Å away from the side chain of residue D198 in the switch-II region of the G-domain (Figure 2.18B). Switch-II is one of the key structural elements of all GTP binding proteins (see section 1.2.1). It has been widely documented that it is the structural rearrangements among the switch-I, switch-II, and P-loop regions, universal in all GTP binding proteins, that lead to GTP hydrolysis<sup>116,128,224,225</sup>. R510 might be involved in the structural arrangements of the G-domain by forming a salt bridge with residue D198 of switch-II.

If so, then the R510H substitution may alter the rate of GTP hydrolysis and/or P<sub>i</sub> release by modifying the interactions between switch-II and domain-III, hence leading to loss of initiation fidelity. It is also possible that by altering the physical interactions between switch-II and domain-III, *R510H* indirectly alters the binding of the Met-tRNA<sub>i</sub> to eIF2 $\gamma$  without altering the rate of GTP hydrolysis and P<sub>i</sub> release since, as discussed in section 1.2.2, the structural arrangements of the switch elements in the G-domain also impact Met-tRNA<sub>i</sub> binding. Yet, it is also possible that *R510H* reduces the affinity or alters the mode of eIF2 binding to the 40S subunit as R510 is located in proximity of the proposed interface between eIF2 and the 40S subunit<sup>127</sup>. This possibility, however, seems less likely because its side chain projects inside the G-domain as explained above (Figure 2.18C).

Interestingly, residue G418 is also located in domain-III and is highly conserved among both eukaryotic and archaeal e/aIF2 $\gamma$  proteins (Figure 2.19). It is in the first  $\beta$ -strand ( $\beta$ 1) of domain-III that projects into the  $\beta$ -barrel structure of domain-II (Figure 2.20A). The three eIF2 $\gamma$  domains are largely autonomous, and this represents the only instance where one domain projects into a neighboring one (Figure 2.20A). The three-dimensional environment of G418 is also conserved. It is surrounded on both sides by strands  $\beta$ 1 and  $\beta$ 3 of domain-II, and its neighboring residues in  $\beta$ 1 include several hydrophobic amino acids that are conserved among different organisms (Figure 2.19 and Figure 2.20A).

In order to examine if other residues in  $\beta$ 1 of domain-III besides G418 are also involved in maintaining the fidelity of start codon recognition, we examined if substitutions at nearby residues Q415, V416, and V417 confer a His<sup>+</sup> phenotype.

Contrary to *G418C*, however, *Q415L*, *V416A*, and *V417L* mutants do not display a His<sup>+</sup> phenotype (Figure 2.21B). We also tested if these mutations confer any growth defects. Cells harboring the above *GCD11* alleles were cultured in the SC-L medium, and their growth phenotypes were examined by spot assays at different temperatures. While *G418C* confers a marked Slg<sup>-</sup> and cold sensitivity (Cs<sup>-</sup>) phenotypes, the *Q415L*, *V416A*, and *V417L* mutant alleles behave like WT *GCD11* in the growth assays (Figure 2.21A).

Residue G418 is not surface-exposed and lacks a side chain with a functional group that may interact with other proteins on the surface of eIF2 $\gamma$  (Figure 2.20A). Therefore, it is unlikely that the phenotypes of the *G418C* allele are a direct result of loss of interactions between eIF2 $\gamma$  and other potential binding proteins. Moreover, it is positioned distant from the proposed binding interface of eIF2 and the 40S subunit (Figure 2.22A). Thus, it also seems unlikely that the phenotypes of *G418C* are a consequence of altered eIF2 binding to the 40S subunit. Domain-II of eIF2 $\gamma$  is thought to be involved in binding the Met-tRNA<sub>i</sub> as well as the  $\alpha$  subunit (see section 1.2.1)<sup>1,113,116,127,138</sup>. Due to its position in  $\beta$ 1 of domain-III, which is inserted inside the  $\beta$ -barrel structure of domain-II, it is possible that the G418C substitution leads to structural rearrangements of domain-II that may affect GTP hydrolysis, Met-tRNA<sub>i</sub> binding, or interactions with the  $\alpha$  subunit as a glycine to cysteine substitution introduces a side chain where none normally exists (Figure 2.22B).

#### *2.3.4 Identification of Mutations in GCD11 that Alter Initiation Fidelity by Site-Directed Mutagenesis*

Since the majority of the mutations we isolated by using the libraries of randomly generated *GCD11* alleles localized to domain-III, we decided to study this domain in

more detail by mutating its remaining conserved surface-exposed residues and examining the mutations for Sui<sup>-</sup> and Ssu<sup>-</sup> phenotypes. Conserved residues in domain-III that are on the surface of eIF2 $\gamma$  were mutated to alanine (A) and, when relevant, to a residue of the opposite charge (glutamic or aspartic acid residues were mutated to alanine and lysine, and arginine or lysine residues were mutated to alanine and glutamic acid) (Figure 2.23 and Figure 2.24). Site-directed mutagenesis was performed with the QuickChange Site-Directed Mutagenesis kit (Agilent Technologies) following the manufacturer's protocol and using primers listed in Table 2.3. Plasmid pNA4 was used as the DNA template. Twenty four mutant alleles were generated by this method, listed in Table 2.6.

The mutant plasmids were introduced into strain NAY13 (*gcd11 $\Delta$ , his4-301, scURA3 GCD11*), and the transformants were streaked on SC-L+FOA medium to select for loss of the *URA3*-containing WT *GCD11* plasmid. Among the mutant alleles created, only those altering the residues E460, R503, and R504 conferred growth defects. Mutant alleles encoding alanine and glutamic acid substitutions of arginine residues at positions 503 and 504 (R503A/E and R504A/E) were recessive lethal (Figure 2.31A). Lysine substitution at position E460 led to a severe Slg<sup>-</sup> phenotype (Figure 2.33A) and an alanine substitution conferred a TS<sup>-</sup>, but not a Slg<sup>-</sup>, phenotype (Figure 2.25A). The temperature sensitivity is unlikely to be a result of unstable mutant eIF2 $\gamma$  protein since Western blot analysis illustrated that even after culturing the cells for 4.4 generations at 37°C, there is no change in the level of *E460A* mutant protein compared to the WT *GCD11* product (Figure 2.25C). The remaining mutations did not confer any growth defects or TS<sup>-</sup> phenotypes (Figure 2.25A) and also did not alter the level of eIF2 $\gamma$  protein (Figure 2.25B).

The mutant alleles were then assayed for their ability to reduce the stringency of start codon recognition by allowing the initiation of *his4-301* translation from a UUG codon, consequently conferring a His<sup>+</sup> phenotype. Strains harboring either the WT or mutant *GCD11* alleles were cultured in SC-L and spotted on medium containing either 0.3mM (+His) or 0.003 mM (-His) histidine to test for suppression of the histidine auxotrophy conferred by the *his4-301* allele. Among all the mutants created, *E460A* presented a clear, albeit weak, His<sup>+</sup> phenotype (Figure 2.26).

In order to examine if any of these *GCD11* mutant alleles reduce the stability of the TC or its binding to the 40S subunit, expression of the *GCN4-lacZ* reporter was measured under nutrient-replete conditions. Among all of the mutant alleles, only *E460A* confers a Gcd<sup>-</sup> phenotype, derepressing expression of the *GCN4-lacZ* reporter by ~7-fold (Figure 2.27). The residue E460 is located on the surface of domain-III on the same face of eIF2 $\gamma$  that contains the binding sites for GTP and Met-tRNA<sub>i</sub> (Figure 2.28A). Remarkably, E460 is positioned in proximity of the proposed binding interface between eIF2 and the 40S subunit (Figure 2.28B). This raises the intriguing possibility that the E460A substitution may alter the affinity or the mode of eIF2 binding to h44 of the 40S subunit, which consequently confers its His<sup>+</sup> and Gcd<sup>-</sup> phenotypes.

E460 is immediately adjacent to residues R503 and R504 in the three-dimensional structure of eIF2 (Figure 2.29A-B). In fact, it is possible that a salt bridge is formed between the side chains of E460 and R503 as they are separated by only 2.9Å (Figure 2.29C). As stated above, both alanine and glutamic acid substitutions at R503 as well as R504 are recessive lethal (Figure 2.31A). Furthermore, the E460K substitution is also extremely slow growing (Figure 2.33A). In order to confirm that the recessive lethality

of the R503/R504 substitutions is not due to reduced expression of the mutant proteins, we performed Western blot analysis and used an antibody against the His<sub>6</sub> epitope (abcam) in strains where the untagged WT *GCD11* was supplied on a sc *URA3* plasmid and the tagged mutant alleles were on a sc *LEU* vector. This analysis indicated that the level of eIF2 $\gamma$  containing the E460K, R503A/E, or R504A/E substitutions is comparable to the level of the WT protein (Figure 2.30B). Furthermore, to examine if these mutants display any dominant phenotypes, we assayed the growth and His<sup>+</sup> phenotypes and measured expression of the *GCN4-lacZ* reporter in cells harboring the WT *GCD11* allele on a sc *TRP1* plasmid and the various recessive lethal mutant alleles on a sc *LEU2* plasmid. These analyses indicated that there is also no dominant phenotype associated with the *E460K*, *R503A/E*, or *R504A/E* mutants as they do not confer a dominant Slg<sup>-</sup> or Ts<sup>-</sup> phenotypes (Figure 2.30A) nor a dominant His<sup>+</sup> or Gcd<sup>-</sup> phenotypes in cells harboring WT *GCD11* (Figure 2.30C-D).

The cluster of residues E460, R503, and R504 seem to carry out a critical function of domain-III. Based on the Sui<sup>-</sup> and Gcd<sup>-</sup> phenotypes of the *E460A* strain, this function likely contributes to the rate or stability of TC binding (Gcd<sup>-</sup>) and the conformation of TC in the P-site needed for accurate start codon recognition (Sui<sup>-</sup>). Because of the position of these three residues on the surface of the proposed binding interface between eIF2 and the 40S subunit (Figure 2.28B), it is possible that the recessive lethality of the indicated mutations is a result of reduced eIF2 binding. If this is the case, then overexpression of the mutant TC might partially suppress this phenotype. In order to test this possibility, we transformed NAY13 (*gcd11 $\Delta$* , *his4-301*, sc *URA3 GCD11*) with hc *LEU2* plasmids co-expressing the four components of the TC (eIF2 $\alpha$ ,  $\beta$ , WT or mutant  $\gamma$ , and Met-



tRNA<sub>i</sub>) and streaked the transformants on SC-L+5-FOA medium to select for loss of the *URA3*-containing WT *GCD11* plasmid. Contrary to this prediction, however, overexpression of the TC containing the R503A or R504A substitutions in eIF2 $\gamma$  does not suppress the recessive lethality of strains harboring these mutations (Figure 2.31A). Furthermore, overexpression of these mutant complexes also does not confer any dominant growth defects, temperature sensitivity, or His<sup>+</sup> phenotypes (Figure 2.32).

Ternary complex binds rapidly to the 40S subunit only when the PIC is in the open conformation. Thus, an increase in the proportion of the PIC in the open conformation is another means by which a reduction in the rate of eIF2 binding can be partially suppressed. The open conformation is stabilized by the binding of the eIF1 and 1A proteins<sup>63</sup>. Consequently, the proportion of the PIC in the open conformation can be increased by overexpressing eIF1. To test this possibility, we introduced a hc *TRP1 SUI1* plasmid into strains harboring the WT *GCD11* on a *URA3* plasmid and the mutant alleles on a sc *LEU2* plasmid. The transformants were then streaked on SC-L-W+FOA medium to select for the loss of *URA3 GCD11* plasmid. Again, contrary to this prediction, overexpression of eIF1 does not suppress the recessive lethality of *R503A* and *R504A* mutants (Figure 2.31B).

We also tested if the recessive lethality conferred by the substitutions at residues R503 and R504 is a result of unstable TC. Overexpression of the Met-tRNA<sub>i</sub> can be expected to partially suppress defects resulting from decreased Met-tRNA<sub>i</sub> binding or an unstable TC. So in order to examine if the overexpression of Met-tRNA<sub>i</sub> can suppress the recessive lethality conferred by these *GCD11* alleles, we introduced a hc *TRP1 IMT4* plasmid into strains harboring the WT *GCD11* on a sc *URA3* plasmid and the mutant

alleles on a sc *LEU2* plasmid. The transformants were then streaked on SC-L-W+FOA medium to select for loss of the *URA3*-containing WT *GCD11* plasmid. Similar to overexpressing eIF1, overexpressing the *IMT4* gene also does not suppress the recessive lethality of these mutations (Figure 2.31B). This result does not support the possibility that the recessive lethality of R503A and R504A is due to reduced Met-tRNA<sub>i</sub> binding or TC stability.

In contrast with *R503A* and *R504A*, overexpression of TC containing the E460K substitution in eIF2 $\gamma$  does improve the severe slow growth defect conferred by the *E460K* allele (Figure 2.33A). Similarly to *R503A* and *R504A*, however, overexpressing *SUI1* or *IMT4* has no effect (Figure 2.33B). Thus, in addition to *G418C* and *R510H*, *E460A/K* mutant alleles are interesting candidates for further analysis in vivo and in vitro (see Chapter 3).

We next set out to determine if any of our site-directed *GCD11* mutant alleles conferred an Ssu<sup>-</sup> phenotype. To test for the Ssu<sup>-</sup> phenotype, we examined all the mutants created by site-directed mutagenesis for their ability to suppress the His<sup>+</sup> phenotype of *SUI3-2*. Derivatives of strain NAY13 (*gcd11 $\Delta$* , *his4-301*) harboring the various *GCD11* mutant alleles and episomal *SUI3-2* were streaked on -His medium to examine their ability to block translation initiation from the UUG codon of *his4-301* and restore histidine auxotrophy. As expected, *E460A* (which has a weak His<sup>+</sup> phenotype on its own) exacerbates the His<sup>+</sup> phenotype of *SUI3-2* (Figure 2.34). This is evident as while the double mutant strain harboring *E460A* and *SUI3-2* displays a Slg<sup>-</sup> phenotype on the +His medium as compared with the strain harboring *SUI3-2* and WT *GCD11*, the two strains display similar growth on the -His medium. The *I466A*, *E494A*, and *E497K*

mutants are all slow growing in combination with *SUI3-2* (Figure 2.34, compare the streaks on the +His medium on top). In this initial screen *S468A*, *K479A/E*, *R484A/E*, *E497K*, and *K498E* conferred partial suppression of the His<sup>+</sup> phenotype of *SUI3-2* without affecting its growth as apparent from their ability to restore histidine auxotrophy in cells harboring the *SUI3-2* allele (Figure 2.34, compare the streaks on the -His medium).

To further confirm the suppression of *SUI3-2* His<sup>+</sup> phenotype, strains harboring the *S468A*, *K479A/E*, *R484A/E*, *E497K*, and *K498E* mutant alleles and episomal *SUI3-2* were cultured in SC-L-W and ten-fold serial dilutions were spotted on SC-L-W medium supplemented with 0.3 mM (+His) or 0.00075 mM (-His) histidine. Interestingly, these mutants display a range in their ability to suppress the His<sup>+</sup> phenotype of *SUI3-2*, with *K479E*, *R484A*, and *R484E* fully suppressing, *K479A* and *E497E* partially suppressing, and *S468A* and *K498E* weakly suppressing the His<sup>+</sup> phenotype (Figure 2.35A).

To quantify the extent to which these mutants suppress initiation from the UUG codon of *his4-301* in cells harboring *SUI3-2*, we used matched *HIS4-lacZ* reporters containing either a UUG or an AUG start codon and measured the ratio of their respective products (UUG/AUG ratio). In WT cells, there is relatively low background level of initiation from a UUG codon, and hence the ratio of *his4(UUG)-lacZ* to *HIS4(AUG)-lacZ* expression is very low. *SUI3-2*, however, reduces the stringency of start codon recognition and increases the translation of *his4(UUG)-lacZ*, which leads to ~2.5-fold increase in the ratio of UUG to AUG initiation compared to the WT cells (Figure 2.35B). The *R484A* and *E497K* mutants display a bona fide Ssu<sup>-</sup> phenotype, partially suppressing the elevated ratio of UUG to AUG initiation in cells expressing the

*SUI3-2* allele by ~40%. The *K479E* mutant also weakly suppresses this ratio by ~15% (Figure 2.35B).

As discussed earlier, *SUI3-2* confers a  $Gcd^-$  phenotype, derepressing expression of the *GCN4-lacZ* reporter by ~2.8-fold (Figure 2.35C). In order to determine if the above *GCD11* mutants also suppress the  $Gcd^-$  phenotype conferred by the *SUI3-2* allele, expression of the *GCN4-lacZ* reporter was measured in strains harboring the various *GCD11* mutants and episomal *SUI3-2*. The mutant *GCD11* alleles also display a range in their ability to suppress the  $Gcd^-$  phenotype of *SUI3-2*, with *K479A/E*, *R484A/E*, and *K498E* partially suppressing, *K479A* failing to suppress, and *S468A* and *E497K* even slightly increasing the derepression of *GCN4-lacZ* conferred by the *SUI3-2* allele (Figure 2.35C).

To examine how universal these *GCD11* mutants were in suppressing the phenotypes of  $Sui^-$  mutations in different initiation factors, strains harboring the *K479A/E*, *R484A/E*, *E497A/K*, and *K498A/E* alleles were transformed with episomal *SUI5* and *tif11-SE1\*SE2\*F131*. Interestingly, the *GCD11* mutants show distinct phenotypic patterns when combined with these  $Sui^-$  mutations. Among them, only *R484E* fully suppresses whereas *K479E*, *R484A*, and *K498E* all partially suppress the  $His^+$  phenotype of *SUI5* (Figure 2.36A). They all also partially suppress both the  $Slg^-$  and the  $Ts^-$  phenotypes of the *SUI5* allele with the *R484A/E*, *K479E*, and *K498E* mutants exhibiting the greatest suppression (Figure 2.36B). Moreover, *K479A/E*, *R484A/E*, and *K498E* all partially suppress the  $Gcd^-$  phenotype of *SUI5* (Figure 2.36C). Note that *K479A*, however, does not suppress the  $His^+$ ,  $Slg^-$ , or  $Ts^-$  of *SUI5* (Figure 2.36A-B). It is interesting to note that while the *E497A* mutant, which does not alter the  $His^+$ ,  $Slg^-$ , or the

Ts<sup>-</sup> phenotypes of *SUI5*, does not derepress the expression *GCN4-lacZ* in otherwise WT cells (Figure 2.27), it further increases the Gcd<sup>-</sup> phenotype of *SUI5* by 2.4-fold (Figure 2.36C). These observations suggest that the Slg<sup>-</sup>, His<sup>+</sup> and the Gcd<sup>-</sup> phenotypes conferred by the *SUI5* allele may have different underlying mechanisms.

In contrast to their phenotypes when combined with *SUI3-2* or *SUI5*, none of the site-directed *GCD11* mutants, suppresses the His<sup>+</sup> phenotype of the *tif11-SE1\*SE2\*F131* Sui<sup>-</sup> allele (Figure 2.37A, compare the first two lanes to the last eight lanes). Moreover, among all the mutants, only *E497A* weakly suppresses its Slg<sup>-</sup> and Ts<sup>-</sup> phenotypes (Figure 2.37B, compare the first two lanes to the last eight lanes). Surprisingly, whereas the *K479A/E*, *E497A/K*, and *K498A/E* alleles have no effect, *R484A* and *R484E* mutations exacerbate the Gcd<sup>-</sup> phenotype conferred by *tif11-SE1\*SE2\*F131*, further derepressing the expression of *GCN4-lacZ* by over 2-fold (Figure 2.37C). Again, note that these mutations do not derepress the expression of *GCN4-lacZ* (Gcd<sup>-</sup>) in otherwise WT cells (Figure 2.27). This phenotype of *R484A/E* is similar to that of the *M482I* and *N433D* mutants that were isolated as suppressors of *SUI5* recessive lethality (Figure 2.37C).

Table 2.7 summarizes our genetic analyses of the Ssu<sup>-</sup> mutations we isolated by either selecting for the suppressors of *SUI5* recessive lethality from a pool of randomly mutagenized *GCD11* alleles or by site-directed mutagenesis of domain-III. It is promising that the mutations in *GCD11* exhibit different phenotypic patterns in combination with the various Sui<sup>-</sup> mutants. Different Sui<sup>-</sup> alleles (*SUI3-2*, *SUI5*, and *tif11-SE1\*SE2\*F131*) have distinct underlying mechanisms. Since our *GCD11* mutants suppress the phenotypes of some Sui<sup>-</sup> mutations but not others, it suggests that they have a specific mechanism and correct for a specific defect.

## 2.4 Discussion

In eukaryotes, base pairing between the start codon of mRNA and the anticodon of Met-tRNA<sub>i</sub> signals the correct start position to the ribosome. The eIF2 complex is a highly conserved initiation factor that binds and delivers the Met-tRNA<sub>i</sub> to the pre-initiation complex. Moreover, hydrolysis of eIF2-bound GTP and P<sub>i</sub> release are required for translation initiation to proceed. Considering these vital functions of the eIF2 complex in start codon selection, we set out to examine this factor in more detail and identify its domains and residues that are involved in establishing the fidelity of this process. To achieve this goal, we embarked on identifying new mutations in eIF2 that alter the accuracy of start codon recognition.

eIF2 $\gamma$  provides the core of the complex that binds GTP and Met-tRNA<sub>i</sub> as well as the  $\alpha$  and  $\beta$  subunits. Thus, we focused our studies on *GCD11* and looked for mutations that altered functions by either lowering the stringency of start codon recognition (Sui<sup>-</sup> phenotype) or, in an opposite manner, restoring initiation fidelity to cells already harboring a Sui<sup>-</sup> mutant (Ssu<sup>-</sup> phenotype). We generated libraries of randomly mutated *GCD11* alleles in order to identify the structural elements that are involved in this process without any bias. To isolate mutations with an Ssu<sup>-</sup> phenotype, we took advantage of the recessive lethality conferred by the *SUI5* allele and from our libraries of random *GCD11* mutants isolated those that suppressed the inviability of cells harboring *SUI5* as the sole source of eIF5 being expressed.

Surprisingly, the majority of the mutant alleles we isolated encode substitutions in domain-III of the  $\gamma$  subunit. Therefore, we decided to further examine domain-III by mutating its conserved surface-exposed residues and screening for an Ssu<sup>-</sup> phenotype.

Twenty four mutations were created by site-directed mutagenesis and screened for their ability to suppress the His<sup>+</sup> phenotype of the *SUI3-2* allele. Multiple additional Ssu<sup>-</sup> mutations were identified in this way.

Among the various *GCD11* alleles we isolated by employing the two aforementioned strategies, the *N433D*, *M482I*, *K479E*, and *R484A* mutants restore the accuracy of start codon selection in vivo and display a bona fide Ssu<sup>-</sup> phenotype by partially suppressing the elevated ratio of UUG to AUG initiation in cells harboring the *SUI3-2* allele. Moreover, they all present a similar pattern in suppressing the His<sup>+</sup> and Gcd<sup>-</sup> phenotypes conferred by *SUI3-2* and *SUI5* as well as the Slg<sup>-</sup> phenotype of *SUI5*. These findings suggest that the above *GCD11* Ssu<sup>-</sup> mutations share a common underlying mechanism.

Remarkably, residues N433, M482, K479, and R484 all cluster to a distinct area with their side chains exposed on the surface of domain-III (Figure 2.38A). This observation suggests that this specific region of eIF2 $\gamma$  domain-III performs an important function in the process of start codon selection. Domain-III has a nicely defined  $\beta$ -barrel structure and encompasses the C-terminal segment of eIF2 $\gamma$ . The area that contains the above residues is distant from the interface of domain-III with the other two domains and is located on the opposite surface of  $\gamma$  that contains the binding sites for GTP and Met-tRNA<sub>i</sub> (Figure 2.38A). Although a crystal structure of eIF2 in complex with the 40S subunit is not currently available, using directed hydroxyl radical cleavage experiments, a model of eIF2 binding to the 40S subunit has been proposed<sup>127</sup>. Interestingly, the surface-exposed area of domain-III that contains the above Ssu<sup>-</sup> mutations is positioned in close proximity of the proposed binding interface between eIF2 and the helix h44 of the

40S subunit (Figure 2.38B). This raises the intriguing possibility that our  $Ssu^-$  mutants restore initiation fidelity by altering the interactions between eIF2 and the 40S subunit so that the PIC would favor the open conformation, which would consequently allow for scanning to continue in order to locate the cognate start codon.

Additional support for this proposal comes from the ability of the *N433D* and *M484I*  $Ssu^-$  mutants to suppress the recessive lethality conferred by the *SUI5* allele. Even though the exact causes of *SUI5* recessive lethality have not yet been experimentally identified, considering the functions of the eIF5 protein in the PIC assembly and translation initiation (see Section 1.1.2), the most likely underlying mechanism(s) may involve alterations in the structural rearrangement of the 43S PIC that occur upon start codon recognition. Thus, it is possible that the isolated mutations in *GCD11* suppress the recessive lethality of *SUI5* by offsetting its detrimental structural rearrangements through adjusting the mode of eIF2 binding to the 40S subunit in the PIC.

In order to isolate novel  $Sui^-$  mutations in *GCD11* that reduce the stringency of start codon recognition, we took advantage of the histidine auxotrophy phenotype conferred by the *his4-301* allele. In order to avoid isolating mutations that reduce initiation fidelity by merely increasing the rate of GTP hydrolysis, we only used the mutant *GCD11* library that contains random mutations in domains –II and –III to select for alleles that conferred a  $His^+$  phenotype by allowing for initiation from the UUG codon of *his4-301*. We isolated the *G418C* and *R510H* alleles by employing this scheme. *R510H* was already identified as a  $Gcd^-$  mutant in a screen for spontaneous revertants of the  $Gcn^-$  phenotype of *gcn2-101 gcn3-101* double mutant<sup>222</sup> and was later shown to also display  $Sui^-$  and  $His^+$  phenotypes by elevating the ratio of UUG to AUG initiation<sup>223</sup>.



This suggests that the selection procedure here worked well to isolate mutations with the desired phenotype.

Residue R510 is located in domain-III of eIF2 $\gamma$ . Because of the structural similarities between eIF2 $\gamma$  and EF-Tu (see section 1.2.1), it was proposed that *R510H* lowers the accuracy of start codon selection by reducing Met-tRNA<sub>i</sub> binding to the eIF2 complex<sup>223</sup>. More recently, however, it has been reported that despite having similar structures, eIF2 $\gamma$  and EF-Tu bind tRNA in different manners. Whereas domain-III of EF-Tu plays a big part in binding tRNA, eIF2 $\gamma$  domain-III it is not involved in Met-tRNA<sub>i</sub> binding<sup>113,127</sup>. Yet, it is possible that *R510H* affects the Met-tRNA<sub>i</sub> binding *indirectly* through altering the structural arrangement of the switch-II region in the G-domain. Although the backbone of residue R510 is positioned on the surface of domain-III, its side chain is not surface-exposed and in fact extends inside the protein toward the G-domain. The side chain of R510 is  $\sim 2.6\text{\AA}$  distant from the side chain of residue D198 in the switch-II region of the G-domain. Thus, it is likely that R510 is involved in maintaining the structural stability of switch-II by forming a salt bridge with D198. Therefore, it is an attractive possibility that the *R510H* mutant reduces initiation fidelity by destabilizing the switch-II region of the G-domain, hence increasing the rate of GTP hydrolysis and/or P<sub>i</sub> release. It is also possible that by altering the structural arrangement of switch-II, *R510H* indirectly affects Met-tRNA<sub>i</sub> binding since, as discussed in Section 1.2.1, the positions of the essential features of the G-domain (switch-I, switch-II, and P-loop) have direct effects on GTP as well as Met-tRNA<sub>i</sub> binding.

Residue G418 is well conserved and is located in the first  $\beta$ -strand of domain-III, which is projected inside the  $\beta$ -barrel structure of domain-II. It is not surface-exposed

and is positioned distant from the proposed binding interface between eIF2 and the 40S subunit. Therefore, it is unlikely that the phenotypes of the *G418C* mutant are a result of altered eIF2 $\gamma$  binding to a partner protein or to the 40S subunit. Domain-II of eIF2 $\gamma$  has been implicated in binding the Met-tRNA<sub>i</sub> as well as the  $\alpha$  subunit<sup>1,113,116,127,138</sup>. Thus, it is possible that *G418C* affects these functions by altering the structure of domain-II, as a cysteine substitution introduces a side chain where none had existed.

We also screened the *GCD11* mutants created by site-directed mutagenesis for the Sui<sup>-</sup> phenotype. Among the twenty four mutations created, the *E460A* allele confers a clear, yet weak, His<sup>+</sup> phenotype. Residue E460 is located on the surface of eIF2 $\gamma$  on the same face that binds GTP and Met-tRNA<sub>i</sub>. It is positioned in close proximity of the proposed binding interface between eIF2 and the 40S subunit. This raises the interesting possibility that *E460A* lowers the fidelity of start codon recognition by altering the binding of eIF2 to the 40s subunit so that the PIC would favor the closed conformation, which would consequently lead to initiation at non-AUG codons.

Our observations suggest that the balance of charge on the surface of eIF2 $\gamma$  domain-III is of vital importance. E460, R503, and R504 residues are all well conserved (Figure 2.23) and are positioned on the surface of eIF2 $\gamma$  that is proposed to be near the binding interface between the eIF2 complex and the 40S subunit (Figure 2.28B and Figure 2.29). As described in detail in Chapter 1, the eIF2 complex binds and maintains the Met-tRNA<sub>i</sub> during the scanning process as the anticodon of Met-tRNA<sub>i</sub> samples the nucleotides on the mRNA in search of the AUG start codon. Thus, the interactions of the Met-tRNA<sub>i</sub> with mRNA on the 40S subunit need to be very dynamic and transient to allow for the sampling of the codons and scanning to proceed. Since it is the eIF2

complex that holds the Met-tRNA<sub>i</sub> during this process, binding of eIF2 (or at least the  $\gamma$  subunit that directly binds the Met-tRNA<sub>i</sub>) to the 40S subunit has to be transient and dynamic. A delicate balance should be maintained: if eIF2 binds too weakly to the 40S subunit, it would fail to initiate even at AUG codons; conversely, if eIF2 binds too tightly to the 40S subunit during the scanning phase, it would stabilize the closed conformation and initiate at non-AUG codons. Therefore, the binding interface between eIF2 $\gamma$  and the 40S subunit should have residues with positive charge to allow for the electrostatic interactions with the negatively charged phosphodiester backbone of the 18S rRNA. This might explain why mutating R504 to other residues is lethal. Moreover, just enough positive charge would be required to allow for a dynamic interaction between eIF2 and the 40S subunit, which might explain why an increase in the net positive charge in the *E460A* mutant leads to the loss of initiation fidelity. There are two positively charged residues R503 and R504 right next to each other, and while the positive side chain of R504 points toward the surface of eIF2 $\gamma$  (where it potentially interacts with the negatively charged backbone of helix h44), the side chain of R503 interacts with the negative side chain of E460. When residue E460 is mutated to alanine, the positive charge of R503 is no longer neutralized. This increases the net positive charge near the surface of eIF2 $\gamma$  where it is proposed to bind to the 40S subunit. Thus, this may alter the way by which eIF2 $\gamma$  interacts with the 40S subunit, which then allows for a non-AUG initiation to take place. Following the same logic, the *E460K* mutant is extremely sick because of the potential electrostatic repulsion with R503, which is likely to destabilize the entire complex. This may explain why overexpressing the *E460K* mutant TC mitigates the extreme growth defect conferred by the *E460K* allele.

By employing three different methods, we isolated two classes of novel mutations in *GCD11*: mutations that lower initiation fidelity allowing for translation initiation from a UUG codon, and those that restore the stringency of start codon selection blocking translation initiation from a UUG codon. Both classes of mutations localize to domain-III of eIF2 $\gamma$ . This suggests that domain-III has a vital function in establishing the stringency of start codon recognition by maintaining the equilibrium between the open and closed conformations. Considering the recent structural model that identifies domain-III as the binding interface between eIF2 and the 40S subunit<sup>127</sup>, our findings point to the intriguing possibility that the mode of eIF2 $\gamma$  binding to the PIC via its domain-III is a determining factor in maintaining the equilibrium between the two conformations of the PIC. To examine this possibility, detailed examination of the *GCD11* mutants that reduce initiation fidelity and those that restore initiation fidelity are presented in Chapters 3 and 4, respectively.

## 2.5 Figures and Tables

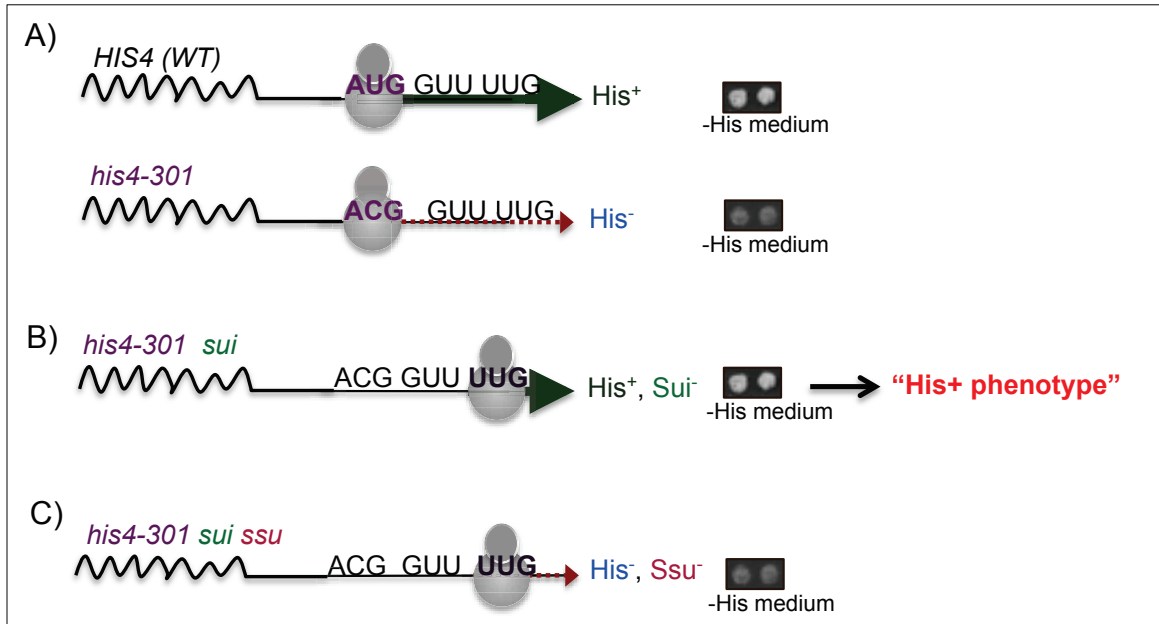


**Figure 2.1 Genetic reporter for monitoring the accuracy of translation initiation in vivo**

(A) *his4-301* is a mutant allele of the *HIS4* gene that lacks a cognate AUG start codon. Thus, in otherwise WT cells, strains harboring the *his4-301* allele exhibit histidine auxotrophy. (B) *Sui*<sup>-</sup> class of mutants lowers the accuracy of start codon recognition and allows for translation initiation from the third in-frame (UUG) codon of the *his4-301* mRNA. Thus, *his4-301* strains harboring a *Sui*<sup>-</sup> mutation display a *His*<sup>+</sup> phenotype by their ability to grow on -His medium (C) *Ssu*<sup>-</sup> alleles, however, reestablish the fidelity of start codon selection and block translation initiation from the UUG codon of *his4-301*. Thus, *his4-301* strains harboring both a *Sui*<sup>-</sup> and an *Ssu*<sup>-</sup> mutation display histidine auxotrophy, as an *Ssu*<sup>-</sup> mutation suppresses the *His*<sup>+</sup> phenotype conferred by a *Sui*<sup>-</sup> allele.

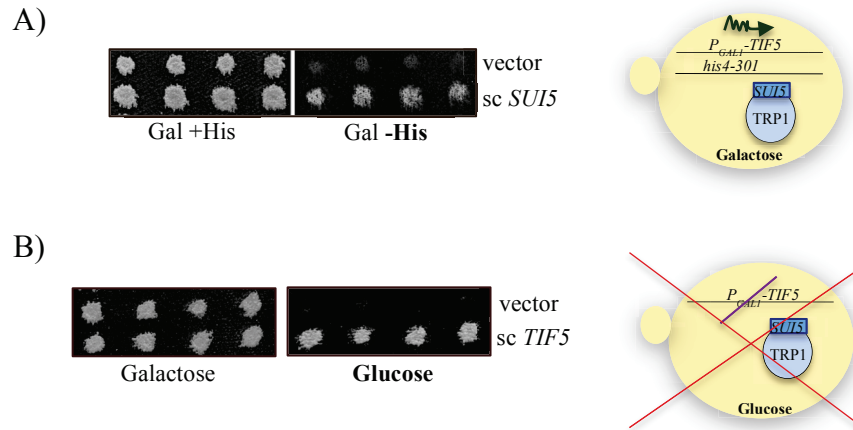


**Figure 2.2 *SUI5* displays dominant  $Sui^-$  and recessive lethal phenotypes**

(A) Strains harboring the *SUI5* allele exhibit a dominant  $Sui^-$  phenotype. Strain NAY17 (*his4-301*,  $P_{GALI-TIF5}$ ) was transformed with either a sc *TRP1 SUI5* plasmid (p4281) or empty *TRP1* vector (YCplac22). Four independent transformants were patched on SCgal-U-W medium and incubated overnight at 30°C. The colonies were then replica plated on the same medium (Gal +His) or the identical medium but lacking histidine (Gal -His). Only colonies that contain *SUI5* are able to initiate translation from the UUG codon of *his4-301* and grow on the -His medium (even in the presence of WT eIF5 expressed from  $P_{GALI-TIF5}$ ). Schematic on the right displays the features of NAY17 relevant for this assay. (B) *SUI5* confers a recessive lethal phenotype. Strain NAY25 ( $P_{GALI-TIF5}$ , sc *TRP1 SUI5*) was transformed with either a sc plasmid harboring the WT *TIF5* allele or vector alone. Four independent transformants were patched on SCgal-U-W medium and incubated overnight at 30°C. The colonies were then replica plated on SC-U-W medium containing glucose as carbon source. Only transformants that express WT eIF5 are able to grow on glucose medium (when the WT chromosomal copy of *TIF5* is transcriptionally shut off). Schematic on the right displays the features of strain NAY25 relevant for this assay.

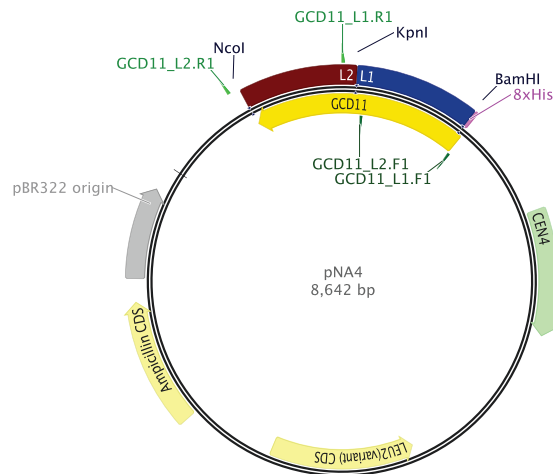
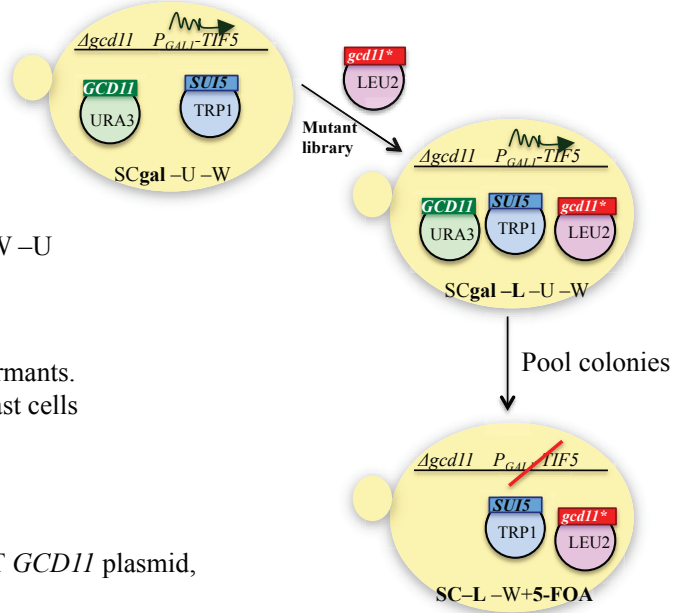


**Figure 2.3 Graphical illustration of the plasmid used for the generation of randomly mutated *GCD11* alleles**

Two libraries of randomly mutated *GCD11* alleles were created corresponding to overlapping regions of the *GCD11* coding region. The first library (L1) encompasses codons 1-306 of the G-domain and was generated using primers GCD11\_L1.F1 and GCD11\_L1.F2. The second library (L2) encompasses codons 251 to 527, which encode the last 59 amino acids in the G-domain and the entirety of domains -II and -III, and was generated using primers GCD11\_L2.F1 and GCD11\_L2.R1. *LEU2 (variant)* and *Ampicillin* alleles code for an essential protein in leucine biosynthesis pathway and ampicillin resistance enzyme, respectively, and are used as selection markers in yeast and *E. coli*, respectively.

1. Transform with mutant library on *LEU2* plasmid



2. Plate transformants on SCgal-L-U-W  
→ no selection

3. When colonies appear, pool transformants.  
→ collect the library in yeast cells

4. Plate the pool on SC-L-W+5-FOA  
→ select for the loss of WT *GCD11* plasmid,  
shut off WT *TIF5*  
=> select for suppression of lethality

**Figure 2.4 Selection scheme for identification of mutations in *GCD11* that suppress the recessive lethality of *SUI5***

Pools of yeast strains containing the mutant alleles of *GCD11* were first generated by transforming strain NAY25 ( $gcd11\Delta$ ,  $P_{GALI-TIF5}$ , sc *TRP1 SUI5*) with the L1 and L2 libraries and growing the cells on SCgal-L-U-W medium (galactose as carbon source to allow for the expression  $P_{GALI-TIF5}$ ). The transformants were pooled, diluted, and spread on SC-L-U-W medium (glucose as carbon source to shut off the expression of  $P_{GALI-TIF5}$ ) with 5-FOA (to select for the loss of *URA3 GCD11* plasmid).

Transformants that could survive and grow on the glucose medium were then selected and streaked on SCgal-L-W medium to isolate single colonies. *gcd11\** denotes randomly mutated *GCD11* alleles.



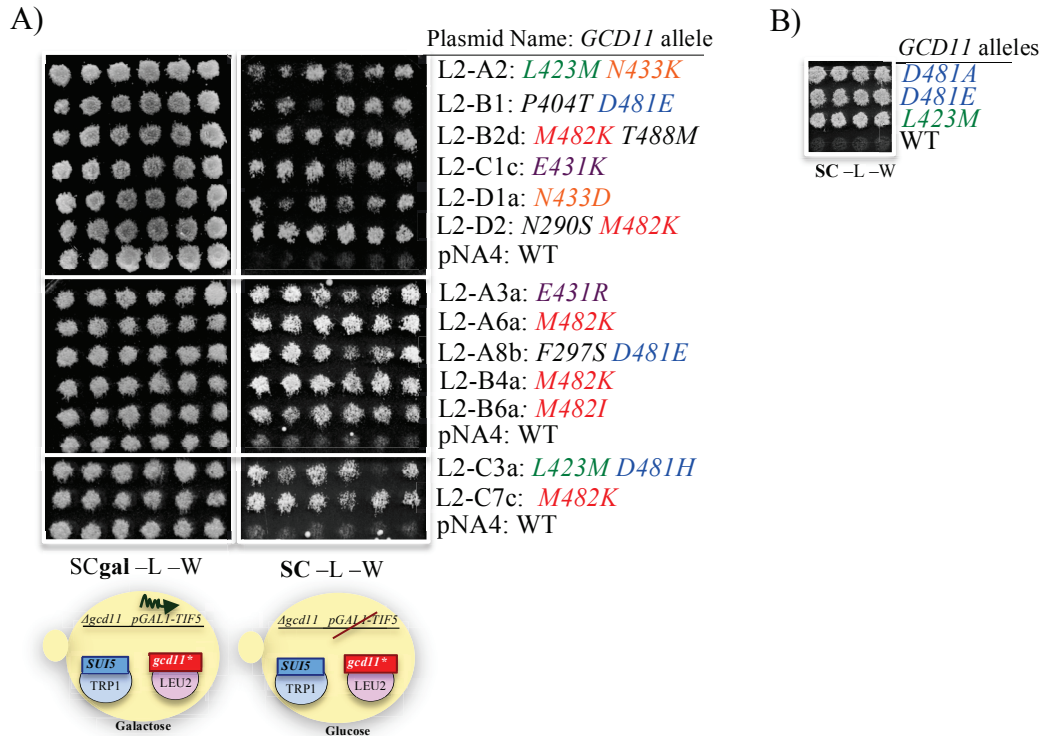


**Figure 2.5 Novel mutations identified in *GCD11* that suppress the recessive lethality of *SUI5***

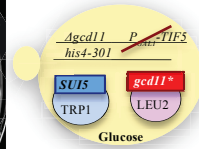
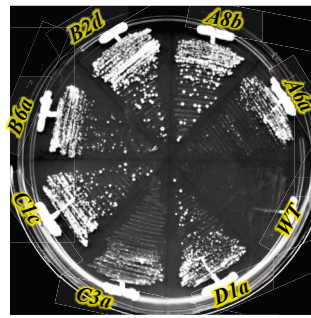
(A) Plasmids rescued from the initial selection process were reintroduced into NAY25 (*gcd11Δ*, *P<sub>GALI</sub>-TIF5*, *sc TRP1 SUI5*), six independent transformants for each plasmid were patched on SCgal-L-W medium, and incubated at 30°C overnight. The colonies were then replica plated on SC-L-W medium (glucose as carbon source) and incubated at 30°C for two (SCgal-L-W plates) and three (SC-L-W plates) days. WT strains expressing the *SUI5* allele as the sole source of the eIF5 protein are inviable (compare the rows corresponding to WT *GCD11* on the SCgal-L-W medium to those on SC-L-W). Only strains harboring mutant alleles of *GCD11* that can suppress the recessive lethality of *SUI5* grow on SC-L-W medium, which contains glucose as carbon source. Color-coding designates substitutions in the same residues that were isolated from independent

mutant plasmids. (B) The *D481A*, *D481E*, and *L423M* mutants of *GCD11* suppress the recessive lethality of *SUI5*. *D481A*, *D481E*, and *L423M* single substitutions were generated in plasmid pNA4 by site-directed mutagenesis using the QuickChange Site-Directed Mutagenesis kit (Agilent Technologies) following the manufacturer's protocol and primer sets g\_D481A.F/g\_D481A.R, g\_D481E.F/g\_D481E.R, and g\_L423M.F/g\_L423M.R, respectively. Same procedure as in panel A.

Plasmid Name: *GCD11* allele

*SUI5*

A6a: *M482K*  
A8b: *F297S D481E*  
B2d: *M482K T488M*  
B6a: *M482I*  
C1c: *E431K*  
C3a: *L423M D481H*  
D1a: *N433D*



SC-L-W

### Figure 2.6 Suppression of *SUI5* recessive lethality by the *GCD11* mutants

(A) Mutations in *GCD11* display a range in ability to restore growth to cells harboring *SUI5* as the sole source of eIF5. Plasmids rescued from the initial selection process were reintroduced into strain NAY25 (*gcd11Δ*, *P<sub>GALI</sub>-TIF5*, *sc TRP1 SUI5*), streaked on SC-L-W medium (where the chromosomal copy of *TIF5* is shut off), and incubated at 30°C for five days to examine the size of individual colonies formed from single cells. WT strain expressing the *SUI5* allele as the sole source of the eIF5 protein is inviable. Only strains harboring mutant alleles of *GCD11* that can suppress the recessive lethality of *SUI5* grow on SC-L-W medium, in the absence of the WT eIF5 protein.

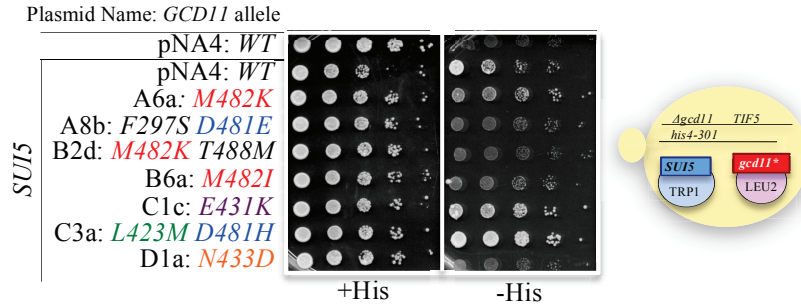


**Figure 2.7 Suppression of *SUI5* His<sup>+</sup> phenotype by the *GCD11* mutants**

The *GCD11* alleles harbored by plasmids A6a, A8b, B2d, B6a, C1c, C3a, and D1a all suppress the dominant Slg<sup>-</sup> phenotype of *SUI5* (compare rows on the +His medium).

Whereas the *GCD11* alleles in plasmids A6a, A8b, B2d, B6a, and D1a fully suppress and that in C1c very weakly suppresses the His<sup>+</sup> phenotype of *SUI5*, the mutant allele

harbored by plasmid C3a does not do so. Derivatives of strain NAY13 (*gcd11Δ*, *his4-301*) harboring the WT or mutant *GCD11* alleles and either expressing *SUI5* from a *sc TRP1* plasmid (p4281) or the empty vector (YCplac22) were cultured in liquid SC-L-W medium, ten-fold serial dilutions were spotted on SC-L-W supplemented with either 0.3 mM (+His) or 0.003 mM (-His) histidine, and incubated at 30°C for two and five days, respectively. Note that in this strain WT eIF5 is expressed in single copy from its endogenous chromosomal locus and is not overexpressed from the *GALI* promoter.

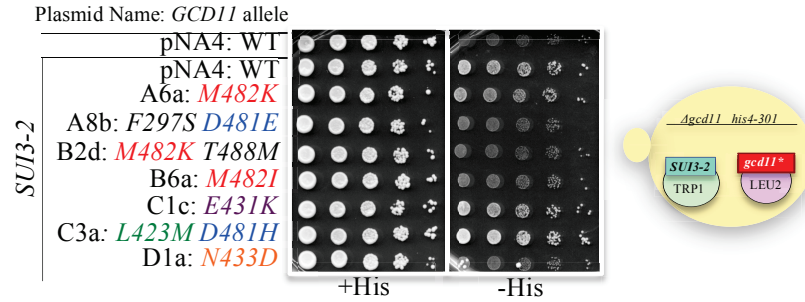


**Figure 2.8 Suppression of *SUI3-2* His<sup>+</sup> phenotype by the *GCD11* mutants**

Whereas the *GCD11* alleles harbored by plasmids A8b, B2d, B6a, and D1a fully suppress and those in plasmids A6a and C1c weakly suppress the His<sup>+</sup> phenotype of *SUI3-2*, the mutant allele harbored by plasmid C3a does not do so. Derivatives of strain NAY13 (*gcd11Δ, his4-301*) harboring the WT or mutant *GCD11* alleles and expressing either *SUI3-2* from a sc *TRP1* plasmid (p4280) or the empty vector (YCplac22) were cultured in liquid SC-L-W, ten-fold serial dilutions were spotted on SC-L-W medium supplemented with either 0.3 mM (+His) or 0.0015 mM (-His) histidine, and incubated at 30°C for two and five days, respectively.

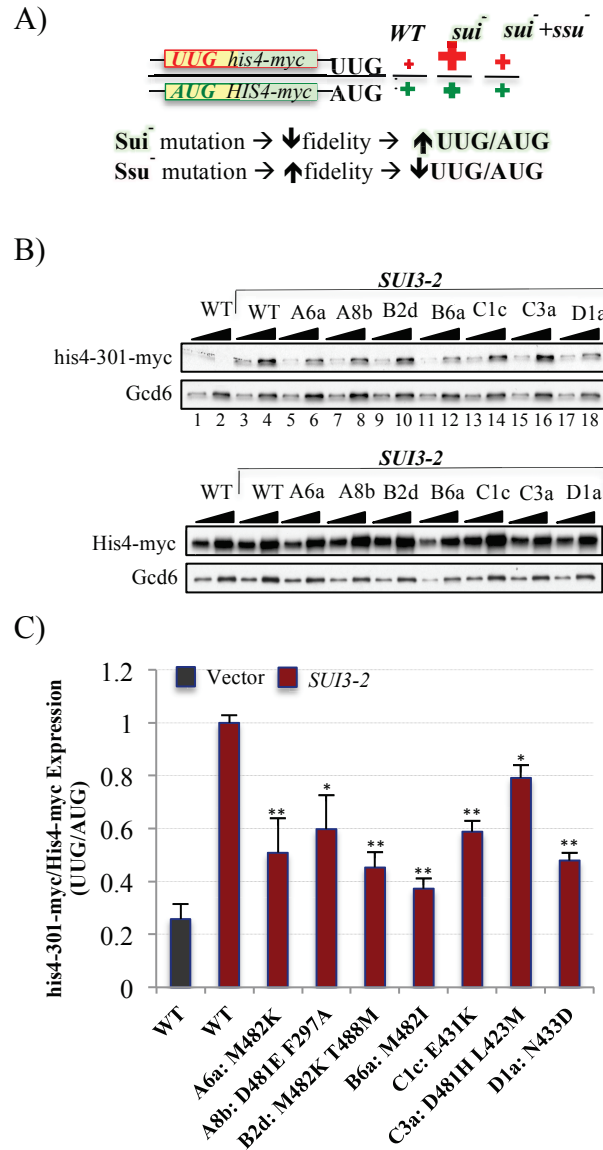


**Figure 2.9 Isolated mutations in *GCD11* restore initiation fidelity in cells harboring the *SUI3-2* mutation**

(A) Expression of the *his4-301-myc*<sub>10</sub> or *HIS4-myc*<sub>10</sub> alleles is used as a genetic reporter to quantify the extent of UUG initiation. *Sui<sup>-</sup>* mutations reduce fidelity and increase the ratio of initiation from a UUG codon to that from an AUG codon (UUG/AUG ratio). *Ssu<sup>-</sup>* mutations, conversely, restore initiation fidelity and suppress the elevated UUG to AUG ratio conferred by the *Sui<sup>-</sup>* alleles. (B) *Ssu<sup>-</sup>* mutations in *GCD11* reduce the

expression of *his4-301-myc<sub>10</sub>* relative to *His4-myc<sub>10</sub>* in cells expressing *SUI3-2*. Ratio of initiation from a UUG codon to that of an AUG codon was assayed by measuring expression levels of the *his4-301-myc* (UUG) and *His4-myc<sub>10</sub>* (AUG) proteins. Strains with the WT or indicated *GCD11* mutant allele harboring episomal *SUI3-2* (p4280) or an empty *TRP1* vector (Ycplac22) and chromosomal *his4-301-myc<sub>10</sub>* (top) or *HIS4-myc<sub>10</sub>* (bottom) were grown to mid exponential phase (OD<sub>600</sub> ~0.5) in SC-L-W medium, and WCEs were subjected to Western blot analysis with antibodies against the Myc-epitope (Sigma) and eIF2Bε/Gcd6 (loading control). Two different amounts of each extract differing by a factor of 2 were loaded in successive lanes. (C) Western signals from repeat experiments (n=4) of panel A were quantified, and the mean ratios of *his4-301-myc<sub>10</sub>* to *His4-myc<sub>10</sub>* (each normalized to the loading control) and standard errors of the mean (SEM, error bars) are plotted. A student *t*-test was used to determine significance (\*p<0.05, \*\*p<0.01).

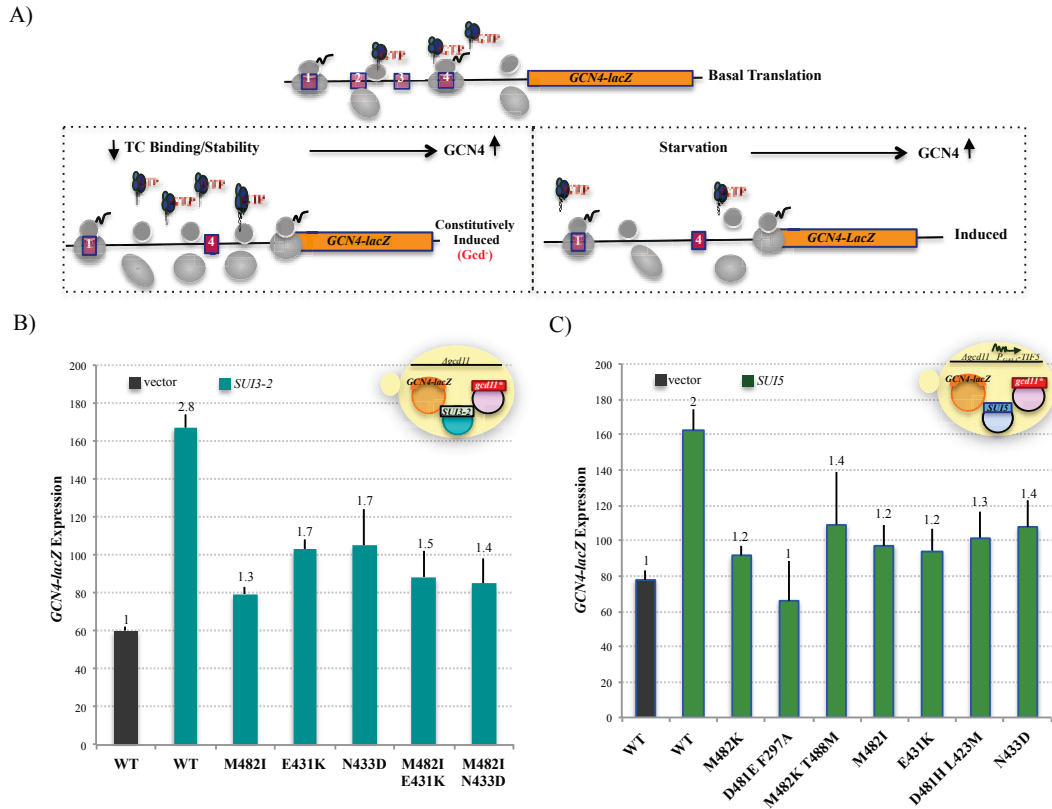


**Figure 2.10 Suppression of *SUI5* and *SUI3-2* *Gcd<sup>-</sup>* phenotypes by the *GCD11* mutants**

(A) *GCN4-lacZ* expression is used as a genetic reporter for the stability and binding of the ternary complex to the PIC. *GCN4* mRNA is translated at low basal levels under normal conditions (top). Amino acid starvation leads to the induction of *GCN4* translation (bottom right). A reduction in TC stability or binding, however, increases the translation of *GCN4* mRNA even under non-starvation conditions, creating a *Gcd<sup>-</sup>* phenotype (bottom left). (B) The *Ssu<sup>-</sup>* mutations in *GCD11* suppress the *Gcd<sup>-</sup>* phenotype of *SUI3-2*. Expression of *GCN4-lacZ*, with all four upstream ORFs, on a single copy plasmid (p180) was measured in derivatives of strain NAY13 harboring the WT or mutant alleles of *GCD11* in the presence of episomal *SUI3-2* (p4280) or an empty *TRP1* vector (YCplac22).  $\beta$ -galactosidase activities (nanomoles of *o*-nitrophenyl- $\beta$ -D-



galactopyranoside cleaved per minute per microgram of protein) were measured in WCEs of exponentially growing cultures ( $OD_{600} \sim 0.5$ ) in SC-L-W medium. Mean of at least eight independent transformants and SEM (error bars) are plotted for each mutant. Double mutant alleles of *GCD11* harboring substitutions at positions 482 and 431 (M42I/E431K) as well as 482 and 433 (M482I/N433D) were generated in pNA4 using the QuickChange Site-Directed Mutagenesis kit (Agilent Technologies) following the manufacturer's protocol. (C) The isolated mutants of *GCD11* that suppress the recessive lethality of *SUI5*, also suppress its  $Gcd^-$  phenotype. Expression of *GCN4-lacZ*, with all four upstream ORFs, on a single copy plasmid (p180) was measured in derivatives of strain NAY25 harboring the WT or mutant alleles of *GCD11* in SCgal-L-W medium (to allow for the expression of *P<sub>GALI</sub>-TIF5*).  $\beta$ -galactosidase assays were performed as in panel B. Mean of at least eight independent transformants and SEM (error bars) are plotted for each mutant.

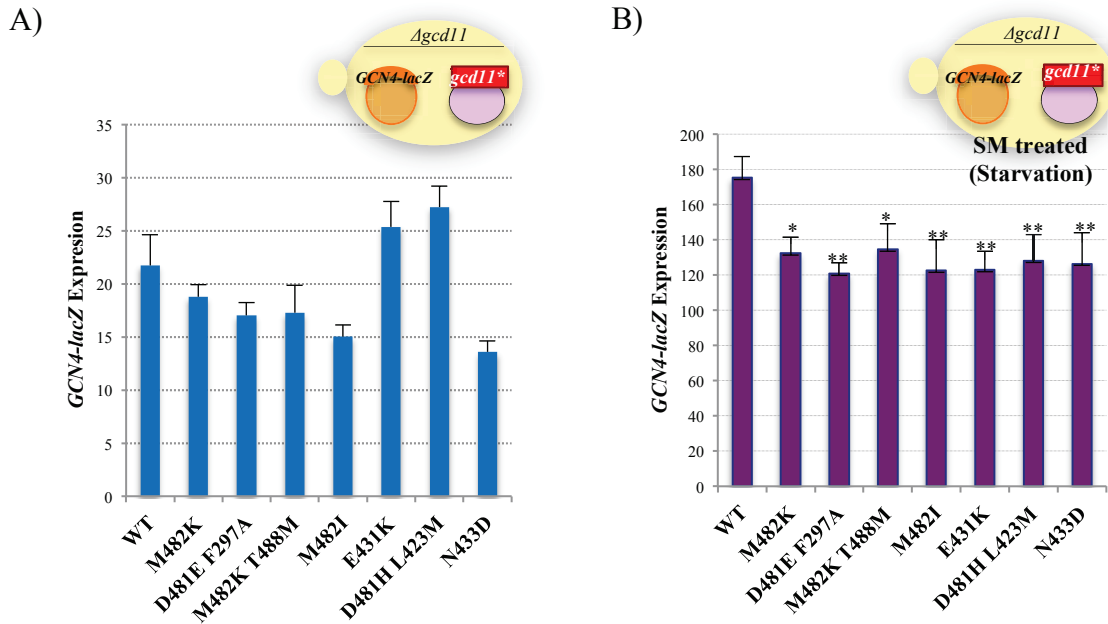
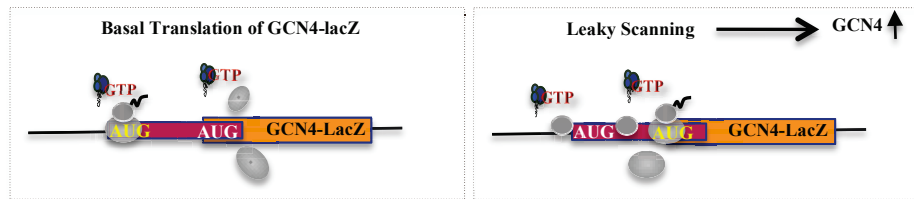


**Figure 2.11 The *Ssu*<sup>-</sup> mutants of *GCD11* display a weak *Gcn*<sup>-</sup> phenotype**

(A) Isolated *Ssu*<sup>-</sup> mutations in *GCD11* do not create a *Gcd*<sup>-</sup> phenotype. Expression of *GCN4-lacZ*, with all four upstream ORFs, on a single copy plasmid (p180) was measured in derivatives of NAY13 harboring the WT or mutant alleles of *GCD11* cultured in SC-L-U medium.  $\beta$ -galactosidase activities (nanomoles of *o*-nitrophenyl- $\beta$ -D-galactopyranoside cleaved per minute per microgram of protein) were measured in WCEs of exponentially growing cultures ( $OD_{600} \sim 0.5$ ). Mean of at least twelve independent transformants and SEM (error bars) are plotted for each mutant. (B) The *Ssu*<sup>-</sup> mutations of *GCD11* create a weak *Gcn*<sup>-</sup> phenotype. Same strains and procedure as in panel B except starvation was induced by the addition of 0.5mg/ml of sulfometuron (SM) for six hours in SC-L-U medium. Mean of at least eight independent transformants and SEM (error bars) are plotted for each mutant. A student *t*-test was used to determine significance (\* $p < 0.05$ , \*\* $p < 0.01$ ). Note that *GCN4-lacZ* expression is ~9-fold higher in the WT strain in starvation versus non-starvation conditions.

A)



B)

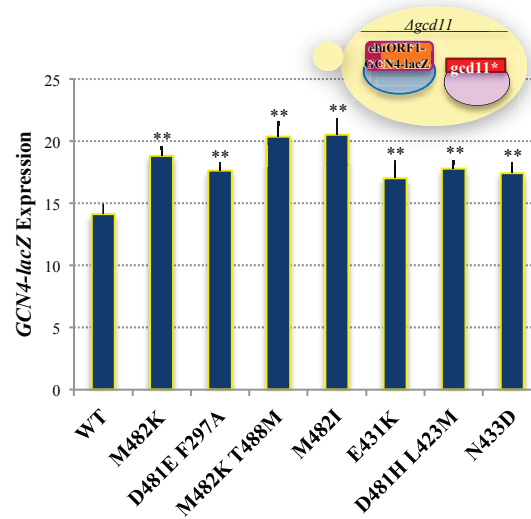


**Figure 2.12 The *Ssu*<sup>-</sup> mutants of *GCD11* exhibit a modest leaky scanning phenotype**

(A) A construct with an elongated upstream ORF1 (el-uORF1) in-frame with and covering the AUG start codon of *GCN4-lacZ* is used as a genetic reporter for leaky scanning. In WT cells, there is low basal translation of *GCN4-lacZ* fusion since most ribosomes translate from the AUG codon of el-uORF1 (left panel). In mutants that have reduced AUG recognition, a greater proportion of ribosomes bypass the AUG codon of el-uORF1 and instead initiate downstream at *GCN4-lacZ* (leaky scanning). Thus, translation of *GCN4-lacZ* mRNA increases in a mutant with a leaky scanning phenotype (right panel) (B) The *Ssu*<sup>-</sup> mutants of *GCD11* display a modest decrease in AUG recognition (weak leaky scanning). Expression of *GCN4-lacZ* was measured in derivatives of NAY13 harboring the WT or indicated mutant alleles of *GCD11*.  $\beta$ -

galactosidase activities (nanomoles of *o*-nitrophenyl- $\beta$ -D-galactopyranoside cleaved per minute per microgram of protein) were measured in WCEs of exponentially growing cultures ( $OD_{600} \sim 0.5$ ) in SC-L-U medium. Mean of at least eight independent transformants and SEM (error bars) are plotted for each mutant. A student *t*-test was used to determine significance (\*\* $p < 0.01$ ).

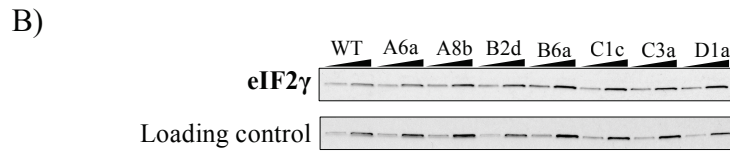
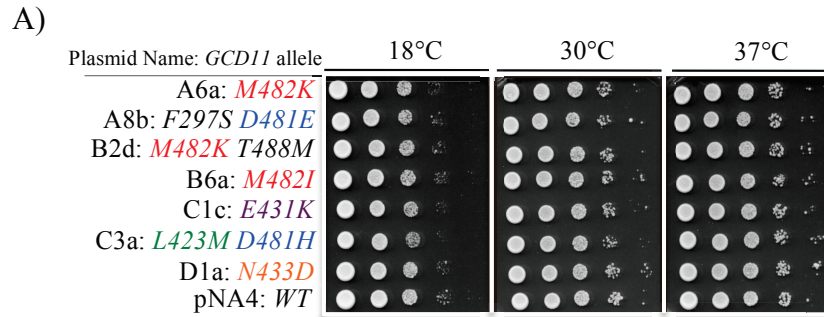


**Figure 2.13 Growth phenotypes and protein levels of the *Ssu*<sup>-</sup> substitutions in eIF2 $\gamma$**

(A) The *GCD11* *Ssu*<sup>-</sup> mutants do not display *Slg*<sup>-</sup> or *TS*<sup>-</sup> phenotypes. Derivatives of NAY13 harboring the WT or mutant alleles of *GCD11* were cultured in SC-L, ten-fold serial dilutions were spotted on SC-L medium, and incubated at the specified temperatures for two (30°C and 37°C) and four days (18°C). (B) The isolated substitutions in eIF2 $\gamma$  do not alter the expression level of their respective proteins. Western blot analysis of WCEs, prepared by TCA extraction, from exponentially growing (OD<sub>600</sub> of ~0.5) strains of panel A were performed with antibodies against the His<sub>6</sub> epitope (abcam) and eIF2B $\epsilon$ /Gcd6 (loading control). Two different amounts of each extract differing by a factor of 2 were loaded in successive lanes.

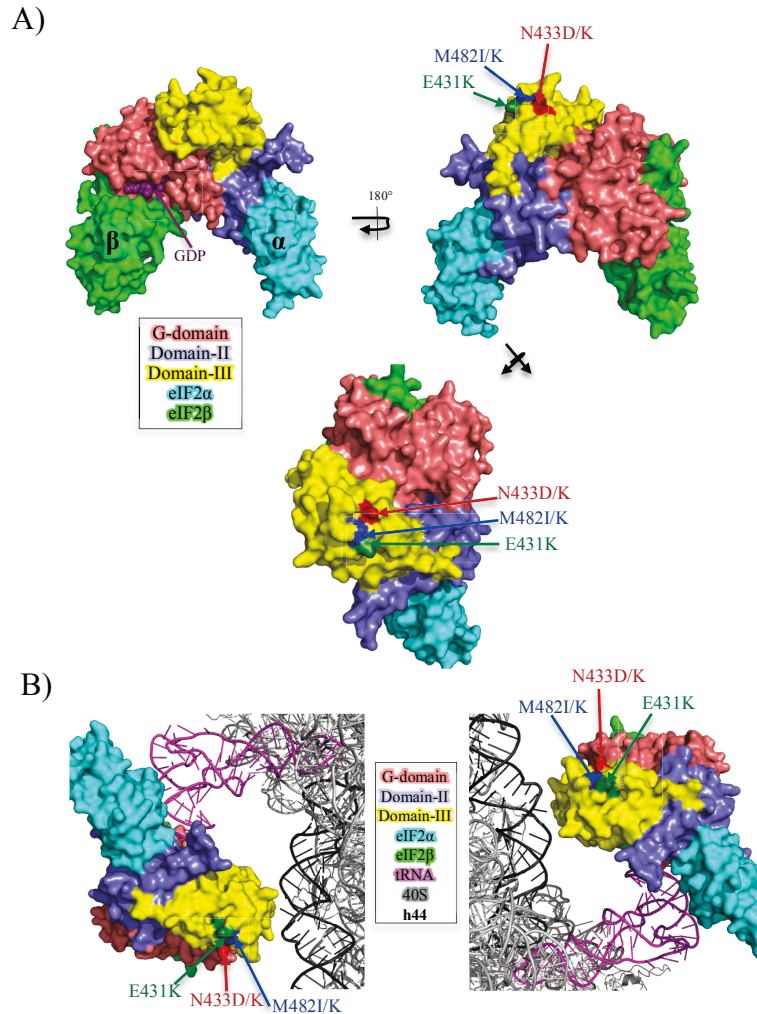


**Figure 2.14 The isolated  $Ssu^-$  substitutions in eIF2 $\gamma$  localize to a discrete region on the surface of domain-III close to h44 of the 40S subunit**

(A) Three different views of a surface representation of eIF2 crystal structure containing the full  $\beta$  and  $\gamma$  but only domain-III of the  $\alpha$  subunit (PDB 2QMU). The identified  $Ssu^-$  mutations cluster to a distinct region on the surface of eIF2 $\gamma$  on the opposite surface that harbors the binding sites for GTP and Met-tRNA<sub>i</sub>. The side chain of the residues harboring the  $Ssu^-$  substitutions are exposed on the surface of eIF2 $\gamma$  (B) Two views of a model of TC binding to the 40S subunit adapted from Shin et al. 2011<sup>127</sup>.  $Ssu^-$  mutations

are located on the surface of domain-III in proximity of h44 of the 40S subunit. Images were created using the PyMOL software<sup>207</sup>.

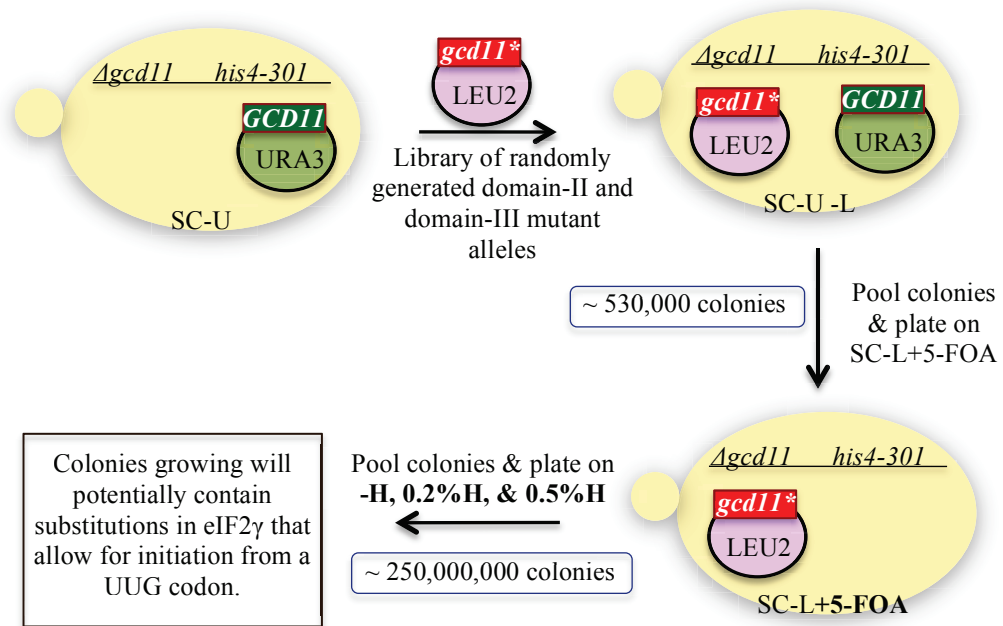


**Figure 2.15 Outline of the selection scheme for isolation of *Sui<sup>-</sup>* mutations in *GCD11***

Strain NAY13 (*gcd11Δ, his4-301, sc URA3 GCD11*) was transformed with the L2 library containing randomly mutated *GCD11* alleles corresponding to domains -II and -III. 530,000 transformants were pooled, diluted, and spread on SC-L medium containing 5-FOA to select for loss of the WT *GCD11 URA3* plasmid. 250 million colonies were then pooled, diluted, and spread on SC-L medium containing 0.015 mM, 0.006 mM, and 0 mM histidine to select for *GCD11* mutant plasmids that allow translation initiation from a non-AUG codon of the *his4-301* allele and suppress the histidine auxotrophy of NAY13.



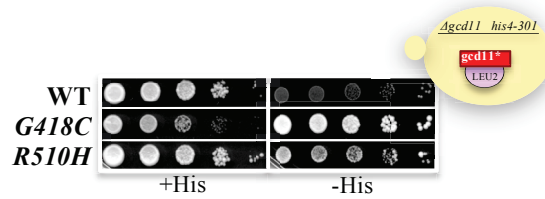


**Figure 2.16 The *G418C* and *R510H* mutants display a  $His^+/Sui^-$  phenotype**

The *G418C* allele confers a stronger  $His^+$  phenotype compared to *R510H* in strains deleted for the chromosomal copy of *GCD11* and harboring the *his4-301* allele.

Additionally, strains expressing *G418C* displays a marked  $Slg^-$  phenotype (compare rows on the +His medium). Derivatives of strain NAY13 (*gcd11 $\Delta$* , *his4-301*) harboring the WT or indicated mutant alleles of *GCD11* were cultured in SC-L, ten-fold serial dilutions were then spotted on SC-L medium supplemented with 0.3 mM (+His) or 0.003 mM (-His) histidine, and incubated at 30°C for two and four days respectively.

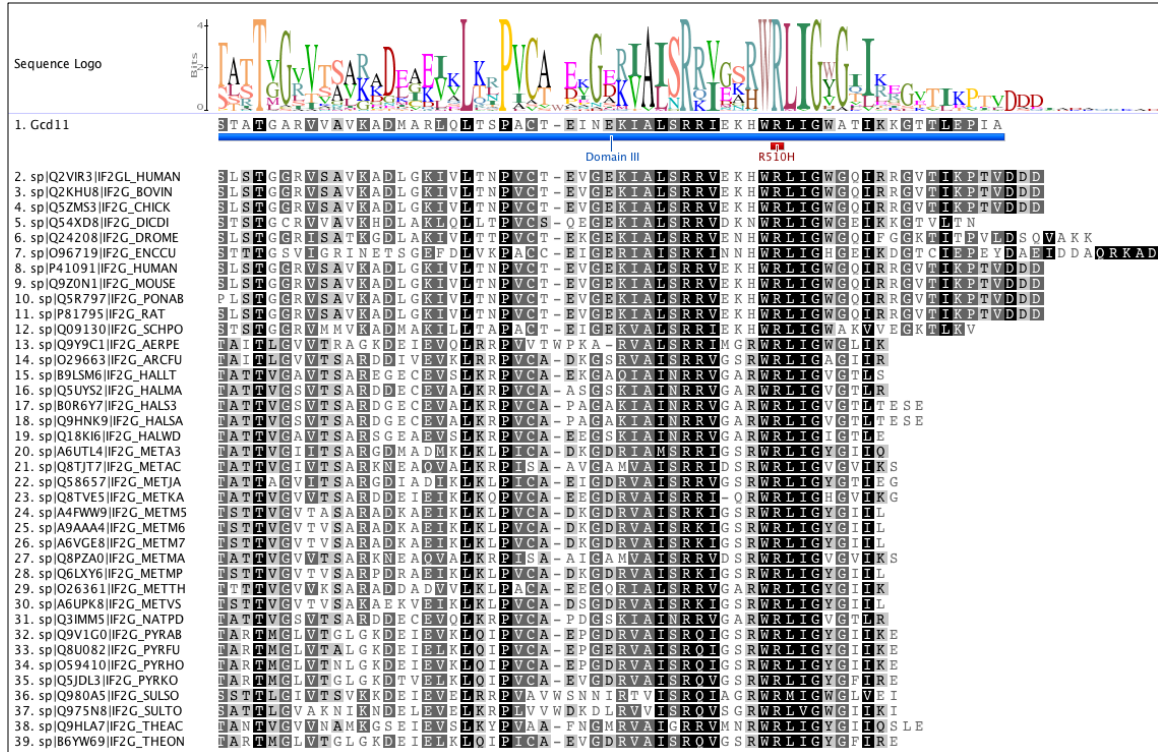


**Figure 2.17 R510 is a highly conserved residue in domain-III of eIF2 $\gamma$**

The region surrounding residue R510, which contains the sequence motif

W<sub>509</sub>R<sub>510</sub>L<sub>511</sub>I<sub>512</sub>G<sub>513</sub> encompassing the last  $\beta$ -strand of domain-III, is highly conserved

among eukaryotes and archaea. 39 Uniprot-reviewed eukaryotic and archaeal e/aIF2 $\gamma$  sequences were aligned using the Geneious software<sup>226</sup>. Only part of the alignment

corresponding to the segment of domain-III containing residue R510 is shown.

Species/sequence names are standard Uniprot identifiers<sup>227</sup>.

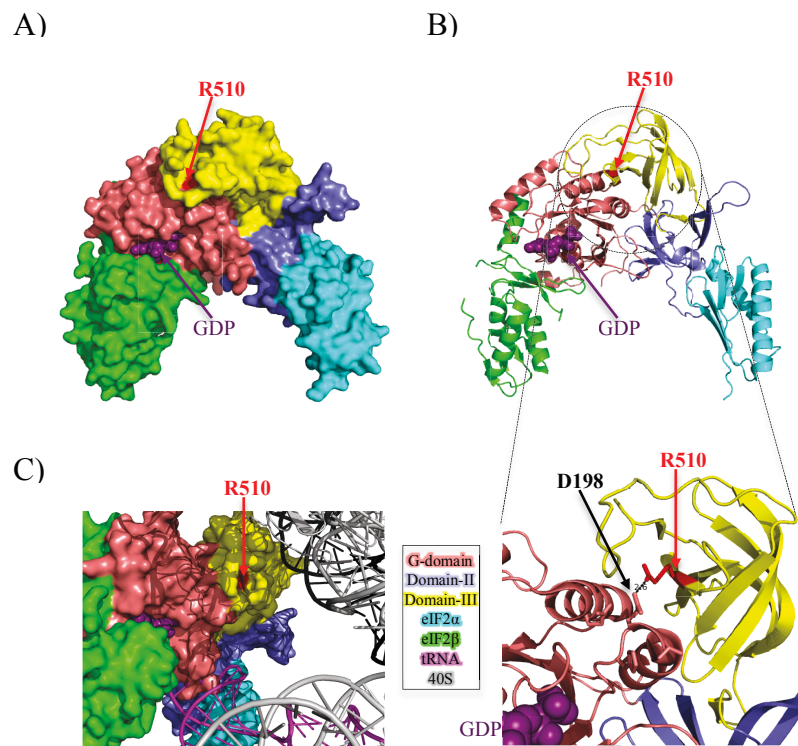


**Figure 2.18 R510 is located on the surface of eIF2 $\gamma$  at the interphase of domain-III and the G-domain**

(A) Front view of a surface representation of aIF2 crystal structure (PDB 2QMU). The main chain of R510 is partially surface-exposed on the same face of eIF2 $\gamma$  that binds GTP and Met-tRNA<sub>i</sub>. (B) A cartoon view of panel A with residue R510 marked (top). A magnified view of the area surrounding R510 is shown at the bottom. R510 is located in the last  $\beta$ -strand of the  $\beta$ -barrel structure of domain-III at the interphase with the G-domain. Side chain of R510 is 2.6Å from D198 in the switch-II region of the G-domain. (C) R510 is also in proximity of the proposed binding interface between eIF2 and the 40S subunit. Its side chain, however, does not project outward from the surface. Instead, it extends inside toward the side chain of D198 in the G-domain, as shown panel B. Model of TC binding to the 40S subunit is adapted Shin et al. 2011<sup>127</sup>. Images were created using the PyMOL software<sup>207</sup>.

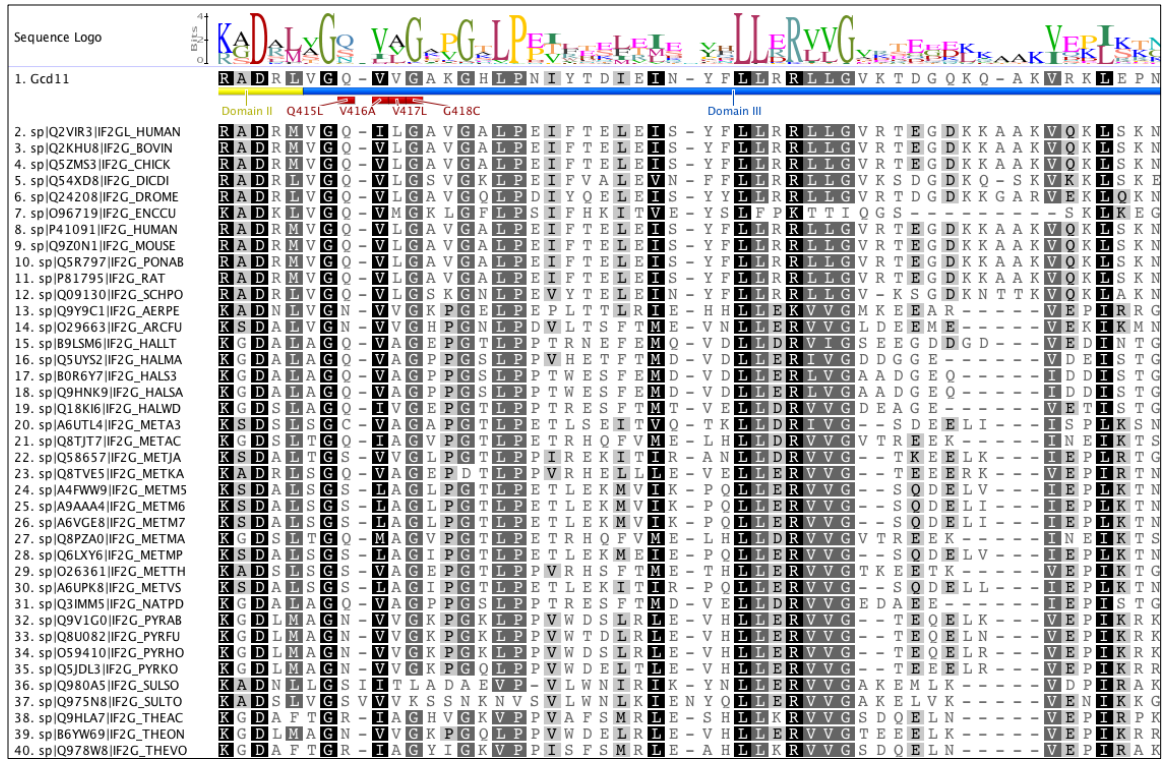
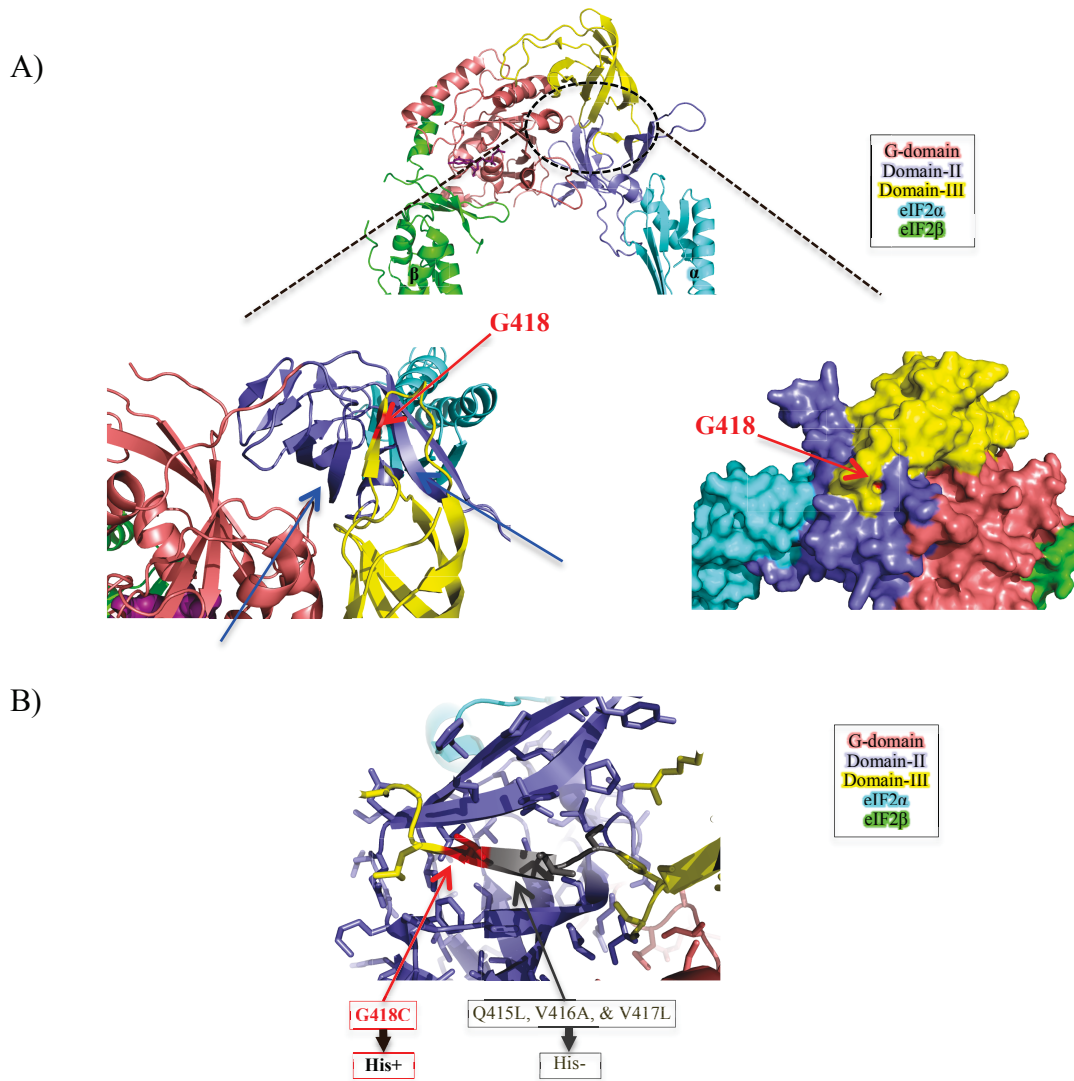


Figure 2.19 G418 is a highly conserved residue in domain-III of eIF2γ

40 Uniprot-reviewed eukaryotic and archaeal e/aIF2γ sequences were aligned using the Geneious software<sup>226</sup>. Only part of the alignment corresponding to the segment of domain-III containing residue G418 is shown. Other substitutions created (by site-directed mutagenesis) in the neighboring residues of G418 in the β1 of domain-III are also marked. Species/sequence names are standard Uniprot identifiers<sup>227</sup>.



**Figure 2.20 G418 is located in the first  $\beta$ -strand of eIF2 $\gamma$  domain-III**

(A) Front view of a cartoon representation of aIF2 (PDB 2QMU) (top panel). Bottom panels are magnified views of the area surrounding G418. G418 is in the  $\beta_1$  of domain-III, which is inserted between  $\beta_1$  and  $\beta_3$  of the  $\beta$ -barrel structure of domain-II (bottom left). G418 is not surface-exposed (bottom right) (B) Among the substitutions of residues in the  $\beta_1$  of domain-III, only G418C displays a His<sup>+</sup> phenotype. Images were created using the PyMOL software<sup>207</sup>.

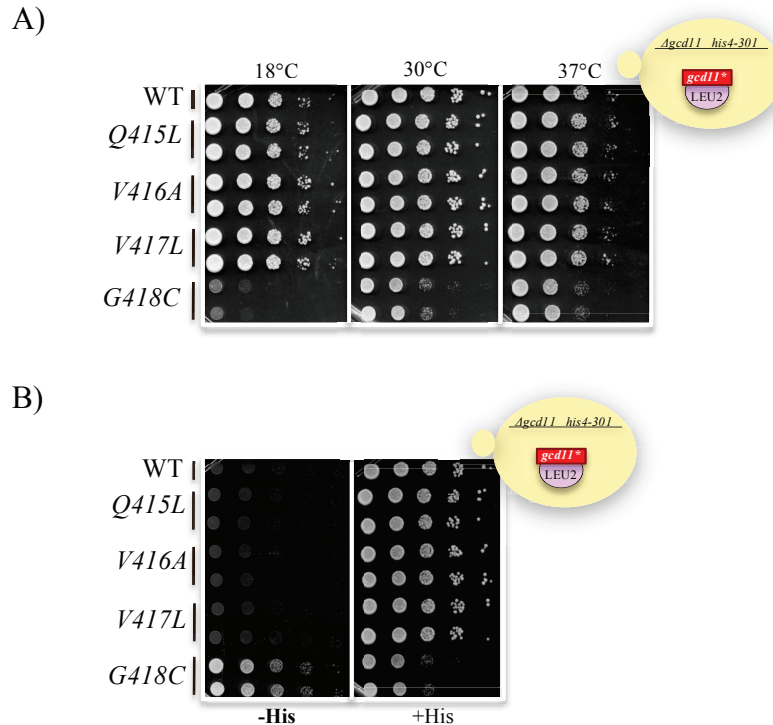


**Figure 2.21 The *G418C* mutant is slow growing, cold sensitive, and displays a strong His<sup>+</sup> phenotype**

(A) The *G418C* allele confers marked Slg<sup>-</sup> and cold sensitivity phenotypes. Substitutions in residues Q415, V416, and V417, which are all located in  $\beta$ 1 of domain-III along with G418, do not create any growth defects, TS<sup>-</sup>, or His<sup>+</sup> phenotypes. Derivatives of strain NAY13 harboring the WT or indicated *GCD11* mutant alleles were cultured in SC-L, ten-fold serial dilutions were spotted on SC-L medium, and incubated at the specified temperatures for two (30°C and 37°C) and four (18°C) days. Two independent transformants of each mutant were spotted. (B) The *G418C* allele confers a strong His<sup>+</sup> phenotype. Same strains and growth conditions as in panel A, except that ten-fold serial dilutions were spotted on SC-L medium supplemented with 0.3 mM (+His) or 0.0006 mM (-His) histidine and incubated at 30°C for two and three days, respectively. Two independent transformants of each mutant were spotted.



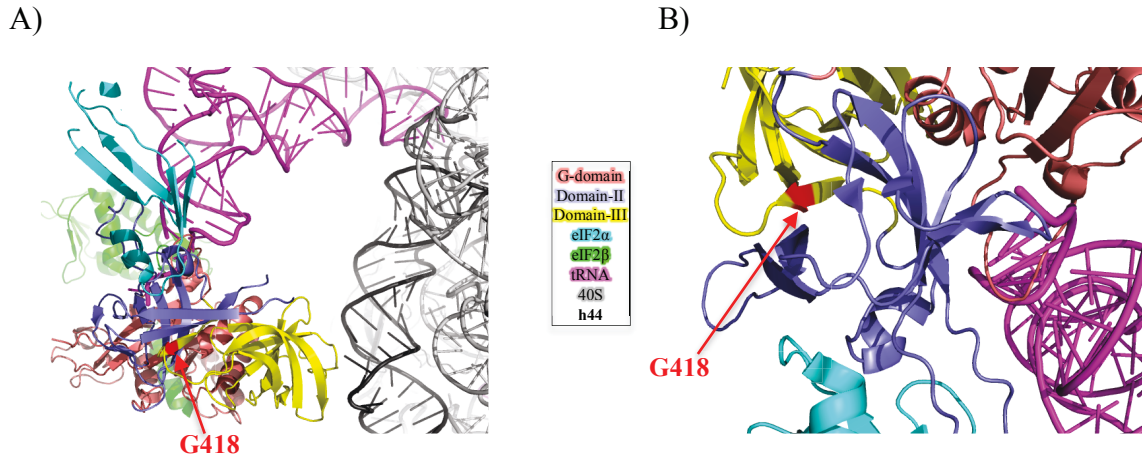


**Figure 2.22 G418 is positioned distant from the proposed interface of eIF2 with the 40S subunit**

(A) Model of TC binding to the 40S subunit adapted from Shin et al. 2011<sup>127</sup>. (B) A magnified view of panel A. Domain-II of eIF2 $\gamma$  has been implicated in binding the Met-tRNA<sub>i</sub> as well as the  $\alpha$  subunit. G418 residue is in  $\beta$ 1 of domain-III that is inserted inside the  $\beta$ -barrel structure of domain-II. Images were created using the PyMOL software<sup>207</sup>.

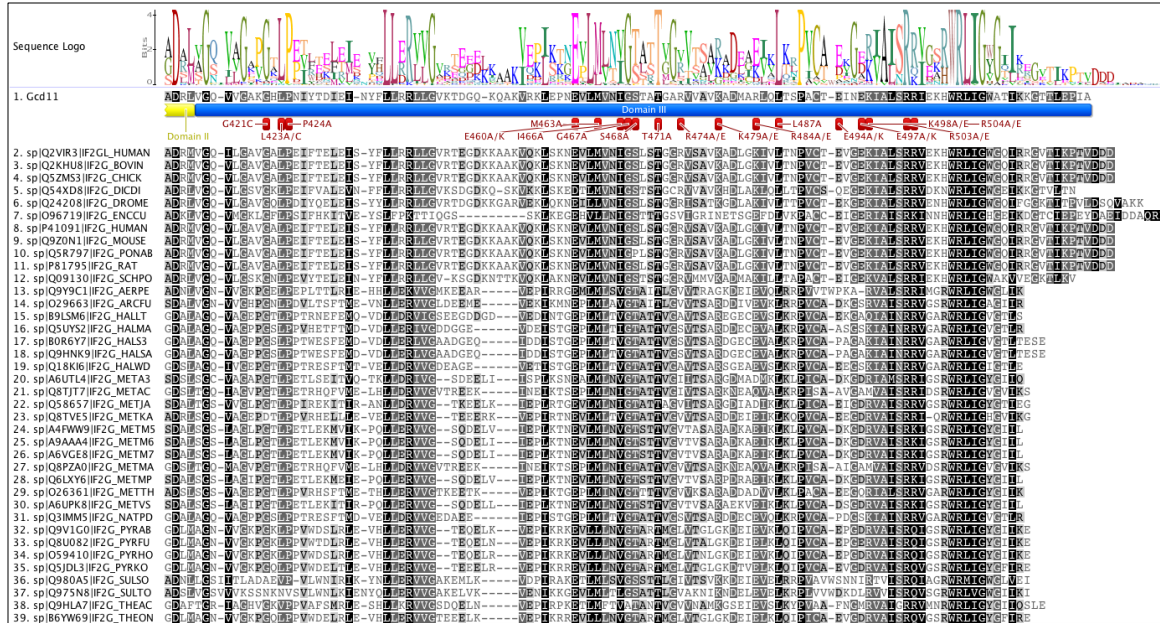


**Figure 2.23 Multiple sequence alignment of eIF2 $\gamma$  domain-III displaying the conserved surface-exposed residues selected for site-directed mutagenesis**

Conserved surface-exposed residues in domain-III were selected for site-directed mutagenesis. The residues were mutated to alanine and, when appropriate, to the residue of the opposite charge. 39 Uniprot-reviewed eukaryotic and archaeal e/aIF2 $\gamma$  sequences were aligned using the Geneious software<sup>226</sup>. Species/sequence names are standard Uniprot identifiers<sup>227</sup>.



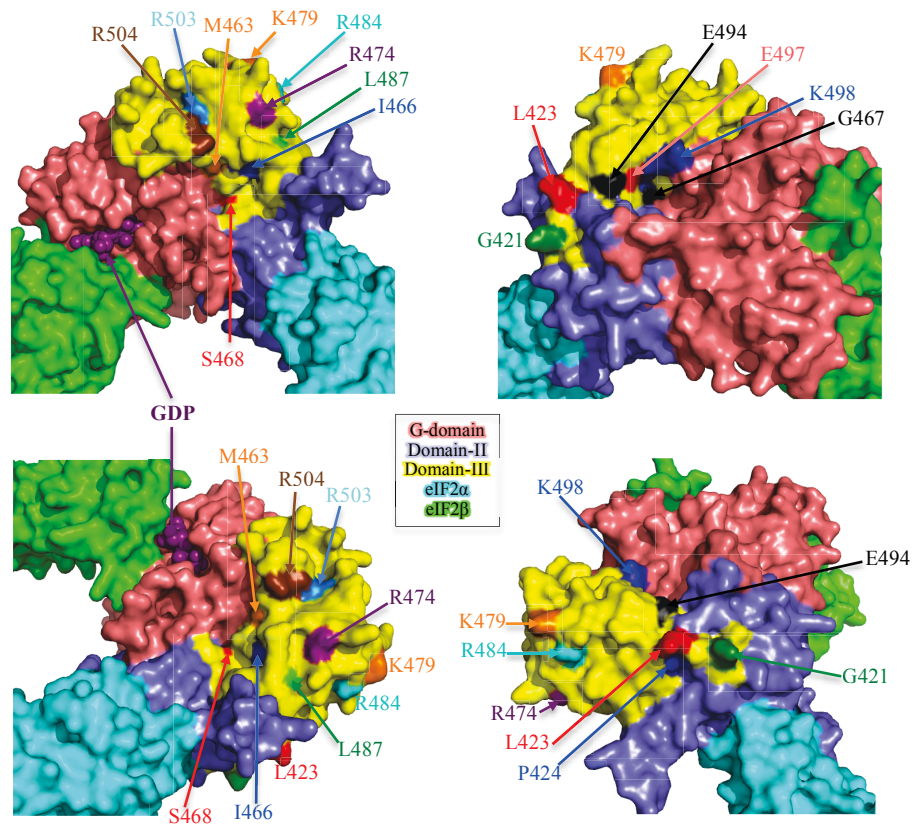
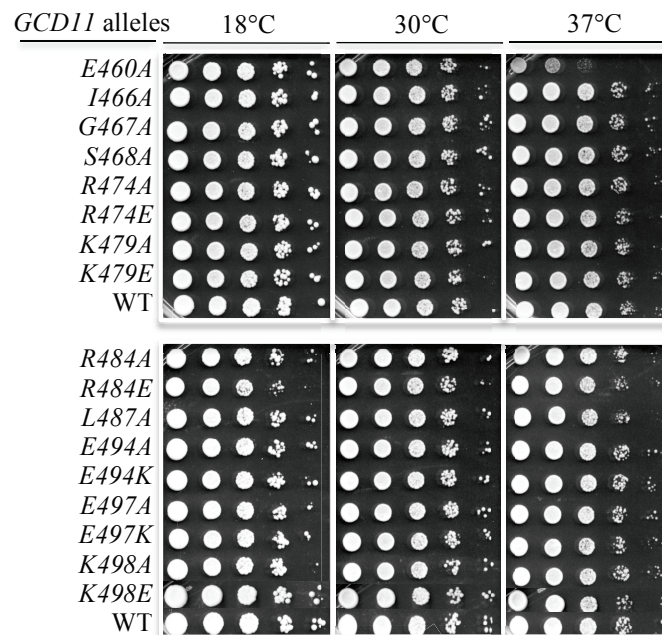


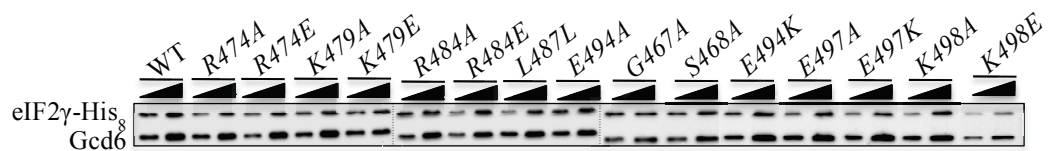
**Figure 2.24 Positions of the eIF2 $\gamma$  residues selected for site-directed mutagenesis on the crystal structure of aIF2**

Four different views displaying a surface representation of aIF2 (PDB 2QMU). eIF2 $\gamma$  residues selected for site-directed mutagenesis are marked. Images were created using the PyMOL software<sup>207</sup>.

A)



B)



C)

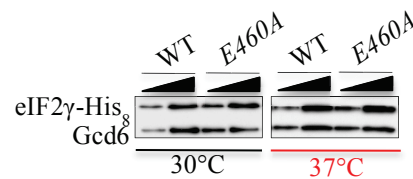


**Figure 2.25 Growth phenotypes and protein levels of *GCD11* mutations created by site-directed mutagenesis**

(A) Among all the mutations created, only *E460A* displays a TS<sup>-</sup> phenotype. Derivatives of strain NAY13 harboring the WT or mutant alleles of *GCD11* were cultured in SC-L medium, ten-fold serial dilutions were spotted on SC-L medium, and incubated at the specified temperatures for two (30°C and 37°C) and four (18°C) days. (B) Mutations do not alter the expression level of eIF2γ protein. Western blot analysis of WCEs of

exponentially growing cultures ( $OD_{600}$  of  $\sim 0.5$ ), prepared by TCA extraction, was performed with antibodies against the His<sub>6</sub> epitope (abcam) and eIF2B $\epsilon$ /Gcd6 (loading control). Same strains and growth conditions as in panel A. Two different amounts of each extract differing by a factor of 2 were loaded in successive lanes. (C) The E460A mutant variant of eIF2 $\gamma$  is stable at 37°C. Derivatives of NAY13 harboring the WT or *E460A* mutant allele of *GCD11* were cultured in SC-L medium either at 30°C or at 37°C for 4.4 generations. Western blot analysis was performed as in panel B.

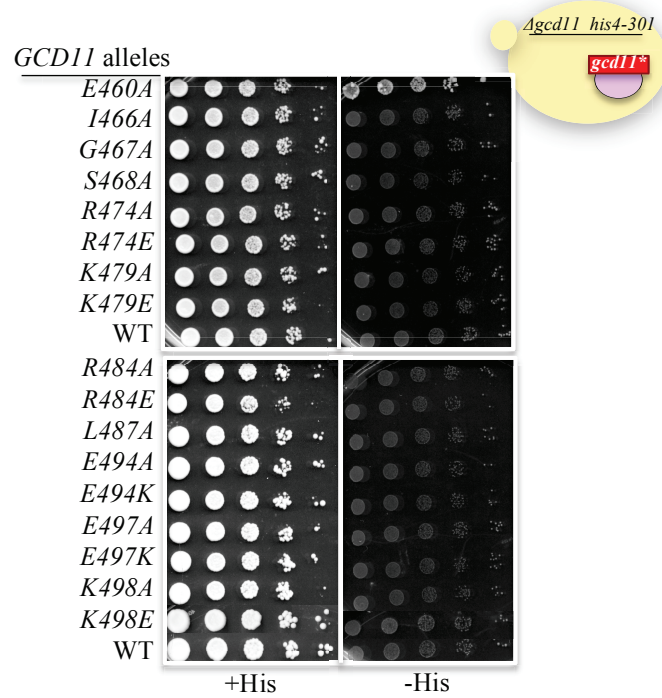


**Figure 2.26 Spot assays for His<sup>+</sup> phenotype of site-directed domain-III mutants**

Among all the point mutations generated, *E460A* displays a weak His<sup>+</sup> phenotype.

Strains (same as in Figure 2.25) were cultured in SC-L medium, ten-fold serial dilutions were spotted on SC-L medium supplemented with 0.3 mM (+His) or 0.003 mM (-His) histidine, and incubated at 30°C for two and seven days respectively.

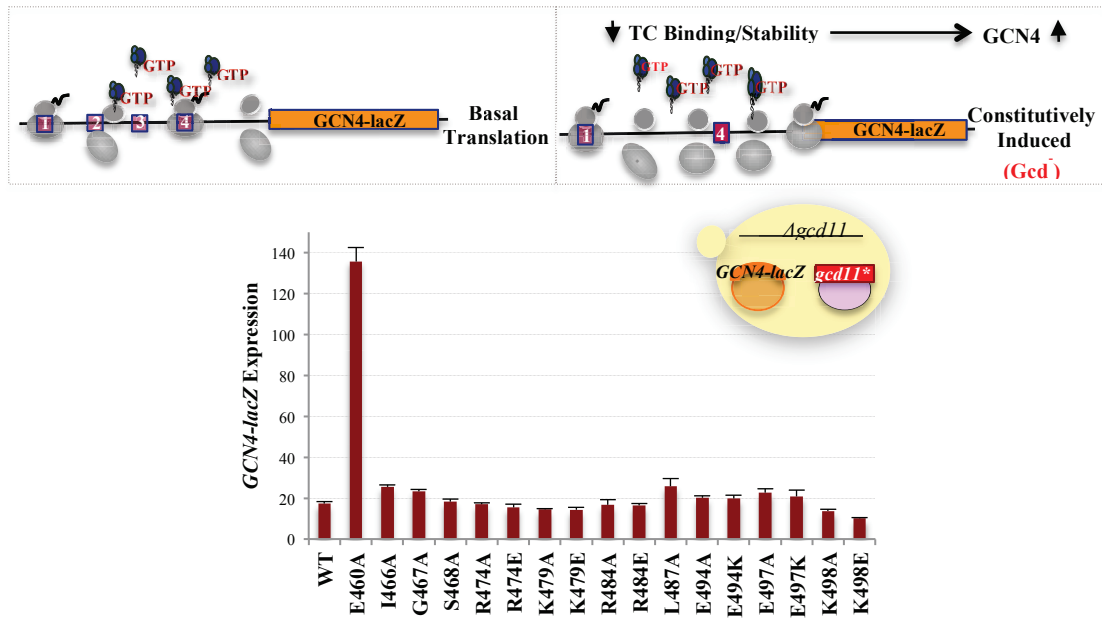


**Figure 2.27 The *E460A* allele confers a *Gcd<sup>-</sup>* phenotype**

*GCN4-lacZ* expression is used as a genetic reporter for the stability and binding of the ternary complex to the PIC. *GCN4-lacZ* mRNA is translated at low basal levels under nutrient-replete (high TC concentration) conditions. Amino acid starvation, however, leads to the induction of *GCN4-lacZ* translation. A reduction in TC stability or binding increases the translation of *GCN4-lacZ* mRNA even under non-starvation conditions, creating a *Gcd<sup>-</sup>* phenotype (schematic on top). Among the mutations generated by site-directed mutagenesis, only *E460A* creates a *Gcd<sup>-</sup>* phenotype, increasing the translation of *GCN4-lacZ* mRNA by ~7-fold in nutrient-replete conditions. Expression of *GCN4-lacZ*, with all four upstream ORFs, on a sc plasmid (p180) was measured in the derivatives of strain NAY13 harboring the WT or mutant alleles of *GCD11*.  $\beta$ -galactosidase activities (nanomoles of *o*-nitrophenyl- $\beta$ -D-galactopyranoside cleaved per minute per microgram of protein) were measured in WCEs of exponentially growing cultures (OD<sub>600</sub> ~0.5) in

SC-L-U medium. Mean of at least four independent transformants and SD (error bars) are plotted for each mutant.

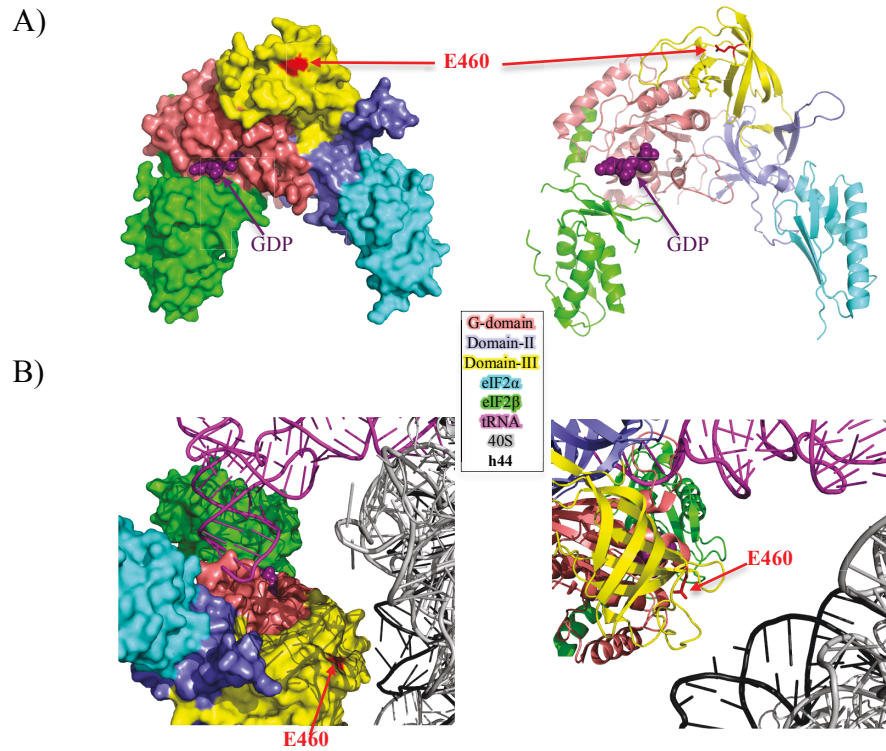
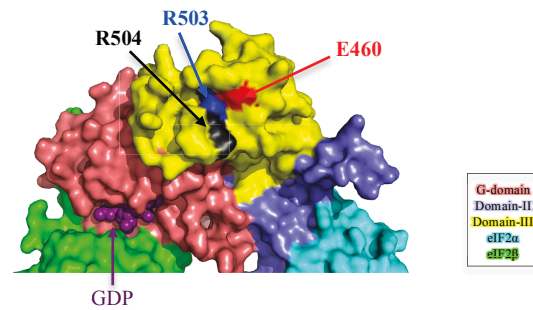


**Figure 2.28 E460 is located on the surface of domain-III in proximity of the interface between eIF2 the 40S subunit**

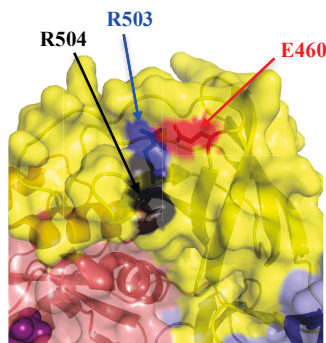
(A) Front view of a surface (left) and cartoon (right) models of aIF2 (PDB 2QMU).

E460 resides in the  $\beta$ -barrel structure of domain-III and is surface-exposed. (B) Two views of the model of eIF2 binding to the 40S subunit. E460 residue is in the proximity of the proposed interface between eIF2 and h44 of the 40S subunit. Position of the side chain of E460 is marked in the right panel. Model of TC binding to the 40S subunit is adapted from Shin et al. 2011<sup>127</sup>. Images were created using the PyMOL software<sup>207</sup>.

A)



B)



C)

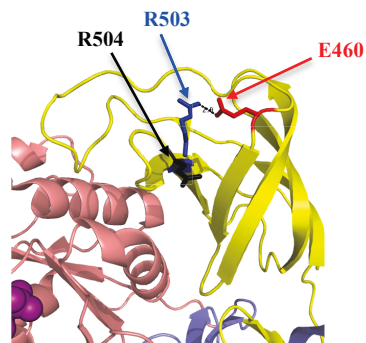


**Figure 2.29 E460 side chain interacts with the side chain of R503**

(A) Front view of a surface representation of aIF2 (PDB 2QMU). R503 and R504 residues cluster with E460 on the surface of domain-III. (B) A magnified view of panel A showing the relative positions of the three residues. Side chain of R504 projects outward from the surface (C) E460 side chain is positioned 2.9Å from the side chain of R503. Images were created using the PyMOL software<sup>207</sup>.



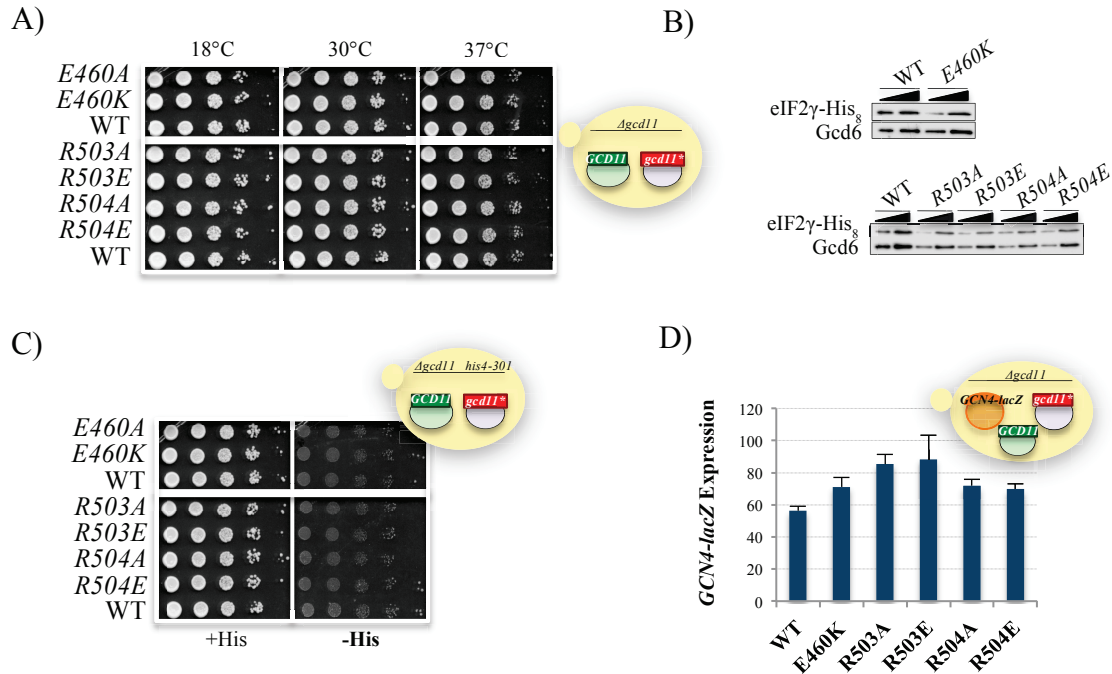


**Figure 2.30** *E460A/K*, *R503A/E*, and *R504A/E* do not display dominant growth defects,  $Gcd^-$ , or  $His^+$  phenotypes.

(A) The *E460A/K*, *R503A/K*, and *R503A/K* mutants do not display dominant  $Slg^-$  or  $TS^-$  phenotypes. Derivatives of strains NAY13 harboring a sc *TRP1 GCD11* plasmid (pNA18) and either the WT or indicated *GCD11* mutant alleles on sc *LEU2* vectors were cultured in SC-L-U, ten-fold serial dilutions were spotted on SC-L-U medium, and incubated at the specified temperatures for two (30°C and 37°C) and four (18°C) days.

(B) *E460K*, *R503A/K*, and *R504A/K* proteins are expressed at similar levels compared to the WT eIF2 $\gamma$  protein. Western blot analysis of WCEs (prepared by TCA extraction) from exponentially growing cells ( $OD_{600}$  of ~0.5) cultured in SC-L-U was performed with antibodies against His<sub>6</sub> epitope (abcam) and eIF2 $\beta$ /GCD6 (loading control). Same strains as in panel A. Two different amounts of each extract differing by a factor of 2 were loaded in successive lanes. Only the mutant *GCD11* alleles (on sc *LEU2* plasmids)

are His<sub>8</sub>-tagged; thus, only expression of the mutant proteins are depicted. (C) *E460A/K*, *R503A/K*, and *R503A/K* do not display a dominant His<sup>+</sup> phenotype. Same strains and growth conditions as in panel A except that ten-fold serial dilutions were spotted on SC-L-U medium supplemented with either 0.3 mM (+His) or 0.003 mM (-His) histidine and incubated at 30°C for two and five days, respectively. (D) The *E460A/K*, *R503A/K*, and *R503A/K* mutants do not display a dominant Gcd<sup>-</sup> phenotype. Expression of *GCN4-lacZ*, with all four upstream ORFs, on a sc plasmid (p180) was measured in strains depicted in panel A.  $\beta$ -galactosidase activities (nanomoles of *o*-nitrophenyl- $\beta$ -D-galactopyranoside cleaved per minute per microgram of protein) were measured in WCEs of exponentially growing cultures (OD<sub>600</sub> ~0.5) in SC-L-U-W. Mean of at least four independent transformants and SD (error bars) are plotted for each mutant.

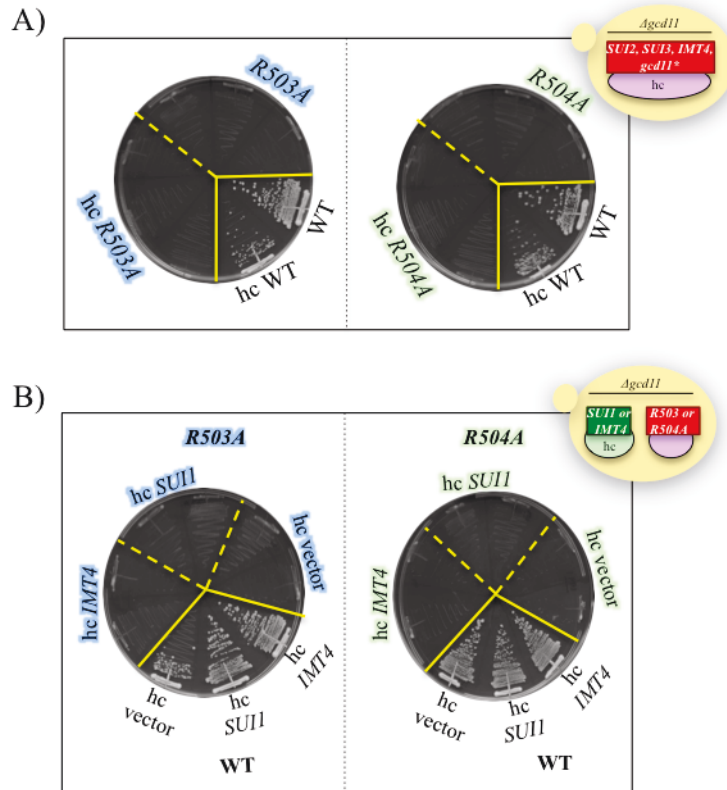


**Figure 2.31 Overexpression of eIF1, Met-tRNA<sub>i</sub>, or TC containing the R503A or R504A mutant variants of eIF2 $\gamma$  do not suppress the recessive lethality conferred by the *R503A* or *R504A* alleles**

(A) Overexpression of TC containing the eIF2 $\gamma$ -R503A or eIF2 $\gamma$ -R504A mutant proteins does not suppress the recessive lethality of strains harboring the R503A and R504 alleles. Strain NAY13 (*gcd11 $\Delta$* , *sc URA3 GCD11*) was transformed with either a *sc LEU2* plasmid expressing the WT, *R403A*, or *R504A* mutant alleles of *GCD11* (pNA4, pNA4-R503A, and pNA4-R504A, respectively) or with a *hc LEU2* plasmid co-expressing the components of the TC (*SUI2*, *SUI3*, *IMT4*, and *GCD11*, *gcd11-R503A* or *gcd11-R504A*) (pNA21, pNA24, and pNA25, respectively). Transformants were streaked on SC-L medium with 5-FOA, to select for loss of the *URA3*-containing WT *GCD11* plasmid, and incubated at 30°C for four days. (B) Overexpression of *SUI1* or *IMT4* does not suppress

the recessive lethality conferred by the *R503A* and *R504A* alleles. Derivatives of strain NAY13 harboring the WT or mutant *R503A* or *R504* alleles were transformed with hc *TRP1 SUII* (pNA19), hc *TRP1 IMT4* (pNA20), or empty hc vector (YEplac122). Transformants were streaked on SC-L-W medium with 5-FOA, to select for loss of the *URA3*-containing WT *GCD11* plasmid, and incubated at 30°C for four days.

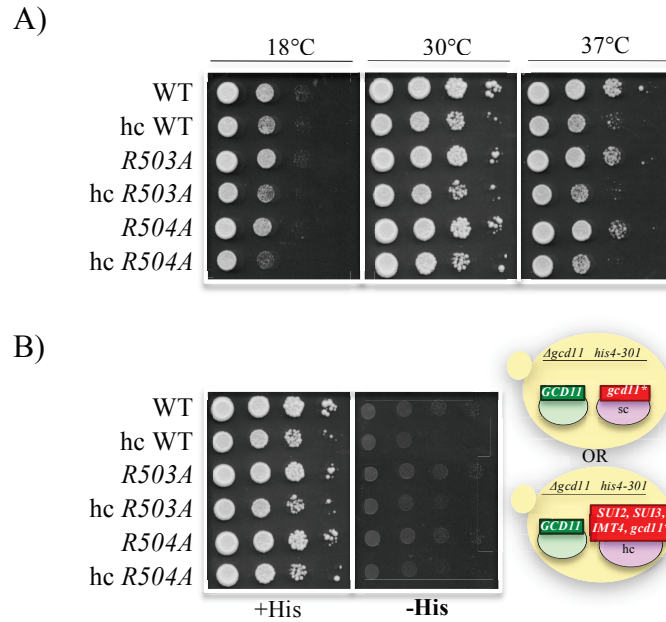


**Figure 2.32 Overexpression of TC containing the R503A or R504A mutant variants of eIF2 $\gamma$  does not create growth defects or a His<sup>+</sup> phenotype**

(A) Overexpression of TC containing the eIF2 $\gamma$ -R503A or eIF2 $\gamma$ -R504A mutant proteins does not create growth defects. NAY13 (*gcd11 $\Delta$ , his4-301, sc URA3 GCD11*) either with a *sc LEU2* plasmid harboring the WT, R503A, or R504A mutant alleles of *GCD11* (pNA4, pNA4-R503A, and pNA4-R504A, respectively) or with a *hc LEU2* vector co-expressing components of the TC (*SUI2, SUI3, IMT4, and GCD11, gcd11-R503A* or *gcd11-R504A*) (pNA21, pNA24, and pNA25, respectively) was cultured in SC-L-U medium, ten-fold serial dilutions were spotted on SC-L-U plates, and incubated at the specified temperatures for two (30°C and 37°C) and four days (18°C). (B) Overexpression of TC containing the eIF2 $\gamma$ -R503A or eIF2 $\gamma$ -R504A mutant proteins also does not create a His<sup>+</sup> phenotype. Same strains and procedures as in panel A except that ten-fold serial dilutions were spotted on SC-L-U medium supplemented with either 0.3

mM (+His) or 0.003 mM (-His) histidine and incubated at 30°C for two and five days respectively.

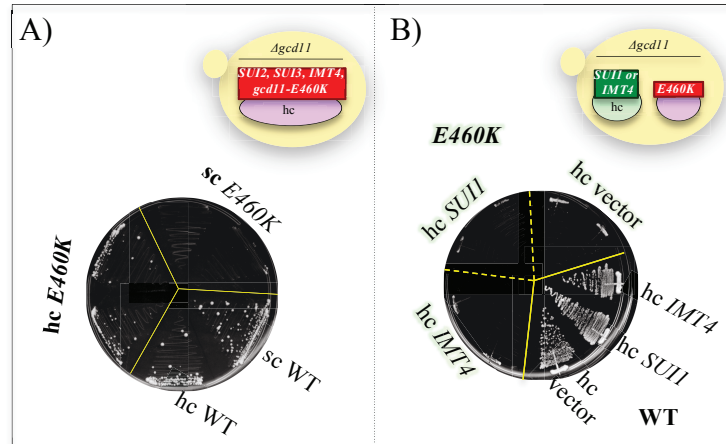


**Figure 2.33 Overexpression of TC containing the E460K substitution in eIF2 $\gamma$  rescues the severe growth defect conferred by the *E460K* allele**

(A) Cells harboring the *E460K* mutant allele of *GCD11* are extremely slow growing. Overexpression of the TC containing the eIF2 $\gamma$ -E460K mutant protein, however, partially rescues this growth defect. Strain NAY13 harboring a *sc URA3 GCD11* plasmid was transformed with either a *sc LEU2* vector expressing the WT or *E460K* mutant allele or with a *hc LEU2* vector co-expressing the components of the TC (*SUI2*, *SUI3*, *IMT4*, and *GCD11* or *gcd11-E460K*). Transformants were streaked on SC-L medium supplemented with 5-FOA to select for the loss of *URA3*-containing WT *GCD11* plasmid. (B) Overexpression of *SUI1* or *IMT4* does not suppress the extreme growth defect conferred by the *E460K* allele. Strain NAY13 harboring a *sc URA3 GCD11* plasmid was transformed with a *sc LEU2* plasmid harboring the *E460K* allele and a *hc TRP1 SUI1* (pNA19), *TRP1 IMT4* (pNA20), or empty vector (YEplac122). Transformants were then streaked on SC-L medium with 5-FOA to select for loss of the *URA3*-containing WT *GCD11* plasmid.

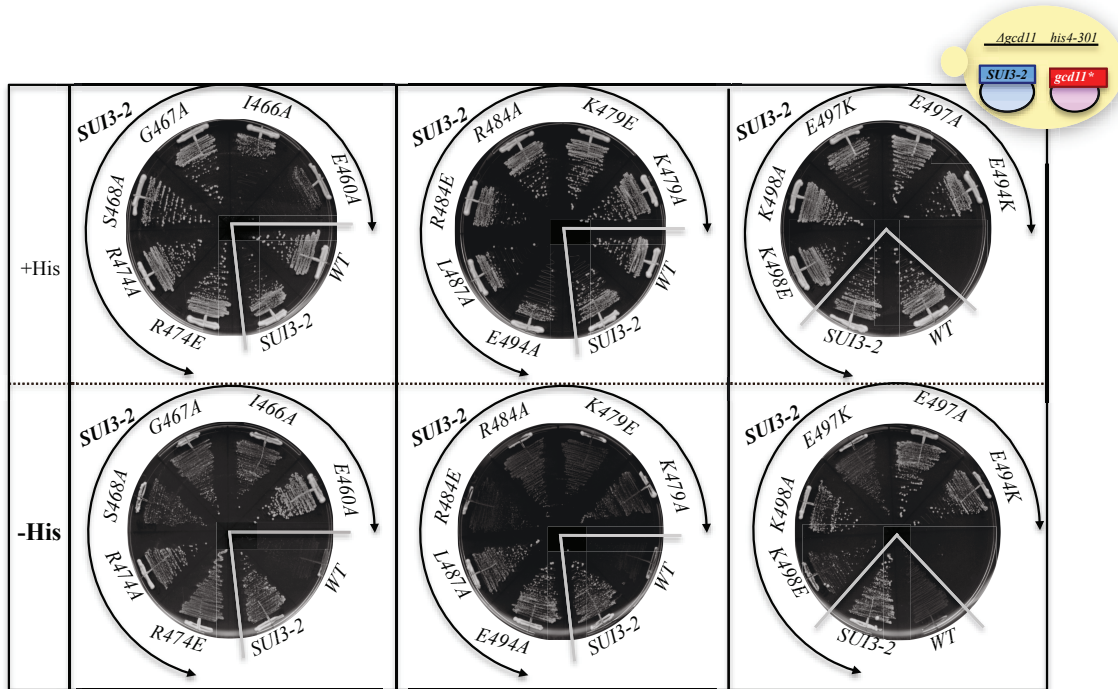


**Figure 2.34** Suppression of *SUI3-2* His<sup>+</sup> phenotype by site-directed mutations in *GCD11*

Double mutant strains harboring the *E460A*, *I466A*, *E494A*, and *E497K* mutant *GCD11* alleles and *SUI3-2* are slow growing. *E460A* enhances the His<sup>+</sup> phenotype of *SUI3-2*. *S468A*, *K479A/E*, *R484A/E*, *E497K*, and *K498E* partially suppress the His<sup>+</sup> phenotype of *SUI3-2*. Derivatives of strain NAY13 expressing the WT or indicated *GCD11* mutant alleles and harboring a sc *TRP1 SUI3-2* plasmid (p4280) were streaked on SC-L-W medium supplemented with either 0.3 mM (+His) or 0.0015 mM (-His) histidine and incubated at 30°C for three and six days respectively.



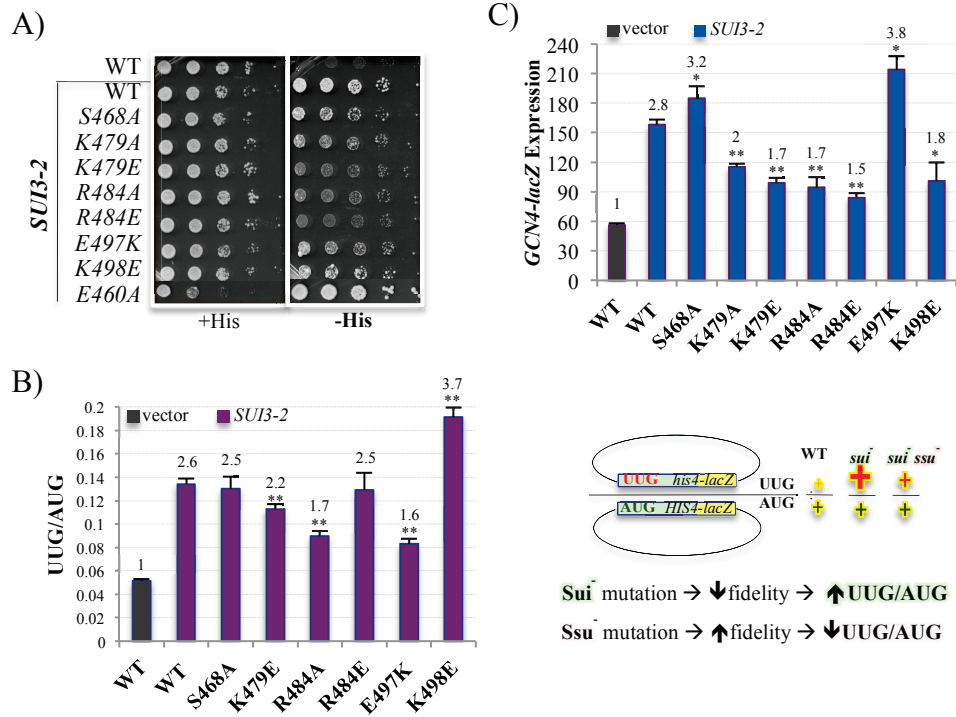


**Figure 2.35** Suppression of *SUI3-2* His<sup>+</sup>, Sui<sup>-</sup>, and Gcd<sup>-</sup> phenotypes by the *GCD11* mutants created by site-directed mutagenesis

(A) The mutant alleles of *GCD11*, generated by site-directed mutagenesis, display a range in suppressing the His<sup>+</sup> phenotype of *SUI3-2*, with *K479E*, *R484A*, and *R484E* fully suppressing, *K479A* and *E497E* partially suppressing, and *S468A* and *K498E* weakly suppressing the His<sup>+</sup> phenotype. Derivatives of NAY13 (*gcd11*Δ, *his4-301*) harboring the WT or indicated *GCD11* alleles with a sc *TRP1 SUI3-2* plasmid (p4280) were cultured in SC-L-W, ten-fold serial dilutions were spotted on SC-L-W medium supplemented with either 0.3 mM (+His) or 0.00075 mM (-His) histidine, and incubated at 30°C for two and five days, respectively. (B) *R484A* and *E497K* partially suppress the elevated ratio of initiation from a UUG codon to that from an AUG codon in cells expressing the *SUI3-2* allele. UUG/AUG ratio was calculated by measuring the β-galactosidase activity from matched *HIS4-lacZ* reporters containing either an AUG or a

UUG codon.  $\beta$ -galactosidase activities (nanomoles of *o*-nitrophenyl- $\beta$ -D-galactopyranoside cleaved per minute per microgram of protein) were measured in WCEs of exponentially growing cultures ( $OD_{600} \sim 0.5$ ) in SC-L medium. Mean of at least eight independent transformants and SEM (error bars) are plotted for each mutant. The schematics of the reporters used are presented on the right. (C) *K479A/E*, *R484A/E*, and *K498E* partially suppress and *K479A* does not alter whereas *S468A* and *E497K* slightly increase the  $Gcd^-$  phenotype conferred by the *SUI3-2* allele. Expression of *GCN4-lacZ*, with all four upstream ORFs, on a sc plasmid (p180) was measured in cells harboring the WT or the mutant alleles of *GCD11* in the presence of episomal *SUI3-2*.  $\beta$ -galactosidase activities (nanomoles of *o*-nitrophenyl- $\beta$ -D-galactopyranoside cleaved per minute per microgram of protein) were measured in the WCEs of exponentially growing cultures ( $OD_{600} \sim 0.5$ ) in SC-L-W medium. Mean of at least eight independent transformants and SEM (error bars) are plotted for each mutant. A student *t*-test was performed to determine significance (\* $p < 0.05$ , \*\* $p < 0.01$ ).

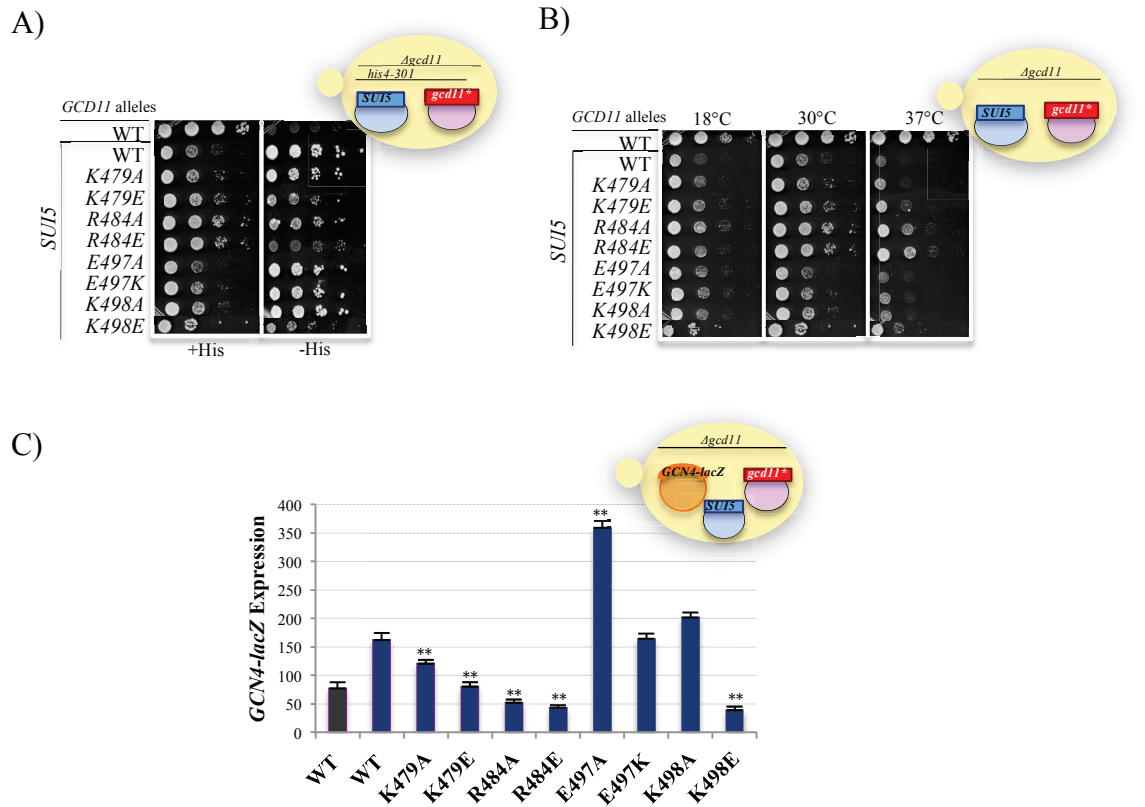


**Figure 2.36 Suppression of *SUI5* Slg<sup>-</sup>, His<sup>+</sup>, and Gcd<sup>-</sup> phenotypes by the *GCD11* mutants created by site-directed mutagenesis**

(A) *K479E*, *R484A*, *R484E*, and *K498E* partially suppress the His<sup>+</sup> phenotype of *SUI5*.

Derivatives of NAY13 (*gcd11Δ*, *his4-301*) harboring the WT or indicated *GCD11* alleles with a sc *TRP1 SUI5* plasmid (p4281) were cultured in SC-L-W, ten-fold serial dilutions were spotted on SC-L-W medium supplemented with either 0.3 mM (+His) or 0.00075 mM (-His) histidine, and incubated at 30°C for two and five days, respectively. (B)

*R484A* and *R484E* partially suppress the Slg<sup>-</sup> and TS<sup>-</sup> phenotypes of *SUI5*. Same strains and growth conditions as in panel A, except that ten-fold serial dilutions were spotted on SC-L-W medium and incubated at the specified temperatures for two (30°C and 37°C) and four (18°C) days. (C) Whereas the *K479E*, *R484A*, *R484E*, and *K498E* mutants suppress and *E497A* increases (by ~2-fold) the Gcd<sup>-</sup> phenotype of *SUI5*, the *E497K* and *K498A*

mutants do not alter the derepression of *GCN4-lacZ* in cells harboring the *SUI5* allele. Expression of *GCN4-lacZ*, with all four upstream ORFs, on a sc plasmid (p180) was measured in cells harboring the WT or mutant alleles of *GCD11* in the presence of episomal *SUI5*.  $\beta$ -galactosidase activities (nanomoles of *o*-nitrophenyl- $\beta$ -D-galactopyranoside cleaved per minute per microgram of protein) were measured in the WCEs of exponentially growing cultures ( $OD_{600} \sim 0.5$ ) in SC-L-W medium. Mean of at least eight independent transformants and SEM (error bars) are plotted for each mutant. A student *t*-test was performed to determine significance (\*\* $p < 0.01$ ).

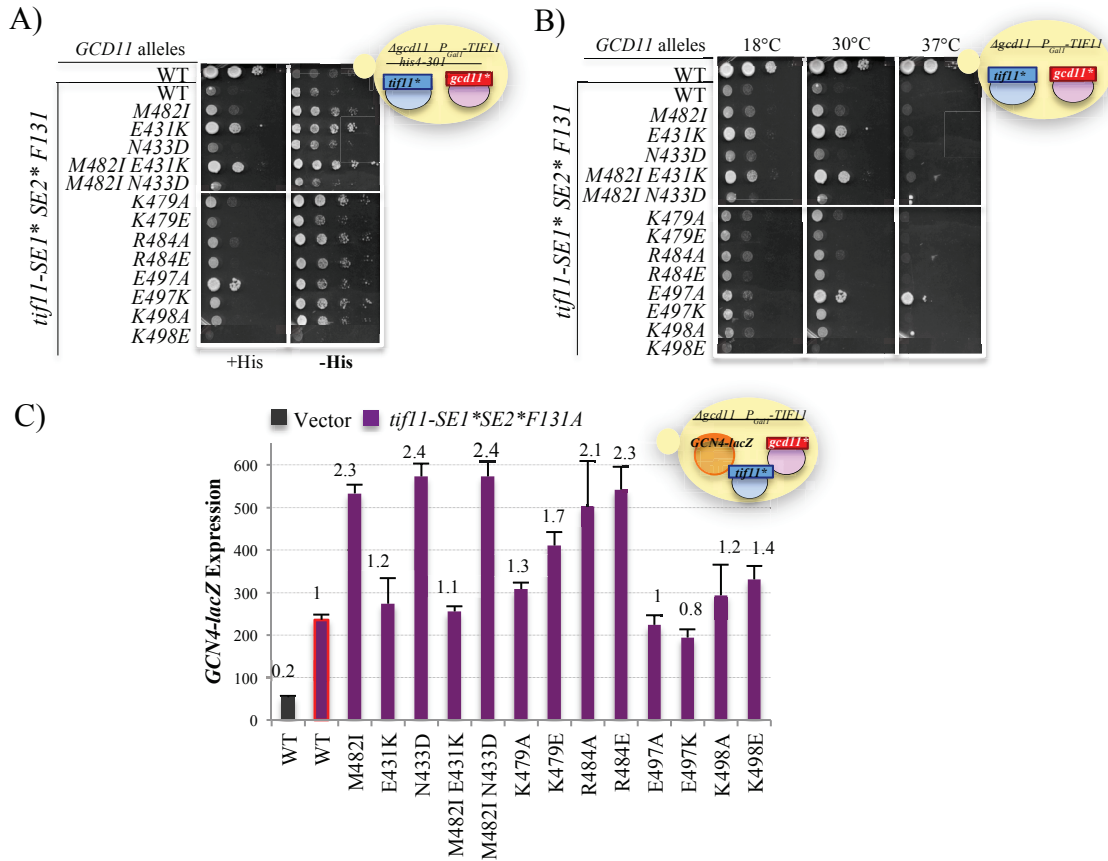


**Figure 2.37** Suppression of *tif11-SE1\*SE2\*F131*  $Slg^-$ ,  $His^+$ , and  $Gcd^-$  phenotypes by the *GCD11* mutants

(A) The *GCD11* mutants do not alter the  $His^+$  phenotype of *tif11-SE1\*SE2\*F131*.

Derivatives of strain NAY74 (*gcd11Δ*, *his4-301*, *P<sub>GALI</sub>-TIF11*) harboring the WT or indicated mutant *GCD11* alleles with either a sc *tif11-SE1\*SE2\*F131 TRP1* plasmid (pAS5-130) or a WT *TIF11 TRP1* plasmid (pAS5-148) were cultured in SC-L-W, ten-fold serial dilutions were spotted on SC-L-W medium supplemented with either 0.3 mM (+His) or 0.0015 mM (-His) histidine, and incubated at 30°C for two and six days, respectively. The *M482I/E431K* and *M482I/N433D* alleles were created by site-directed mutagenesis as described in Figure 2.10. (B) *E431K* and *E497A* partially suppress the  $Slg^-$ , but only *E497A* weakly suppresses the  $TS^-$  phenotype of the *tif11-SE1\*SE2\*F131*

*Sui*<sup>-</sup> mutation whereas *K498E* exacerbates the *Slg*<sup>-</sup>. Same strains and conditions as in panel A, except that ten-fold serial dilutions were spotted on SC-L-W medium, and incubated at the specified temperatures for two (30°C and 37°C) and four (18°C) days.

(C) *M482I*, *N433D*, *R484A*, and *R484E* increase the *Gcd*<sup>-</sup> phenotype of *tif11-SE1\*SE2\*F131* by over 2-fold. Expression of *GCN4-lacZ*, with all four upstream ORFs, on a sc plasmid (p180) was measured in the same strains as in panel A.  $\beta$ -galactosidase activities (nanomoles of *o*-nitrophenyl- $\beta$ -D-galactopyranoside cleaved per minute per microgram of protein) were measured in the WCEs of exponentially growing cultures ( $OD_{600} \sim 0.5$ ) in SC-L-U-W medium. Mean of at least eight independent transformants and SEM (error bars) are plotted for each mutant.

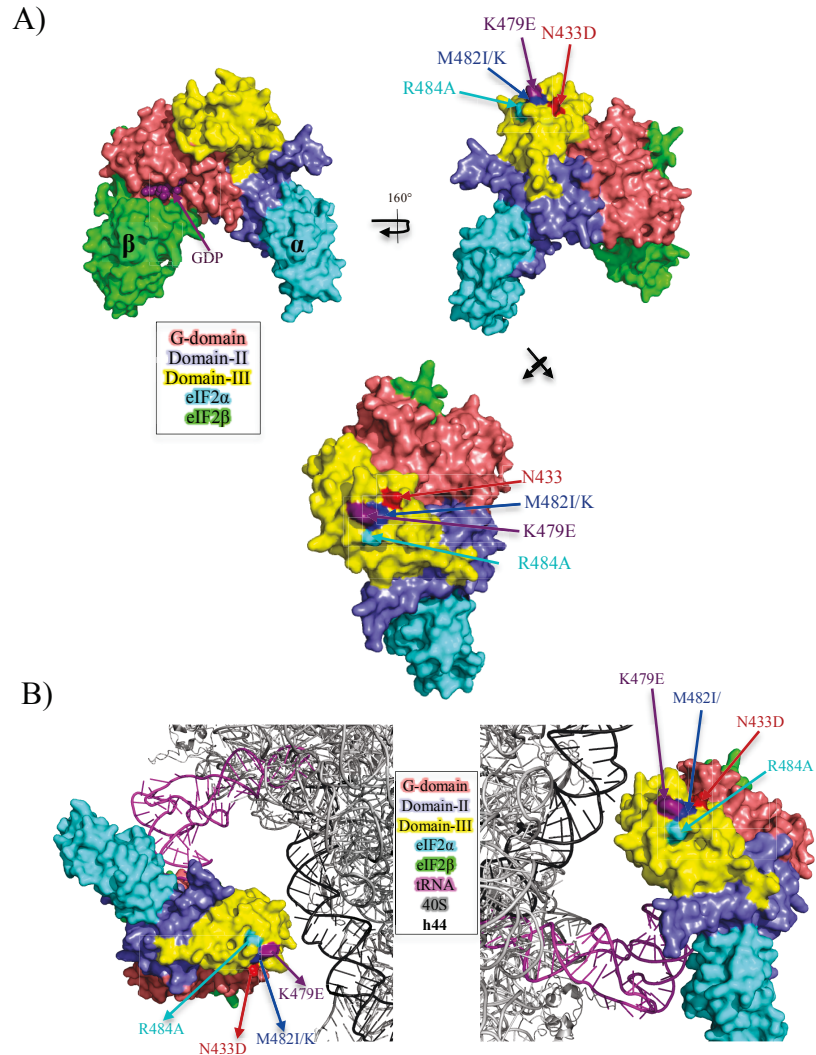


**Figure 2.38 The *Ssu<sup>-</sup>* substitutions in eIF2 $\gamma$  localize to a discrete region on the surface of domain-III**

(A) Three different views of a surface representation of eIF2 (PDB 2QMU). Bona fide *Ssu<sup>-</sup>* mutations, which were isolated from a pool of randomly mutated *GCD11* alleles or site-directed mutagenesis and suppress the *His<sup>+</sup>*, *Sui<sup>-</sup>*, and *Gcd<sup>-</sup>* phenotypes of *SUI3-2*, cluster to a distinct area in domain-III of eIF2 $\gamma$  with their side chains extending toward the surface. (B) The *Ssu<sup>-</sup>* mutations of *GCD11*, isolated from a library of randomly mutated alleles or site-directed mutagenesis, localize to a surface-exposed area in

proximity of the proposed interface between eIF2 and h44 of the 40S subunit. Model of TC binding to the 40S subunit adapted from Shin et al. 2011<sup>127</sup>. Images were created using the PyMOL software<sup>207</sup>.



**Table 2.1 List of *S. cerevisiae* Strains**

<b>Strain</b>	<b>Genotype</b>	<b>Source</b>
EY647	<i>Mata ura3-52 leu2-3,112 ino1-13 his4-301(ACG) gcd11Δ::hisG Ep293&lt;GCD11 URA3 CEN4/ARS1&gt;</i>	223
JCY04	<i>MATa ura3-52 leu2-3 leu2-112 trp1Δ-63 his4-301(ACG)-myc10::KanMX sui1Δ::hisG p1200&lt;sc URA3 SUI1&gt;</i>	228
H4	<i>Mata leu2-3 leu2-112 ura3-52</i>	A. Hinnebusch
NAY7	<i>Mata ura3-52 leu2-3,112 ino1-13 his4-301(ACG) gcd11Δ::hisG Ep517&lt;GCD11 LEU2 CEN/ARS&gt;</i>	This Study
NAY11	<i>Mata ura3-52 leu2-3,112 ino1-13 his4-301(ACG) gcd11Δ::hisG Δtrp1::hisG Ep517&lt;GCD11 LEU2 CEN/ARS&gt;</i>	This Study
NAY13	<i>Mata ura3-52 leu2-3,112 ino1-13 his4-301(ACG) gcd11Δ::hisG trp1Δ::hisG Ep293&lt;GCD11 URA3 CEN4/ARS1&gt;</i>	This Study
NAY17	<i>Mata ura3-52 leu2-3,112 ino1-13 his4-301(ACG) gcd11Δ::hisG trp1Δ::hisG kanMX6-pGAL1-TIF5 Ep293&lt;GCD11 URA3 CEN4/ARS1&gt;</i>	This Study
NAY25	<i>Mata ura3-52 leu2-3,112 ino1-13 his4-301(ACG) gcd11Δ::hisG trp1Δ::hisG kanMX6-pGAL1-TIF5 Ep293&lt;GCD11 URA3 CEN4/ARS1&gt; p4281&lt;TIF5-G31R TRP1 CEN&gt;</i>	This Study
NAY41	<i>Mata ura3-52 leu2-3,112 ino1-13 his4-301(ACG) gcd11Δ::hisG trp1Δ::hisG kanMX6-pGAL1-TIF5 Ep293&lt;GCD11 URA3 CEN4/ARS1&gt; p1990&lt;TRP1 CEN4/ARS&gt;</i>	This Study
NAY45	<i>Mata ura3-52 leu2-3,112 ino1-13 his4-301(ACG) gcd11Δ::hisG trp1Δ::hisG kanMX6-pGAL1-TIF5 Ep293&lt;GCD11 URA3 CEN4/ARS1&gt; p4280&lt;SUI3-2 TRP1 CEN&gt;</i>	This Study
NAY64	<i>Mata ura3-52 leu2-3,112 ino1-13 HIS4(AUG)-myc<sub>10</sub>-kanMx6 gcd11Δ::hisG trp1Δ::hisG Ep293&lt;GCD11 URA3 CEN4/ARS1&gt;</i>	This Study
NAY66	<i>Mata ura3-52 leu2-3,112 ino1-13 his4-301(UUG)- myc<sub>10</sub>-kanMx6 gcd11Δ::hisG trp1Δ::hisG Ep293 &lt;GCD11 URA3 CEN4/ARS1&gt;</i>	This Study
NAY74	<i>Mata ura3-52 leu2-3,112 ino1-13 his4-301(ACG) gcd11Δ::hisG trp1Δ::hisG KanMX-pGAL1-TIF11 Ep293&lt;GCD11 URA3 CEN4/ARS1&gt;</i>	This Study
NAY93	<i>Mata ura3-52 leu2-3,112 ino1-13 his4-301(ACG) gcd11Δ::hisG trp1Δ::hisG pNA4&lt;GCD11-His<sub>8</sub> LEU2 CEN4/ARS1&gt;</i>	This Study

**Table 2.2 List of Plasmids**

<b>Plasmid</b>	<b>Description<sup>a</sup></b>	<b>Source</b>
YCplac111	sc <i>LEU2</i> yeast- <i>E. coli</i> shuttle vector	229
YCplac22	sc <i>TRP1</i> yeast- <i>E. coli</i> shuttle vector	229
YCP50	sc <i>URA3</i> yeast- <i>E. coli</i> shuttle vector	230
pSB32	lc <i>LEU2</i> yeast- <i>E. coli</i> shuttle vector	
YEplac122	hc <i>TRP1</i> yeast- <i>E. coli</i> shuttle vector	229
YEplac181	hc <i>LEU2</i> yeast- <i>E. coli</i> shuttle vector	229
pRS425	hc <i>LEU2</i> yeast- <i>E. coli</i> shuttle vector	231
Ep293	sc <i>URA3 GCD11</i> in YCP50	223
Ep517	lc <i>LEU2 GCD11</i> in pSB32	223
pC2872	sc <i>LEU2 GCD11-His<sub>8</sub></i> in YCplac111	P. Alone
pNA4	sc <i>LEU2 GCD11-His<sub>8</sub></i> in pC2872	This study
p4281	sc <i>TRP1 TIF5-G31R</i> in YCplac22	81
p4280	sc <i>TRP1 SUI3-S264Y</i> in YCplac22	81
p367	sc <i>URA3 HIS4(ATG)-lacZ</i>	209
p391	sc <i>URA3 HIS4(TTG)-lacZ (his4-301)</i>	209
p180	sc <i>URA3 GCN4-lacZ</i> in YCp50	232
pM226 (p4164)	sc <i>URA3 GCN4-lacZ</i> with elongated uORF1 extending into <i>GCN4</i>	233
pPMB24	sc <i>URA3 SUI1-lacZ</i> in YCP50	234
pPMB25	sc <i>URA3 SUI1<sub>opt</sub>-lacZ</i> in YCP50	234
pPMB28	sc <i>URA3 SUI1<sub>UUU</sub>-lacZ</i> in YCP50	234
pCFB04	hc <i>LEU2 SUI1</i> in YEplac181	97
pAS5-148 (p5366)	sc <i>TRP1 TIF11</i> in YCplac22	A. Saini
pAS5-130 (p5312)	sc <i>TRP1 tif11-SE1*-SE2*-F131</i> in YCplac22	A. Saini
pNA4-A6a	sc <i>LEU2 gcd11-His<sub>8</sub>-M482K</i>	This study
pNA4-A8b	sc <i>LEU2 gcd11-His<sub>8</sub>-F297S,D481E</i>	This study
pNA4-B2d	sc <i>LEU2 gcd11-His<sub>8</sub>-M482K,T488M</i>	This study
pNA4-B6a	sc <i>LEU2 gcd11-His<sub>8</sub>-M482I</i>	This study
pNA4-C1c	sc <i>LEU2 gcd11-His<sub>8</sub>-E431K</i>	This study
pNA4-C3a	sc <i>LEU2 gcd11-His<sub>8</sub>-L423M,D481H</i>	This study
pNA4-D1a	sc <i>LEU2 gcd11-His<sub>8</sub>-N433D</i>	This study
pNA4-D2c	sc <i>LEU2 gcd11-His<sub>8</sub>-N290S,M482K</i>	This study
pNA4-MK	sc <i>LEU2 gcd11-His<sub>8</sub>-M484I,E431K</i>	This study
pNA4-ME	sc <i>LEU2 gcd11-His<sub>8</sub>-M482I,N433D</i>	This study
pNA4-G421C	sc <i>LEU2 gcd11-His<sub>8</sub>-G421C</i>	This study
pNA4-L423A	sc <i>LEU2 gcd11-His<sub>8</sub>-L423A</i>	This study
pNA4-P424A	sc <i>LEU2 gcd11-His<sub>8</sub>-P424A</i>	This study
pNA4-E460A	sc <i>LEU2 gcd11-His<sub>8</sub>-E460A</i>	This study
pNA4-E460K	sc <i>LEU2 gcd11-His<sub>8</sub>-E460K</i>	This study
pNA4-M463A	sc <i>LEU2 gcd11-His<sub>8</sub>-M463A</i>	This study
pNA4-I466A	sc <i>LEU2 gcd11-His<sub>8</sub>-I466A</i>	This study
pNA4-G467A	sc <i>LEU2 gcd11-His<sub>8</sub>-G467A</i>	This study
pNA4-S468A	sc <i>LEU2 gcd11-His<sub>8</sub>-S468A</i>	This study
pNA4-T471A	sc <i>LEU2 gcd11-His<sub>8</sub>-T471A</i>	This study
pNA4-R474A	sc <i>LEU2 gcd11-His<sub>8</sub>-R474A</i>	This study
pNA4-R474E	sc <i>LEU2 gcd11-His<sub>8</sub>-R474E</i>	This study
pNA4-K479A	sc <i>LEU2 gcd11-His<sub>8</sub>-K479A</i>	This study
pNA4-K479E	sc <i>LEU2 gcd11-His<sub>8</sub>-K479E</i>	This study
pNA4-R484A	sc <i>LEU2 gcd11-His<sub>8</sub>-R484A</i>	This study
pNA4-R484E	sc <i>LEU2 gcd11-His<sub>8</sub>-R484E</i>	This study
pNA4-L487A	sc <i>LEU2 gcd11-His<sub>8</sub>-L487A</i>	This study
pNA4-E494A	sc <i>LEU2 gcd11-His<sub>8</sub>-E494A</i>	This study

<b>Plasmid</b>	<b>Description<sup>a</sup></b>	<b>Source</b>
pNA4-E494K	sc <i>LEU2 gcd11-His<sub>8</sub>-E494K</i>	This study
pNA4-E497A	sc <i>LEU2 gcd11-His<sub>8</sub>-E497A</i>	This study
pNA4-E497K	sc <i>LEU2 gcd11-His<sub>8</sub>-E497K</i>	This study
pNA4-K498A	sc <i>LEU2 gcd11-His<sub>8</sub>-K498A</i>	This study
pNA4-K498E	sc <i>LEU2 gcd11-His<sub>8</sub>-K498E</i>	This study
pNA4-R503A	sc <i>LEU2 gcd11-His<sub>8</sub>-R503A</i>	This study
pNA4-R503E	sc <i>LEU2 gcd11-His<sub>8</sub>-R503E</i>	This study
pNA4-R504A	sc <i>LEU2 gcd11-His<sub>8</sub>-R504A</i>	This study
pNA4-R504E	sc <i>LEU2 gcd11-His<sub>8</sub>-R504E</i>	This study
pNA18	sc <i>TRP1 GCD11</i> in YCplac22	This study
pNA19	hc <i>TRP1 SUI1</i> in YEplac122	This study
pNA20	hc <i>TRP1 IMT4</i> in YEplac122	This study
pAV1732	hc <i>LEU2 GCD11-His<sub>6</sub> SUI3 SUI2 IMT4</i> in pRS425	G. Pavitt
pNA21	hc <i>LEU2 GCD11-His<sub>8</sub> SUI3 SUI2 IMT4</i> in pAV1732	This study
pNA23	hc <i>LEU2 gcd11-His<sub>8</sub>-E460K SUI3 SUI2 IMT4</i> in pNA21	This study
pNA24	hc <i>LEU2 gcd11-His<sub>8</sub>-R503A SUI3 SUI2 IMT4</i> in pNA21	This study
pNA25	hc <i>LEU2 gcd11-His<sub>8</sub>-R504A SUI3 SUI2 IMT4</i> in pNA21	This study

<sup>a</sup> sc: single copy number; hc: high copy number; lc: low copy number

**Table 2.3 List of Primers**

<b>Primer</b>	<b>Sequence</b>	<b>Usage</b>
CHA209 <sup>a</sup>	<i>CCAACCTATGGTTACGCTAGGC</i>	Generation of strain NAY66
CHA210 <sup>a</sup>	<i>CGCTATTGATACCCACTCTTGC</i>	
PM-18 <sup>b</sup>	<i>GAGCATTGCGATACGATGGG</i>	Generation of strain NAY64
PM-19 <sup>b</sup>	<i>CGGTCTGT ACGTACTTCACC</i>	
g_NcoI.F1	<i>GCAGTGGTTTCCATGGTTCCTTAAGCGATGGG</i>	SDM <sup>c</sup> , to create NcoI site at 3' end of <i>GCD11</i> CDS <sup>d</sup>
g_NcoI.F2	<i>CCCATCGCTTAAGGAACCATGGAAACCACTGC</i>	
g_KpnI.F1	<i>GGCGACATGACCGATCGTTCGATGTTTATTGTAGC</i>	SDM, to remove first internal KpnI site in <i>GCD11</i> CDS
g_KpnI.R1	<i>GCTACAATAAACATCGGAACGATCGGTCATGTCGCC</i>	
IMT4_HindIII.F1	<i>GACATTGCAAAGCTTTGCCCAAATGAGCCAAATGCCA</i>	To amplify <i>IMT4</i> gene for insertion into HindIII site of YEplac122
IMT4_HindIII.R1	<i>GACATTGCAAAGCTTGCCGTAGACGGCCTATTTTCATTGC</i>	
GCD11_L1.F1	<i>TCGCGCATTAGAGGTAGACA</i>	Generation of L1 library
GCD11_L1.R1	<i>TGGTGGTACGGGAATAGTCT</i>	
GCD11_L2.F1	<i>AGGTCGATTTAATGCGTGAAGA</i>	Generation of L2 library
GCD11_L2.R1	<i>GTTTCCCTTCCTCCTAGCCC</i>	
TIF5_pGAL.F	<i>CTACATTAAGAGTATCTCGTGTGTTCTTTTTTTTTC CGAATTCGAGCTCGTTAAAC</i>	<i>TIF5</i> promoter replacement
TIF5_pGAL.R	<i>GTAATAATGGATCATGATTATCTCTACAAATATTAATAGA CATTTTGAGATCCGGGTTTT</i>	
TIF5.F2	<i>CGTCACATATACATAAGCTC</i>	Verification of <i>TIF5</i> promoter replacement
TIF5.R2	<i>GAGCACCTAATTCGAAACCA</i>	
g_Q415L.F	<i>GATCGTCTTGTCGGTCTAGTCGTCGGTGCTAAG</i>	SDM, Q415L
g_Q415L.R	<i>CTTAGCACCGGACTAGACCGACAAGACGATC</i>	
g_V416A.F	<i>GATCGTCTTGTCGGTCAAGCTGTCGGTGCTAAGGG</i>	SDM, V416A
g_V416A.R	<i>CCCTTAGCACCGGACTGACCGACAAGACGATC</i>	
g_V417L.F	<i>CGTCTTGTCGGTCAAGTCTCGGTGCTAAGGG</i>	SDM, V417L
g_V417L.R	<i>CCCTTAGCACCGGACTGACCGACAAGACG</i>	
g_G418C.F	<i>CTTGTCGGTCAAGTCTGTCGCTAAGGGTCATTTGC</i>	SDM, G418C
g_G418C.R	<i>GCAAATGACCCCTAGCACAGACTGACCGACAAG</i>	
g_G421C.F	<i>GTCGTCGGTGTAAAGTGTCATTTGCCAAAC</i>	SDM, G421C
g_G421C.R	<i>GTTTGGCAAATGACACTTAGCACCGGACGAC</i>	
g_L423A.F	<i>CGGTGCTAAGGGTCAATGCTCCAAACATTTATACTG</i>	SDM, L423A
g_L423A.R	<i>CAGTATAAATGTTTGGAGCATGACCCTTAGCACCG</i>	
g_L423M.F	<i>GGTTGCCGTTAAAGCTCATATGGCAAGATTACAG</i>	SDM, L423M
g_L423M.R	<i>CTGTAATCTTGCCATATGAGCTTTAACGGCAACC</i>	
g_P424A.F	<i>GGTGCTAAGGGTCATTTGGCTAACATTTATACTG</i>	SDM, P424A
g_P424A.R	<i>CAGTATAAATGTTAGCCAAATGACCCCTTAGCACC</i>	
g_E460A.F	<i>GAAAATTAGAGCCAAATGCTGTTCTTATGGTCAAC</i>	SDM, E460A
g_E460A.R	<i>GTTGACCATAAGAAGCAGCATTTGGCTCTAATTTTC</i>	
g_E460K.F	<i>GAAAATTAGAGCCAAATAAAGTTCTTATGGTCAAC</i>	SDM, E460K
g_E460K.R	<i>GTTGACCATAAGAATTTATTTGGCTCTAATTTTC</i>	
g_M463A.F	<i>CCAAATGAAGTTCTTGCTGTCAACATTGGTTCTACC</i>	SDM, M463A
g_M463A.R	<i>GGTAGAACCAATGTTGACAGCAAGAATTCATTTGG</i>	
g_I466A.F	<i>GTTCTTATGGTCAACGCTGGTTCTACCGCTACGGGGG</i>	SDM, I466A
g_I466A.R	<i>CCCCCGTAGCGGTAGAACCAGCGTTGACCATAAGAA</i>	
g_G467A.F	<i>CTTATGGTCAACATTGCTTCTACCGCTACGG</i>	SDM, G467A
g_G467A.R	<i>CCGTAGCGGTAGAAGCAATGTTGACCATAAG</i>	
g_S468A.F	<i>CTTATGGTCAACATTGGTGCTACCGCTACGGGGG</i>	SDM, S468A
g_S468A.R	<i>CCCCCGTAGCGGTAGACCAATGTTGACCATAAG</i>	

<b>Primer</b>	<b>Sequence</b>	<b>Usage</b>
g_T471A.F	<i>CATTGGTTCTACCGCTGCTGGGGCTCGTGTGG</i>	SDM, T471A
g_T471A.R	<i>CCACACGAGCCCCAGCAGCGGTAGAACCAATG</i>	
g_R474A.F	<i>CCGCTACGGGGGCTGCTGTGGTTGCCGTTAAAG</i>	SDM, R474A
g_R474A.R	<i>CTTTAACGGCAACCACAGCAGCCCCCGTAGCGG</i>	
g_R474E.F	<i>CCGCTACGGGGGCTGAAGTGGTTGCCGTTAAAG</i>	SDM, R474E
g_R474E.R	<i>CTTTAACGGCAACCACCTTCAGCCCCCGTAGCGG</i>	
g_K479A.F	<i>CGTGTGGTTGCCGTTGCTGCTGATATGGCAAG</i>	SDM, K479A
g_K479A.R	<i>CTTGCCATATCAGCAGCAACGGCAACCACACG</i>	
g_K479E.F	<i>CGTGTGGTTGCCGTTGAAGCTGATATGGCAAG</i>	SDM, K479E
g_K479E.R	<i>CTTGCCATATCAGCTTCAACGGCAACCACACG</i>	
g_D481A.F	<i>GGTTGCCGTTAAAGCTGCTATGGCAAGATTACAG</i>	SDM, D481A
g_D481A.R	<i>CTGTAATCTTGCCATAGCAGCTTTAACGGCAACC</i>	
g_D481E.F	<i>GGTTGCCGTTAAAGCTGAAATGGCAAGATTACAG</i>	SDM, D481E
g_D481E.R	<i>CTGTAATCTTGCCATTTACAGCTTTAACGGCAACC</i>	
g_R484A.F	<i>GCTGATATGGCAGCTTTACAGTTAACGTCGCCCG</i>	SDM, R484A
g_R484A.R	<i>CGGGCGACGTTAACTGTAAAGCTGCCATATCAGC</i>	
g_R484E.F	<i>GCTGATATGGCAGAAATTACAGTTAACGTCGCCCG</i>	SDM, R484E
g_R484E.R	<i>CGGGCGACGTTAACTGTAACTTGCCATATCAGC</i>	
g_L487A.F	<i>GATATGGCAAGATTACAGGCTACGTCGCCCGCTTG</i>	SDM, L487A
g_L487A.R	<i>CAAGCGGGCGACGTAGCCTGTAATCTTGCCATATC</i>	
g_E494A.F	<i>CGCCCCGTTGTACTGCTATTAACGAGAAGATTGC</i>	SDM, E494A
g_E494A.R	<i>GCAATCTTCTCGTTAATAGCAGTACAAGCGGGCG</i>	
g_E494K.F	<i>CGCCCCGTTGTACTAAAATTAACGAGAAGATTGC</i>	SDM, E494K
g_E494K.R	<i>GCAATCTTCTCGTTAATTTAGTACAAGCGGGCG</i>	
g_E497A.F	<i>CGCTTGTACTGAAATTAACGCTAAGATTGCTTTGTTCG</i>	SDM, E497A
g_E497A.R	<i>CGACAAAGCAATCTTAGCGTTAATTTAGTACAAGCG</i>	
g_E497K.F	<i>CGCTTGTACTGAAATTAACAAGAAGATTGCTTTGTTCG</i>	SDM, E497K
g_E497K.R	<i>CGACAAAGCAATCTTCTTGTTAATTTAGTACAAGCG</i>	
g_K498A.F	<i>CTGAAATTAACGAGGCTATTGCTTTGTCGAG</i>	SDM, K498A
g_K498A.R	<i>CTCGACAAAGCAATAGCCTCGTTAATTTAG</i>	
g_K498E.F	<i>CTGAAATTAACGAGGAAATTGCTTTGTCGAG</i>	SDM, K498E
g_K498E.R	<i>CTCGACAAAGCAATTTCTCGTTAATTTAG</i>	
g_R503A.F	<i>GAAAGATTGCTTTGTCGGCTCGTATCGAAAAGC</i>	SDM, R503A
g_R503A.R	<i>GCTTTTCGATACGAGCCGACAAAGCAATCTTC</i>	
g_R503E.F	<i>GAAAGATTGCTTTGTCGGAACGTATCGAAAAGC</i>	SDM, R503E
g_R503E.R	<i>GCTTTTCGATACGTTCCGACAAAGCAATCTTC</i>	
g_R504A.F	<i>GATTGCTTTGTCGAGAGCTATCGAAAAGCATTGG</i>	SDM, R504A
g_R504A.R	<i>CCAATGCTTTTCGATAGCTCTCGACAAAGCAATC</i>	
g_R504E.F	<i>GATTGCTTTGTCGAGAGAAATCGAAAAGCATTGG</i>	SDM, R504E
g_R504E.R	<i>CCAATGCTTTTCGATTCTCTCGACAAAGCAATC</i>	


<sup>a</sup>. Ref<sup>228</sup>

<sup>b</sup>. Ref<sup>234</sup>

<sup>c</sup>. SDM: Site-Directed Mutagenesis

<sup>d</sup>. CDS: Coding Sequence

**Table 2.4 Frequency and type of mutations in the libraries of randomly mutated *GCD11* alleles**



The diagram shows a yellow arrow labeled 'GCD11' pointing to the right. Above the arrow is a blue box labeled 'L1' and below it is a red box labeled 'L2'.

		L1	L2
<i>Frequency of mutation</i>		72.4%	86.4%
<i>Number of clones</i>		~19,000	~152,000
<i>Distribution of # of mutations per plasmid</i>	1 mutation	57.1%	57.9%
	2 mutations	19.0%	5.30%
	≥3 mutations	23.8%	36.8%
<i>Distribution of type of mutations in each library</i>	<i>Missense</i>	65.0%	60.0%
	<i>Synonymous</i>	30.0%	34.3%
	<i>Nonsense</i>	5.00%	5.70%

\*Frequencies are calculated from sequencing a random sample of at least 30 plasmids for each library

**Table 2.5 List of isolated mutant alleles of *GCD11* that suppressed the recessive lethality of *SUI5***

Mutant <sup>a</sup>	Substitutions <sup>b</sup>	Mutations in CDS <sup>c</sup>
A2a	<i>L423M N433K</i>	T1269A 1301CG
A3a	<i>E431R</i>	G1291A
A6a	<i>M482K</i>	T1445A
A8b	<i>F297S D481E</i>	T890C T1443A
B1a	<i>P404T D481E</i>	C1212A T1445A
B2d	<i>M482K T488M</i>	T1447A C1465T
B4a	<i>M482K</i>	T1445A
B6a	<i>M482I</i>	G1446T
C1c	<i>E431K</i>	G1293A
C3a	<i>L423M D481H</i>	T1267A G1441C
C7c	<i>M482K</i>	T1445A
D1a	<i>N433D</i>	A1299G
D2c	<i>N290S M482K</i>	A871G T1447A

<sup>a</sup> Plasmid name

<sup>b</sup> Missense mutations in the plasmid recovered. Color-coding designates substitutions in the same residues that were isolated from independent mutant plasmids.

<sup>c</sup> CDS: Coding Sequence

**Table 2.6 List of site-directed mutations created in domain-III of *GCD11***

#	Mutation	Residue in CDS <sup>a</sup>	Phenotype <sup>b</sup>	#	Mutation	Residue in CDS <sup>a</sup>	Phenotype <sup>b</sup>
1	<i>G421C</i>	T <sub>1261</sub> GT	-	12	<i>R484A</i>	G <sub>1451</sub> CT	Sup. His <sup>+</sup>
2	<i>L423A</i>	G <sub>1267</sub> CT	-	13	<i>R484E</i>	G <sub>1451</sub> AA	Sup. His <sup>+</sup>
3	<i>P424A</i>	G <sub>1270</sub> CT	-	14	<i>L487A</i>	G <sub>1460</sub> CT	-
4	<i>E460A</i>	G <sub>1378</sub> CT	Sui <sup>-</sup>	15	<i>E494A</i>	G <sub>1481</sub> CT	Sup. His <sup>+</sup>
5	<i>E460K</i>	A <sub>1378</sub> AA	Strong Slg <sup>-</sup>	16	<i>E494K</i>	A <sub>1481</sub> AA	Sup. His <sup>+</sup>
6	<i>M463A</i>	G <sub>1384</sub> CT	-	17	<i>E497A</i>	G <sub>1490</sub> CT	Sup. His <sup>+</sup>
7	<i>I466A</i>	G <sub>1397</sub> CT	-	18	<i>E497K</i>	A <sub>1490</sub> AG	Sup. His <sup>+</sup>
8	<i>G467A</i>	G <sub>1400</sub> CT	-	19	<i>K498A</i>	G <sub>1493</sub> CT	Sup. His <sup>+</sup>
9	<i>S468A</i>	G <sub>1402</sub> CT	Sup. His <sup>++</sup>	20	<i>K498E</i>	G <sub>1493</sub> AA	Sup. His <sup>+</sup>
10	<i>T471A</i>	G <sub>1412</sub> CT	-	21	<i>R503A</i>	G <sub>1508</sub> CT	Recessive lethal
11	<i>R474A</i>	G <sub>1421</sub> CT	-	22	<i>R503E</i>	G <sub>1508</sub> AA	Recessive lethal
12	<i>R474E</i>	G <sub>1421</sub> AA	-	23	<i>R504A</i>	G <sub>1511</sub> CT	Recessive lethal
13	<i>K479A</i>	G <sub>1436</sub> CT	Sup. His <sup>+</sup>	24	<i>R504E</i>	G <sub>1511</sub> AA	Recessive lethal
14	<i>K479E</i>	G <sub>1436</sub> AA	Sup. His <sup>+</sup>				

<sup>a</sup> CDS: Coding Sequence

<sup>b</sup> Sui<sup>-</sup> or \*Suppression of *SUI3-2* His<sup>+</sup>

**Table 2.7 Suppression of the Sui<sup>-</sup>, His<sup>+</sup>, Gcd<sup>-</sup>, Slg<sup>-</sup>, and TS<sup>-</sup> phenotypes of different Sui<sup>-</sup> mutants by the *GCD11* Ssu<sup>-</sup> alleles**

<i>GCD11</i> alleles	<i>SUI3-2</i>			<i>SUI5</i>				<i>tif11-SE1*SE2*F131</i>			
	His <sup>++</sup>	Gcd <sup>-b</sup>	UUG/AUG <sup>-b</sup>	Slg <sup>-a</sup>	Ts <sup>-a</sup>	His <sup>++</sup>	Gcd <sup>-b</sup>	Slg <sup>-a</sup>	Ts <sup>-a</sup>	His <sup>++</sup>	Gcd <sup>-b</sup>
<i>N433D</i>	+++	40%↓	50%↓	+	NA <sup>c</sup>	+++	40%↓	-	-	-	2.4X↑
<i>M482I</i>	+++	40%↓	60%↓	+	NA	+++	52%↓	-	-	-	2.3X↑
<i>E431K</i>	+/-	40%↓	40%↓	+	NA	+/-	40%↓	+/-	+/-	-	-
<i>K479E</i>	+++	40%↓	15%↓	+/-	-	++/-	50%↓	-	-	-	-
<i>R484A</i>	+++	44%↓	40%↓	+	+	++/-	70%↓	-	-	-	2.1X↑
<i>E497K</i>	+++	-	40%↓	-	-	-	-	-	-	-	-

<sup>a</sup> '+' indicates suppression, '-' indicates no effect

<sup>b</sup> Numbers indicate percentage or fold change in the double mutant with respect to *SUI3-2*, *SUI5*, or *tif11-SE1\*SE2\*F131*

<sup>c</sup> Not available

**CHAPTER 3: CHARACTERIZATION OF THE MUTANT ALLELES OF *GCD11*  
THAT REDUCE THE STRINGENCY OF START CODON RECOGNITION**



### 3.1 Introduction

The main characterized function of the eIF2 complex in the process of scanning and start codon recognition is binding the Met-tRNA<sub>i</sub> in a GTP dependent manner and delivering it to the P-site of the 40S subunit of the ribosome. The hydrolysis of its bound GTP and the release of P<sub>i</sub> are required for the dissociation of Met-tRNA<sub>i</sub> upon start codon recognition so that initiation can proceed. The  $\gamma$ -subunit of eIF2 forms the core of the complex that binds to both GTP and Met-tRNA<sub>i</sub>. Due to these properties of eIF2 $\gamma$ , the most likely underlying mechanism for the loss of initiation fidelity in its Sui<sup>-</sup> class of mutants would be an increase in the rate of GTP hydrolysis/P<sub>i</sub> release or the dissociation of the Met-tRNA<sub>i</sub>. Two Sui<sup>-</sup> mutations have been previously identified in *GCD11*. A lysine or aspartic acid substitution of the asparagine residue at position 135 (N135K/D), located in the switch-I region of the G-domain, has indeed been illustrated to lower the initiation fidelity by increasing the dissociation of Met-tRNA<sub>i</sub> from the eIF2 complex<sup>163,235</sup>. Furthermore, intragenic suppressors of *gcd11-N135D* were shown to suppress its Sui<sup>-</sup> phenotype by restoring the Met-tRNA<sub>i</sub> binding<sup>235</sup>.

As elucidated in Section 2.3.3, *R510H* was identified as a spontaneous mutation that constitutively derepressed the translation of *GCN4* mRNA (Gcd<sup>-</sup> phenotype)<sup>222</sup> and was later shown to also reduce the initiation fidelity creating a Sui<sup>-</sup> phenotype<sup>223</sup>. X-ray crystallography of eIF2 $\gamma$  homologues in archaea have revealed a three-dimensional structure that closely resembles that of EF-Tu (see Section 1.2.1)<sup>119</sup>. This is consistent with the function of both proteins in binding tRNA in a GTP dependent manner and delivering it to the ribosome. Due to this structural similarity between eIF2 $\gamma$  and EF-Tu, it was proposed that the *R510H* mutant displays Gcd<sup>-</sup> and Sui<sup>-</sup> phenotypes by also

lowering the Met-tRNA<sub>i</sub> binding to eIF2<sup>223</sup>. More recently, however, it has been reported that despite their similar structures, eIF2 $\gamma$  and EF-Tu bind tRNA and 40S in different manners<sup>113,127,236</sup>, whereas domain-III of EF-Tu plays an important part in binding the tRNA during the elongation phase of protein synthesis, eIF2 $\gamma$  domain-III is not involved in the Met-tRNA<sub>i</sub> binding. Thus, it is unlikely that the R510H substitution *directly* reduces the Met-tRNA<sub>i</sub> binding to eIF2. As discussed in Chapter 2, it is, however, possible that *R510H indirectly* affects Met-tRNA<sub>i</sub> binding by altering the relative position and stability of the switch-II region in the G-domain.

As elucidated earlier, we set out to identify new structural elements in eIF2 $\gamma$  that are involved in establishing the fidelity of translation initiation by isolating new mutations that alter the stringency of start codon recognition. We isolated three such mutants (*G418C*, *E460A*, and *R510H*) that reduce the accuracy of start codon selection and allow for translation initiation from a near-cognate UUG codon. Among them, *gcd11-R510H* was already identified as a Sui<sup>-</sup> mutant but, as stated above, was not described in detail. We employed genetic techniques to characterize these three alleles in vivo. Based on their genetic phenotypes and their position in the three-dimensional structure of eIF2, which can be indicative of their potential underlying mechanisms, the *E460A* and *G418C* mutants were then further characterized in an in vitro reconstituted yeast translation initiation system.

## 3.2 Materials and Methods

Standard methods were used for culturing, transforming, plasmid shuffling, and construction of *S. cerevisiae* strains<sup>210-212</sup>. For yeast growth assays, cultures were grown to saturation, diluted to OD<sub>600</sub> of 1 or 0.5, and 5µl of 10X serial dilutions were spotted on the appropriate medium.

### 3.2.1 Yeast Strain Constructions

For a list of yeast strains see Table 3.1. The strains used for the large-scale purification of eIF2 were generated in multiple steps by deleting the *GCN2*, *PEP4*, *SUI3*, and *SUI2* genes and replacing the *his4-301* allele with WT *HIS4* in NAY11. Briefly, *GCN2* was deleted by transforming NAY11 with the *gcn2Δ::hisG::ura3* disruption fragment of plasmid pHQ1093 and growing the resulting transformants on 5-FOA-containing medium as described previously<sup>213</sup> to generate NAY69. Deletion of *GCN2* was confirmed by PCR analysis. *LEU2*-containing plasmid Ep517 was then replaced with Ep293, which carries the *URA3* marker, to create NAY71. To do this NAY69 was transformed with Ep293 using the method of lithium acetate transformation<sup>210</sup>, and plasmid replacement was achieved as described in section 2.2.1 for NAY13. The loss of Ep517 was established by confirming leucine auxotrophy in NAY71. Next, the *his4-301* allele was replaced with WT *HIS4* to generate NAY72. This was achieved by transforming strain NAY71 with a PCR fragment corresponding to a portion of the *HIS4* gene from 340 bp upstream to 437 bp downstream of the start ATG codon and selecting for transformants on SC-U-H medium. Integration of the *HIS4* fragment at the correct locus was confirmed by PCR analysis. To obtain NAY76, the *URA3*-containing plasmid Ep293 was then shuffled with pNA4, which carries the *LEU2* marker, by transforming

NAY72 with pNA4 and selecting for transformants on SC-L medium with 5-FOA. The *PEP4* gene was then deleted by replacing its coding region with the hphMX4 cassette using the one-step PCR strategy<sup>237</sup> and selecting for hygromycin B resistance to generate NAY81. Deletion of *PEP4* was confirmed by PCR analysis. To obtain NAY82, pNA4 was then replaced with a sc *URA3*-containing plasmid pNA28 harboring the three genes (*GCD11*, *SUI2*, and *SUI3*) encoding the eIF2 complex using similar procedure explained above for NAY71. The *SUI3* gene was deleted by replacing its coding region with the kanMX4 cassette using the one-step PCR strategy<sup>214</sup> and selecting for kanamycin resistance to create NAY84. Deletion of *SUI3* was confirmed by PCR analysis. Finally, NAY86 was obtained by replacing the coding region of *SUI2* with the natMX4 cassette using the one-step PCR strategy<sup>237</sup> and selecting for nourseothricin resistance. Deletion of *SUI2* was confirmed by PCR analysis.

To obtain strains NAY87, NAY89, and NAY91, which were used to purify the eIF2 complexes containing the WT, G418C, and E460A mutant eIF2 $\gamma$  proteins, respectively, NAY86 was transformed with pNA21, pNA26, and pNA22, and the transformants were plated on SC-L medium containing 5-FOA to select for loss of the *URA3*-containing plasmid pNA28. The strains were verified again by rescuing their respective plasmids and subjecting them to DNA sequence analysis of the three genes encoding the WT or mutant eIF2 complexes.

### 3.2.2. Plasmid Constructions

For the list of plasmids used in this study see Table 3.2. pNA28 was created by inserting a 7.8 SacI-XhoI fragment containing the three eIF2 genes (*GCD11-His<sub>6</sub>*, *SUI2*, and *SUI3*) from pAV1726 between the SacI-SalI sites of YCplac33. pNA26 was made

by replacing the 2.57 kb SacI-SbfI fragment of pNA21 (containing *GCD11-His<sub>8</sub>*) with the SacI-SbfI fragment from pNA4-G418C that contains the mutant *gcd11-G418C* allele. The plasmid was verified by DNA sequence analysis of the *GCD11*, *SUI2*, and *SUI3* genes. See Section 2.2.2 for details of the construction procedures for plasmids pNA4, pNA19, pNA20, pNA21, pNA22, pNA23, pNA4-E460A, and pNA4-G418C.

### 3.2.3. Biochemical Assays with Yeast Extracts

$\beta$ -galactosidase assays with yeast WCEs obtained from exponentially growing cells (OD<sub>600</sub> of ~0.5) were performed as described previously<sup>218</sup>. To measure luminescence in cells harboring the dual luciferase reporter (pRaugFFuug), exponentially growing cultures (OD<sub>600</sub> of ~0.5) were collected by centrifugation and resuspended in PBS buffer (137 mM NaCl, 2.7 mM KCl, 10 mM Na<sub>2</sub>HPO<sub>4</sub>•2H<sub>2</sub>O, 2 mM KH<sub>2</sub>PO<sub>4</sub>, pH 7.4) with Complete Protease Inhibitor Cocktail (Roche), and whole cell lysates were generated by adding glass beads and vortexing at 4°C. Luminescence was measured with a microplate luminometer (Berthold) using the Dual-Luciferase Reporter 1000 Assay System (Promega) following the manufacturer's procedure.

### 3.2.4. In Vitro Reconstitution Assays

Purification of reagents. Eukaryotic initiation factors 1, 1A, and 5 were purified from BL21(DE3) CodonPlus *E. coli* (Agilent Technologies) using the IMPAC system (New England Biolabs) for the purification of intein fusion proteins as described before<sup>238</sup>. To generate eIF1A-Fl, eIF1A was labeled at its C-terminus with a Cys-Lys-fluorescein dipeptide using the expressed protein ligation system as previously described<sup>75,239</sup>. His<sub>8</sub>-tagged WT and mutant eIF2 complexes were overexpressed in yeast and purified as described<sup>127</sup>. 40S subunit was purified from yeast based on a procedure

described previously<sup>238</sup>. Yeast initiator tRNA was transcribed from a hammerhead fusion template using T7 polymerase run off transcription, and radiolabeled [<sup>35</sup>S]Met-tRNA<sub>i</sub> and stoichiometrically charged Met-tRNA<sub>i</sub> were prepared as previously described<sup>238</sup>. The sequence of the model mRNAs used were GGAA(UC)<sub>7</sub>UNNN(CU)<sub>10</sub>C where NNN was either AUG or UUG. For all experiments the reaction buffer was composed of 30 mM HEPES (pH 7.5), 100 mM potassium acetate, 3 mM magnesium acetate, and 2 mM dithiothreitol.

Affinity of Met-tRNA<sub>i</sub> binding to the eIF2 complex. Binding of the Met-tRNA<sub>i</sub> to eIF2 was measured by a filter-binding assay as described before<sup>165</sup>. Briefly, a limiting amount of [<sup>35</sup>S]Met-tRNA<sub>i</sub> (1 nM) was incubated with GDPNP (1 mM) and increasing concentrations of eIF2. The reactions were filtered through an upper nitrocellulose membrane (Millipore), which retains the eIF2•GDPNP•Met-tRNA<sub>i</sub> complexes, and a lower Nytran Supercharge membrane (Millipore), which retains the unbound [<sup>35</sup>S]Met-tRNA<sub>i</sub>. The filters were then air-dried, and the radioactivity on each membrane was determined by the liquid scintillation counting method.

Bench-top GTP hydrolysis. Bench-top GTP hydrolysis assays were performed essentially as described before<sup>92</sup>. A limiting concentration of [ $\gamma$ -<sup>32</sup>P]GTP (80 nM) was mixed with saturating amounts of eIF2 (0.8  $\mu$ M). To measure GTP hydrolysis in eIF2 alone, the reactions were incubated at 26°C and then stopped by adding 100 mM EDTA at different time points. To measure GTP hydrolysis in the TC, eIF2 (0.8  $\mu$ M) was first incubated with [ $\gamma$ -<sup>32</sup>P]GTP (80 nM) for 10 min. Met-tRNA<sub>i</sub> (0.8  $\mu$ M) was then added, and the reactions were stopped by adding 100 mM EDTA at different time points. The fraction of GTP hydrolyzed over time was then measured by employing thin layer

chromatography (TLC). The samples were run on PEI-cellulose TLC using 0.3 M KPO<sub>4</sub>, pH 4.4 as the mobile phase to separate the [ $\gamma$ -<sup>32</sup>P]GTP and <sup>32</sup>P<sub>i</sub> entities and were quantified by Phosphorimager analysis.

Affinity and kinetics of TC binding to the 40S subunit. Native gel shift assays were used to measure both the affinity and the kinetics of TC binding to the 40S subunit as described<sup>63,240</sup>. To measure the affinity of TC binding to the 40S subunit, TC preassembled with eIF2 (0.8  $\mu$ M), GDPNP (1 mM), and [<sup>35</sup>S]Met-tRNA<sub>i</sub> (1 nM) was incubated with eIF1 (1  $\mu$ M), eIF1A (1  $\mu$ M), mRNA (1  $\mu$ M), and a range of 40S concentrations from 0.5 to 50 nM. The 43S•mRNA complex formation was then measured by native gel electrophoresis. The dissociation constants (K<sub>d</sub> values) were calculated by fitting the data with a hyperbolic or a quadratic equation. To measure the rate of TC binding to the 40S subunit, 43S•mRNA complexes were formed by mixing TC preassembled with eIF2 (250 nM), GDPNP (1 mM), and [<sup>35</sup>S]Met-tRNA<sub>i</sub> (0.6 nM) with eIF1 (1  $\mu$ M), eIF1A (1  $\mu$ M), 40S (20 nM), and mRNA (10  $\mu$ M). The reactions were stopped at different time points by adding  $\geq$ 300-fold excess of unlabeled TC, and the rate of complex formation was measured by native gel electrophoresis. Curves were fit to a single exponential equation to determine the observed rate constants (k<sub>obs</sub> values).

Kinetics of TC dissociation. Dissociation of TC from the 43S•mRNA complex was monitored as described previously<sup>63</sup>. 43S•mRNA complexes were formed by mixing TC preassembled with eIF2 (250 nM), GDPNP (1 mM), and [<sup>35</sup>S]Met-tRNA<sub>i</sub> (1 nM) with eIF1 (1  $\mu$ M), eIF1A (1  $\mu$ M), 40S (20 nM), and mRNA (10  $\mu$ M). The reactions were then initiated by adding  $\geq$ 370-fold excess of unlabeled TC and were stopped by

loading on a running native gel. The dissociation rate constants ( $k_{\text{off}}$  values) were calculated by fitting the data with a single exponential equation.

eIF1A dissociation kinetics. Kinetics of eIF1A dissociation was measured by anisotropy as previously described<sup>75</sup>. 43S•mRNA complexes were first formed by incubating saturating amounts of TC preassembled with eIF2 (300 nM), GDPNP (1 mM), and Met-tRNA<sub>i</sub> (150 nM), eIF1 (1  $\mu$ M), eIF5 (1  $\mu$ M), 40S (120 nM), and mRNA (10 $\mu$ M) with a limiting concentration of eIF1A-F1 (15 nM). A saturating concentration of unlabeled eIF1A (1  $\mu$ M) was then added to chase the reaction, and changes in the anisotropy were measured over time using a T-format Spex Fluorolog-3 (J.Y. Horiba).



### 3.3 Results

#### 3.3.1 Novel Mutations in *GCD11* Reduce the Fidelity of Start Codon Recognition

A mutant allele of the *HIS4* gene (*his4-301*) lacking a cognate start codon was used as a genetic reporter for the identification of mutations in *GCD11* that would allow for initiation from a non-AUG codon. His4 is an essential protein that is required for histidine biosynthesis in yeast. Thus, in otherwise WT cells, yeast harboring the *his4-301* allele is unable to grow on medium lacking histidine. Mutations that lower the initiation fidelity would consequently allow for initiation from the UUG triplet at the third in-frame codon of *his4-301*, suppress its histidine auxotrophy, and grow in the absence of histidine in the medium (His<sup>+</sup> phenotype)<sup>208,209</sup>. The *G418C*, *E460A*, and *R510H* mutant alleles isolated in *GCD11* (as described in Chapter 2) all confer a His<sup>+</sup> phenotype, presumably by allowing translation initiation from the in-frame UUG codon of *his4-301* (Figure 3.1A). These mutants exhibit a range of histidine independence as *G418C* presents a strong, *R510H* a medium, and *E460A* a weak His<sup>+</sup> phenotype, suggesting that they elevate initiation at UUG codons to different extents.

In order to quantify the extent of non-AUG initiation in these mutants, we used genetic reporters containing either a UUG or an AUG start codon and calculated the ratio of their respective products (UUG/AUG ratio). Two different sets of reporters were used: matched *HIS4-lacZ* alleles with an AUG or a UUG start codon (see Section 2.3.4) or a dual luciferase reporter system with the Renilla luciferase gene (*P<sub>adh</sub>-Renilla*) containing an AUG start codon and the Firefly luciferase (*P<sub>cyc</sub>-Firefly*) containing a UUG start codon. In WT cells, there is a small amount of background translation initiation from a UUG codon, and hence the ratio of UUG to AUG initiation is low (Figure 3.1B). The

*G418C*, *E460A*, and *R510H* mutants, however, increase the ratio of initiation from a UUG codon to that from an AUG codon (Figure 3.1B). The amount of increase in the UUG to AUG ratio in these mutants is consistent with the strength of their His<sup>+</sup> phenotypes, so that *G418C* confers the biggest increase, *R510H* a moderate increase, and *E460A* produces a weak but significant increase in the ratio of UUG to AUG initiation. Thus, the *G418C*, *E460A*, and *R510H* mutations in *GCD11* reduce the stringency of the start codon recognition and consequently confer Sui<sup>-</sup> and His<sup>+</sup> phenotypes.

To examine if the Sui<sup>-</sup> and His<sup>+</sup> phenotypes of these mutants are a result of reduced TC formation or impaired TC binding to the PIC, we measured the expression of a *GCN4-lacZ* reporter in the WT and mutant *GCD11* strains. As elucidated in the previous chapters, expression of *GCN4* can serve as a genetic reporter for monitoring the stability and the loading of the ternary complex to the PIC. In nutrient-replete conditions, translation of *GCN4* mRNA is repressed. A reduction in TC stability or in its rate of binding to the 40S subunit, however, leads to an increase in the expression of *GCN4* even in nutrient-replete conditions (a Gcd<sup>-</sup> phenotype)<sup>206,220</sup>. In WT cells, when nutrients are abundant, there is low basal translation of the *GCN4-lacZ* reporter (Figure 3.2A). Cells harboring the *G418C*, *E460A*, or *R510H* mutant alleles, however, exhibit a Gcd<sup>-</sup> phenotype by increasing expression of the *GCN4-lacZ* reporter in nutrient-replete conditions (Figure 3.2A). The extent to which these mutants derepress *GCN4-lacZ* expression correlates with the strength of their Sui<sup>-</sup> and His<sup>+</sup> phenotypes, which may suggest these phenotypes have a common underlying mechanism in these mutants.

A Gcd<sup>-</sup> phenotype can result from a reduced rate of TC binding to the scanning 40S subunits on the *GCN4* mRNA (as discussed above and in Section 1.2.3). Ternary

complex binds rapidly to the 40S subunit only when the pre-initiation complex is in the open conformation<sup>60</sup>. Increasing the proportion of PIC in the open conformation can then be expected to partially suppress a Gcd<sup>-</sup> phenotype by further stabilizing the open conformation and allowing a greater fraction of the scanning 40S subunits to bind TC before reaching uORF4. The eIF1 protein, along with eIF1A, binds and stabilizes the PIC in the open conformation<sup>63</sup>. Consequently, overexpression of eIF1 can be expected to partially suppress an increase in the expression of the *GCN4-lacZ* reporter. Thus, in order to examine if overexpression of the eIF1 protein (Sui1 in yeast) suppresses the Gcd<sup>-</sup> phenotype of *G418C*, *R510H*, and *E460A*, expression of the *GCN4-lacZ* reporter was measured in cells harboring the WT or *GCD11* mutant alleles and expressing *SUI1* from a hc *TRP1* plasmid. In agreement with this expectation, overexpressing the eIF1 protein, partially suppresses the Gcd<sup>-</sup> phenotype of the *G418C*, *E460A*, and *R510H* mutants (Figure 3.2A).

As elucidated above, overexpressing the eIF1 protein further stabilizes the open conformation and allows for the PIC to continue scanning, which consequently leads to a reduction in the formation of closed conformation and initiation at a near-cognate UUG codon. Thus, to examine if overexpression of eIF1 can similarly reduce the elevated ratio of UUG to AUG initiation in these mutants, we measured expression of the *HIS4-lacZ* reporters in isogenic strains harboring either the WT or the mutant *E460A* or *G418C* alleles and expressing *SUI1* from a hc *TRP1* plasmid. Consistent with this reasoning, eIF1 overexpression partially suppresses the elevated ratio of UUG to AUG initiation in the *G418C* and *E460A* mutants (Figure 3.2B).

Since overexpression of eIF1 could partially suppress the elevated ratio of UUG to AUG initiation and the Gcd<sup>-</sup> phenotype of the *GCD11* mutants, we next tested if it can also suppress the His<sup>+</sup> and the growth defects conferred by these alleles. Spot assays were performed with isogenic strains (*gcd11Δ, his4-301*) harboring the WT or mutant alleles of *GCD11* and expressing *SUI1* from a hc *TRP1* plasmid. In agreement with partially reducing the ratio of UUG to AUG initiation (Figure 3.2B), overexpressing eIF1 also partially suppresses the His<sup>+</sup> phenotype of the *GCD11* mutants (Figure 3.3A). It, however, does not suppress the Slg<sup>-</sup> and the Cs<sup>-</sup> phenotypes conferred by the *G418C* allele, nor does it suppress the TS<sup>-</sup> phenotype of the *E460A* mutant (Figure 3.3B).

While overexpression of the eIF1 protein is likely to partially suppress a Gcd<sup>-</sup> phenotype by stabilizing the open conformation of the PIC, overexpression of the Met-tRNA<sub>i</sub> can be expected to do so by increasing the concentration of TC. Met-tRNA<sub>i</sub> binds to eIF2 only when in complex with GTP<sup>165,241</sup>. In fact, it is the irreversible hydrolysis of eIF2-bound GTP upon AUG recognition that leads to the dissociation of the Met-tRNA<sub>i</sub> from the eIF2 complex<sup>191,242</sup>. It has also been reported that Met-tRNA<sub>i</sub> binding to eIF2 stabilizes the binding of the GTP<sup>164</sup>. Moreover, we found here that binding of the Met-tRNA<sub>i</sub> to the purified eIF2 complex also reduces the spontaneous rate of GTP hydrolysis by eIF2 in vitro (Figure 3.4). This was assayed by comparing the rate of GTP hydrolysis in the eIF2•GTP complex with that in the TC (eIF2•GTP•Met-tRNA<sub>i</sub>). Hence, overexpression of the Met-tRNA<sub>i</sub> can be expected to suppress an increase in the rate of GTP hydrolysis. Yet, Met-tRNA<sub>i</sub> overexpression could also be expected to increase TC assembly by mass action, driving a higher proportion of the available eIF2•GTP into TC.

Mass action may explain how overexpression of Met-tRNA<sub>i</sub> reduces the depression of *GCN4-lacZ* in nutrient-starved cells<sup>206</sup>.

Therefore, in order to examine if overexpressing the Met-tRNA<sub>i</sub> can suppress the Gcd<sup>-</sup> phenotype of the *GCD11* mutants, expression of the *GCN4-lacZ* reporter was measured in cells harboring either the WT or the mutant *G418C* or *R510H* alleles and expressing *IMT4* from a hc *TRP1* plasmid. The overexpression of Met-tRNA<sub>i</sub> partially suppresses the derepression of *GCN4-lacZ* expression in the *G418C* and *R510H* mutants (Figure 3.2A). Remarkably, overexpressing the Met-tRNA<sub>i</sub> reduces expression of the *GCN4-lacZ* reporter in the *R510H* strain by 92%, as compared to 44% and 72% in the WT and *G418C* strains, respectively. This is in good agreement with our proposal that the R510H substitution is likely to increase the rate of GTP hydrolysis and/or P<sub>i</sub> release by destabilizing the switch-II region of the G-domain, which then leads to an increase in the ratio of UUG to AUG initiation and in the expression of the *GCN4-lacZ* reporter (this hypothesis was explained in detail in Section 2.3.3 and will be discussed again at the end of this chapter).

### 3.3.2 The *E460A* Mutant Promotes Formation of the Closed Conformation at a UUG Codon

In an effort to uncover the mechanism for the loss of initiation fidelity conferred by the *E460A* mutant allele of *GCD11*, we employed biochemical assays in a reconstituted yeast translation initiation system<sup>238</sup> to test our hypotheses directly. As discussed in Section 2.3.4, E460 is a highly conserved surface-exposed residue that is positioned in domain-III of eIF2 $\gamma$  in proximity of the proposed binding interface between the eIF2 complex and the 40S subunit. Thus, based on its genetic characteristics, as

explained above, and its position in the three-dimensional structure of eIF2, we proposed that E460A substitution is likely to reduce the stringency of start codon recognition by altering the mode of eIF2 binding so that the PIC now favors the closed conformation even at non-AUG codons. To test this hypothesis directly, we measured the affinity and the rate of TC binding to the 40S subunit in the yeast reconstituted translation initiation system.

To measure the affinity of the ternary complex for the 40S subunit, we first examined if the eIF2 $\gamma$ -E460A mutant protein can form a TC with WT stability. We determined the affinity of Met-tRNA<sub>i</sub> for eIF2 using a filter-binding assay, by measuring the binding of radiolabeled [<sup>35</sup>S]Met-tRNA<sub>i</sub> at increasing concentrations of eIF2. The results indicated that the E460A mutant protein does not have a defect in binding Met-tRNA<sub>i</sub> and forming a stable TC as we obtained similar K<sub>d</sub> values for the E460A and WT eIF2 $\gamma$  proteins that were within the range of published results (Figure 3.5). To measure the binding affinity of TC for the 40S subunit, we then performed electrophoretic mobility shift assays (EMSA) to monitor PIC formation. The PIC was assembled in vitro using saturating amounts of eIF2 (containing WT or the E460A mutant eIF2 $\gamma$ ), eIF1, eIF1A, and mRNA (with an AUG or a UUG codon), a limiting amount of [<sup>35</sup>S]Met-tRNA<sub>i</sub>, and a range of 40S concentrations. The fraction of TC bound to the 40S subunit (PIC formation) was then measured by native gel electrophoresis (see Material and Methods for more detail on all the biochemical assays performed). Consistent with previous reports, we observed a tight binding of the TC to the 43•mRNA complexes. Moreover, our results indicate that E460A substitution in eIF2 $\gamma$  does not significantly alter the affinity of the TC for the 40S subunit with either a UUG- or an AUG-containing

model mRNA as we obtained similar  $K_d$  values for TC assembled with WT or the E460A variant of eIF2 $\gamma$  (Figure 3.6). Therefore, it is unlikely that the *E460A* mutant reduces the initiation fidelity by altering the binding affinity of TC for the PIC.

To measure the rate of TC binding to the 40S subunit, we next determined the kinetics of PIC formation using a similar gel shift assay. Preformed TC (eIF2•GDPNP•[<sup>35</sup>S]Met-tRNA<sub>i</sub>) was mixed with saturating concentrations of eIF1, eIF1A, 40S, and mRNA. The reaction was stopped at different time points by adding an excess of unlabeled TC, and the fraction of TC bound to the 40S subunit was monitored by native gel electrophoresis. Remarkably, the E460A substitution increases the rate of TC binding exclusively at a UUG codon by 5-fold (Figure 3.7). It has been demonstrated previously that the binding of TC to the 40S subunit is biphasic<sup>95</sup>. The first phase corresponds to the codon-independent rapid recruitment of TC to the 40S subunit in the open conformation, which occurs during scanning. The second phase is the codon-dependent structural rearrangements that stabilizes TC binding upon cognate codon:anticodon base pairing and formation of the closed conformation<sup>95</sup>. Stabilization of TC binding upon formation of the closed conformation is apparent as the observed rate of TC binding to the 40S subunit is faster at an AUG codon versus a UUG codon (Figure 3.7, compare the rate of WT with an AUG mRNA to that with a UUG mRNA). The E460A substitution alters the *codon-dependent* phase of TC binding as it only increases the rate at a UUG codon. These results suggest that *E460A* reduces the stringency of start codon recognition by promoting the formation of the closed conformation at a near-cognate UUG codon. Based on the position of residue E460 near the proposed binding interface between eIF2 and h44 of the 40S subunit (Figure 2.28), it is likely that *E460A*

stabilizes TC binding and the closed conformation by adjusting the mode of eIF2 binding to the 40S subunit through altering the physical interactions between domain-III of eIF2 $\gamma$  and helix h44 of the 40S subunit, which consequently leads to translation initiation at non-AUG codons.

In order to determine if the steady state equilibrium between the open and closed conformations is altered in *E460A*, we measured the rate of eIF1A dissociation from reconstituted PIC. Kinetics of eIF1A dissociation is biphasic and serves as a proxy for the two conformations of the pre-initiation complex<sup>75</sup>. It has been demonstrated that start codon recognition induces structural rearrangements in the PIC that stabilizes eIF1A binding and reduces the rotational freedom of its CTT through an interaction with the eIF5 protein<sup>75</sup>. This is apparent as the rate of eIF1A dissociation is slower from the PIC reconstituted with an AUG versus a non-AUG codon (Figure 3.10A, compare the WT curve with an AUG to that with a UUG mRNA). The tighter binding of eIF1A upon start codon recognition is manifested as an increase in the amplitude of the slower phase of the biphasic dissociation reaction. Therefore, the relative amplitudes of the two kinetic phases of eIF1A dissociation is thought to represent the partitioning of the PIC between the open, scanning-conducive and closed, scanning-arrested conformations<sup>75</sup> (Figure 3.8). An apparent equilibrium constant between the two conformations of the PIC can then be defined as the ratio of the amplitudes of the two kinetic phases of eIF1A dissociation ( $K_{amp}$ ). Higher  $K_{amp}$  values indicate that the closed conformation is more favored

We used a fluorescence anisotropy-based assay to measure the kinetics of eIF1A dissociation from reconstituted PIC<sup>75</sup> (see Figure 3.9 for a brief description of the principles of fluorescence anisotropy). eIF1A was labeled with fluorescein at its CTT



using the expressed protein ligation method<sup>239,243</sup>. PIC was first assembled with a limiting amount of fluorescein-labeled eIF1A (eIF1A-FI) and saturating concentrations of TC, eIF1, eIF5, 40S, and mRNA. An excess of unlabeled eIF1A was then added and changes in the anisotropy were measured over time. In agreement with previous reports<sup>70,75,104</sup>, and as elucidated above, we observed reduced dissociation of eIF1A from the reconstituted PIC with an AUG versus a UUG codon (Figure 3.10A, compare the WT curve with an AUG to that with a UUG mRNA)). This is manifested as the  $K_{amp}$  value for the WT with an AUG mRNA is ~4-fold larger than with a UUG mRNA (Figure 3.10B, compare the  $K_{amp}$  values for the WT). The E460A substitution in eIF2 $\gamma$  does not alter the dissociation kinetics of eIF1A from the 43S•mRNA PIC (Figure 3.10, compare the curves and the  $K_{amp}$  values). Thus, it is unlikely that the *E460A* mutant alters the steady state equilibrium between the two conformations of the PIC.

### 3.3.3 Biochemical Analysis of the *G418C Sui<sup>-</sup>* Mutant

To determine the underlying mechanism for the *Sui<sup>-</sup>* phenotype conferred by the *G418C* allele, we performed similar assays in the yeast reconstituted translation initiation system to assess TC stability and binding to the PIC. We first examined the binding of Met-tRNA<sub>i</sub> to the eIF2 complex containing the *G418C* substitution in the  $\gamma$  subunit. As discussed in Section 2.3.3, *G418* residue is located in the first  $\beta$ -strand of domain-III that is projected in-between the  $\beta$ -barrel structure of domain-II. Since domain-II has been implicated in Met-tRNA<sub>i</sub> binding<sup>1,113,127,138</sup>, we hypothesized that *G418C* may lower the stringency of start codon recognition by reducing the binding of Met-tRNA<sub>i</sub> to eIF2 through altering the three-dimensional structure of domain-II. Thus, in order to determine the binding affinity of Met-tRNA<sub>i</sub> for eIF2, we performed filter-binding assays

as described before<sup>165</sup>. A limiting amount of [<sup>35</sup>S]Met-tRNA<sub>i</sub> and a range of eIF2 concentrations were used to measure the fraction of [<sup>35</sup>S]Met-tRNA<sub>i</sub> bound to the eIF2 complex. In contrast with our hypothesis, as compared to the WT protein, the G418C variant does not significantly alter the affinity of Met-tRNA<sub>i</sub> binding to the eIF2 complex (Figure 3.11).

Because of its location, as elucidated above, it is also possible that the G418C substitution may alter the intrinsic rate of GTP hydrolysis in eIF2 by altering the relative position of domain-II with respect to the G-domain. Thus, we measured the spontaneous rate of GTP hydrolysis in eIF2 containing either WT or mutant eIF2 $\gamma$ . A limiting amount of [ $\gamma$ -<sup>32</sup>P]GTP was incubated with a saturating concentration of eIF2, and the fraction of GTP hydrolyzed was measured over time by separating the [ $\gamma$ -<sup>32</sup>P]GTP and <sup>32</sup>P<sub>i</sub> entities using thin layer chromatography. These experiments illustrated that the G418C substitution also does not increase the intrinsic rate of GTP hydrolysis in eIF2 (Figure 3.12).

Next we tested the possibility that the Sui<sup>-</sup> phenotype conferred by the *G418C* allele is a result of altered TC binding to the 40S subunit. Thus, we measured the affinity and the rate of TC loading on the 40S subunit using a similar set up explained above for the *E460A* mutant and established that the G418C substitution does not alter the affinity (Figure 3.13A) or the rate of TC binding to the PIC (Figure 3.13B) at either an AUG or a UUG codon. This finding is not unexpected because considering that G418 is not exposed on the surface of eIF2 $\gamma$  and is positioned away from the proposed binding interface between eIF2 and the 40S (Figure 2.20 and Figure 2.22), it would be unlikely that the G418C substitution would affect the loading of the eIF2 complex on the PIC.

In order to establish if the loss of initiation fidelity in *G418C* is due to an altered equilibrium between the two conformations of the PIC, we then measured the kinetics of eIF1A dissociation using a similar procedure described in above for the *E460A* mutant. The G418C substitution also does not alter the steady state equilibrium between the open and closed conformations of the PIC as it does not alter the equilibrium between the two phases of eIF1A dissociation as compared to WT eIF2 $\gamma$  (Figure 3.14). Thus, the genetic phenotypes conferred by the *G418C* allele are unlikely to be a result of reduced TC stability, altered TC binding to the 40S subunit, or an increased stability of the closed conformation at a near-cognate UUG codon.

### 3.4 Discussion

During the initiation stage of protein synthesis, the eIF2 complex has the vital function of delivering the Met-tRNA<sub>i</sub> to the P-site of the 40S subunit and maintaining it in a proper orientation during the scanning phase so that the anticodon of the Met-tRNA<sub>i</sub> can sample the codons of the mRNA leader sequence for complementarity in search of the start codon. Upon arrival at the AUG start codon, the hydrolysis of eIF2-bound GTP and P<sub>i</sub> release then allow for the dissociation of Met-tRNA<sub>i</sub> from eIF2. With the dissociation of eIF2•GDP and other initiation factors from the PIC and joining of the large subunit of the ribosome, the process of protein synthesis then continues to the elongation stage<sup>90</sup>.

eIF2 $\gamma$  is the core subunit of the eIF2 complex that provides the binding sites for GTP and Met-tRNA<sub>i</sub> through its G-domain and domain-II<sup>1,113,127,138</sup>. Contrary to the other two domains, domain-III of eIF2 $\gamma$  has mainly remained uncharacterized. Recently, however, by using a directed hydroxyl radical probing approach, a model for the loading of eIF2 on the 40S subunit was proposed in which domain-III provides a key binding interface between eIF2 and helix h44 of the 40S subunit<sup>127</sup>. Here, we have provided genetic and biochemical evidence for the involvement of eIF2 $\gamma$  domain-III in establishing the accuracy of start codon selection. We have identified three Sui<sup>-</sup> mutations that map to domain-III of eIF2 $\gamma$ . Interestingly, the three mutant alleles (*G418C*, *R510H*, and *E460A*) seem to lower the stringency of start codon recognition by different mechanisms, which suggests domain-III is involved in multiple functions during the initiation stage of protein synthesis.

All three mutant alleles we isolated confer a His<sup>+</sup> phenotype, albeit to different degrees, by allowing for the initiation of *his4-301* translation from a UUG codon. In order to quantify the amount of non-AUG initiation in these mutants, we measured the expression of reporter genes with either a UUG or an AUG start codon and calculated the ratio of their respective products. In agreement with their His<sup>+</sup> phenotypes, all three Sui<sup>-</sup> mutants present an elevated ratio of UUG to AUG initiation compared to WT cells to extents that correlate with the strength of their His<sup>+</sup> phenotype. Moreover, all three mutants display a Gcd<sup>-</sup> phenotype, which is partially suppressed by overexpression of the eIF1 protein as well as the Met-tRNA<sub>i</sub>.

Partial suppression of the Gcd<sup>-</sup> phenotype by eIF1 overexpression may imply that the *GCD11* Sui<sup>-</sup> mutants reduce the rate of TC loading on the reinitiating 40S subunits so that increasing the prevalence of the open conformation, as a result of eIF1 overexpression, can partially compensate for this defect. This mechanism may also explain the ability of eIF1 overexpression to dampen the derepression of *GCN4-lacZ* under nutrient-starved conditions when the rate of TC loading is reduced as a result of low TC concentration caused by the phosphorylation of eIF2 $\alpha$  (explained in Section 1.2.3). Furthermore, the partial suppression of the Sui<sup>-</sup> phenotype by eIF1 overexpression may suggest that the *GCD11* mutants favor the closed conformation of the PIC. It is, however, possible that the *GCD11* Sui<sup>-</sup> mutants elevate UUG initiation by a different mechanism, and that eIF1 overexpression suppresses this defect *indirectly* by maintaining the PIC in the open conformation, which is presumably the mechanism by which eIF1 overexpression reduces UUG recognition even in otherwise WT cells. Since the *E460A*, *R510H*, and *G418C* mutants seem to reduce the fidelity of start codon recognition by

different mechanisms, it is more likely that the overexpression of the eIF1 protein partially suppresses their His<sup>+</sup>, Sui<sup>-</sup>, and Gcd<sup>-</sup> phenotypes indirectly through increasing the prevalence of the PIC in the open conformation. Moreover, the failure to observe a suppression of the Slg<sup>-</sup>, Ts<sup>-</sup>, and Cs<sup>-</sup> phenotypes by eIF1 overexpression may suggest that the impact of overexpressing eIF1 is indeed indirect. Yet, it is also possible that the *GCD11* mutant alleles impair other aspects of the initiation pathway that cannot be rescued by overexpressing the eIF1 protein.

As elucidated earlier in Section 3.3.2, overexpression of the Met-tRNA<sub>i</sub> can be expected to increase the concentration of TC (by mass action) and to partially suppress an increase in the background rate of GTP hydrolysis in eIF2. Interestingly, in agreement with our proposal that *R510H* mutant is likely to reduce the initiation fidelity by increasing the intrinsic rate of GTP hydrolysis, through destabilizing the structure of switch-II region in the G-Domain (see Section 2.3.3), overexpressing the Met-tRNA<sub>i</sub> suppresses the Gcd<sup>-</sup> phenotype of the *R510H* mutant by over 90%. Yet, this result is also consistent with the possibility that *R510H* indirectly affects Met-tRNA<sub>i</sub> binding to the eIF2 complex. In vitro GTPase and Met-tRNA<sub>i</sub> binding assays are required to differentiate between these two hypotheses and establish the true underlying mechanism for the Sui<sup>-</sup> phenotype of *R510H*. Residue R510 is very well conserved and is located in the last  $\beta$ -strand of domain-III that provides the interface between domain-III and the G-domain. Moreover, the entire sequence motif (W<sub>509</sub>R<sub>510</sub>L<sub>511</sub>I<sub>512</sub>G<sub>513</sub>) of the last  $\beta$ -strand of domain-III is highly conserved, which may suggest the side chains of its residues may play a vital function in eIF2 $\gamma$  (for example, by stabilizing the switch-II region as

discussed earlier). Thus, it would be interesting to examine if substitutions in the neighboring residues of R510 also alter the fidelity of translation initiation.

Among our three *Sui<sup>-</sup>* mutants, *G418C* displayed the strongest *His<sup>+</sup>* and *Gcd<sup>-</sup>* phenotypes and had the largest increase in the ratio of initiation from a UUG codon to that from an AUG codon. Therefore, we performed in-depth biochemical assays to determine the underlying mechanism for the loss of initiation fidelity in *G418C*. Due to its position in the first  $\beta$ -strand of domain-III that is inserted inside the  $\beta$ -barrel structure of domain-II, we hypothesized that the G418C substitution reduces the binding of Met-tRNA<sub>i</sub> to eIF2 as domain-II has been implicated in Met-tRNA<sub>i</sub> binding<sup>1,113,124,127,138</sup>. In contrast with our hypothesis, however, the G418C variant of eIF2 $\gamma$  does not seem to significantly alter the affinity of the Met-tRNA<sub>i</sub> for eIF2.

We also confirmed that the G418C substitution does not alter the spontaneous rate of GTP hydrolysis in the eIF2 complex. We cannot, however, rule out the possibility that it may alter the eIF5-dependent GTP hydrolysis or the dissociation of P<sub>i</sub> in the context of the PIC. This hypothesis can be examined by performing GTPase assays using a rapid quench method as described previously<sup>92</sup>. Additionally, we tested the possibilities that the G418C substitution alters binding of the TC to the 40S subunit or directly disrupts the steady state equilibrium between the two conformations of the PIC, by stabilizing the closed conformation on a near-cognate UUG codon. Thus, we measured the affinity and the kinetics of TC binding to the 40S subunit with eIF2 containing the G418C substitution and determined that it does not alter the binding affinity or the rate of TC loading on the 40S subunit. Furthermore, the *Sui<sup>-</sup>* phenotype of *G418C* is also not

due to an increase in the stability of the closed conformation at a UUG codon, as the G418C substitution does not alter the dissociation kinetics of eIF1A.

Albeit these results, it is still a likely possibility that *G418C* reduces the stringency of start codon recognition by altering the conformation of Met-tRNA<sub>i</sub> binding, without affecting its binding affinity for eIF2 since it has been previously proposed that structural alterations in eIF2 $\gamma$  can subtly alter the conformation of Met-tRNA<sub>i</sub> on the 40S subunit and consequently affect the fidelity of start codon recognition independent of the binding affinity of Met-tRNA<sub>i</sub> for eIF2<sup>235</sup>. Unfortunately, this possibility can only be directly examined via determining the crystal structure of TC with the WT or the mutant G418C eIF2 $\gamma$  proteins.

Despite its weaker in vivo Sui<sup>-</sup> phenotype, *E460A* was chosen for an in-depth biochemical analysis over the *R510H* mutant because, as discussed in much detail in Section 2.3.4, it was more likely that it plays a direct role in promoting the formation of closed conformation at a UUG codon through altering the physical interactions between eIF2 and the 40S subunit (see Section 2.3.4). We examined if the E460A substitution alters the affinity or the rate of TC binding to the 40S subunit and established that whereas the E460A substitution does not alter the affinity, it increases the rate of TC loading on the 40S subunit *exclusively* at a UUG codon. It has been previously demonstrated that binding of the TC to the 40S subunit is stabilized upon AUG recognition and follows a biphasic kinetics. While the first phase represents the rapid recruitment of the TC to the 40S subunit, the second phase signifies the codon-dependent structural rearrangements that take place upon AUG recognition and formation of the closed conformation<sup>95</sup>. Thus, *E460A* promotes formation of the closed conformation of



the PIC at a UUG codon, which consequently leads to initiation and loss of fidelity. This is quite interesting since *E460A* marks the first mutant of its kind identified so far; it is the first *Sui<sup>-</sup>* mutant that promotes formation of the closed conformation at a UUG codon, by increasing the rate of TC loading, without affecting it at an AUG codon. Considering the position of residue E460 on the proposed interface between eIF2 and the 40S subunit (Figure 2.28), it is a likely possibility that the E460A substitution allows for the formation of the closed conformation at a UUG codon by adjusting the way eIF2 binds to the PIC through altering its physical interactions with helix h44 of the 40S subunit. In other words, it is likely that *E460A* allows for UUG initiation by allowing eIF2 $\gamma$  to bind in a *start codon recognition mode* at a UUG codon.

Although *E460A* promotes formation of the closed conformation by stabilizing binding of the TC to the 40S subunit at a UUG codon, it does not seem to alter the steady state equilibrium between the two conformations of the PIC as measured by the dissociation kinetics of the eIF1A protein. It is important to note that the dissociation of eIF1A is measured by adding the chase (unlabeled eIF1A) only after the PIC has fully formed and reached a steady state. The two assays, kinetics of TC loading and eIF1A dissociation, have very different set up and are indicative of different functions. Whereas the kinetics of TC loading reveals how likely it is that the closed conformation is formed, the kinetics of eIF1A dissociation is a proxy for the steady state stability of each conformation. In other words, it does not measure how likely it is that formation of the closed conformation is promoted; it measures how stable it is after forming. Thus, *E460A* seems to promote formation of the closed conformation without affecting its steady state stability. This is consistent with our current understanding of the two

conformations of the PIC. Start codon recognition requires the coordinated action of a number of events in the PIC that collectively commit the complex to form a stable closed conformation and begin translation. For example, it is not only the mode of eIF2 binding that participates in promoting the formation of the closed conformation (as we propose here), as physical interactions between eIF5 and eIF1 have to be disrupted<sup>70,72</sup>, new interactions between the eIF1A and eIF5 proteins should be formed<sup>72,75</sup>, and the eIF2-bound GTP has to hydrolyzed irreversibly with the dissociation of  $P_i$ <sup>92</sup> among many other events that cooperatively lead to *formation* and *stabilization* of the closed conformation upon start codon recognition.

Our genetic and biochemical findings here provide evidence for the involvement of eIF2 $\gamma$  domain-III in establishing the stringency of start codon recognition. Domain-III seems to perform multiple functions during the initiation stage of protein synthesis. It is likely to participate in stabilizing GTP binding, through physical interactions with the switch-II region of the G-domain, and perhaps in maintaining the Met-tRNA<sub>i</sub> in the proper conformation for binding to the 40S subunit, through physical interactions with domain-II. As elucidated earlier, however, further experiments are required to directly confirm the above hypotheses. Most interestingly, our genetic and biochemical findings suggest that domain-III of eIF2 $\gamma$  is involved in promoting formation of the closed conformation upon cognate base pairing between the start codon and the anticodon of Met-tRNA<sub>i</sub>. To our knowledge, this is the first report of such function for the eIF2 complex.

### 3.5 Figures and Tables

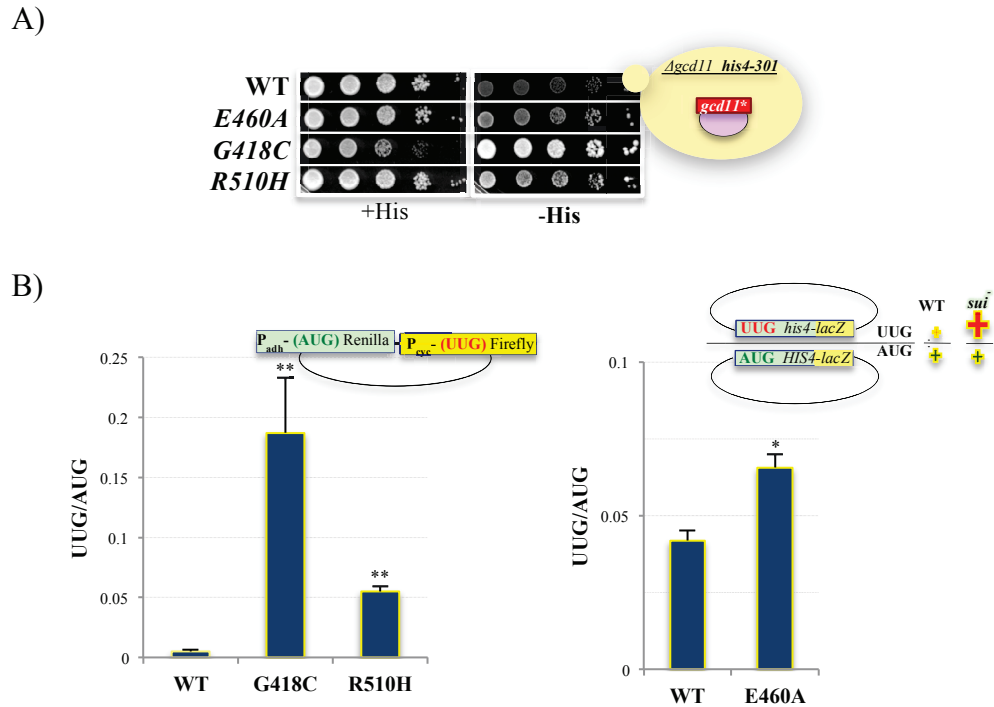


**Figure 3.1 The *Sui*<sup>-</sup> mutants of *GCD11* display a His<sup>+</sup> phenotype and an increased UUG to AUG ratio**

(A) The *E460A*, *G418C*, and *R510H* alleles of *GCD11* confer a range of His<sup>+</sup> phenotypes, with *G418C* producing a strong, *R510H* a medium, and *E460A* a weak phenotype. Cells harboring the *G418C* allele are also slow growing (compare the rows on the +His medium). Derivatives of strain NAY13 harboring the WT or mutant alleles of *GCD11* were cultured in SC-L, ten-fold serial dilutions were spotted on SC-L medium supplemented with 0.3 mM (+His) or 0.003 mM (-His) histidine, and incubated at 30°C for two and five days, respectively. The schematic on the right displays the features of the strain important for this assay. *gcd11*\* represents either the WT or mutant *GCD11* alleles. (B) Consistent with their His<sup>+</sup> phenotype, the *GCD11* mutants exhibit a *Sui*<sup>-</sup>

phenotype by increasing the ratio of initiation from a UUG codon to that from an AUG codon. UUG to AUG ratio was calculated by measuring the  $\beta$ -galactosidase activity from matched *HIS4-lacZ* reporters with either an AUG or a UUG start codon (on the right) or by measuring the luminescence from a dual luciferase reporter system with the Renilla luciferase gene (*P<sub>adh</sub>-Renilla*) containing an AUG start codon and the Firefly luciferase (*P<sub>cyc</sub>-Firefly*) containing a UUG start codon.  $\beta$ -galactosidase activities (nanomoles of *o*-nitrophenyl- $\beta$ -D-galactopyranoside cleaved per minute per microgram of protein) were measured in WCEs of exponentially growing cultures (OD<sub>600</sub> ~0.5) in SC-L medium. Luminescence was measured from exponentially growing cultures (OD<sub>600</sub> ~0.5) in SC-L medium, and relative luminescence of Firefly (UUG) to Renilla (AUG) genes are plotted. Mean of at least eight independent transformants and SEM (error bars) are plotted for each mutant. The schematics of the reporters used are presented on the graphs. A student *t*-test was used to determine significance (\**p*<0.05, \*\**p*<0.01).

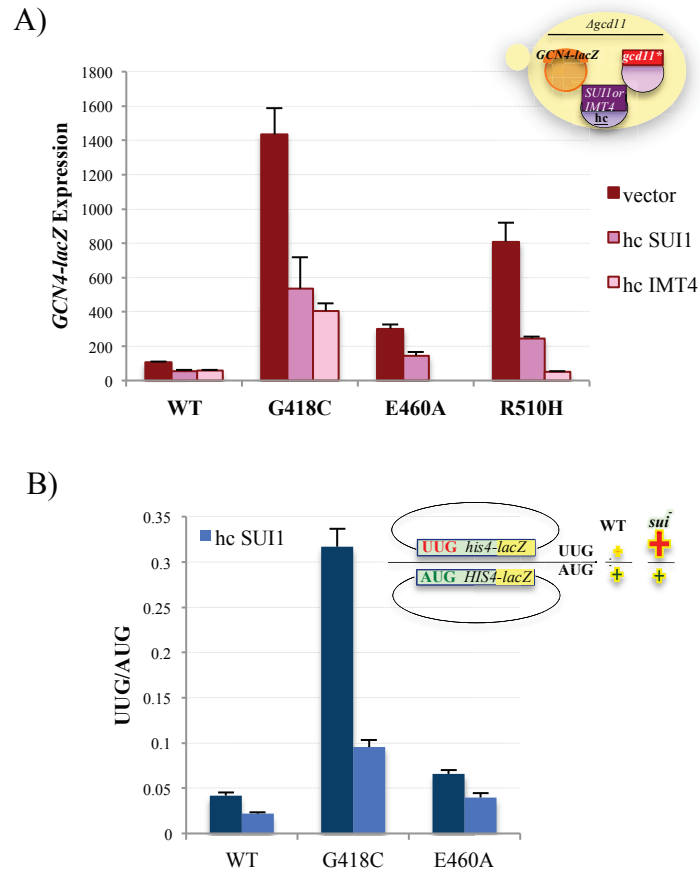


**Figure 3.2 The *Gcd<sup>-</sup>* phenotype and the elevated UUG/AUG initiation ratio of the *GCD11 Sui<sup>-</sup>* mutants are partially suppressed by overexpression of the eIF1 protein**

(A) The *G418C*, *E460A*, and *R510H Sui<sup>-</sup>* alleles of *GCD11* all confer a *Gcd<sup>-</sup>* phenotype, increasing expression of the *GCN4-lacZ* reporter in nutrient-replete conditions.

Overexpressing eIF1 and Met-tRNA<sub>i</sub> partially suppresses the *Gcd<sup>-</sup>* phenotype of the *GCD11* mutants. Expression of the *GCN4-lacZ* reporter was measured in derivatives of strain NAY13 harboring the WT or mutant alleles of *GCD11* with either an empty hc *TRP1* vector (YEplac122) or overexpressing *SUI1* or *IMT4* on hc *TRP1* plasmids (pNA19 and pNA20, respectively).  $\beta$ -galactosidase activities (nanomoles of *o*-nitrophenyl- $\beta$ -D-galactopyranoside cleaved per minute per microgram of protein) were measured in the WCEs of exponentially growing cultures (OD<sub>600</sub> ~0.5) in SC-L-W medium. Mean of at

least eight independent transformants and SEM (error bars) are plotted for each mutant.

(B) Overexpression of eIF1 reduces the ratio of initiation from a UUG codon to that from an AUG codon. UUG to AUG ratio was calculated by measuring the  $\beta$ -galactosidase activity from matched *HIS4-lacZ* reporters (as described in Figure 3.1) in derivatives of NAY13 harboring the WT or mutants alleles of *GCD11* with either an empty vector (YEplac122) or overexpressing *SUI1* from a hc *TRPI* plasmid (pNA19). Same growth conditions and procedure as in panel A. A diagram of the reporter used is presented on the graph.

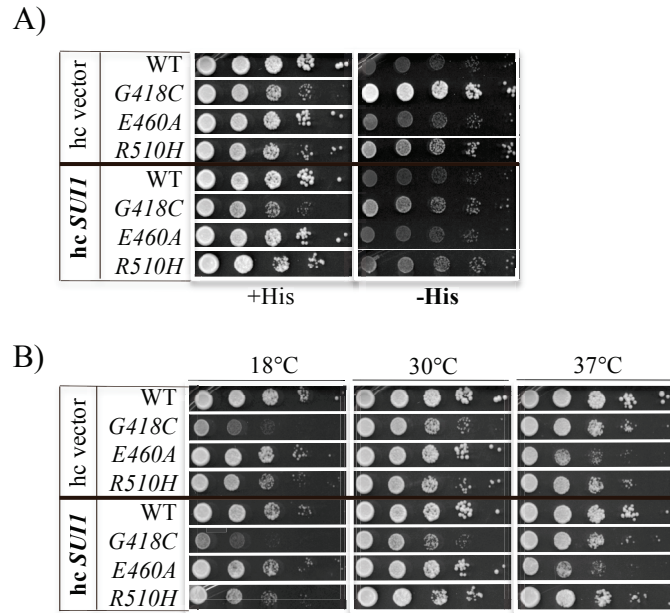


**Figure 3.3 eIF1 overexpression partially suppresses the His<sup>+</sup> phenotype of the *GCD11* Sui<sup>-</sup> mutants but does not alter their growth phenotypes**

(A) Overexpression of the eIF1 protein partially suppresses the His<sup>+</sup> phenotype of the *GCD11* Sui<sup>-</sup> mutants. Strains (same as in Figure 3.2) were cultured in SC-L-W, ten-fold serial dilutions were spotted on SC-L-W medium supplemented with 0.3 mM (+His) or 0.003 mM (-His) histidine, and incubated at 30°C for two and five days, respectively.

(B) Overexpression of the eIF1 protein does not suppress the Slg<sup>-</sup> and the CS<sup>-</sup> phenotypes conferred by the *G418C* allele nor does it mitigate the TS<sup>-</sup> phenotype of the *E460A* mutant. Same strains and growth conditions as in panel A, except that ten-fold serial dilutions were spotted on SC-L-W medium and incubated at the specified temperatures for two (30°C and 37°C) and four (18°C) days.

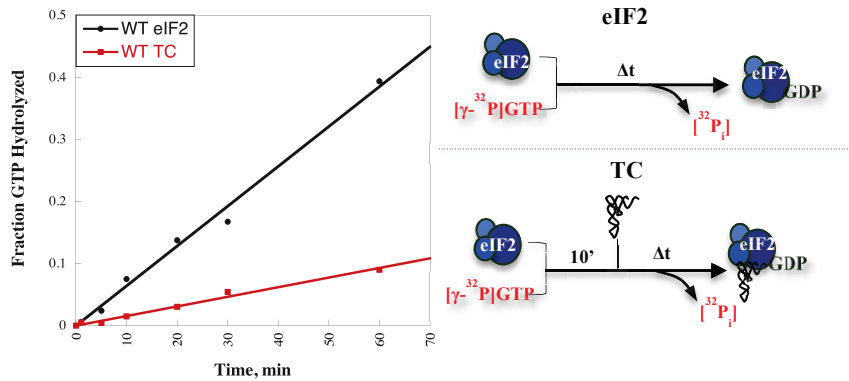


**Figure 3.4 Binding of the Met-tRNA<sub>i</sub> reduces the spontaneous rate of GTP hydrolysis in eIF2**

Met-tRNA<sub>i</sub> binding to the eIF2 complex lowers its intrinsic rate of GTP hydrolysis. GTP hydrolysis was measured by adding a limiting amount of [ $\gamma$ -<sup>32</sup>P]GTP (80 nM) to a saturating concentration of eIF2 (0.8  $\mu$ M). To measure GTP hydrolysis in eIF2 alone, the reactions were incubated at 26°C and stopped by adding 100 mM EDTA at the specified time points. To measure GTP hydrolysis in the TC, eIF2 was first incubated with [ $\gamma$ -<sup>32</sup>P]GTP for 10 min. Met-tRNA<sub>i</sub> (0.8  $\mu$ M) was then added, and the reactions were stopped by adding 100 mM EDTA at the specified time points. [ $\gamma$ -<sup>32</sup>P]GTP and <sup>32</sup>P<sub>i</sub> were separated by thin layer chromatography (PEI-cellulose TLC) and the fraction of total <sup>32</sup>P<sub>i</sub> released was quantified by PhosphorImager analysis. All values were normalized to the fraction of GTP hydrolyzed (<sup>32</sup>P<sub>i</sub> released) at 0 min for eIF2 and at 10 min for the TC. The curves were fit a linear regression equation. Slopes of the regression lines are 0.41±0.040 and 0.088±0.014 for eIF2 and TC, respectively.



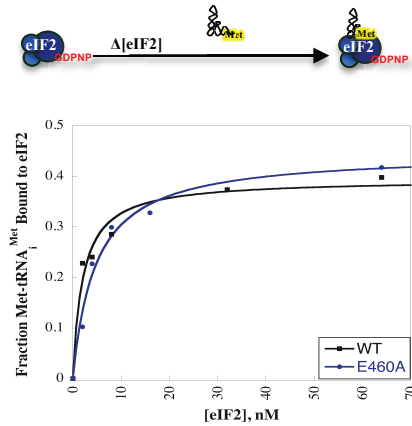


**Figure 3.5 E460A substitution in eIF2 $\gamma$  does not alter the affinity of Met-tRNA<sub>i</sub> binding to the eIF2 complex**

Binding of the Met-tRNA<sub>i</sub> to eIF2 was measured in vitro by filter-binding assays. A limiting amount of [<sup>35</sup>S]Met-tRNA<sub>i</sub> (1 nM) was incubated with GDPNP (1 mM) and a range of eIF2 concentrations. The reactions were filtered through an upper nitrocellulose membrane (Millipore), which retains the eIF2•GDPNP•Met-tRNA<sub>i</sub> complexes, and a lower Nytran Supercharge membrane (Millipore), which retains the unbound [<sup>35</sup>S]Met-tRNA<sub>i</sub>. The filters were then air-dried, and the radioactivity on each membrane was determined by the liquid scintillation counting method. The fraction of [<sup>35</sup>S]Met-tRNA<sub>i</sub> bound to eIF2 at each concentration is plotted. Data were fit with hyperbolic binding curves to determine the K<sub>d</sub> values of 46.0±10.0 and 17±18 nM for WT and the E460A variant of eIF2 $\gamma$ , respectively.

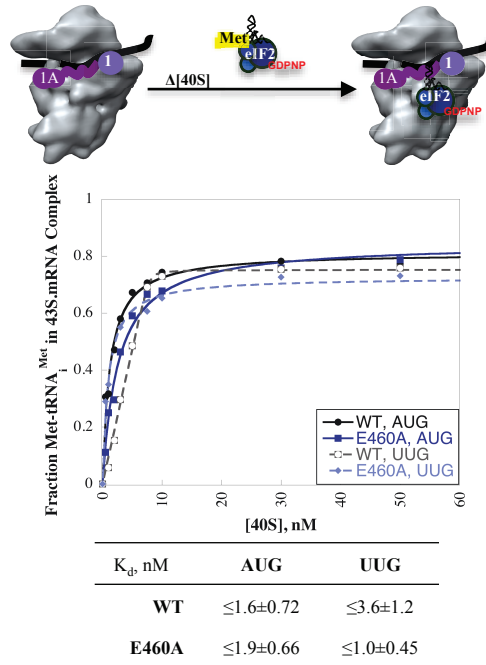


**Figure 3.6 E460A does not alter the affinity of TC binding to the 43S•mRNA PIC**

Preformed TC (0.8  $\mu$ M eIF2, 1 mM GDPNP, 1 nM [ $^{35}$ S]Met-tRNA<sub>i</sub>) was mixed with saturating concentrations of eIF1 (1  $\mu$ ), eIF1A (1  $\mu$ ), mRNA (1  $\mu$ M), and a range of 40S concentrations. The fraction of [ $^{35}$ S]Met-tRNA<sub>i</sub> bound to the 40S subunits (PIC formation) was measured by native gel electrophoresis. Data were fit with hyperbolic binding curves to determine the  $K_d$  values. Averages of at least three experiments and SDs are reported. The detection limit of this assay is  $\leq 1$  nM, as TC binds very tightly to the 40S subunit in the presence of eIF1, 1A, and mRNA.

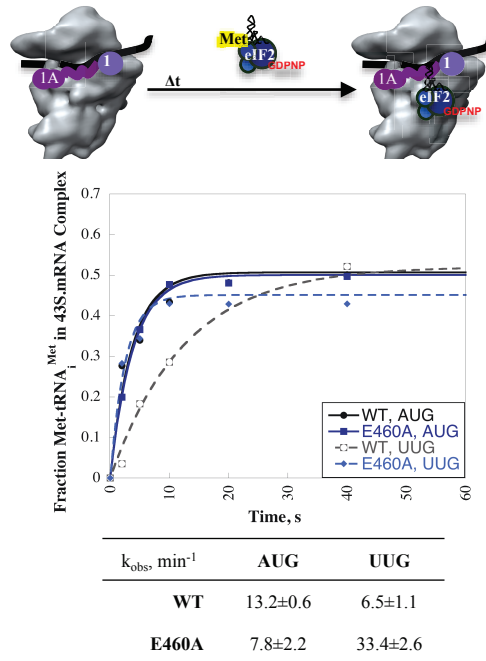


**Figure 3.7 The E460A substitution in eIF2 $\gamma$  increases the rate of TC binding to the 43S•mRNA PIC exclusively with a UUG start codon**

Preformed TC (250 nM eIF2, 1 mM GDPNP•, 1 nM [<sup>35</sup>S]Met-tRNA<sub>i</sub>) was mixed with saturating concentrations of eIF1 (1  $\mu$ ), eIF1A (1  $\mu$ M), 40S (20 nM), and mRNA (10  $\mu$ M) with an AUG or a UUG codon. The reactions were stopped by adding excess amount of unlabeled TC, and the fraction of [<sup>35</sup>S]Met-tRNA<sub>i</sub> bound to the 40S subunits (PIC formation) was measured over time by native gel electrophoresis. The curves were fit with a single exponential equation. Mean values from at least four experiments and SEMs are reported.

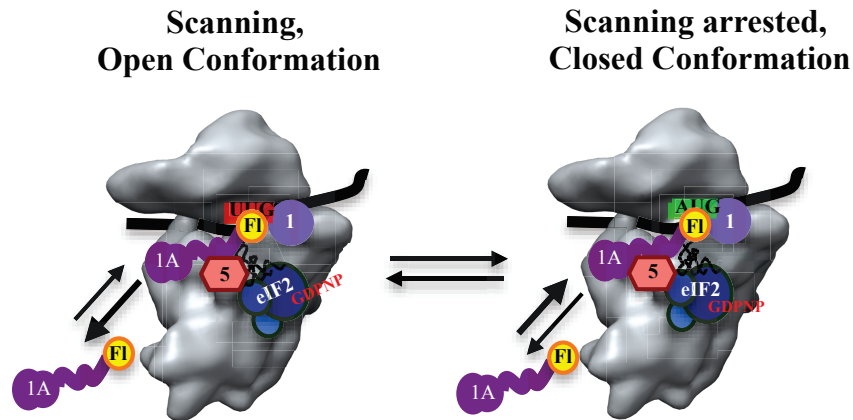


**Figure 3.8** The eIF1A dissociation kinetics from the 43S•mRNA complex serves as a proxy for partitioning between the open and closed conformations of the PIC

Kinetics of eIF1A dissociation from the 43S•mRNA PIC is biphasic. Previous studies have indicated that the fast phase corresponds to eIF1A dissociation from the open, scanning-conductive PIC whereas the slow phase represents the dissociation of eIF1A from the closed, scanning-arrested conformation<sup>75</sup>. Start codon recognition induces structural rearrangements in the PIC that stabilizes eIF1A binding and reduces the rotational freedom of its CTT through an interaction with the eIF5 protein. The tighter binding of eIF1A upon start codon recognition is manifested as an increase in the amplitude of the slower phase of the biphasic dissociation reaction. Therefore, the relative amplitudes of the two kinetic phases of eIF1A dissociation is thought to represent the partitioning of the PIC between the open and closed conformations<sup>75</sup>.

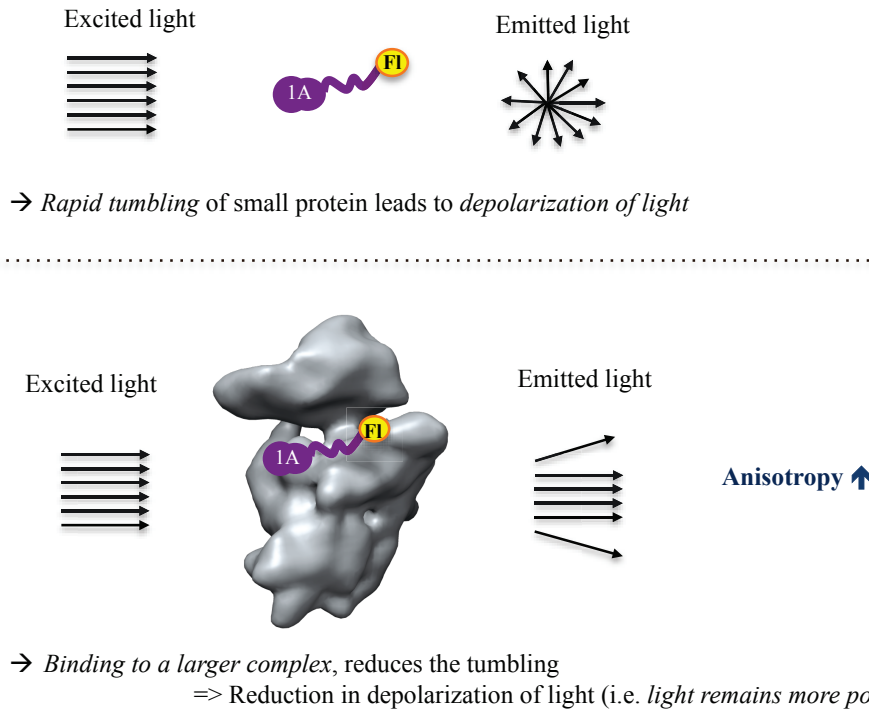


### Figure 3.9 Principles of fluorescence anisotropy

When a fluorescence molecule is excited with a polarized light, the extent of the polarization of the emitted light can be described in terms of anisotropy. Fluorescence anisotropy can be used to measure the steady state or the kinetics of binding reactions that can cause a change in the intrinsic tumbling of molecules. Smaller molecules have a rapid molecular tumbling that leads to a greater depolarization of the excited light (top). Upon binding to a larger complex, however, the tumbling of the smaller molecule is reduced, which subsequently reduces the depolarization of the excited light increasing the anisotropy (bottom). The extent of change in the depolarization of light upon binding of the smaller molecule to a bigger complex (i.e. change in the anisotropy of the fluorescence molecule) represents the binding affinity of the two molecules, which can be measured either at the steady state to obtain the dissociation constant or over time to calculate the rate of a reaction.

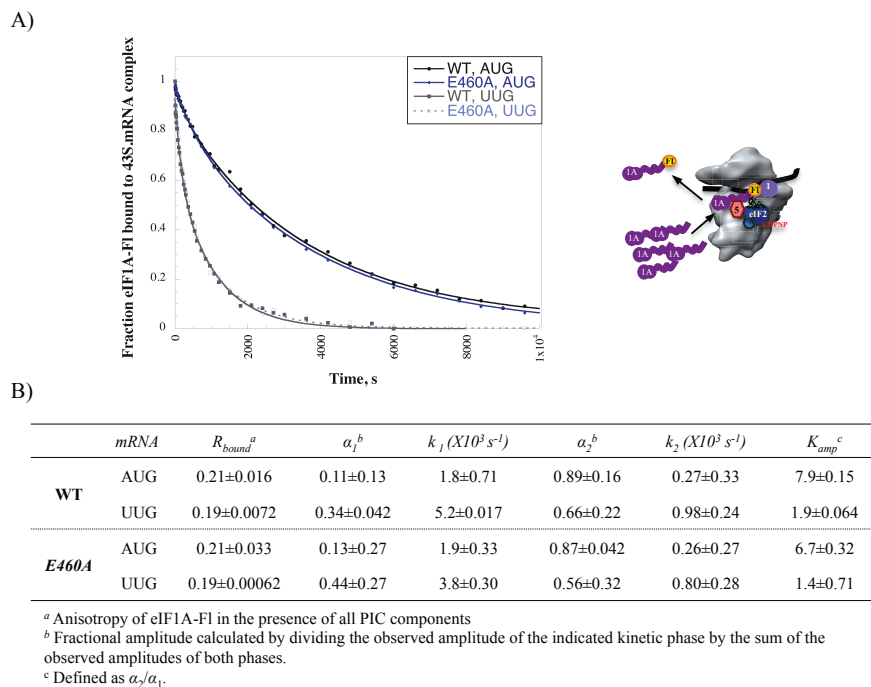


**Figure 3.10 The E460A substitution in eIF2 $\gamma$  does not alter the dissociation kinetics of eIF1A from reconstituted PIC**

(A) 43S•mRNA complexes were first assembled by incubating saturating amounts of TC (0.8  $\mu$ M eIF2, 1 mM GDPNP, 150 nM Met-tRNA<sub>i</sub>), eIF1 (1  $\mu$ M), eIF5 (1  $\mu$ M), 40S (20 nM), and mRNA (10  $\mu$ M) with a limiting amount of eIF1A-FI (15 nM). An excess of unlabeled eIF1A (1  $\mu$ M) was then added, and changes in anisotropy were measured over time. (B) The E460A variant of eIF2 $\gamma$  does not alter the  $K_{amp}$  values with either an AUG or a UUG mRNA. The amplitudes ( $\alpha_1$  and  $\alpha_2$ ), and the rates ( $k_1$  and  $k_2$ ) corresponding to the two phases of eIF1A dissociation are also not altered with the E460A variant compared to the WT eIF2 $\gamma$  protein. Curves from panel A were fit with a double exponential equation. Mean values from at least two experiments and mean deviations are reported.

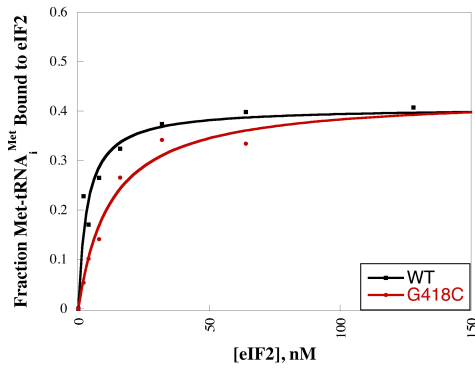


**Figure 3.11 The G418C substitution in eIF2 $\gamma$  does not alter the affinity of Met-tRNA<sub>i</sub> binding to the eIF2 complex**

Binding of the Met-tRNA<sub>i</sub> to eIF2 was measured in vitro by filter-binding assays. Same procedure as in Figure 3.5. The  $K_d$  values are  $46 \pm 10$  and  $48 \pm 12$  for WT and the G418C variant of eIF2 $\gamma$ , respectively.

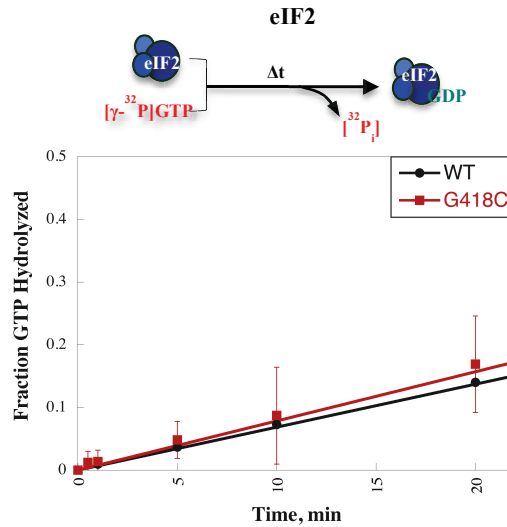


**Figure 3.12 The G418C substitution in eIF2 $\gamma$  does not alter the intrinsic rate of GTP hydrolysis in the eIF2 complex**

Same procedure as in Figure 3.4. Mean value of at least two experiments and mean deviation (error bar) is represented for each time point. Values are normalized to the background rate of hydrolysis ( $^{32}\text{P}_i$  released) in the  $[\gamma\text{-}^{32}\text{P}]\text{GTP}$  molecule alone exposed to the same temperature and buffer conditions of the assay. The curves were fit a linear regression equation. Slopes of the regression lines are  $0.41\pm 0.040$  and  $0.47\pm 0.20$  for the WT and mutant G418C proteins, respectively.



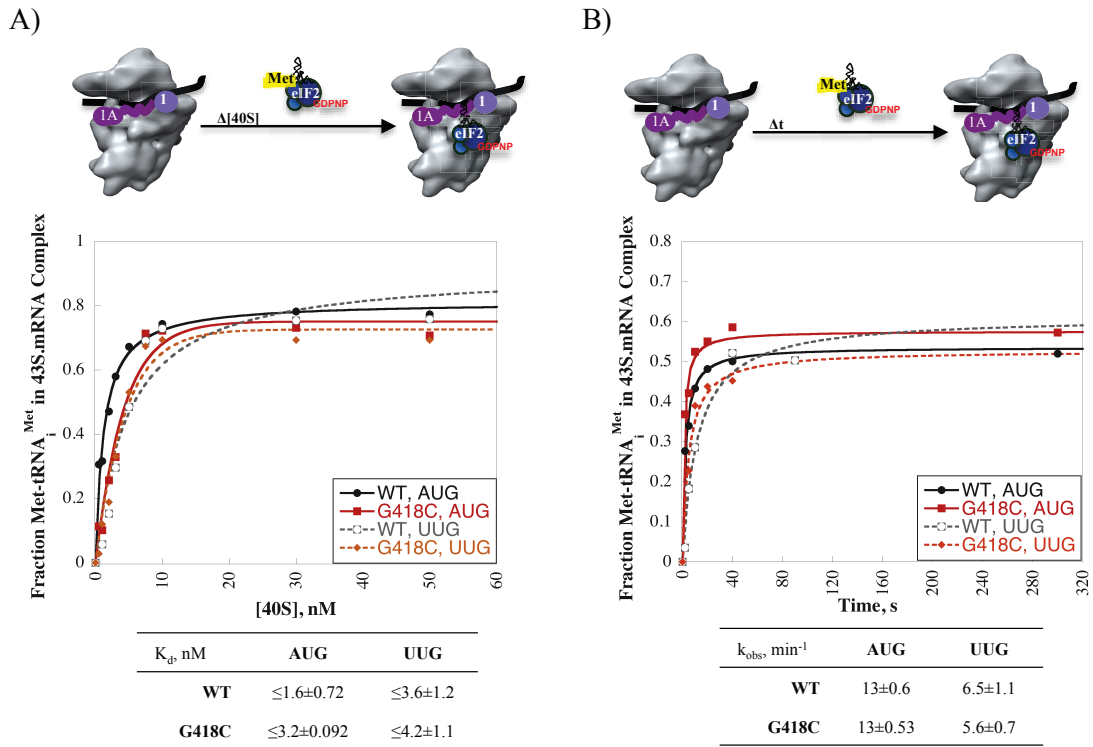
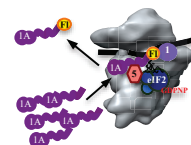
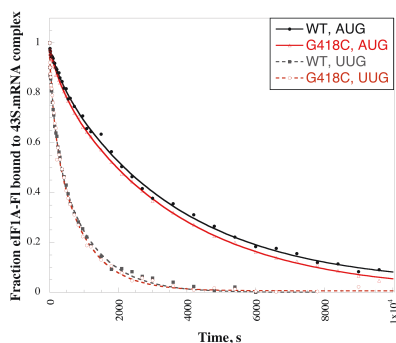


**Figure 3.13 G418C does not alter the affinity or the rate of TC binding to the 43S•mRNA PIC**

(A) The G418C variant of eIF2γ does not alter the affinity of TC binding to reconstituted PIC. Same procedure as in Figure 3.6. Means of at least two experiments and mean deviations are reported. (B) The G418C substitution in eIF2γ does not alter the rate of TC loading on reconstituted PIC. Same procedure as in Figure 3.7. Means of at least three experiments and SDs are reported.

A)



B)

	<i>mRNA</i>	$R_{bound}^a$	$\alpha_1^b$	$k_1 (X10^3)$	$\alpha_2^b$	$k_2 (X10^3)$	$K_{amp}^c$
<b>WT</b>	AUG	0.21±0.016	0.11±0.13	1.8±0.71	0.89±0.16	0.27±0.33	7.9±0.15
	UUG	0.19±0.0072	0.34±0.042	5.2±0.017	0.66±0.22	0.98±0.24	1.9±0.064
<b>G418C</b>	AUG	0.20±0.012	0.11±0.44	2.6±0.12	0.89±0.056	0.28±0.050	8.3±0.50
	UUG	0.19±0.011	0.25±0.079	8.1±0.017	0.75±0.027	1.1±0.0	3.0±0.10

<sup>a</sup> Anisotropy of eIF1A-F1 in the presence of all PIC components  
<sup>b</sup> Fractional amplitude calculated by dividing the observed amplitude of the indicated kinetic phase by the sum of the observed amplitudes of both phases.  
<sup>c</sup> Defined as  $\alpha_2/\alpha_1$ .

**Figure 3.14 The G418C variant of eIF2 $\gamma$  does not alter the dissociation kinetics of eIF1A from reconstituted PIC**

(A) Same procedure as in Figure 3.10. (B) The G418C substitution in eIF2 $\gamma$  does not alter the  $K_{amp}$  values with either an AUG or a UUG mRNA. The amplitudes ( $\alpha_1$  and  $\alpha_2$ ), and the rates ( $k_1$  and  $k_2$ ) corresponding to the two phases of eIF1A dissociation are also not altered with the G418C variant compared to the WT eIF2 $\gamma$  protein. Curves from panel A were fit with a double exponential equation. Mean values from at least two experiments and mean deviations are reported.

**Table 3.1 List of *S. cerevisiae* Strains**

<b>Strain</b>	<b>Genotype</b>	<b>Source</b>
NAY11	<i>Mata ura3-52 leu2-3,112 ino1-13 his4-301(ACG) gcd11Δ::hisG trp1Δ::hisG Ep517&lt;GCD11 LEU2 CEN/ARS&gt;</i>	This Study
NAY13	<i>Mata ura3-52 leu2-3,112 ino1-13 his4-301(ACG) gcd11Δ::hisG trp1Δ::hisG Ep293&lt;GCD11 URA3 CEN4/ARS1&gt;</i>	This Study
NAY93	<i>Mata ura3-52 leu2-3,112 ino1-13 his4-301(ACG) gcd11Δ::hisG trp1Δ::hisG pNA4&lt;GCD11-His<sub>8</sub> LEU2 CEN4/ARS1&gt;</i>	This Study
NAY95	<i>Mata ura3-52 leu2-3,112 ino1-13 his4-301(ACG) gcd11Δ::hisG trp1Δ::hisG pNA4-G418C&lt;gcd11-G418C-His<sub>8</sub> LEU2 CEN4/ARS1&gt;</i>	This Study
NAY97	<i>Mata ura3-52 leu2-3,112 ino1-13 his4-301(ACG) gcd11Δ::hisG trp1Δ::hisG pNA4-E460A&lt;gcd11-E460A-His<sub>8</sub> LEU2 CEN4/ARS1&gt;</i>	This Study
NAY99	<i>Mata ura3-52 leu2-3,112 ino1-13 his4-301(ACG) gcd11Δ::hisG trp1Δ::hisG pNA4-R510H&lt;gcd11-R510H-His<sub>8</sub> LEU2 CEN4/ARS1&gt;</i>	This Study
NAY69	<i>Mata ura3-52 leu2-3,112 ino1-13 his4-301(ACG) gcd11Δ::hisG trp1Δ::hisG gen2Δ::hisG Ep517&lt;GCD11 LEU2 CEN/ARS&gt;</i>	This Study
NAY71	<i>Mata ura3-52 leu2-3,112 ino1-13 his4-301(ACG) gcd11Δ::hisG trp1Δ::hisG gen2Δ::hisG Ep293&lt;GCD11 URA3 CEN4/ARS1&gt;</i>	This Study
NAY72	<i>Mata ura3-52 leu2-3,112 ino1-13 HIS4<sup>+</sup> gcd11Δ::hisG trp1Δ::hisG gen2Δ::hisG Ep293 &lt;GCD11 URA3 CEN4/ARS1&gt;</i>	This Study
NAY76	<i>Mata ura3-52 leu2-3,112 ino1-13 HIS4<sup>+</sup> gcd11Δ::hisG trp1Δ::hisG gen2Δ::hisG pNA4&lt;GCD11-His<sub>8</sub> LEU2 CEN4/ARS1&gt;</i>	This Study
NAY81	<i>Mata ura3-52 leu2-3,112 ino1-13 HIS4<sup>+</sup> gcd11Δ::hisG trp1Δ::hisG gen2Δ::hisG pep4Δ::hygB pNA4&lt;GCD11-His<sub>8</sub> LEU2 CEN4/ARS1&gt;</i>	This Study
NAY82	<i>Mata ura3-52 leu2-3,112 ino1-13 HIS4<sup>+</sup> gcd11Δ::hisG trp1Δ::hisG gen2Δ::hisG pep4Δ::hygB pNA28&lt;sc URA3 GCD11-His<sub>6</sub> SUI3 SUI2&gt;</i>	This Study
NAY84	<i>Mata ura3-52 leu2-3,112 ino1-13 HIS4<sup>+</sup> gcd11Δ::hisG trp1Δ::hisG gen2Δ::hisG pep4Δ::hygB sui3Δ::kanMX4 pNA28&lt;sc URA3 GCD11-His<sub>6</sub> SUI3 SUI2&gt;</i>	This Study
NAY86	<i>Mata ura3-52 leu2-3,112 ino1-13 HIS4<sup>+</sup> gcd11Δ::hisG trp1Δ::hisG gen2Δ::hisG pep4Δ::hygB sui3Δ::kanMX4 sui2Δ::hphMX4 pNA28&lt;sc URA3 GCD11-His<sub>6</sub> SUI3 SUI2&gt;</i>	This Study
NAY87	<i>Mata ura3-52 leu2-3,112 ino1-13 HIS4<sup>+</sup> gcd11Δ::hisG trp1Δ::hisG gen2Δ::hisG pep4Δ::hygB sui3Δ::kanMX4 sui2Δ::hphMX4 pNA21&lt;hc LEU2 GCD11-His<sub>8</sub> SUI3 SUI2 IMT4&gt;</i>	This Study
NAY89	<i>Mata ura3-52 leu2-3,112 ino1-13 HIS4<sup>+</sup> gcd11Δ::hisG trp1Δ::hisG gen2Δ::hisG pep4Δ::hygB sui3Δ::kanMX4 sui2Δ::hphMX4 pNA26&lt;hc LEU2 gcd11-G418C-His<sub>8</sub> SUI3 SUI2 IMT4&gt;</i>	This Study
NAY91	<i>Mata ura3-52 leu2-3,112 ino1-13 HIS4<sup>+</sup> gcd11Δ::hisG trp1Δ::hisG gen2Δ::hisG pep4Δ::hygB sui3Δ::kanMX4 sui2Δ::hphMX4 pNA22&lt;hc LEU2 gcd11-E460A-His<sub>8</sub> SUI3 SUI2 IMT4&gt;</i>	This Study

**Table 3.2 List of Plasmids**

<b>Plasmid</b>	<b>Description<sup>a</sup></b>	<b>Source</b>
YCplac111	sc <i>LEU2</i> yeast- <i>E. coli</i> shuttle vector	229
YCplac22	sc <i>TRP1</i> yeast- <i>E. coli</i> shuttle vector	229
YCP50	sc <i>URA3</i> yeast- <i>E. coli</i> shuttle vector	230
pSB32	lc <i>LEU2</i> yeast- <i>E. coli</i> shuttle vector	
YEplac122	hc <i>TRP1</i> yeast- <i>E. coli</i> shuttle vector	229
YEplac181	hc <i>LEU2</i> yeast- <i>E. coli</i> shuttle vector	229
pRS425	hc <i>LEU2</i> yeast- <i>E. coli</i> shuttle vector	231
YCplac33	sc <i>URA3</i> yeast- <i>E. coli</i> shuttle vector	229
Ep293	sc <i>URA3 GCD11</i> in YCP50	223
Ep517	lc <i>LEU2 GCD11</i> in pSB32	223
pC2872	sc <i>LEU2 GCD11-His<sub>8</sub></i> in YCplac111	P. Alone
pNA4	sc <i>LEU2 GCD11-His<sub>8</sub></i> in pC2872	This study
pNA4-E460A	sc <i>LEU2 gcd11-His<sub>8</sub>-E460A</i>	This study
pNA4-G418C	sc <i>LEU2 gcd11-His<sub>8</sub>-G418C</i>	This study
pNA4-R510H	sc <i>LEU2 gcd11-His<sub>8</sub>-R510H</i>	This study
p367	sc <i>URA3 HIS4(ATG)-lacZ</i>	209
p391	sc <i>URA3 HIS4(TTG)-lacZ (his4-301)</i>	209
p180	sc <i>URA3 GCN4-lacZ</i> in YCp50	232
pCFB04	hc <i>LEU2 SUI1</i> in YEplac181	97
pNA19	hc <i>TRP1 SUI1</i> in YEplac122	This study
pNA20	hc <i>TRP1 IMT4</i> in YEplac122	This study
pRaugFFuug / pJDR1Fuug	sc <i>URA3 P<sub>adh</sub>-(AUG)Renilla-luciferase P<sub>cyc</sub>-(UUG)Firefly-luciferase</i>	97
pAV1726	hc <i>LEU2 GCD11-His<sub>6</sub> SUI3 SUI2</i> in pRS425	G. Pavitt
pAV1732	hc <i>LEU2 GCD11-His<sub>6</sub> SUI3 SUI2 IMT4</i> in pAV1726	G. Pavitt
pNA28	sc <i>URA3 GCD11-His<sub>6</sub> SUI2 SUI3</i> in YCplac33	This study
pNA21	hc <i>LEU2 GCD11-His<sub>8</sub> SUI3 SUI2 IMT4</i> in pAV1732	This study
pNA22	hc <i>LEU2 gcd11-His<sub>8</sub>-E460A SUI3 SUI2 IMT4</i> in pNA21	This study
pNA26	hc <i>LEU2 gcd11-His<sub>8</sub>-G418C SUI3 SUI2 IMT4</i> in pNA21	This study

<sup>a</sup>. sc: single copy number; hc: high copy number; lc: low copy number

**CHAPTER 4: CHARACTERIZATION OF THE MUTANT ALLELES OF *GCD11*  
THAT RESTORE INITIATION FIDELITY**

## 4.1 Introduction

In eukaryotes, the initiation of protein synthesis is governed by base pairing between the anticodon of the Met-tRNA<sub>i</sub> and the start codon of the mRNA. eIF2 is a heterotrimeric complex that delivers the Met-tRNA<sub>i</sub> to the P-site of the small subunit of the ribosome in a GTP dependent manner, maintains the Met-tRNA<sub>i</sub> in the proper orientation for scanning the leader sequence of the mRNA with the PIC in the open conformation, and finally releases the Met-tRNA<sub>i</sub> upon start codon recognition and formation of the closed conformation. Thus, eIF2 is intimately involved in the identification and selection of the start codon in eukaryotes. In order to identify the structural elements in eIF2 that are essential for the accuracy of start codon selection, we set out to identify mutations that alter the fidelity of this process. We focused on the  $\gamma$ -subunit as it forms the core of the eIF2 complex that provides the binding sites for GTP and the Met-tRNA<sub>i</sub>.

As discussed in Chapter 2, to identify the essential features of eIF2 $\gamma$  involved in scanning and start codon recognition, we employed three different strategies to isolate mutant alleles that either reduce the accuracy of initiation (Sui<sup>-</sup> phenotype) or conversely restore it in cells harboring a Sui<sup>-</sup> mutant (Ssu<sup>-</sup> phenotype). Our genetic and biochemical analysis of the Sui<sup>-</sup> alleles of *GCD11* suggested a novel function for the eIF2 complex in which domain-III of the  $\gamma$ -subunit is involved in promoting the formation of the closed conformation (see Chapter 3). We also isolated multiple mutant alleles of *GCD11* that restore the stringency of start codon recognition and confer an Ssu<sup>-</sup> phenotype (see Chapter 2). Among them, we selected the *gcd11-N433D* and *gcd11-R484A* alleles that presented the strongest genetic phenotype in suppressing the His<sup>+</sup> and the elevated UUG

initiation in Sui<sup>-</sup> mutant cells (with reduced initiation fidelity) for further in-depth biochemical analysis in a reconstituted yeast translation initiation system. These results are presented in this chapter.

## 4.2 Materials and Methods

Standard methods were used for culturing, transforming, plasmid shuffling, and construction of *S. cerevisiae* strains<sup>210-212</sup>. For yeast growth assays, cultures were grown to saturation, diluted to OD<sub>600</sub> of 1 or 0.5, and 5µl of 10X serial dilutions were spotted on the appropriate medium.

### 4.2.1 Yeast Strain Constructions

For a list of yeast strains see Table 4.1. Strain NAY116 was generated by transforming NAY13 (*gcd11Δ, his4-301, sc URA3 GCD11*) with a *sc TRP1 SUI3-2* plasmid (p4280) and selecting for transformants on SC-U-W medium. NAY156, NAY135, and NAY137 were created by transforming NAY116 with plasmids pNA4, pNA4-N433D, and pNA4-R484A, respectively. The transformants were plated on SC-L-W medium containing 5-FOA to select for loss of the *URA3*-containing plasmid Ep293.

To obtain strains NAY105, NAY109, and NAY111, which were used to purify the eIF2 complexes containing the S264Y substitution in eIF2β and the WT, N433D, and R484A mutant variants of eIF2γ, respectively, NAY86 was transformed with plasmids pNA29, pNA30, and pNA31. Transformants were plated on SC-L medium containing 5-FOA to select for loss of the *URA3*-containing plasmid pNA28. The strains were verified again by rescuing their respective plasmids and subjecting them to DNA sequence analysis of the three genes (*SUI2, SUI3, and GCD11*) encoding the eIF2 complex. See Section 2.2.1 for details on the construction of NAY13 and Section 3.2.1 for NAY86 and NAY87.



#### 4.2.2. Plasmid Constructions

For the list of plasmids used in this study see Table 4.2. Plasmid pNA29 was generated by replacing the XhoI-MluI fragment of pNA21 containing the WT *SUI3* gene with the 0.85 kb SalI-MluI fragment of p4280 harboring the mutant *SUI3-2* allele. The plasmid was verified by DNA sequence analysis of *GCD11*, *SUI2*, and *SUI3* genes. pNA30 and pNA31 were obtained by replacing the 2.57 kb SacI-SbfI fragment of pNA29 (containing WT *GCD11-His<sub>8</sub>*) with the SacI-SbfI fragments from plasmids pNA4-N433D and pNA4-R484A, respectively. The plasmids were verified by DNA sequence analysis of *GCD11*, *SUI2*, and *SUI3* genes. See Section 2.2.2 for details of the construction procedures for plasmids pNA4-N433D and pNA-R484A and Section 3.2.2 for pNA28 and pNA29.

#### 4.2.3. Biochemical Assays with Yeast Extracts

$\beta$ -galactosidase assays with yeast WCEs obtained from exponentially growing cells ( $OD_{600}$  of  $\sim 0.5$ ) were performed as described previously<sup>218</sup>.

#### 4.2.4. In Vitro Reconstitution Assays

All the biochemical assays in the in vitro reconstituted yeast translation initiation system were performed as described in Chapter 3 (see Section 3.2.4).

## 4.3 Results

### 4.3.1 The *Ssu*<sup>-</sup> Mutants of *GCD11* Restore Initiation Fidelity in Cells Harboring the *SUI3-2* Allele in Vivo

A tyrosine substitution of the serine residue at position 264 (S264Y) of eIF2 $\beta$ , encoded by the *SUI3-2* allele, reduces the stringency of start codon recognition and confers a dominant *Sui*<sup>-</sup> phenotype<sup>109,152,163</sup>. We again took advantage of the *his4-301* allele to monitor the accuracy of initiation in vivo<sup>209</sup> (Figure 4.1A). *his4-301* is a mutant variant of the *HIS4* gene that lacks a cognate AUG codon, which consequently confers histidine auxotrophy in otherwise WT cells (Figure 4.1B, compare the WT row on the +His and -His medium). The *SUI3-2* allele, however, reduces the fidelity of start codon selection and allows for translation initiation from the third in-frame (UUG) codon of *his4-301*<sup>109,152,163</sup>. Consequently, *SUI3-2* suppresses the histidine auxotrophy of cells harboring the *his4-301* allele and confers a His<sup>+</sup> phenotype (Figure 4.1B, compare WT and *SUI3-2* on the -His medium). The *N433D* and *R484A* mutant alleles of *GCD11* when expressed in cells harboring *SUI3-2*, both suppress its His<sup>+</sup> phenotype to nearly WT levels (Figure 4.1B). Thus, the *GCD11* mutants reestablish the fidelity of start codon selection in vivo and block translation initiation from the UUG codon of the *his4-301* allele so that cells expressing the *SUI3-2* allele are again histidine auxotrophs.

To quantify the extent by which these mutants suppress initiation from the UUG codon of *his4-301* in cells harboring *SUI3-2*, we used matched *HIS4-lacZ* reporters containing either a UUG (*his4-lacZ*) or an AUG (*HIS4-lacZ*) start codon and measured the ratio of their respective products (UUG to AUG ratio) (Figure 4.1C). In WT cells, there is relatively low background level of initiation from a UUG codon, and hence the

ratio of *his4-lacZ* to *HIS4-lacZ* expression is very low. *SUI3-2*, however, reduces the stringency of start codon recognition and increases the frequency of UUG initiation elevating the UUG to AUG ratio by ~2.6-fold (Figure 4.1D, compare WT to *SUI3-2*). In cells expressing the *N433D* and *R484A* mutant alleles of *GCD11* together with *SUI3-2*, however, the ratio of initiation from a UUG codon to that from an AUG codon is reduced (Figure 4.1D). As a result, *gcd11-N433D* completely eliminates and *gcd11-R484A* substantially reduces the elevated UUG initiation conferred by *SUI3-2* restoring the accuracy of start codon selection in vivo.

#### 4.3.2 *SUI3-2* Stabilizes the Closed Conformation of the PIC

In order to identify the underlying mechanism by which the Ssu<sup>-</sup> mutants of *GCD11* reinstate the fidelity of start codon recognition, we took advantage of a reconstituted yeast translation initiation system<sup>238</sup> to directly assay the various steps involved in the formation of a functional pre-initiation complex. It was originally proposed that *SUI3-2* allows for initiation from a non-AUG codon by increasing the intrinsic rate of GTP hydrolysis in the eIF2 complex<sup>163</sup>. Thus, we first examined if the S264Y substitution in the  $\beta$  subunit (the point mutation encoded by the *SUI3-2* allele) increases the spontaneous rate of GTP hydrolysis in purified eIF2. A limiting amount of [ $\gamma$ -<sup>32</sup>P]GTP was incubated with a saturating concentration of eIF2, and the fraction of GTP hydrolyzed was measured over time by separating the [ $\gamma$ -<sup>32</sup>P]GTP and <sup>32</sup>P<sub>i</sub> entities using thin layer chromatography. Consistent with previous reports, we observed a low rate of GTP hydrolysis in WT eIF2 (Figure 4.2). In this assay, however, the S264Y substitution in eIF2 $\beta$  does not increase the intrinsic rate of GTP hydrolysis compared to the WT protein (Figure 4.2).

*SUI3-2* allows for translation initiation from a UUG codon in vivo. Since the formation of the closed conformation is needed for start codon recognition, we hypothesized that *SUI3-2* further stabilizes the closed conformation of the PIC, which consequently leads to initiation at non-AUG codons. Therefore, we next determined the relative stability of the two conformations of the PIC by measuring the dissociation rate of the eIF1A protein from the in vitro reconstituted 43S•mRNA complex.

As elucidated in Chapter 3, kinetics of eIF1A dissociation from the 43S•mRNA complexes is biphasic and serves as a proxy for measuring the partitioning of the PIC between the open and closed conformations<sup>75</sup>. It has been demonstrated that start codon recognition induces structural rearrangements in the PIC that stabilizes eIF1A binding and reduces the rotational freedom of its CTT through an interaction with the eIF5 protein<sup>75</sup>. This is apparent as the rate of eIF1A dissociation is slower from the PIC reconstituted with an AUG versus a non-AUG codon (Figure 4.3A, compare the WT curve with an AUG to that with a UUG mRNA). The tighter binding of eIF1A upon start codon recognition is manifested as an increase in the amplitude of the slower phase of the biphasic dissociation reaction. Therefore, the relative amplitudes of the two kinetic phases of eIF1A dissociation are thought to represent the partitioning of the PIC between the open, scanning-conductive and closed, scanning-arrested conformations. An apparent equilibrium constant ( $K_{amp}$ ) between the two PIC conformations can then be defined as the ratio of the amplitudes of the two kinetic phases of eIF1A dissociation. Higher  $K_{amp}$  values indicate that the closed conformation is more favored (Figure 3.8).

We determined the dissociation kinetics of eIF1A from reconstituted PIC using a fluorescence anisotropy-based assay<sup>75</sup>. 43S•mRNA PIC was first assembled with a

limiting amount of fluorescein labeled eIF1A (eIF1A-F1) and saturating concentrations of the TC, eIF1, eIF5, 40S, and mRNA (with an AUG or a UUG codon). An excess of unlabeled eIF1A was then added and changes in the anisotropy were measured over time. In agreement with previous studies<sup>70,75,104</sup>, and as elucidated above, we observed reduced dissociation of eIF1A from the reconstituted PIC with an AUG versus a UUG codon (Figure 4.3A, compare the WT curve with an AUG to that with a UUG mRNA). This is apparent as the  $K_{amp}$  value with an AUG codon, when the majority of the PIC is in the closed conformation, is ~4-fold larger than that for a UUG codon (Figure 4.3B, compare the  $K_{amp}$  values for the WT with an AUG versus a UUG mRNA). Moreover, as previously reported<sup>75</sup>, we observed that the starting anisotropy of the complex ( $R_{bound}$ ) is greater for the PIC assembled with an AUG mRNA compared to that with a UUG mRNA (Figure 4.3B, compare the WT  $R_{bound}$  values), which presumably reflects the reduced rotational flexibility of the eIF1A CTT in the closed versus the open conformations of the PIC.

Remarkably, the S264Y substitution in eIF2 $\beta$  increases the fraction of the PIC in the closed conformation relative to the open conformation at a UUG codon, increasing the  $K_{amp}$  by ~6-fold (Figure 4.3B, compare the  $K_{amp}$  values of WT with S264Y). Interestingly, we could not calculate a  $K_{amp}$  value for S264Y at an AUG codon as the dissociation kinetics of eIF1A is no longer biphasic and the data is fit with a single exponential function. This indicates that the S264Y substitution in eIF2 $\beta$  increases the proportion of the PIC in the closed conformation to the point where the open conformation is essentially nonexistent at an AUG codon. Thus, S264Y increases the steady state stability of the closed conformation at both an AUG and a UUG codon.

Under normal circumstances, the majority of the PICs at an AUG start codon are in the scanning-arrested, closed conformation whereas at a UUG codon the majority of PICs are in the scanning-conductive, open conformation. Therefore, a further increase in the proportion of the PIC in the closed conformation is likely to have a smaller impact on initiation frequency at an AUG codon than at a UUG codon. Hence, stabilization of the closed conformation provides a logical explanation for the loss of initiation fidelity and the Sui<sup>-</sup> phenotype of cells expressing the *SUI3-2* mutant allele.

It has been previously demonstrated that start codon recognition and formation of the closed conformation stabilizes binding of the TC to the 40S subunit<sup>95</sup>. Thus, to confirm that the loss of initiation fidelity in *SUI3-2* is indeed due to the stabilization of the closed conformation at a UUG codon, we measured the dissociation kinetics of the TC from reconstituted PIC. PIC was first assembled with saturating amounts of eIF2, eIF1, eIF1A, 40S, and mRNA and a limiting concentration of [<sup>35</sup>S]Met-tRNA<sub>i</sub>. The reactions were then initiated by adding an excess of unlabeled TC and were stopped by loading on a running native gel. The fraction of TC that remained bound to the 43S•mRNA PIC was then quantified to calculate the dissociation rate of TC. Stabilization of the TC binding upon formation of the closed conformation is apparent as while there is almost no TC dissociated at an AUG codon even after 24 hours, only 50% of the TC remains bound to the PIC at a UUG codon after 4 hours (Figure 4.4, compare the WT curves with an AUG and a UUG mRNA). Consistent with stabilizing the closed conformation, S264Y reduces the dissociation rate of TC from the PIC at a UUG codon by ~2-fold (Figure 4.4). Thus, our results from the dissociation kinetics of eIF1A and TC both suggest that the reduced accuracy of start codon recognition in *SUI3-2* is due to the

stabilization of the closed conformation, which consequently leads to initiation at non-AUG codons. This finding is consistent with the current understanding of the translation initiation mechanism in eukaryotes (discussed in Section 1.1.1) as start codon selection does require the formation of the closed conformation.

#### *4.3.3. The Ssu<sup>-</sup> Mutants of GCD11 Reduce the Stability of the Closed Conformation of the PIC*

As elucidated above, *SUI3-2* allows for UUG initiation by stabilizing the closed conformation of the PIC. Based on their ability to block translation initiation from a UUG codon in cells expressing the *SUI3-2* allele in vivo, we hypothesized that the *N433D* and *R484A* Ssu<sup>-</sup> mutants of *GCD11* reestablish the accuracy of start codon recognition by reducing the stability of the closed conformation, and hence allowing for the PIC to continue scanning the leader sequence of the mRNA in search of a cognate AUG start codon. This hypothesis is in agreement with our proposed model that domain-III of eIF2 $\gamma$  is involved in maintaining the equilibrium between the two PIC conformations (see Section 3.3.2) as residues N433 and R484 are positioned on a discrete surface-exposed locus in domain-III (Section 2.3.4 and Figure 4.7A).

Therefore, to establish if the Ssu<sup>-</sup> mutants of *GCD11* alter the stability of the two conformations of the PIC, we measured the dissociation kinetics of eIF1A from reconstituted PIC, with eIF2 containing the S264Y substitution in the  $\beta$  subunit and the *N433D* or *R484A* substitutions in the  $\gamma$  subunit, using the same procedure explained above. Remarkably, the *N433D* and *R484A* mutants of eIF2 $\gamma$  both partially suppress the effects of S264 and increase the dissociation of eIF1A from the 43S•mRNA complexes (Figure 4.3A). *N433D* and *R484A* reduce the fraction of PIC in the closed conformation

lowering the  $K_{amp}$  value by ~3-fold at a UUG codon (Figure 4.3B, compare the  $K_{amp}$  values). They also lower the prevalence of the closed conformation at an AUG codon so that the biphasic kinetics is restored to eIF1A dissociation from PIC containing the S264Y substitution, albeit the  $K_{amp}$  values are still higher compared to the WT values (Figure 4.3B).

Consistent with lowering the occurrence of the close conformation, the N433D and R484A mutants also reduce the  $R_{bound}$  values (Figure 4.3B). As elucidated above, a higher  $R_{bound}$  value reflects reduced rotational flexibility of the eIF1A CTT in the closed conformation. Thus, a reduction in the  $R_{bound}$  value suggests that the fraction of PIC in the closed conformation is reduced. Remarkably, the N433D and R484A substitutions, when present with S264Y, reduce the  $R_{bound}$  at both AUG and UUG codons to values even lower than that of the WT eIF2. Thus, our results suggest that the *N433D* and *R484A* mutants of *GCD11* suppress the loss of initiation fidelity in cells expressing the *SUI3-2* allele by reducing the prevalence of the closed conformation of the PIC.

To confirm that the *Ssu*<sup>-</sup> mutants of *GCD11* reduce the stability of the closed conformation by employing an alternative method, we measured the kinetics of TC dissociation from reconstituted PIC with eIF2 containing the S264Y substitution in the  $\beta$  subunit and the N433D or R484A substitutions in the  $\gamma$  subunit. As discussed earlier, formation of the closed conformation stabilizes the binding of the TC to the PIC. We showed above that S264Y mutant of eIF2 $\beta$  increases the stability of the closed conformation, and consequently reduces the dissociation of TC from the PIC at a UUG codon (Figure 4.4, compare the S264Y curve with the WT). If the N433D and R484A substitutions in eIF2 $\gamma$  indeed reduce the stability of the closed conformation, they should



then increase the dissociation rate of TC containing the S264Y mutant from reconstituted PIC. Confirming this expectation, N433D and R484A both increase the dissociation rate of TC from the 43S•mRNA PIC at a UUG codon to WT levels (Figure 4.4). Thus, our findings from the dissociation kinetics of eIF1A and TC from reconstituted PIC, both indicate that the Ssu<sup>-</sup> mutants of *GCD11* block translation initiation at a UUG codon by reducing the stability of the closed conformation.

Next, to examine if the loading of the TC on the 40S subunit is altered with the mutant eIF2 complexes containing the S264Y substitution in  $\beta$  and the N433D or R484A mutant variants of  $\gamma$ , we measured the affinity and the kinetics of TC binding to reconstituted PIC. To determine the affinity of the TC binding to the 40S subunit, we performed electrophoretic mobility shift assays to monitor the PIC formation (as explained in Chapter 3). The PIC was assembled in vitro using saturating concentrations of eIF2 (WT, S264Y, S264Y/N433D, and S264Y/R484A), eIF1, eIF1A, and mRNA (with an AUG or a UUG codon), a limiting amount of radiolabeled [<sup>35</sup>S]Met-tRNA<sub>i</sub>, and a range of 40S concentrations. The fraction of TC bound to the 40S (PIC formation) was then measured by native gel electrophoresis. In agreement with previous studies, we observed a tight binding of TC to the 43S•mRNA complexes (Figure 4.5). Moreover, our results indicate that none of the eIF2 mutant complexes significantly alter the affinity of the TC for the 40S subunit at either a UUG or an AUG codon (Figure 4.5).

To measure the rate of TC binding to the 40S subunit, we next determined the kinetics of PIC formation using a similar gel shift assay. Preformed TC (eIF2•GDPNP•[<sup>35</sup>S]Met-tRNA<sub>i</sub>) was mixed with saturating concentrations of eIF1, eIF1A, 40S, and mRNA. The reaction was stopped at different time points by adding an

excess of unlabeled TC, and the fraction of TC bound to the 40S was monitored by native gel electrophoresis. As discussed in Sections 1.1.2 and 3.3.2, start codon recognition stabilizes the binding of the TC to the 40S subunit. Consistent with previous reports<sup>63,95</sup>, we observed a higher rate of TC binding to the PIC with an AUG versus a UUG codon (Figure 4.6, compare the  $k_{\text{obs}}$  for the WT with an AUG to that with a UUG mRNA). Furthermore, these experiments established that none of the mutant eIF2 complexes significantly alter the observed rate of TC loading on the 40S subunit at either an AUG or a UUG codon (Figure 4.6). Thus, the altered accuracy of start codon recognition conferred by *SUI3-2* and the *GCD11* Ssu<sup>-</sup> alleles is unlikely to be a result of altered rate TC loading on the PIC.

Lastly, to eliminate the possibility that the mutant *GCD11* alleles alter the intrinsic rate of GTP hydrolysis in eIF2, we measured GTP hydrolysis in purified eIF2 containing the S264Y variant of  $\beta$  and the N433D or R484A substitutions in  $\gamma$  (as described above in Section 3.3.2) and established that the spontaneous rate of GTP hydrolysis is unaffected in these mutant complexes compared to WT eIF2 (Figure 4.2). Therefore, our findings suggest that the Ssu<sup>-</sup> mutants of *GCD11* reestablish the fidelity of start codon recognition by *specifically* reducing the prevalence of the closed conformation of the PIC.

#### 4.4 Discussion

To identify the structural elements in eIF2 $\gamma$  involved in establishing the fidelity of start codon recognition, we used different strategies to isolate mutations that alter the fidelity of this process (see Chapter 2). We successfully identified multiple mutant alleles in *GCD11* that either lower the accuracy of the start codon selection (Sui $^-$  phenotype) or conversely reinstate it in cells with reduced initiation fidelity (Ssu $^-$  phenotype). The characterization of our Sui $^-$  alleles, presented in Chapter 3, suggested a new function for domain-III of eIF2 $\gamma$  in maintaining the equilibrium between the two conformations of the PIC, which is essential for the fidelity of translation initiation. In this chapter, we presented our in-depth analysis on two of the *GCD11* Ssu $^-$  alleles, *gcd11-N433D* and *gcd11-R484A*, that we had identified (see Chapter 2). Our findings here provide further evidence for the role of domain-III of eIF2 $\gamma$  in establishing the accuracy of start codon recognition by maintaining the equilibrium between the open and closed conformations of the PIC.

We first illustrated that the Ssu $^-$  mutants of *GCD11* reestablish the accuracy of start codon selection in vivo by suppressing the Sui $^-$  phenotype of *SUI3-2*. The *SUI3-2* allele, which encodes the S264Y substitution in the  $\beta$  subunit of the eIF2 complex, reduces the stringency of start codon recognition and confers a dominant Sui $^-$  phenotype<sup>163</sup>. It suppresses the histidine auxotrophy in cells harboring the *his4-301* allele (His $^+$  phenotype) by allowing for translation initiation from a near-cognate UUG codon. The N433D and R484 substitutions in eIF2 $\gamma$ , however, suppress the His $^+$  phenotype conferred by the *SUI3-2* allele by blocking the translation of *his4-301*. In agreement with this phenotype, both mutants also partially suppress the elevated ratio of UUG to AUG

initiation conferred by the *SUI3-2* allele, measured by matched *HIS4-lacZ* reporters expressed either from a UUG or an AUG start codon. Thus, the *N433D* and *R484A* mutants of *GCD11* restore initiation fidelity in cells harboring *SUI3-2* in vivo.

In order to determine the underlying mechanism for our Ssu<sup>-</sup> mutants, we took advantage of an in vitro reconstituted yeast translation initiation system<sup>238</sup> to monitor the various steps involved in the process of start codon recognition directly. It was originally proposed that *SUI3-2* increases the intrinsic rate of GTP hydrolysis in eIF2<sup>163</sup>. In our assays, however, we did not detect any increase in the spontaneous rate of GTP hydrolysis in purified eIF2 containing the S264Y substitution. This difference may result from variations in the set up of the two assays. We employed a GTPase assay where we incubated a limiting amount of [ $\gamma$ -<sup>32</sup>P]GTP with a saturating concentration of eIF2 at 26°C, stopped the reactions by adding 100 mM EDTA at different time points, separated the hydrolyzed  $\gamma$ -phosphate (<sup>32</sup>P<sub>i</sub>) and the [ $\gamma$ -<sup>32</sup>P]GTP entities by thin layer chromatography, and calculated the fraction of <sup>32</sup>P<sub>i</sub> released by PhosphorImager analysis. In the original assay, however, the fraction of GTP hydrolyzed was inferred by the loss of <sup>32</sup>P<sub>i</sub> signal in a filter-binding assay<sup>163</sup>. In this assay [ $\gamma$ -<sup>32</sup>P]GTP and [<sup>3</sup>H]GTP were incubated at a ratio of 1:1000 with eIF2 at 37°C, the samples were applied to pre-wet membranes, and the amount of [ $\gamma$ -<sup>32</sup>P]GTP remaining bound to eIF2 was determined by counting the air-dried membranes without scintillation liquid. A likely reason for the difference observed in the results can be attributed to the temperature at which the two assays were conducted. While the original filter-binding assay was performed at 37°C, we measured the rate of GTP hydrolysis at 26°C. It has been reported that the *SUI3-2* allele confers a temperature sensitivity phenotype<sup>61,244</sup>. Thus, it is likely that the increase

in the spontaneous rate of GTP hydrolysis observed in the original report is due to the higher temperature at which the assay was conducted. Interestingly, this may suggest that the underlying mechanism for the temperature sensitivity of *SUI3-2* is an increase in the intrinsic rate of GTP hydrolysis in eIF2.

It should also be noted that the standard laboratory growth temperature for *S. cerevisiae* is 30°C, which has been used as part of the default growth conditions throughout our study. Furthermore, our biochemical assays were all performed at 26°C that is close to the temperature at which our in vivo experiments were conducted. Regardless of whether *SUI3-2* increases the intrinsic rate of GTP hydrolysis, however, its in vivo Sui<sup>-</sup> phenotype cannot be fully explained by this defect since while the Ssu<sup>-</sup> mutants of *GCD11* suppress the loss of initiation fidelity conferred by the *SUI3-2* allele in vivo (at 30°C), they do not alter the intrinsic rate of GTP hydrolysis compared to WT eIF2.

*SUI3-2* allows for non-AUG start codon recognition, and since a stable closed conformation is needed for the process of initiation to ensue, we hypothesized that *SUI3-2* increases the stability of the PIC in the closed conformation at near-cognate UUG codons. We measured the fraction of PIC in each conformation by determining the kinetics of eIF1A dissociation, and confirmed that *SUI3-2* does indeed increase the occurrence of the closed conformation. The increase in the stability of the PIC, however, is regardless of the start codon as *SUI3-2* increases the proportion of PIC in the closed conformation both with an AUG and a UUG containing mRNA. This is consistent with the report that *SUI3-2* does not specifically prefer a UUG codon and increases translation initiation at non-AUG codons irrespective of their exact sequence<sup>163</sup>. Our result is also in

agreement with a recent report implicating eIF2 $\beta$  is stabilizing the closed conformation, as it was illustrated that physical interactions between eIF2 $\beta$  and eIF5 are required for the stabilization of the closed conformation<sup>70</sup>. Although the S264Y substitution is located in a different domain of eIF2 $\beta$  than the one interacting with eIF5, it is possible that it increases the stability of the closed conformation by further strengthening the interactions between the eIF2 $\beta$  and eIF5 proteins, for example by allosterically altering the structure of the N-terminal domain of  $\beta$  that contact eIF5.

Another possibility is that *SUI3-2* stabilizes the closed conformation by indirectly increasing the interactions between the NTD of eIF5 and the CTT of eIF1A. As elucidated in Chapter 1, the NTD of eIF5 is reported to directly contact the G-domain of eIF2 $\gamma$ <sup>69</sup>. Since interactions between the NTD of eIF5 and CTT of eIF1A have been reported to form upon a cognate codon:anticodon interaction<sup>72</sup>, which stabilizes the closed conformation, the NTD of eIF5 is then expected to move away from the G-domain of eIF2 $\gamma$ , which can also potentially contribute to the release of P<sub>i</sub>. This is indeed consistent with a recent report that the interaction between eIF5 NTD and eIF1A CTT is required for P<sub>i</sub> release and eIF1 dissociation<sup>72</sup>. Moreover, the ZBD of eIF2 $\beta$ , where the S264Y substitution is located, exhibits a high degree of flexibility and has been observed to potentially interact with the G-domain of  $\gamma$ <sup>114,116,126</sup>. Furthermore, the NTD of eIF5 contains a ZBD and an  $\alpha$ - $\beta$  fold domain that bear structural homology to the equivalent domains of eIF2 $\beta$ <sup>116,158</sup>. Therefore, they can potentially compete for binding to similar substrates, such as the switch-I element of eIF2 $\gamma$  G-domain. Moreover, as elucidated above, it has recently been reported that interactions between the CTD of eIF5 and the N-terminal domain of eIF2 $\beta$  strengthen upon a cognate codon:anticodon interaction and is

needed for the stabilization of the closed conformation<sup>70</sup>. Thus, it is likely that upon cognate codon:anticodon base pairing, the interactions between eIF5 CTD and eIF2 $\beta$  N-terminal domain stabilizes the interactions between the ZBD of eIF2 $\beta$  and the G-domain of eIF2 $\gamma$ . This then allows for the ZBD of the  $\beta$  subunit to replace eIF5 NTD in binding to eIF2 $\gamma$  G-domain. Any substitution in the ZBD of eIF2 $\beta$ , such as S264Y, that would increase its interactions with the G-domain can then be expected to stabilize the closed conformation by increasing the dissociation rate of eIF5 NTD from the G-domain, and hence indirectly increasing its association with eIF1A CTT, which in turn leads to the stabilization of the closed conformation.

We established that the N433D and R484A substitutions in eIF2 $\gamma$  reduce the occurrence of the closed conformation by illustrating that these mutations offset the effects of S264Y and increase the dissociation rate of eIF1A and TC from reconstituted PIC. Residues N433 and R484 are positioned on a discrete surface-exposed area in domain-III of eIF2 $\gamma$  that is in proximity of the proposed binding interface between eIF2 and helix h44 of the 40S subunit (Figure 4.7). As discussed in Chapter 2, many of the *Ssu*<sup>-</sup> alleles we isolated in *GCD11* localize to this very specific region of domain-III (Figure 2.38). This raises the intriguing possibility that the affects of the *N433D* and *R484A* mutants on the equilibrium between the two conformations of the PIC is through altered physical interactions between domain-III of eIF2 $\gamma$  and helix h44 of the 40S subunit.

As described in detail in Chapter 1, the eIF2 complex delivers the Met-tRNA<sub>i</sub> to the P-site of the 40S subunit in a GTP dependent manner and maintains it throughout the scanning process as the anticodon of Met-tRNA<sub>i</sub> samples the codons on the mRNA for

complementarity in search of the AUG start codon. Thus, the interactions of Met-tRNA<sub>i</sub> with the mRNA on the 40S subunit should be dynamic and transient to allow for the sampling of codons during the scanning stage of initiation. Since it is the eIF2 complex that holds the Met-tRNA<sub>i</sub> during this process, we expect that when the PIC is in the open conformation, the binding of eIF2 $\gamma$  to the 40S subunit has to be transient to allow for dynamic interactions between the Met-tRNA<sub>i</sub> and the mRNA. Upon correct base pairing between the Met-tRNA<sub>i</sub> and the start codon, however, a series of events takes place in the PIC that collectively leads to the stabilization of the Met-tRNA<sub>i</sub> binding and the closed conformation, which then signals translation initiation.

As the free energy differences between cognate and near-cognate base pairing is not sufficient to explain the fidelity of start codon recognition<sup>245-250</sup>, the binding of the Met-tRNA<sub>i</sub> to the P-site should be stabilized through additional interactions and structural rearrangements in the PIC upon a cognate codon:anticodon interaction. Thus, as the open conformation has to have the flexibility and the dynamics to allow for scanning of the mRNA leader sequence, the closed conformation has to stabilize the binding of the Met-tRNA<sub>i</sub> in the P-site to allow for initiation to proceed. Here we propose that domain-III of eIF2 $\gamma$  participates in stabilizing the closed conformation and the binding of the Met-tRNA<sub>i</sub> in the P-site upon cognate base pairing between the Met-tRNA<sub>i</sub> and mRNA.

Multiple lines of evidence provide support for this proposal. It has been demonstrated that start codon recognition and formation of the closed conformation does indeed stabilize the binding of the TC to the 40S subunit<sup>95</sup>. Moreover, our *E460A* Sui<sup>-</sup> mutant, as described in Chapter 3, increases the rate of TC loading on the 40S subunit at a UUG codon, which consequently leads to the formation of the closed conformation and



translation initiation. Therefore, as our proposed model predicts, an increase in stability of the (transient) interactions between eIF2 $\gamma$  and the 40S subunit can lead to the formation of the closed conformation and start codon recognition at non-AUG codons.

Furthermore, although recent cryo-EM reconstitution of a mammalian PIC places domain-III of eIF2 $\gamma$  facing helix h44 of the 40S subunit, which is consistent with the result of the previous hydroxyl radical probing study<sup>127</sup>, it does not detect any direct contacts between the two as domain-III is observed about 34Å away from helix h44<sup>151</sup>. It is important to note that the cryo-EM model depicts the PIC in the open conformation as it was assembled without an mRNA. In the hydroxyl radical probing experiment, however, the eIF2 complex was mapped on the 40S subunit presumably in the closed conformation of the PIC since it was assembled in the presence of an mRNA. Significantly, it was also noted that eIF2 in the cryo-EM reconstruction showed conformational variability indicating that eIF2 $\gamma$  can potentially approach helix h44 of the 40S subunit upon codon-anticodon base pairing<sup>151</sup>.

Since our *Ssu*<sup>-</sup> mutants that reduce the stability of the closed conformation are localized to a specific region on the surface of domain-III, it is likely that upon cognate base pairing between the anticodon of the Met-tRNA<sub>i</sub> and the start codon, subtle structural rearrangements, perhaps a result of the small changes in the free energy of base pairing, translates into a movement of domain-III toward helix h44 and creation of new contact points with the 40S subunit that help stabilize the closed conformation and consequently the Met-tRNA<sub>i</sub> in the P-site. In this case the *GCD11* *Ssu*<sup>-</sup> mutants reduce the stability of the closed conformation because they prevent the formation of contact points between domain-III and helix h44 upon codon:anticodon base pairing. Start codon

recognition requires the coordinated action of a number of events in the PIC that collectively commit the complex to form a stable closed conformation and begin translation. Here we have introduced a new player in this process and suggested a function for the domain-III of eIF2 $\gamma$  in establishing the equilibrium between the two conformations of the PIC, which ultimately establishes the fidelity of translation initiation.

## 4.5 Figures and Tables

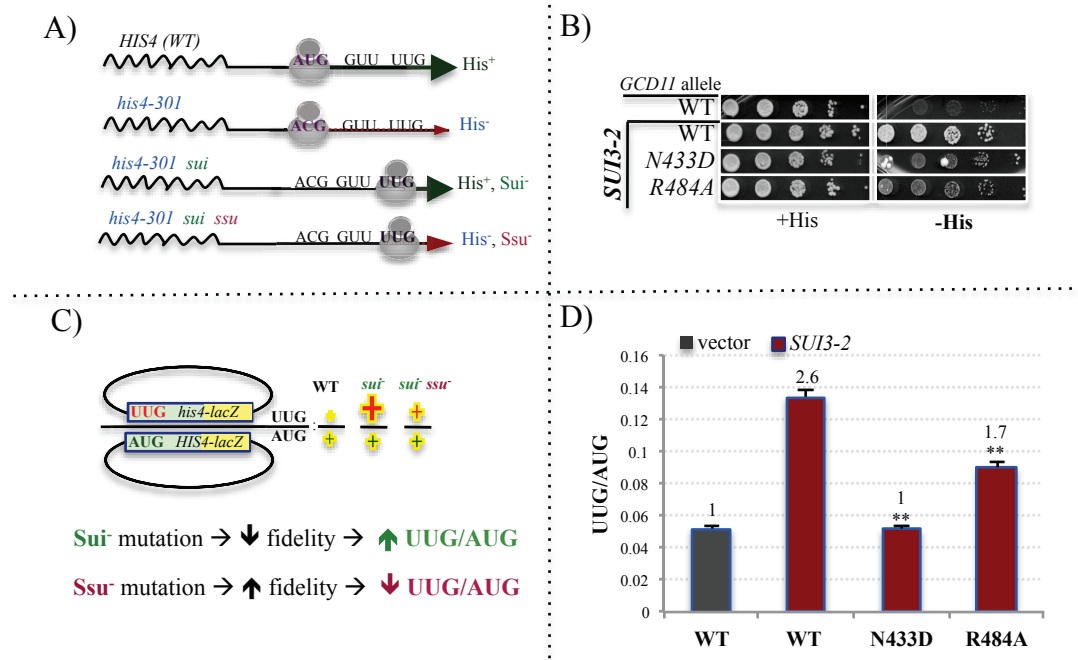


**Figure 4.1** The *Ssu*<sup>-</sup> mutants of *GCD11* suppress the His<sup>+</sup> phenotype and the elevated ratio of UUG to AUG initiation conferred by the *SUI3-2* allele

(A) A variant of the *HIS4* allele is used as a genetic reporter to monitor the accuracy of start codon selection. *his4-301* is a mutant allele of the *HIS4* gene that lacks a cognate AUG start codon, which consequently confers histidine auxotrophy in otherwise WT cells. The *Sui*<sup>-</sup> class of mutations, which lower the stringency of start codon recognition, allows for translation initiation from a near-cognate UUG codon of *his4-301* suppressing the histidine auxotrophy (His<sup>+</sup> phenotype). The *Ssu*<sup>-</sup> class of mutations, however, reestablishes the fidelity of start codon selection and blocks translation initiation from the UUG codon of *his4-301*, hence restoring the histidine auxotrophy. (B) The *gcd11-N433D* and *gcd11-R484A* mutants suppress the His<sup>+</sup> phenotype of cells expressing the *SUI3-2* allele. Derivatives of strain NAY13 with the WT or mutant *GCD11* alleles on a

sc *LEU2* plasmid and harboring episomal *SUI3-2* (p4280) or the empty *TRP1* vector (YCplac22) were cultured in SC-L-W, ten-fold serial dilutions were spotted on SC-L-W medium supplemented with 0.3 mM (+His) or 0.003 mM (-His) histidine, and incubated at 30°C for two and five days, respectively. (C) Matched *HIS4-lacZ* reporters, containing a UUG (*his4-lacZ*) or an AUG (*HIS4-lacZ*) start codon, are used to measure the ratio of initiation from a UUG codon to that from an AUG codon. *Sui*<sup>-</sup> mutations elevate the ratio of UUG to AUG initiation compared to WT cells by reducing the stringency of start codon recognition and increasing the expression of *his4-lacZ* from a UUG codon. The *Ssu*<sup>-</sup> mutants, on the other hand, suppress the elevated ratio of UUG to AUG initiation observed in cells harboring a *Sui*<sup>-</sup> allele by restoring initiation fidelity and reducing the expression of *his4-lacZ* from a UUG codon. (D) The *gcd11-N433D* and *gcd11-R484A* mutants suppress the elevated ratio of initiation from a UUG codon to that from an AUG codon in cells expressing the *SUI3-2* allele. UUG/AUG ratio was calculated in the same strains as in panel B by measuring the  $\beta$ -galactosidase activity of the *HIS4-lacZ* reporters described in panel C.  $\beta$ -galactosidase activities (nanomoles of *o*-nitrophenyl- $\beta$ -D-galactopyranoside cleaved per minute per microgram of protein) were measured in WCEs of exponentially growing cultures (OD<sub>600</sub> ~0.5) in SC-L-W medium. Mean of at least eight independent transformants and SEM (error bars) are plotted for each mutant. A student *t*-test was used to determine significance (\*\**p*<0.01).

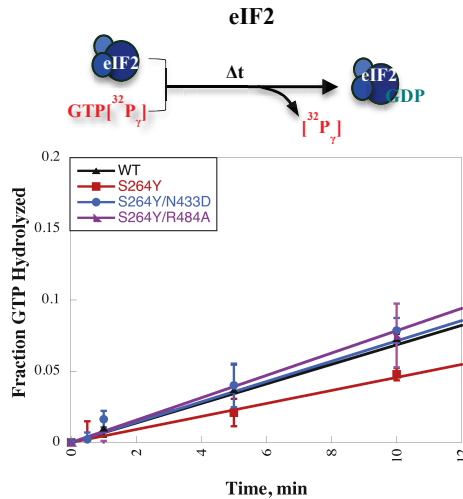


**Figure 4.2 GTP hydrolysis in the mutant eIF2 complexes**

The S264Y substitution in the  $\beta$  subunit and the N433D or R484A mutant variants of the  $\gamma$  subunit do not significantly alter the intrinsic rate of GTP hydrolysis in eIF2. GTP hydrolysis was measured by adding a limiting amount of  $[\gamma\text{-}^{32}\text{P}]\text{GTP}$  (80 nM) to a saturating concentration of eIF2 (0.8  $\mu\text{M}$ ). The reactions were incubated at 26°C and stopped by adding 100 mM EDTA at the specified time points.  $[\gamma\text{-}^{32}\text{P}]\text{GTP}$  and  $^{32}\text{P}_i$  were separated by thin layer chromatography (PEI-cellulose TLC) and the fraction of total  $^{32}\text{P}_i$  released was quantified by PhosphorImager analysis. Mean value of at least two experiments and mean deviation (error bar) is represented for each time point. Values are normalized to the background rate of hydrolysis ( $^{32}\text{P}_i$  release) in the  $[\gamma\text{-}^{32}\text{P}]\text{GTP}$  molecule alone exposed to the same temperature and buffer conditions of the assay. The curves were fit a linear regression equation. Slopes of the regression lines are  $0.41\pm 0.040$ ,  $0.24\pm 0.014$ ,  $0.43\pm 0.076$ , and  $0.47\pm 0.072$  for the WT, eIF2 $\beta$ -S264Y, eIF2 $\beta$ -S264Y/eIF2 $\gamma$ -N433D, and eIF2 $\beta$ -S264Y/eIF2 $\gamma$ -R484A complexes, respectively.

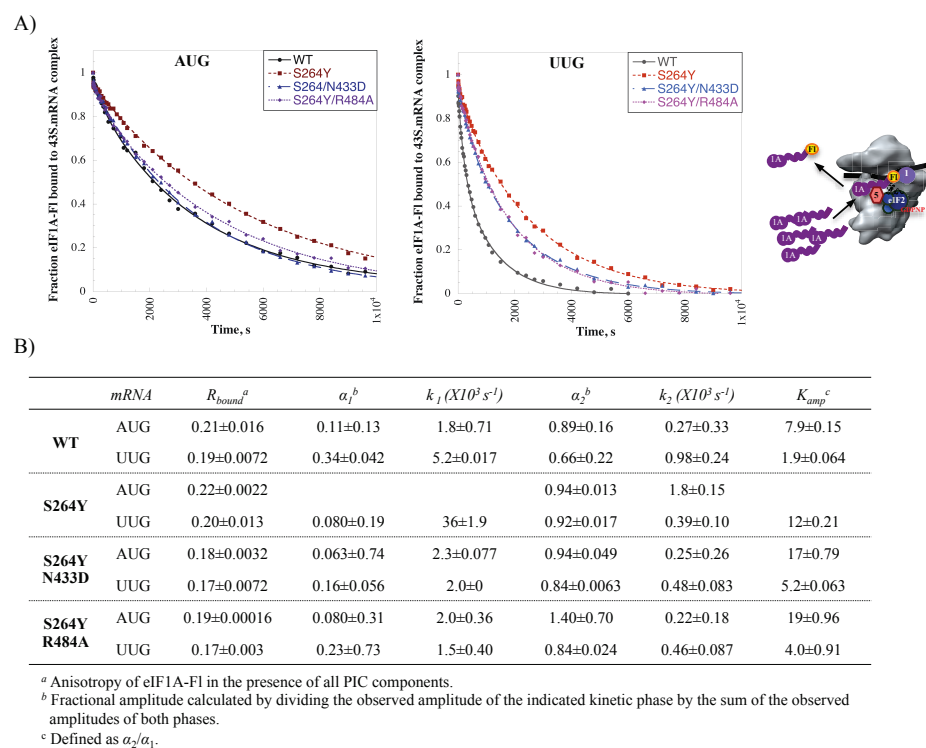


### Figure 4.3 Kinetic of eIF1A dissociation from reconstituted PIC containing the WT or the mutant variants of the eIF2 complex

The S264Y substitution in eIF2 $\beta$  reduces the dissociation of eIF1A from reconstituted PIC with AUG or UUG codons. The N433D and R484A variants of eIF2 $\gamma$  suppress this defect and, conversely, increase the dissociation of eIF1A from reconstituted PIC. (A) 43S•mRNA complexes were first assembled by incubating saturating concentrations of TC (0.8  $\mu$ M eIF2, 1 mM GDPNP, 150 nM Met-tRNA<sub>i</sub>), eIF1 (1  $\mu$ M), eIF5 (1 $\mu$ M), 40S (120 nM), and mRNA (10  $\mu$ M) with a limiting amount of eIF1A-FI (15 nM). An excess of unlabeled eIF1A was then added, and changes in anisotropy were measured over time. (B) S264Y increases the  $K_{amp}$  value at a UUG codon by 6-fold. A  $K_{amp}$  value for S264Y at an AUG codon could not be calculated as the dissection kinetics of eIF1A was no longer biphasic. The N433D and R484A variants of eIF2 $\gamma$  suppress the elevated  $K_{amp}$

value of S264Y by  $\sim 3$ -fold at a UUG codon. They also restore the biphasic kinetics of eIF1A dissociation at an AUG codon. N433D and R484A also reduce the  $R_{\text{bound}}$  values both with a UUG and an AUG containing mRNA. Curves from panel A were fit with a double exponential equation, except for S264Y with an AUG mRNA that was fit with a single exponential function. Mean values from at least two experiments and mean deviations are reported.

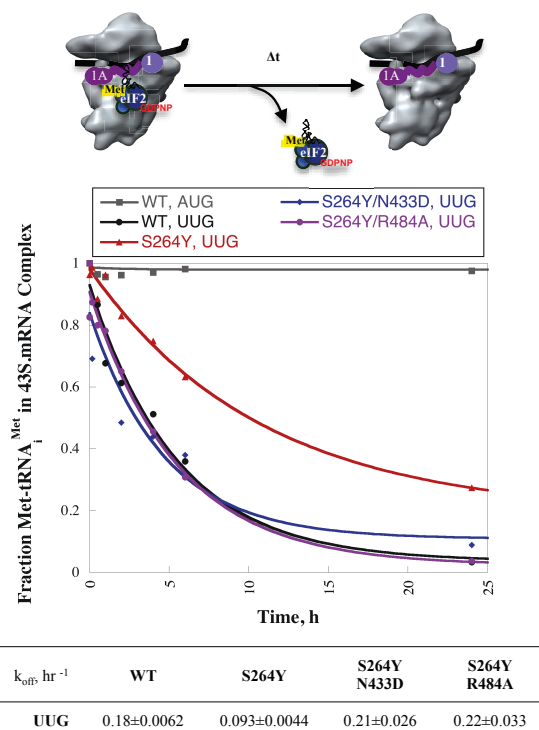


**Figure 4.4 Dissociation kinetics of TC from reconstituted PIC with WT and mutant eIF2**

TC dissociates more rapidly from the 43S•mRNA complexes with a UUG versus an AUG codon as start codon recognition stabilizes the binding of the TC to the PIC. The S264Y variant of eIF2 $\beta$ , however, reduces the dissociation rate of TC at a UUG codon by ~2-folds. The N433D and R484A substitutions in eIF2 $\gamma$ , on the other hand, suppress this defect restoring the rate of TC dissociation to WT levels. PIC was assembled by mixing saturating concentrations of eIF2 (250 nM), GDPNP (1 mM), eIF1 (1  $\mu$ M), eIF1A (1  $\mu$ M), 40S (20 nM), and mRNA (10  $\mu$ M) and a limiting amount of [<sup>35</sup>S]Met-tRNA<sub>i</sub> (1 nM). To measure the  $k_{\text{off}}$ , the reactions were then initiated by adding an excess of unlabeled TC and were stopped by loading on a running native gel. Curves were fit with a single exponential equation. Means of at least three experiments and SDs are reported.



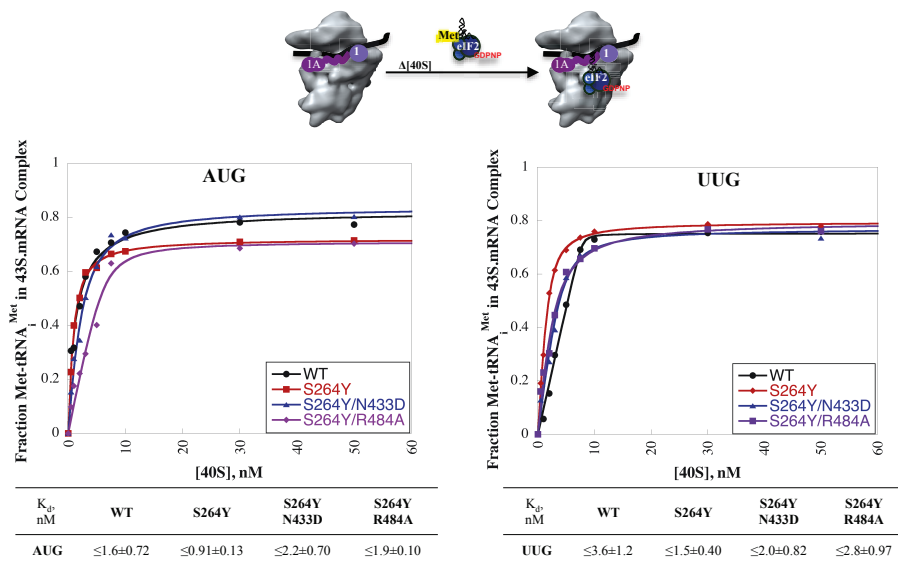


**Figure 4.5 Affinity of TC binding to reconstituted PIC assembled with WT and mutant eIF2**

eIF2 containing the S264Y variant of  $\beta$  and the N433D or R484A substitutions in  $\gamma$  does not significantly alter the rate of TC loading on 43•SmRNA complexes with an AUG or a UUG codon. Preformed TC (0.8  $\mu$ M eIF2, 1 mM GDPNP, 1 nM [ $^{35}$ S]Met-tRNA<sub>i</sub>) was mixed with saturating concentrations of eIF1 (1  $\mu$ ), eIF1A (1  $\mu$ ), mRNA (1  $\mu$ M), and a range of 40S concentrations. The fraction of [ $^{35}$ S]Met-tRNA<sub>i</sub> bound to the 40S subunits (PIC formation) was measured by native gel electrophoresis. The data were fit with hyperbolic or quadratic binding curves to determine the  $K_d$  values. Means of at least two experiments and mean deviations are reported. The detection limit of this assay is  $\leq 1$  nM since TC binds very tightly to the 40S subunit in the presence of eIF1, 1A, and mRNA

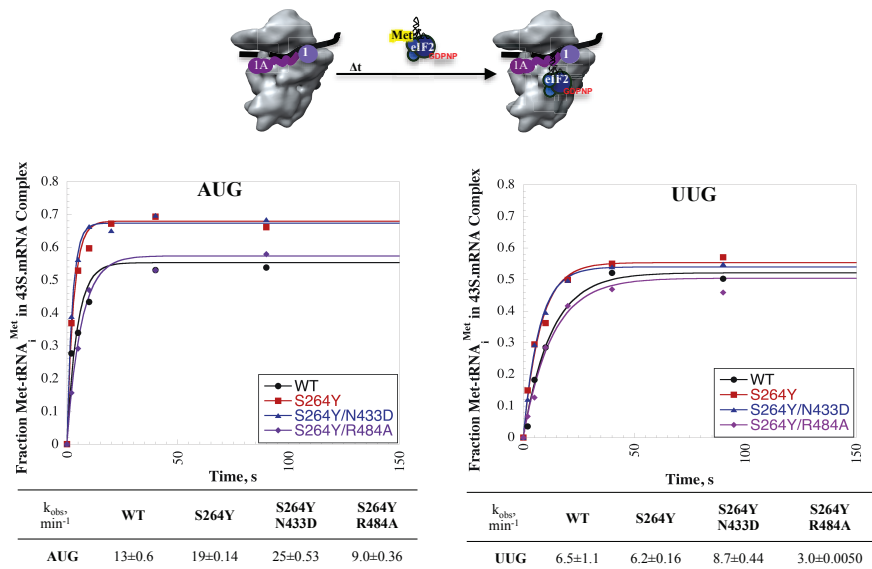


**Figure 4.6 Kinetics of TC binding to reconstituted PIC assembled with WT and mutant eIF2**

eIF2 containing the S264Y substitution in the  $\beta$  subunit and the N433D or R484A mutant variants of the  $\gamma$  subunit does not significantly alter the rate of TC loading on 43•SmRNA complexes with an AUG or a UUG codon. Preformed TC (250 nM eIF2, 1 mM GDPNP, 1 nM [ $^{35}$ S]Met-tRNA<sub>i</sub>) was mixed with saturating concentrations of eIF1 (1  $\mu$ ), eIF1A (1  $\mu$ M), 40S (20 nM), and mRNA (10  $\mu$ M). The reactions were stopped by adding excess amount of unlabeled TC, and the fraction of [ $^{35}$ S]Met-tRNA<sub>i</sub> bound to the 40S subunits (PIC formation) was measured over time by native gel electrophoresis. The curves were fit with a single exponential function. Means of at least two experiments and mean deviations are reported.

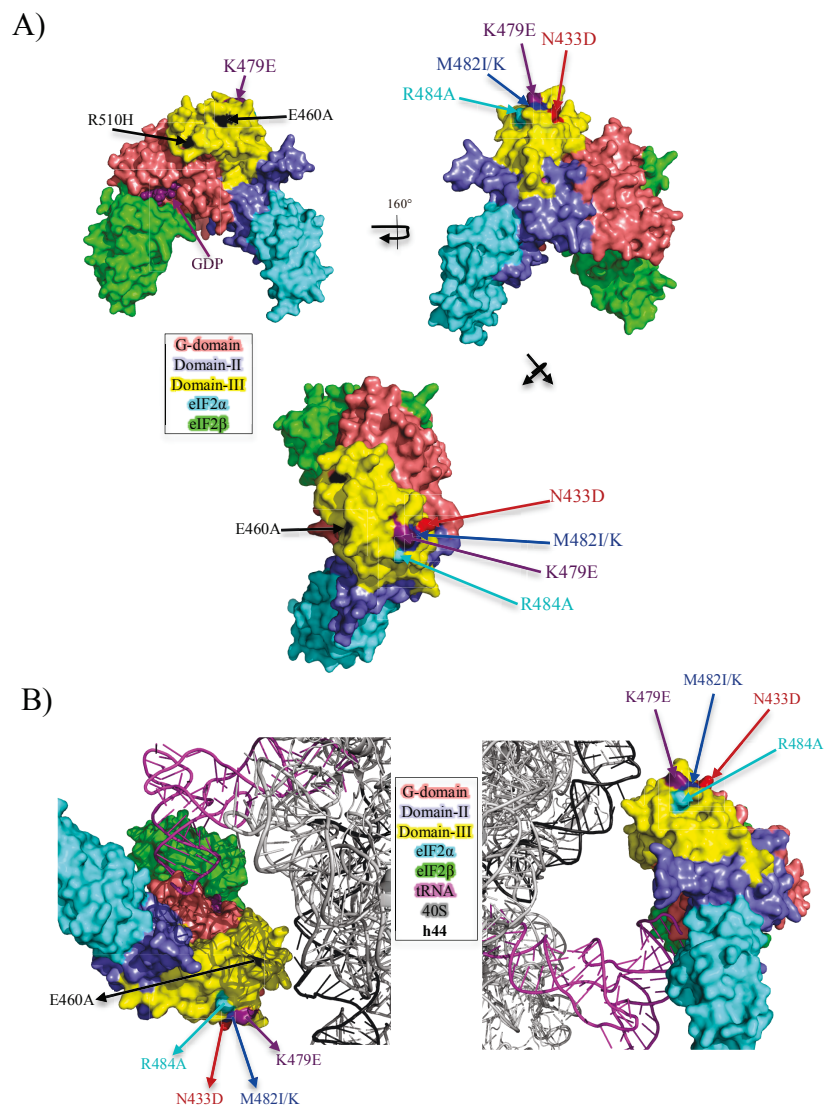


**Figure 4.7 Positions of the isolated Sui<sup>-</sup> and Ssu<sup>-</sup> mutations on the structure of eIF2**

(A) Three views of a surface-exposed representation of eIF2 (PDB 2QMU) with the positions of the isolated Sui<sup>-</sup> (E460A, R510H) and Ssu<sup>-</sup> (N433D, K479E, R484A, M482I/K) substitutions in domain-III marked. (B) Two views of the model of eIF2 binding to h44 of the 40S subunit. The Isolated Sui<sup>-</sup> and Ssu<sup>-</sup> substitutions in eIF2 $\gamma$  are in proximity of the proposed binding interface between eIF2 and helix h44. Model of TC binding to the 40S subunit is adapted from Shin et al. 2011<sup>127</sup>. Images were created using the PyMOL software<sup>207</sup>.

**Table 4.1 List of *S. cerevisiae* Strains**

<b>Strain</b>	<b>Genotype</b>	<b>Source</b>
NAY13	<i>Mata</i> <i>ura3-52 leu2-3,112 ino1-13 his4-301(ACG) gcd11Δ::hisG trp1Δ::hisG Ep293&lt;GCD11 URA3 CEN4/ARS1&gt;</i>	This Study
NAY116	<i>Mata</i> <i>ura3-52 leu2-3,112 ino1-13 his4-301(ACG) Δgcd11::hisG Δtrp1::hisG Ep293&lt;GCD11 URA3 CEN4/ARS1&gt; p4280 &lt;SUI3-2 TRP1, CEN&gt;</i>	This Study
NAY156	<i>Mata</i> <i>ura3-52 leu2-3,112 ino1-13 his4-301(ACG) Δgcd11::hisG Δtrp1::hisG pNA4&lt; GCD11-His<sub>8</sub> LEU2 CEN4/ARS1&gt; p4280&lt;SUI3-2 TRP1 CEN&gt;</i>	This Study
NAY135	<i>Mata</i> <i>ura3-52 leu2-3,112 ino1-13 his4-301(ACG) Δgcd11::hisG Δtrp1::hisG pNA4-N433D&lt; gcd11-N433D-His<sub>8</sub> LEU2 CEN4/ARS1&gt; p4280&lt;SUI3-2 TRP1 CEN&gt;</i>	This Study
NAY137	<i>Mata</i> <i>ura3-52 leu2-3,112 ino1-13 his4-301(ACG) Δgcd11::hisG Δtrp1::hisG pNA4-R484A&lt; gcd11-R484A-His<sub>8</sub> LEU2 CEN4/ARS1&gt; p4280&lt;SUI3-2 TRP1 CEN&gt;</i>	This Study
NAY86	<i>Mata</i> <i>ura3-52 leu2-3,112 ino1-13 HIS4<sup>+</sup> gcd11Δ::hisG trp1Δ::hisG gcn2Δ::hisG pep4Δ::hygB sui3Δ::kanMX4 sui2Δ::hphMX4 pNA28&lt;sc URA3 GCD11-His<sub>6</sub> SUI3 SUI2&gt;</i>	This Study
NAY87	<i>Mata</i> <i>ura3-52 leu2-3,112 ino1-13 HIS4<sup>+</sup> gcd11Δ::hisG trp1Δ::hisG gcn2Δ::hisG pep4Δ::hygB sui3Δ::kanMX4 sui2Δ::hphMX4 pNA21&lt;hc LEU2 GCD11-His<sub>8</sub> SUI3 SUI2 IMT4&gt;</i>	This Study
NAY105	<i>Mata</i> <i>ura3-52 leu2-3,112 ino1-13 HIS4<sup>+</sup> gcd11Δ::hisG trp1Δ::hisG gcn2Δ::hisG pep4Δ::hygB sui3Δ::kanMX4 sui2Δ::hphMX4 pNA29&lt;hc LEU2 GCD11-His<sub>8</sub> SUI3-2 SUI2 IMT4&gt;</i>	This Study
NAY109	<i>Mata</i> <i>ura3-52 leu2-3,112 ino1-13 HIS4<sup>+</sup> gcd11Δ::hisG trp1Δ::hisG gcn2Δ::hisG pep4Δ::hygB sui3Δ::kanMX4 sui2Δ::hphMX4 pNA30&lt;hc LEU2 gcd11-N433D-His<sub>8</sub> SUI3-2 SUI2 IMT4&gt;</i>	This Study
NAY111	<i>Mata</i> <i>ura3-52 leu2-3,112 ino1-13 HIS4<sup>+</sup> gcd11Δ::hisG trp1Δ::hisG gcn2Δ::hisG pep4Δ::hygB sui3Δ::kanMX4 sui2Δ::hphMX4 pNA31&lt;hc LEU2 gcd11-N433D-His<sub>8</sub> SUI3-2 SUI2 IMT4&gt;</i>	This Study

**Table 4.2 List of Plasmids**

<b>Plasmid</b>	<b>Description<sup>a</sup></b>	<b>Source</b>
YCplac111	sc <i>LEU2</i> yeast- <i>E. coli</i> shuttle vector	229
YCplac22	sc <i>TRP1</i> yeast- <i>E. coli</i> shuttle vector	229
YCP50	sc <i>URA3</i> yeast- <i>E. coli</i> shuttle vector	230
pSB32	lc <i>LEU2</i> yeast- <i>E. coli</i> shuttle vector	
pRS425	hc <i>LEU2</i> yeast- <i>E. coli</i> shuttle vector	231
YCplac33	sc <i>URA3</i> yeast- <i>E. coli</i> shuttle vector	229
Ep293	sc <i>URA3 GCD11</i> in YCP50	223
Ep517	lc <i>LEU2 GCD11</i> in pSB32	223
pC2872	sc <i>LEU2 GCD11-His<sub>8</sub></i> in YCplac111	P. Alone
pNA4	sc <i>LEU2 GCD11-His<sub>8</sub></i> in pC2872	This study
pNA4-N433D	sc <i>LEU2 gcd11-His<sub>8</sub>-N433D</i>	This study
pNA4-R484A	sc <i>LEU2 gcd11-His<sub>8</sub>-R484A</i>	This study
p4280	sc <i>TRP1 SUI3-2</i> in YCplac22	81
p367	sc <i>URA3 HIS4(ATG)-lacZ</i>	209
p391	sc <i>URA3 HIS4(TTG)-lacZ (his4-301)</i>	209
p180	sc <i>URA3 GCN4-lacZ</i> in YCp50	232
pAV1726	hc <i>LEU2 GCD11-His<sub>6</sub> SUI3 SUI2</i> in pRS425	G. Pavitt
pAV1732	hc <i>LEU2 GCD11-His<sub>6</sub> SUI3 SUI2 IMT4</i> in pAV1726	G. Pavitt
pNA28	sc <i>URA3 GCD11-His<sub>6</sub> SUI2 SUI3</i> in YCplac33	This study
pNA21	hc <i>LEU2 GCD11-His<sub>8</sub> SUI3 SUI2 IMT4</i> in pAV1732	This study
pNA29	hc <i>LEU2 GCD11-His<sub>8</sub> SUI3-2 SUI2 IMT4</i> in pNA21	This study
pNA30	hc <i>LEU2 gcd11-N433D-His<sub>8</sub> SUI3-2 SUI2 IMT4</i> in pNA29	This study
pNA31	hc <i>LEU2 gcd11-R484A-His<sub>8</sub> SUI3-2 SUI2 IMT4</i> in pNA29	This study

<sup>a</sup> sc: single copy number; hc: high copy number; lc: low copy number

## **CHAPTER 5: CONCLUDING REMARKS**

Initiation, elongation, termination, and recycling of the ribosomal complexes constitute the four major stages of protein synthesis. Initiation is the most heavily regulated stage that sets the reading frame for the translation of the mRNA sequence into a fully functional protein product. In eukaryotes, this process is governed by base pairing between the anticodon of the Met-tRNA<sub>i</sub> and the start codon of the mRNA and is mediated through the actions of at least twelve initiation factors and the small subunit of the ribosome. The stage of initiation itself can be divided into two main phases of scanning and start codon selection, and the PIC exists in two conformations corresponding to each phase. During the scanning of the mRNA 5' UTR, the PIC is in an 'open' conformation, which allows for the Met-tRNA<sub>i</sub> to search the mRNA leader sequence for complementary to identify the start codon. Upon cognate codon:anticodon base pairing, however, the coordinated actions of a number of events in the PIC collectively commit the complex to form a more stable 'closed' conformation and begin translation. For example, physical interactions between eIF5 and eIF1 has to be disrupted<sup>70,72</sup>, new interactions between the eIF1A and eIF5 proteins should be formed<sup>72,75</sup>, and the eIF2-bound GTP has to get hydrolyzed irreversibly with the dissociation of P<sub>i</sub><sup>92</sup> among many other events that cooperatively lead to formation and stabilization of the closed conformation.

The ultimate goal of the structural rearrangements in the PIC, upon a cognate codon:anticodon interaction, is to stabilize the binding of the Met-tRNA<sub>i</sub> in a fully accommodated mode in the P-site of the 40S subunit as multiple lines of evidence have suggested that the Met-tRNA<sub>i</sub> is not fully inserted in the P-site during the scanning phase of initiation<sup>30,60</sup>. Since the Met-tRNA<sub>i</sub> has to interact with each and every nucleotide in

the mRNA 5' UTR to identify the start codon, it is logical that it has to maintain a dynamic and transient interaction with the mRNA during the scanning phase of initiation. Moreover, preventing the full accommodation of the Met-tRNA<sub>i</sub> in the P-site reduces the stability of its binding, which consequently lowers the probability of initiation at near-cognate codons.

Since the free energy difference between a cognate and a near-cognate base pairing is not sufficient to explain the fidelity of start codon recognition<sup>245-250</sup>, however, the binding of the Met-tRNA<sub>i</sub> to the P-site should be stabilized through additional interactions and structural rearrangements in the PIC upon formation of the cognate codon:anticodon interaction. eIF2 is a logical candidate to perform a critical function in this process since it is the complex that binds and holds the Met-tRNA<sub>i</sub> during the entire process of initiation. Our findings in this study indeed have provided support for the involvement of the  $\gamma$  subunit of eIF2 in stabilizing the closed conformation upon cognate base pairing between the Met-tRNA<sub>i</sub> and mRNA.

Our genetic and biochemical analyses here have confirmed the involvement of eIF2 $\gamma$  domain-III in establishing the stringency of start codon recognition. Domain-III seems to perform multiple functions during the initiation stage of protein synthesis. It is likely to participate in stabilizing GTP binding, through physical interactions with the switch-II region of the G-domain, and perhaps in maintaining the Met-tRNA<sub>i</sub> in the proper conformation for binding to the 40S subunit, through physical interactions with domain-II. As elucidated earlier, however, further experiments are required to directly confirm the above hypotheses. Most interestingly, our findings suggested that domain-III



of eIF2 $\gamma$  is involved in stabilizing the closed conformation of the PIC upon cognate base pairing between the start codon and the anticodon of Met-tRNA<sub>i</sub>.

Based on our evidence and our current understanding of the mechanism of start codon recognition in eukaryotes, we proposed a model in which domain-III of eIF2 $\gamma$  maintains a transient interaction with helix h44 of the 40S subunit during the scanning phase of initiation. A cognate codon:anticodon interaction, however, leads to subtle structural rearrangements in the Met-tRNA<sub>i</sub>, for example due to the free energy of cognate base pairing, that induces a movement of eIF2 $\gamma$  domain-III toward h44, which consequently leads to the formation of more stable contact points between eIF2 and the 40S subunit. This, in turn, contributes to the stabilization of Met-tRNA<sub>i</sub> binding in the P-site of the 40S subunit.

It is important to note that during the entire process of translation initiation, the PIC maintains a dynamic structure and exists in equilibrium between the *open* and *closed* conformations. A collection of small structural rearrangements in the many components of the PIC can then further stabilize one or the other conformation depending on the environment, for example the sequence or structure of the mRNA 5' UTR. Dividing the vital decision of start codon selection among multiple different protein factors creates resilience and allows the process to have a buffer zone against environmental assaults, for example spontaneous mutations in any of its essential players. It also allows for multiple levels of regulation, which makes the entire process adaptable to external factors. Therefore, to fully understand how exactly start codon selection is achieved, the intricate network of interactions among its many players need to be established. In this study, we

defined a new interaction in this network. Many more, however, still have to be determined.

## REFERENCES

- 1 Marintchev, A. & Wagner, G. Translation initiation: structures, mechanisms and evolution. *Q Rev Biophys* **37**, 197-284 (2004).
- 2 Garret, R. A. *et al.* *The ribosome: structure, function, antibiotics, and cellular interactions*. (ASM Press, 2000).
- 3 Sonenberg, N., Hershey, J. W. B. & Mathews, M. B. *Translational control of gene expression*. (Cold Spring Harbor Laboratory Press, 2000).
- 4 Savelsbergh, A., Rodnina, M. V. & Wintermeyer, W. Distinct functions of elongation factor G in ribosome recycling and translocation. *RNA* **15**, 772-780, doi:10.1261/rna.1592509 (2009).
- 5 Pavlov, M. Y., Antoun, A., Lovmar, M. & Ehrenberg, M. Complementary roles of initiation factor 1 and ribosome recycling factor in 70S ribosome splitting. *EMBO J* **27**, 1706-1717, doi:10.1038/emboj.2008.99 (2008).
- 6 Pisarev, A. V., Hellen, C. U. & Pestova, T. V. Recycling of eukaryotic posttermination ribosomal complexes. *Cell* **131**, 286-299, doi:10.1016/j.cell.2007.08.041 (2007).
- 7 Nurenberg, E. & Tampe, R. Tying up loose ends: ribosome recycling in eukaryotes and archaea. *Trends in biochemical sciences* **38**, 64-74, doi:10.1016/j.tibs.2012.11.003 (2013).
- 8 Peske, F., Rodnina, M. V. & Wintermeyer, W. Sequence of steps in ribosome recycling as defined by kinetic analysis. *Mol Cell* **18**, 403-412, doi:10.1016/j.molcel.2005.04.009 (2005).
- 9 von der Haar, T. A quantitative estimation of the global translational activity in logarithmically growing yeast cells. *BMC systems biology* **2**, 87, doi:10.1186/1752-0509-2-87 (2008).
- 10 Kozma, S. C., Um, S. H. & Thomas, G. in *Translational Control in Biology and Medicine* (eds Michael Mathews, Nahum Sonenberg, & J.W.B. Hershey) 459-484 (Cold Spring Harbor Laboratory Press, 2007).
- 11 Novoa, I., Gallego, J., Ferreira, P. G. & Mendez, R. Mitotic cell-cycle progression is regulated by CPEB1 and CPEB4-dependent translational control. *Nature cell biology* **12**, 447-456, doi:10.1038/ncb2046 (2010).
- 12 Blazquez-Domingo, M., Grech, G. & von Lindern, M. Translation initiation factor 4E inhibits differentiation of erythroid progenitors. *Mol Cell Biol* **25**, 8496-8506, doi:10.1128/MCB.25.19.8496-8506.2005 (2005).
- 13 Thompson, B., Wickens, M. & Kimble, J. in *Translational Control in Biology and Medicine* (eds Michael Mathews, Nahum Sonenberg, & J.W.B. Hershey) 486-507 (Cold Spring Harbor Laboratory Press, 2007).
- 14 Kong, J. & Lasko, P. Translational control in cellular and developmental processes. *Nature reviews. Genetics* **13**, 383-394, doi:10.1038/nrg3184 (2012).
- 15 Klann, E. & Richter, J. D. in *Translational Control in Biology and Medicine* (eds M. Mathews, N Sonenberg, & J.W.B. Hershey) 485-506 (Cold Spring Harbor Laboratory Press, 2007).
- 16 Mendez, R. & Wells, D. Location, location, location: translational control in development and neurobiology. *Trends in cell biology* **12**, 407-409 (2002).

- 17 Sonenberg, N. & Hinnebusch, A. G. New modes of translational control in development, behavior, and disease. *Mol Cell* **28**, 721-729 (2007).
- 18 Sonenberg, N. & Hinnebusch, A. G. Regulation of translation initiation in eukaryotes: mechanisms and biological targets. *Cell* **136**, 731-745 (2009).
- 19 Abbott, C. M. & Proud, C. G. Translation factors: in sickness and in health. *Trends in biochemical sciences* **29**, 25-31, doi:10.1016/j.tibs.2003.11.006 (2004).
- 20 Belsham, G. J., McNerney, G. M. & Ross-Smith, N. Foot-and-mouth disease virus 3C protease induces cleavage of translation initiation factors eIF4A and eIF4G within infected cells. *Journal of virology* **74**, 272-280 (2000).
- 21 Calkhoven, C. F., Muller, C. & Leutz, A. Translational control of gene expression and disease. *Trends in molecular medicine* **8**, 577-583 (2002).
- 22 Cazzola, M. & Skoda, R. C. Translational pathophysiology: a novel molecular mechanism of human disease. *Blood* **95**, 3280-3288 (2000).
- 23 Cuesta, R., Gupta, M. & Schneider, R. J. The regulation of protein synthesis in cancer. *Progress in molecular biology and translational science* **90**, 255-292, doi:10.1016/S1877-1173(09)90007-2 (2009).
- 24 Le Quesne, J. P., Spriggs, K. A., Bushell, M. & Willis, A. E. Dysregulation of protein synthesis and disease. *The Journal of pathology* **220**, 140-151, doi:10.1002/path.2627 (2010).
- 25 Scheper, G. C., Proud, C. G. & van der Knaap, M. S. Defective translation initiation causes vanishing of cerebral white matter. *Trends in molecular medicine* **12**, 159-166, doi:10.1016/j.molmed.2006.02.006 (2006).
- 26 Scheper, G. C., van der Knaap, M. S. & Proud, C. G. Translation matters: protein synthesis defects in inherited disease. *Nature reviews. Genetics* **8**, 711-723, doi:10.1038/nrg2142 (2007).
- 27 Borck, G. *et al.* eIF2 $\gamma$  mutation that disrupts eIF2 complex integrity links intellectual disability to impaired translation initiation. *Mol Cell* **48**, 641-646, doi:10.1016/j.molcel.2012.09.005 (2012).
- 28 Kash, J. C., Goodman, A. G., Korth, M. J. & Katze, M. G. Hijacking of the host-cell response and translational control during influenza virus infection. *Virus research* **119**, 111-120, doi:10.1016/j.virusres.2005.10.013 (2006).
- 29 Santini, E. *et al.* Exaggerated translation causes synaptic and behavioural aberrations associated with autism. *Nature* **493**, 411-415, doi:10.1038/nature11782 (2013).
- 30 Jackson, R. J., Hellen, C. U. & Pestova, T. V. The mechanism of eukaryotic translation initiation and principles of its regulation. *Nature reviews. Molecular cell biology* **11**, 113-127, doi:10.1038/nrm2838 (2010).
- 31 Malys, N. & McCarthy, J. E. Translation initiation: variations in the mechanism can be anticipated. *Cellular and molecular life sciences : CMLS* **68**, 991-1003, doi:10.1007/s00018-010-0588-z (2011).
- 32 Selmer, M. *et al.* Structure of the 70S ribosome complexed with mRNA and tRNA. *Science* **313**, 1935-1942, doi:10.1126/science.1131127 (2006).
- 33 Steitz, T. A. A structural understanding of the dynamic ribosome machine. *Nature reviews. Molecular cell biology* **9**, 242-253, doi:10.1038/nrm2352 (2008).
- 34 Guillon, J. M. *et al.* Nucleotides of tRNA governing the specificity of Escherichia coli methionyl-tRNA(fMet) formyltransferase. *J Mol Biol* **224**, 359-367 (1992).

- 35 Laursen, B. S., Sorensen, H. P., Mortensen, K. K. & Sperling-Petersen, H. U. Initiation of protein synthesis in bacteria. *Microbiol Mol Biol Rev* **69**, 101-123, doi:10.1128/MMBR.69.1.101-123.2005 (2005).
- 36 Lee, C. P., Seong, B. L. & RajBhandary, U. L. Structural and sequence elements important for recognition of Escherichia coli formylmethionine tRNA by methionyl-tRNA transformylase are clustered in the acceptor stem. *J Biol Chem* **266**, 18012-18017 (1991).
- 37 Wu, X. Q. & RajBhandary, U. L. Effect of the amino acid attached to Escherichia coli initiator tRNA on its affinity for the initiation factor IF2 and on the IF2 dependence of its binding to the ribosome. *J Biol Chem* **272**, 1891-1895 (1997).
- 38 Kozak, M. Regulation of translation via mRNA structure in prokaryotes and eukaryotes. *Gene* **361**, 13-37, doi:10.1016/j.gene.2005.06.037 (2005).
- 39 Yusupova, G. Z., Yusupov, M. M., Cate, J. H. & Noller, H. F. The path of messenger RNA through the ribosome. *Cell* **106**, 233-241 (2001).
- 40 Schmeing, T. M. & Ramakrishnan, V. What recent ribosome structures have revealed about the mechanism of translation. *Nature* **461**, 1234-1242, doi:10.1038/nature08403 (2009).
- 41 Shine, J. & Dalgarno, L. The 3'-terminal sequence of Escherichia coli 16S ribosomal RNA: complementarity to nonsense triplets and ribosome binding sites. *Proc Natl Acad Sci U S A* **71**, 1342-1346 (1974).
- 42 Simonetti, A. *et al.* A structural view of translation initiation in bacteria. *Cellular and molecular life sciences : CMLS* **66**, 423-436, doi:10.1007/s00018-008-8416-4 (2009).
- 43 La Teana, A., Gualerzi, C. O. & Brimacombe, R. From stand-by to decoding site. Adjustment of the mRNA on the 30S ribosomal subunit under the influence of the initiation factors. *RNA* **1**, 772-782 (1995).
- 44 Karimi, R., Pavlov, M. Y., Buckingham, R. H. & Ehrenberg, M. Novel roles for classical factors at the interface between translation termination and initiation. *Mol Cell* **3**, 601-609 (1999).
- 45 Petrelli, D. *et al.* Translation initiation factor IF3: two domains, five functions, one mechanism? *EMBO J* **20**, 4560-4569, doi:10.1093/emboj/20.16.4560 (2001).
- 46 Boelens, R. & Gualerzi, C. O. Structure and function of bacterial initiation factors. *Current protein & peptide science* **3**, 107-119 (2002).
- 47 Carter, A. P. *et al.* Crystal structure of an initiation factor bound to the 30S ribosomal subunit. *Science* **291**, 498-501 (2001).
- 48 Dahlquist, K. D. & Puglisi, J. D. Interaction of translation initiation factor IF1 with the E. coli ribosomal A site. *J Mol Biol* **299**, 1-15, doi:10.1006/jmbi.2000.3672 (2000).
- 49 Petersen, H. U., Roll, T., Grunberg-Manago, M. & Clark, B. F. Specific interaction of initiation factor IF2 of E. coli with formylmethionyl-tRNA f Met. *Biochemical and biophysical research communications* **91**, 1068-1074 (1979).
- 50 Grigoriadou, C., Marzi, S., Pan, D., Gualerzi, C. O. & Cooperman, B. S. The translational fidelity function of IF3 during transition from the 30 S initiation complex to the 70 S initiation complex. *J Mol Biol* **373**, 551-561, doi:10.1016/j.jmb.2007.07.031 (2007).

- 51 Gualerzi, C., Risuleo, G. & Pon, C. L. Initial rate kinetic analysis of the mechanism of initiation complex formation and the role of initiation factor IF-3. *Biochemistry* **16**, 1684-1689 (1977).
- 52 Milon, P., Konevega, A. L., Gualerzi, C. O. & Rodnina, M. V. Kinetic checkpoint at a late step in translation initiation. *Mol Cell* **30**, 712-720, doi:10.1016/j.molcel.2008.04.014 (2008).
- 53 Pon, C. L., Brimacombe, R. & Gualerzi, C. Cross-linking of Escherichia coli initiation factor IF-3 to the RNA moiety of the 30S ribosomal subunits. *Biochemistry* **16**, 5681-5686 (1977).
- 54 Fabbretti, A. *et al.* The real-time path of translation factor IF3 onto and off the ribosome. *Mol Cell* **25**, 285-296, doi:10.1016/j.molcel.2006.12.011 (2007).
- 55 Tomsic, J. *et al.* Late events of translation initiation in bacteria: a kinetic analysis. *EMBO J* **19**, 2127-2136, doi:10.1093/emboj/19.9.2127 (2000).
- 56 Ben-Shem, A. *et al.* The structure of the eukaryotic ribosome at 3.0 Å resolution. *Science* **334**, 1524-1529, doi:10.1126/science.1212642 (2011).
- 57 Kozak, M. How do eucaryotic ribosomes select initiation regions in messenger RNA? *Cell* **15**, 1109-1123 (1978).
- 58 Kozak, M. Evaluation of the "scanning model" for initiation of protein synthesis in eucaryotes. *Cell* **22**, 7-8 (1980).
- 59 Kozak, M. The scanning model for translation: an update. *J Cell Biol* **108**, 229-241 (1989).
- 60 Hinnebusch, A. G. & Lorsch, J. R. The mechanism of eukaryotic translation initiation: new insights and challenges. *Cold Spring Harbor perspectives in biology* **4**, doi:10.1101/cshperspect.a011544 (2012).
- 61 Asano, K., Clayton, J., Shalev, A. & Hinnebusch, A. G. A multifactor complex of eukaryotic initiation factors eIF1, eIF2, eIF3, eIF5, and initiator tRNA<sup>Met</sup> is an important translation initiation intermediate in vivo. *Genes & development* **14**, 2534-2546 (2000).
- 62 Merrick, W. C. Mechanism and regulation of eukaryotic protein synthesis. *Microbiological reviews* **56**, 291-315 (1992).
- 63 Passmore, L. A. *et al.* The eukaryotic translation initiation factors eIF1 and eIF1A induce an open conformation of the 40S ribosome. *Mol Cell* **26**, 41-50 (2007).
- 64 Kolupaeva, V. G., Unbehaun, A., Lomakin, I. B., Hellen, C. U. & Pestova, T. V. Binding of eukaryotic initiation factor 3 to ribosomal 40S subunits and its role in ribosomal dissociation and anti-association. *RNA* **11**, 470-486, doi:10.1261/rna.7215305 (2005).
- 65 Majumdar, R., Bandyopadhyay, A. & Maitra, U. Mammalian translation initiation factor eIF1 functions with eIF1A and eIF3 in the formation of a stable 40 S preinitiation complex. *J Biol Chem* **278**, 6580-6587, doi:10.1074/jbc.M210357200 (2003).
- 66 Sokabe, M., Fraser, C. S. & Hershey, J. W. The human translation initiation multi-factor complex promotes methionyl-tRNA<sub>i</sub> binding to the 40S ribosomal subunit. *Nucleic Acids Res* **40**, 905-913, doi:10.1093/nar/gkr772 (2012).
- 67 Das, S. & Maitra, U. Functional significance and mechanism of eIF5-promoted GTP hydrolysis in eukaryotic translation initiation. *Progress in nucleic acid research and molecular biology* **70**, 207-231 (2001).

- 68 Paulin, F. E., Campbell, L. E., O'Brien, K., Loughlin, J. & Proud, C. G. Eukaryotic translation initiation factor 5 (eIF5) acts as a classical GTPase-activator protein. *Current biology : CB* **11**, 55-59 (2001).
- 69 Alone, P. V. & Dever, T. E. Direct binding of translation initiation factor eIF2gamma-G domain to its GTPase-activating and GDP-GTP exchange factors eIF5 and eIF2B epsilon. *J Biol Chem* **281**, 12636-12644 (2006).
- 70 Luna, R. E. *et al.* The C-Terminal Domain of Eukaryotic Initiation Factor 5 Promotes Start Codon Recognition by Its Dynamic Interplay with eIF1 and eIF2beta. *Cell Rep* **1**, 689-702, doi:10.1016/j.celrep.2012.04.007 (2012).
- 71 Yamamoto, Y. *et al.* The eukaryotic initiation factor (eIF) 5 HEAT domain mediates multifactor assembly and scanning with distinct interfaces to eIF1, eIF2, eIF3, and eIF4G. *Proc Natl Acad Sci U S A* **102**, 16164-16169, doi:10.1073/pnas.0507960102 (2005).
- 72 Nanda, J. S., Saini, A. K., Munoz, A. M., Hinnebusch, A. G. & Lorsch, J. R. Coordinated Movements of Eukaryotic Translation Initiation Factors eIF1, eIF1A and eIF5 Trigger Phosphate Release from eIF2 in response to Start Codon Recognition by the Ribosomal Pre-initiation Complex. *J Biol Chem*, doi:10.1074/jbc.M112.440693 (2013).
- 73 Singh, C. R., Yamamoto, Y. & Asano, K. Physical association of eukaryotic initiation factor (eIF) 5 carboxyl-terminal domain with the lysine-rich eIF2beta segment strongly enhances its binding to eIF3. *J Biol Chem* **279**, 49644-49655, doi:10.1074/jbc.M409609200 (2004).
- 74 Asano, K. *et al.* Multiple roles for the C-terminal domain of eIF5 in translation initiation complex assembly and GTPase activation. *EMBO J* **20**, 2326-2337, doi:10.1093/emboj/20.9.2326 (2001).
- 75 Maag, D., Algire, M. A. & Lorsch, J. R. Communication between eukaryotic translation initiation factors 5 and 1A within the ribosomal pre-initiation complex plays a role in start site selection. *J Mol Biol* **356**, 724-737 (2006).
- 76 Pestova, T. V. & Kolupaeva, V. G. The roles of individual eukaryotic translation initiation factors in ribosomal scanning and initiation codon selection. *Genes & development* **16**, 2906-2922. (2002).
- 77 Lomakin, I. B., Kolupaeva, V. G., Marintchev, A., Wagner, G. & Pestova, T. V. Position of eukaryotic initiation factor eIF1 on the 40S ribosomal subunit determined by directed hydroxyl radical probing. *Genes & development* **17**, 2786-2797 (2003).
- 78 Rabl, J., Leibundgut, M., Ataide, S. F., Haag, A. & Ban, N. Crystal structure of the eukaryotic 40S ribosomal subunit in complex with initiation factor 1. *Science* **331**, 730-736 (2011).
- 79 Weisser, M., Voigts-Hoffmann, F., Rabl, J., Leibundgut, M. & Ban, N. The crystal structure of the eukaryotic 40S ribosomal subunit in complex with eIF1 and eIF1A. *Nat Struct Mol Biol* **20**, 1015-1017, doi:10.1038/nsmb.2622 (2013).
- 80 Singh, C. R., He, H., Ii, M., Yamamoto, Y. & Asano, K. Efficient incorporation of eukaryotic initiation factor 1 into the multifactor complex is critical for formation of functional ribosomal preinitiation complexes in vivo. *J Biol Chem* **279**, 31910-31920, doi:10.1074/jbc.M313940200 (2004).

- 81 Valasek, L., Nielsen, K. H., Zhang, F., Fekete, C. A. & Hinnebusch, A. G. Interactions of eukaryotic translation initiation factor 3 (eIF3) subunit NIP1/c with eIF1 and eIF5 promote preinitiation complex assembly and regulate start codon selection. *Mol Cell Biol* **24**, 9437-9455 (2004).
- 82 Reibarkh, M. *et al.* Eukaryotic initiation factor (eIF) 1 carries two distinct eIF5-binding faces important for multifactor assembly and AUG selection. *J Biol Chem* **283**, 1094-1103, doi:10.1074/jbc.M708155200 (2008).
- 83 Yu, Y. *et al.* Position of eukaryotic translation initiation factor eIF1A on the 40S ribosomal subunit mapped by directed hydroxyl radical probing. *Nucleic Acids Res* **37**, 5167-5182, doi:10.1093/nar/gkp519 (2009).
- 84 Olsen, D. S. *et al.* Domains of eIF1A that mediate binding to eIF2, eIF3 and eIF5B and promote ternary complex recruitment in vivo. *EMBO J* **22**, 193-204, doi:10.1093/emboj/cdg030 (2003).
- 85 Chiu, W. L. *et al.* The C-terminal region of eukaryotic translation initiation factor 3a (eIF3a) promotes mRNA recruitment, scanning, and, together with eIF3j and the eIF3b RNA recognition motif, selection of AUG start codons. *Mol Cell Biol* **30**, 4415-4434, doi:10.1128/MCB.00280-10 (2010).
- 86 Pisarev, A. V., Kolupaeva, V. G., Yusupov, M. M., Hellen, C. U. & Pestova, T. V. Ribosomal position and contacts of mRNA in eukaryotic translation initiation complexes. *EMBO J* **27**, 1609-1621, doi:10.1038/emboj.2008.90 (2008).
- 87 Siridechadilok, B., Fraser, C. S., Hall, R. J., Doudna, J. A. & Nogales, E. Structural roles for human translation factor eIF3 in initiation of protein synthesis. *Science* **310**, 1513-1515, doi:10.1126/science.1118977 (2005).
- 88 Valášek, L. *et al.* The Yeast eIF3 Subunits TIF32/a and NIP1/c and eIF5 Make Critical Connections with the 40S Ribosome in vivo. *Genes & development* **17**, 786-799 (2003).
- 89 Valášek, L., Nielsen, K. H. & Hinnebusch, A. G. Direct eIF2-eIF3 contact in the multifactor complex is important for translation initiation in vivo. *EMBO J* **21**, 5886-5898 (2002).
- 90 Hinnebusch, A. G. Molecular mechanism of scanning and start codon selection in eukaryotes. *Microbiol Mol Biol Rev* **75**, 434-467, first page of table of contents (2011).
- 91 Pestova, T. V., Borukhov, S. I. & Hellen, C. U. Eukaryotic ribosomes require initiation factors 1 and 1A to locate initiation codons. *Nature* **394**, 854-859, doi:10.1038/29703 (1998).
- 92 Algire, M. A., Maag, D. & Lorsch, J. R. Pi release from eIF2, not GTP hydrolysis, is the step controlled by start-site selection during eukaryotic translation initiation. *Mol Cell* **20**, 251-262 (2005).
- 93 Allen, G. S., Zavialov, A., Gursky, R., Ehrenberg, M. & Frank, J. The cryo-EM structure of a translation initiation complex from *Escherichia coli*. *Cell* **121**, 703-712, doi:10.1016/j.cell.2005.03.023 (2005).
- 94 Simonetti, A. *et al.* Structure of the 30S translation initiation complex. *Nature* **455**, 416-420, doi:10.1038/nature07192 (2008).
- 95 Kolitz, S. E., Takacs, J. E. & Lorsch, J. R. Kinetic and thermodynamic analysis of the role of start codon/anticodon base pairing during eukaryotic translation initiation. *Rna* **15**, 138-152 (2009).



- 96 Unbehaun, A., Borukhov, S. I., Hellen, C. U. & Pestova, T. V. Release of initiation factors from 48S complexes during ribosomal subunit joining and the link between establishment of codon-anticodon base-pairing and hydrolysis of eIF2-bound GTP. *Genes & development* **18**, 3078-3093, doi:10.1101/gad.1255704 (2004).
- 97 Cheung, Y. N. *et al.* Dissociation of eIF1 from the 40S ribosomal subunit is a key step in start codon selection in vivo. *Genes & development* **21**, 1217-1230 (2007).
- 98 Martin-Marcos, P. *et al.* beta-hairpin loop of eIF1 mediates 40S ribosome binding to regulate initiator tRNA<sup>Met</sup> recruitment and accuracy of AUG selection in vivo. *J Biol Chem*, doi:10.1074/jbc.M113.498642 (2013).
- 99 Pestova, T. V. *et al.* The joining of ribosomal subunits in eukaryotes requires eIF5B. *Nature* **403**, 332-335, doi:10.1038/35002118 (2000).
- 100 Acker, M. G., Shin, B. S., Dever, T. E. & Lorsch, J. R. Interaction between eukaryotic initiation factors 1A and 5B is required for efficient ribosomal subunit joining. *J Biol Chem* **281**, 8469-8475, doi:10.1074/jbc.M600210200 (2006).
- 101 Acker, M. G. *et al.* Kinetic analysis of late steps of eukaryotic translation initiation. *J Mol Biol* **385**, 491-506, doi:10.1016/j.jmb.2008.10.029 (2009).
- 102 Marintchev, A., Kolupaeva, V. G., Pestova, T. V. & Wagner, G. Mapping the binding interface between human eukaryotic initiation factors 1A and 5B: a new interaction between old partners. *Proc Natl Acad Sci U S A* **100**, 1535-1540, doi:10.1073/pnas.0437845100 (2003).
- 103 Fekete, C. A. *et al.* The eIF1A C-terminal domain promotes initiation complex assembly, scanning and AUG selection in vivo. *Embo J* **24**, 3588-3601 (2005).
- 104 Fekete, C. A. *et al.* N- and C-terminal residues of eIF1A have opposing effects on the fidelity of start codon selection. *EMBO* **26**, 1602-1614 (2007).
- 105 Saini, A. K., Nanda, J. S., Lorsch, J. R. & Hinnebusch, A. G. Regulatory elements in eIF1A control the fidelity of start codon selection by modulating tRNA(i)(Met) binding to the ribosome. *Genes & development* **24**, 97-110 (2010).
- 106 Barrieux, A. & Rosenfeld, M. G. Characterization of GTP-dependent Met-tRNA<sup>f</sup> binding protein. *J Biol Chem* **252**, 3843-3847 (1977).
- 107 Lloyd, M. A., Osborne, J. C., Jr., Safer, B., Powell, G. M. & Merrick, W. C. Characteristics of eukaryotic initiation factor 2 and its subunits. *J Biol Chem* **255**, 1189-1193 (1980).
- 108 Cigan, A. M., Pabich, E. K., Feng, L. & Donahue, T. F. Yeast translation initiation suppressor *sui2* encodes the alpha subunit of eukaryotic initiation factor 2 and shares sequence identity with the human alpha subunit. *Proc Natl Acad Sci U S A* **86**, 2784-2788 (1989).
- 109 Donahue, T. F., Cigan, A. M., Pabich, E. K. & Valavicius, B. C. Mutations at a Zn(II) finger motif in the yeast eIF-2 beta gene alter ribosomal start-site selection during the scanning process. *Cell* **54**, 621-632 (1988).
- 110 Hannig, E. M., Cigan, A. M., Freeman, B. A. & Kinzy, T. G. GCD11, a negative regulator of GCN4 expression, encodes the gamma subunit of eIF-2 in *Saccharomyces cerevisiae*. *Mol Cell Biol* **13**, 506-520 (1993).
- 111 Kimball, S. R. Eukaryotic initiation factor eIF2. *The international journal of biochemistry & cell biology* **31**, 25-29 (1999).

- 112 Schmitt, E., Blanquet, S. & Mechulam, Y. The large subunit of initiation factor aIF2 is a close structural homologue of elongation factors. *EMBO J* **21**, 1821-1832, doi:10.1093/emboj/21.7.1821 (2002).
- 113 Schmitt, E. *et al.* Structure of the ternary initiation complex aIF2-GDPNP-methionylated initiator tRNA. *Nat Struct Mol Biol* **19**, 450-454, doi:10.1038/nsmb.2259 (2012).
- 114 Stolboushkina, E. *et al.* Crystal structure of the intact archaeal translation initiation factor 2 demonstrates very high conformational flexibility in the alpha- and beta-subunits. *J Mol Biol* **382**, 680-691, doi:10.1016/j.jmb.2008.07.039 (2008).
- 115 Stolboushkina, E. *et al.* Crystal structure of the archaeal translation initiation factor 2 in complex with a GTP analogue and Met-tRNA<sup>f</sup>(Met.). *J Mol Biol* **425**, 989-998, doi:10.1016/j.jmb.2012.12.023 (2013).
- 116 Yatime, L., Mechulam, Y., Blanquet, S. & Schmitt, E. Structure of an archaeal heterotrimeric initiation factor 2 reveals a nucleotide state between the GTP and the GDP states. *Proc Natl Acad Sci U S A* **104**, 18445-18450, doi:10.1073/pnas.0706784104 (2007).
- 117 Hashimoto, N. N., Carnevalli, L. S. & Castilho, B. A. Translation initiation at non-AUG codons mediated by weakened association of eukaryotic initiation factor (eIF) 2 subunits. *The Biochemical journal* **367**, 359-368, doi:10.1042/BJ20020556 (2002).
- 118 Pedulla, N. *et al.* The archaeal eIF2 homologue: functional properties of an ancient translation initiation factor. *Nucleic Acids Res* **33**, 1804-1812, doi:10.1093/nar/gki321 (2005).
- 119 Schmitt, E., Blanquet, S. & Mechulam, Y. The large subunit of initiation factor aIF2 is a close structural homologue of elongation factors. *EMBO J* **21**, 1821-1832. (2002).
- 120 Thompson, G. M., Pacheco, E., Melo, E. O. & Castilho, B. A. Conserved sequences in the beta subunit of archaeal and eukaryal translation initiation factor 2 (eIF2), absent from eIF5, mediate interaction with eIF2gamma. *The Biochemical journal* **347 Pt 3**, 703-709 (2000).
- 121 Rajesh, K., Iyer, A., Suragani, R. N. & Ramaiah, K. V. Intersubunit and interprotein interactions of alpha- and beta-subunits of human eIF2: Effect of phosphorylation. *Biochemical and biophysical research communications* **374**, 336-340, doi:10.1016/j.bbrc.2008.07.022 (2008).
- 122 Suragani, R. N., Kamindla, R., Ehtesham, N. Z. & Ramaiah, K. V. Interaction of recombinant human eIF2 subunits with eIF2B and eIF2alpha kinases. *Biochemical and biophysical research communications* **338**, 1766-1772, doi:10.1016/j.bbrc.2005.10.150 (2005).
- 123 Nikonov, O. *et al.* New insights into the interactions of the translation initiation factor 2 from archaea with guanine nucleotides and initiator tRNA. *J Mol Biol* **373**, 328-336, doi:10.1016/j.jmb.2007.07.048 (2007).
- 124 Roll-Mecak, A., Alone, P., Cao, C., Dever, T. E. & Burley, S. K. X-ray structure of translation initiation factor eIF2gamma: implications for tRNA and eIF2alpha binding. *J Biol Chem* **279**, 10634-10642, doi:10.1074/jbc.M310418200 (2004).

- 125 Schmitt, E., Naveau, M. & Mechulam, Y. Eukaryotic and archaeal translation initiation factor 2: a heterotrimeric tRNA carrier. *FEBS Lett* **584**, 405-412, doi:10.1016/j.febslet.2009.11.002 (2010).
- 126 Sokabe, M., Yao, M., Sakai, N., Toya, S. & Tanaka, I. Structure of archaeal translational initiation factor 2 betagamma-GDP reveals significant conformational change of the beta-subunit and switch 1 region. *Proc Natl Acad Sci U S A* **103**, 13016-13021, doi:10.1073/pnas.0604165103 (2006).
- 127 Shin, B. S. *et al.* Initiation factor eIF2gamma promotes eIF2-GTP-Met-tRNA(i)(Met) ternary complex binding to the 40S ribosome. *Nat Struct Mol Biol* (2011).
- 128 Vetter, I. R. & Wittinghofer, A. The guanine nucleotide-binding switch in three dimensions. *Science* **294**, 1299-1304, doi:10.1126/science.1062023 (2001).
- 129 Berchtold, H. *et al.* Crystal structure of active elongation factor Tu reveals major domain rearrangements. *Nature* **365**, 126-132, doi:10.1038/365126a0 (1993).
- 130 Nissen, P. *et al.* Crystal structure of the ternary complex of Phe-tRNA<sup>Phe</sup>, EF-Tu, and a GTP analog. *Science* **270**, 1464-1472 (1995).
- 131 Polekhina, G. *et al.* Helix unwinding in the effector region of elongation factor EF-Tu-GDP. *Structure* **4**, 1141-1151 (1996).
- 132 Yatime, L., Mechulam, Y., Blanquet, S. & Schmitt, E. Structural switch of the gamma subunit in an archaeal aIF2 alpha gamma heterodimer. *Structure* **14**, 119-128, doi:10.1016/j.str.2005.09.020 (2006).
- 133 Ito, T., Marintchev, A. & Wagner, G. Solution structure of human initiation factor eIF2alpha reveals homology to the elongation factor eEF1B. *Structure* **12**, 1693-1704, doi:10.1016/j.str.2004.07.010 (2004).
- 134 Dhaliwal, S. & Hoffman, D. W. The crystal structure of the N-terminal region of the alpha subunit of translation initiation factor 2 (eIF2alpha) from *Saccharomyces cerevisiae* provides a view of the loop containing serine 51, the target of the eIF2alpha-specific kinases. *J Mol Biol* **334**, 187-195 (2003).
- 135 Nonato, M. C., Widom, J. & Clardy, J. Crystal structure of the N-terminal segment of human eukaryotic translation initiation factor 2alpha. *J Biol Chem* **277**, 17057-17061, doi:10.1074/jbc.M111804200 (2002).
- 136 Yatime, L., Schmitt, E., Blanquet, S. & Mechulam, Y. Functional molecular mapping of archaeal translation initiation factor 2. *J Biol Chem* **279**, 15984-15993, doi:10.1074/jbc.M311561200 (2004).
- 137 Yatime, L., Schmitt, E., Blanquet, S. & Mechulam, Y. Structure-function relationships of the intact aIF2alpha subunit from the archaeon *Pyrococcus abyssi*. *Biochemistry* **44**, 8749-8756, doi:10.1021/bi050373i (2005).
- 138 Naveau, M. *et al.* Roles of yeast eIF2alpha and eIF2beta subunits in the binding of the initiator methionyl-tRNA. *Nucleic Acids Res* **41**, 1047-1057, doi:10.1093/nar/gks1180 (2013).
- 139 Kozak, M. Point mutations define a sequence flanking the AUG initiator codon that modulates translation by eukaryotic ribosomes. *Cell* **44**, 283-292 (1986).
- 140 Pestova, T. V., Lorsch, J. R. & Hellen, C. U. T. in *Translational Control in Biology and Medicine* (eds M. Mathews, N. Sonenberg, & J.W.B. Hershey) 87-128 (Cold Spring Harbor Laboratory Press, 2007).

- 141 Kozak, M. Compilation and analysis of sequences upstream from the translation  
start site in eukaryotic mRNAs. *Nucleic Acids Research* **12**, 857-872 (1984).
- 142 Agarwal, S., Jha, S., Sanyal, I. & Amla, D. V. Effect of point mutations in  
translation initiation context on the expression of recombinant human alpha(1)-  
proteinase inhibitor in transgenic tomato plants. *Plant cell reports* **28**, 1791-1798,  
doi:10.1007/s00299-009-0779-y (2009).
- 143 Davies, M. V. & Kaufman, R. J. The sequence context of the initiation codon in  
the encephalomyocarditis virus leader modulates efficiency of internal translation  
initiation. *Journal of virology* **66**, 1924-1932 (1992).
- 144 Kochetov, A. V., Kolchanov, N. A. & Sarai, A. Interrelations between the  
efficiency of translation start sites and other sequence features of yeast mRNAs.  
*Mol Gen Genomics* **270**, 442-447 (2003).
- 145 Rangan, L., Vogel, C. & Srivastava, A. Analysis of context sequence surrounding  
translation initiation site from complete genome of model plants. *Molecular  
biotechnology* **39**, 207-213, doi:10.1007/s12033-008-9036-9 (2008).
- 146 LaGrandeur, T. & Parker, R. The cis acting sequences responsible for the  
differential decay of the unstable MFA2 and stable PGK1 transcripts in yeast  
include the context of the translational start codon. *Rna* **5**, 420-433 (1999).
- 147 McCarthy, J. E. Posttranscriptional control of gene expression in yeast. *Microbiol  
Mol Biol Rev* **62**, 1492-1553 (1998).
- 148 Vilela, C., Ramirez, C. V., Linz, B., Rodrigues-Pousada, C. & McCarthy, J. E.  
Post-termination ribosome interactions with the 5'UTR modulate yeast mRNA  
stability. *EMBO J* **18**, 3139-3152, doi:10.1093/emboj/18.11.3139 (1999).
- 149 Yun, D. F., Laz, T. M., Clements, J. M. & Sherman, F. mRNA sequences  
influencing translation and the selection of AUG initiator codons in the yeast  
*Saccharomyces cerevisiae*. *Molecular microbiology* **19**, 1225-1239 (1996).
- 150 Pisarev, A. V. *et al.* Specific functional interactions of nucleotides at key -3 and  
+4 positions flanking the initiation codon with components of the mammalian 48S  
translation initiation complex. *Genes & development* **20**, 624-636,  
doi:10.1101/gad.1397906 (2006).
- 151 Hashem, Y. *et al.* Structure of the Mammalian Ribosomal 43S Preinitiation  
Complex Bound to the Scanning Factor DHX29. *Cell* **153**, 1108-1119,  
doi:10.1016/j.cell.2013.04.036 (2013).
- 152 Castilho-Valavicius, B., Yoon, H. & Donahue, T. F. Genetic characterization of  
the *Saccharomyces cerevisiae* translational initiation suppressors *sui1*, *sui2* and  
*SUI3* and their effects on *HIS4* expression. *Genetics* **124**, 483-495 (1990).
- 153 Cho, S. & Hoffman, D. W. Structure of the beta subunit of translation initiation  
factor 2 from the archaeon *Methanococcus jannaschii*: a representative of the  
eIF2beta/eIF5 family of proteins. *Biochemistry* **41**, 5730-5742 (2002).
- 154 Gutierrez, P. *et al.* Structure of the archaeal translation initiation factor aIF2 beta  
from *Methanobacterium thermoautotrophicum*: implications for translation  
initiation. *Protein science : a publication of the Protein Society* **13**, 659-667,  
doi:10.1110/ps.03506604 (2004).
- 155 Asano, K., Krishnamoorthy, T., Phan, L., Pavitt, G. D. & Hinnebusch, A. G.  
Conserved bipartite motifs in yeast eIF5 and eIF2Bepsilon, GTPase-activating  
and GDP-GTP exchange factors in translation initiation, mediate binding to their

- common substrate eIF2. *EMBO J* **18**, 1673-1688, doi:10.1093/emboj/18.6.1673 (1999).
- 156 Das, S., Maiti, T., Das, K. & Maitra, U. Specific interaction of eukaryotic translation initiation factor 5 (eIF5) with the beta-subunit of eIF2. *J Biol Chem* **272**, 31712-31718 (1997).
- 157 Koonin, E. V. Multidomain organization of eukaryotic guanine nucleotide exchange translation initiation factor eIF-2B subunits revealed by analysis of conserved sequence motifs. *Protein science : a publication of the Protein Society* **4**, 1608-1617, doi:10.1002/pro.5560040819 (1995).
- 158 Conte, M. R., Kelly, G., Babon, J. & Proud, C. G. Resonance assignment for the N-terminal region of the eukaryotic initiation factor 5 (eIF5). *Journal of biomolecular NMR* **36 Suppl 1**, 42, doi:10.1007/s10858-006-9014-0 (2006).
- 159 Laurino, J. P., Thompson, G. M., Pacheco, E. & Castilho, B. A. The beta subunit of eukaryotic translation initiation factor 2 binds mRNA through the lysine repeats and a region comprising the C2-C2 motif. *Mol Cell Biol* **19**, 173-181 (1999).
- 160 Flynn, A., Shatsky, I. N., Proud, C. G. & Kaminski, A. The RNA-binding properties of protein synthesis initiation factor eIF-2. *Biochimica et biophysica acta* **1219**, 293-301 (1994).
- 161 Flynn, A., Oldfield, S. & Proud, C. G. The role of the beta-subunit of initiation factor eIF-2 in initiation complex formation. *Biochimica et biophysica acta* **1174**, 117-121 (1993).
- 162 Nika, J., Rippel, S. & Hannig, E. M. Biochemical analysis of the eIF2beta gamma complex reveals a structural function for eIF2alpha in catalyzed nucleotide exchange. *J Biol Chem* **276**, 1051-1056, doi:10.1074/jbc.M007398200 (2001).
- 163 Huang, H. K., Yoon, H., Hannig, E. M. & Donahue, T. F. GTP hydrolysis controls stringent selection of the AUG start codon during translation initiation in *Saccharomyces cerevisiae*. *Genes & development* **11**, 2396-2413 (1997).
- 164 Erickson, F. L. & Hannig, E. M. Ligand interactions with eukaryotic translation initiation factor 2: role of the  $\beta$ -subunit. *EMBO J* **15**, 6311-6320 (1996).
- 165 Kapp, L. D. & Lorsch, J. R. GTP-dependent recognition of the methionine moiety on initiator tRNA by translation factor eIF2. *J Mol Biol* **335**, 923-936 (2004).
- 166 Levin, D. H., Kyner, D. & Acs, G. Protein initiation in eukaryotes: formation and function of a ternary complex composed of a partially purified ribosomal factor, methionyl transfer RNA, and guanosine triphosphate. *Proc Natl Acad Sci U S A* **70**, 41-45 (1973).
- 167 Safer, B., Adams, S. L., Anderson, W. F. & Merrick, W. C. Binding of MET-TRNA<sup>f</sup> and GTP to homogeneous initiation factor MP. *J Biol Chem* **250**, 9076-9082 (1975).
- 168 Anthony, D. D., Jr., Kinzy, T. G. & Merrick, W. C. Affinity labeling of eukaryotic initiation factor 2 and elongation factor 1 alpha beta gamma with GTP analogs. *Archives of biochemistry and biophysics* **281**, 157-162 (1990).
- 169 Drabkin, H. J., Helk, B. & RajBhandary, U. L. The role of nucleotides conserved in eukaryotic initiator methionine tRNAs in initiation of protein synthesis. *J Biol Chem* **268**, 25221-25228 (1993).

- 170 Farruggio, D., Chaudhuri, J., Maitra, U. & RajBhandary, U. L. The A1 x U72 base pair conserved in eukaryotic initiator tRNAs is important specifically for binding to the eukaryotic translation initiation factor eIF2. *Mol Cell Biol* **16**, 4248-4256 (1996).
- 171 Mechulam, Y., Guillon, L., Yatime, L., Blanquet, S. & Schmitt, E. Protection-based assays to measure aminoacyl-tRNA binding to translation initiation factors. *Methods Enzymol* **430**, 265-281, doi:10.1016/S0076-6879(07)30011-6 (2007).
- 172 Mouat, M. F. & Manchester, K. An alpha subunit-deficient form of eukaryotic protein synthesis initiation factor eIF-2 from rabbit reticulocyte lysate and its activity in ternary complex formation. *Molecular and cellular biochemistry* **183**, 69-78 (1998).
- 173 von Pawel-Rammingen, U., Astrom, S. & Bystrom, A. S. Mutational analysis of conserved positions potentially important for initiator tRNA function in *Saccharomyces cerevisiae*. *Mol Cell Biol* **12**, 1432-1442 (1992).
- 174 Wagner, T., Gross, M. & Sigler, P. B. Isoleucyl initiator tRNA does not initiate eucaryotic protein synthesis. *J Biol Chem* **259**, 4706-4709 (1984).
- 175 Marck, C. & Grosjean, H. tRNomics: analysis of tRNA genes from 50 genomes of Eukarya, Archaea, and Bacteria reveals anticodon-sparing strategies and domain-specific features. *RNA* **8**, 1189-1232 (2002).
- 176 Kozak, M. Initiation of translation in prokaryotes and eukaryotes. *Gene* **234**, 187-208 (1999).
- 177 RajBhandary, U. L. Initiator transfer RNAs. *Journal of bacteriology* **176**, 547-552 (1994).
- 178 RajBhandary, U. L. & Ming Chow, C. in *tRNA: structure, biosynthesis, and function* (eds D. Soll & U. L. RajBhandary) 511-528 (American Society for Microbiology, 1995).
- 179 Astrom, S. U., von Pawel-Rammingen, U. & Bystrom, A. S. The yeast initiator tRNA<sup>Met</sup> can act as an elongator tRNA(Met) in vivo. *J Mol Biol* **233**, 43-58, doi:10.1006/jmbi.1993.1483 (1993).
- 180 Astrom, S. U. & Bystrom, A. S. Rit1, a tRNA backbone-modifying enzyme that mediates initiator and elongator tRNA discrimination. *Cell* **79**, 535-546 (1994).
- 181 Basavappa, R. & Sigler, P. B. The 3 A crystal structure of yeast initiator tRNA: functional implications in initiator/elongator discrimination. *EMBO J* **10**, 3105-3111 (1991).
- 182 Desgres, J., Keith, G., Kuo, K. C. & Gehrke, C. W. Presence of phosphorylated O-ribosyl-adenosine in T-psi-stem of yeast methionine initiator tRNA. *Nucleic Acids Res* **17**, 865-882 (1989).
- 183 Forster, C., Chakraborty, K. & Sprinzl, M. Discrimination between initiation and elongation of protein biosynthesis in yeast: identity assured by a nucleotide modification in the initiator tRNA. *Nucleic Acids Res* **21**, 5679-5683 (1993).
- 184 Kiesewetter, S., Ott, G. & Sprinzl, M. The role of modified purine 64 in initiator/elongator discrimination of tRNA(iMet) from yeast and wheat germ. *Nucleic Acids Res* **18**, 4677-4682 (1990).
- 185 Naveau, M., Lazennec-Schurdevin, C., Panvert, M., Mechulam, Y. & Schmitt, E. tRNA binding properties of eukaryotic translation initiation factor 2 from

- Encephalitozoon cuniculi. *Biochemistry* **49**, 8680-8688, doi:10.1021/bi1009166 (2010).
- 186 Dale, T., Sanderson, L. E. & Uhlenbeck, O. C. The affinity of elongation factor Tu for an aminoacyl-tRNA is modulated by the esterified amino acid. *Biochemistry* **43**, 6159-6166, doi:10.1021/bi036290o (2004).
- 187 LaRiviere, F. J., Wolfson, A. D. & Uhlenbeck, O. C. Uniform binding of aminoacyl-tRNAs to elongation factor Tu by thermodynamic compensation. *Science* **294**, 165-168, doi:10.1126/science.1064242 (2001).
- 188 Sanderson, L. E. & Uhlenbeck, O. C. The 51-63 base pair of tRNA confers specificity for binding by EF-Tu. *RNA* **13**, 835-840, doi:10.1261/rna.485307 (2007).
- 189 Sanderson, L. E. & Uhlenbeck, O. C. Directed mutagenesis identifies amino acid residues involved in elongation factor Tu binding to yeast Phe-tRNAPhe. *J Mol Biol* **368**, 119-130, doi:10.1016/j.jmb.2007.01.075 (2007).
- 190 Pavitt, G. D., Ramaiah, K. V., Kimball, S. R. & Hinnebusch, A. G. eIF2 independently binds two distinct eIF2B subcomplexes that catalyze and regulate guanine-nucleotide exchange. *Genes & development* **12**, 514-526 (1998).
- 191 Hinnebusch, A. G. in *Translational Control of Gene Expression* (eds N. Sonenberg, J. W. B. Hershey, & M. B. Mathews) 185-243 (Cold Spring Harbor Laboratory Press, 2000).
- 192 Kimball, S. R., Fabian, J. R., Pavitt, G. D., Hinnebusch, A. G. & Jefferson, L. S. Regulation of guanine nucleotide exchange through phosphorylation of eukaryotic initiation factor eIF2 $\alpha$ . Role of the  $\alpha$ - and  $\delta$ -subunits of eIF2b. *J Biol Chem* **273**, 12841-12845 (1998).
- 193 Proud, C. G. Protein phosphorylation in translational control. *Current topics in cellular regulation* **32**, 243-369 (1992).
- 194 Dever, T. E., Yang, W., Astrom, S., Bystrom, A. S. & Hinnebusch, A. G. Modulation of tRNA(iMet), eIF-2, and eIF-2B expression shows that GCN4 translation is inversely coupled to the level of eIF-2.GTP.Met-tRNA(iMet) ternary complexes. *Mol Cell Biol* **15**, 6351-6363 (1995).
- 195 Rowlands, A. G., Panniers, R. & Henshaw, E. C. The catalytic mechanism of guanine nucleotide exchange factor action and competitive inhibition by phosphorylated eukaryotic initiation factor 2. *J Biol Chem* **263**, 5526-5533 (1988).
- 196 Siekierka, J., Manne, V. & Ochoa, S. Mechanism of translational control by partial phosphorylation of the  $\alpha$  subunit of eukaryotic initiation factor 2. *Proc Natl Acad Sci U S A* **81**, 352-356 (1984).
- 197 Dar, A. C., Dever, T. E. & Sicheri, F. Higher-order substrate recognition of eIF2 $\alpha$  by the RNA-dependent protein kinase PKR. *Cell* **122**, 887-900, doi:10.1016/j.cell.2005.06.044 (2005).
- 198 Dever, T. E., Dar, A. C. & Sicheri, F. in *Translational control in Biology and Medicine* (eds M.B. Mathews, N. Sonenberg, & J.W.B. Hershey) 319-344 (Cold Spring Harbor Laboratory Press, 2007).
- 199 Dong, J., Qiu, H., Garcia-Barrido, M., Anderson, J. & Hinnebusch, A. G. Uncharged tRNA activates GCN2 by displacing the protein kinase moiety from a bipartite tRNA-binding domain. *Mol Cell* **6**, 269-279 (2000).

- 200 Clemens, M. J. PKR--a protein kinase regulated by double-stranded RNA. *The international journal of biochemistry & cell biology* **29**, 945-949 (1997).
- 201 Sadler, A. J. & Williams, B. R. Structure and function of the protein kinase R. *Current topics in microbiology and immunology* **316**, 253-292 (2007).
- 202 Garcia, M. A., Meurs, E. F. & Esteban, M. The dsRNA protein kinase PKR: virus and cell control. *Biochimie* **89**, 799-811, doi:10.1016/j.biochi.2007.03.001 (2007).
- 203 Dalton, L. E., Healey, E., Irving, J. & Marciniak, S. J. Phosphoproteins in stress-induced disease. *Progress in molecular biology and translational science* **106**, 189-221, doi:10.1016/B978-0-12-396456-4.00003-1 (2012).
- 204 Ron, D. & Harding, H. P. Protein-folding homeostasis in the endoplasmic reticulum and nutritional regulation. *Cold Spring Harbor perspectives in biology* **4**, doi:10.1101/cshperspect.a013177 (2012).
- 205 Lu, L., Han, A. P. & Chen, J. J. Translation initiation control by heme-regulated eukaryotic initiation factor 2 $\alpha$  kinase in erythroid cells under cytoplasmic stresses. *Mol Cell Biol* **21**, 7971-7980, doi:10.1128/MCB.21.23.7971-7980.2001 (2001).
- 206 Hinnebusch, A. G. Translational regulation of GCN4 and the general amino acid control of yeast. *Annu Rev Microbiol* **59**, 407-450 (2005).
- 207 The PyMOL Molecular Graphics System v. 1.5.0.4.
- 208 Yoon, H. J. & Donahue, T. F. The suil suppressor locus in *Saccharomyces cerevisiae* encodes a translation factor that functions during tRNA(iMet) recognition of the start codon. *Mol Cell Biol* **12**, 248-260 (1992).
- 209 Donahue, T. F. & Cigan, A. M. Genetic selection for mutations that reduce or abolish ribosomal recognition of the *HIS4* translational initiator region. *Mol Cell Biol* **8**, 2955-2963 (1988).
- 210 Schiestl, R. H. & Gietz, R. D. High efficiency transformation of intact yeast cells using single stranded nucleic acids as a carrier. *Curr Genet* **16**, 339-346 (1989).
- 211 Sherman, F., Fink, G. & Lawrence, C. Vol. 34 61-64 (Cold Spring Harbor Laboratory, New York, 1974).
- 212 Boeke, J. D., Trueheart, J., Natsoulis, G. & Fink, G. R. 5-fluoroorotic acid as a selective agent in yeast molecular genetics. *Methods Enzymol* **154**, 164-175 (1987).
- 213 Alani, E., Cao, L. & Kleckner, N. A method for gene disruption that allows repeated use of *URA3* selection in the construction of multiply disrupted yeast strains. *Genetics* **116**, 541-545 (1987).
- 214 Longtine, M. S. *et al.* Additional modules for versatile and economical PCR-based gene deletion and modification in *Saccharomyces cerevisiae*. *Yeast* **14**, 953-961 (1998).
- 215 Reid, G. A. & Schatz, G. Import of Proteins into Mitochondria. *J Biol Chem* **257**, 13062-13067. (1982).
- 216 Dever, T. E. *et al.* Phosphorylation of initiation factor 2 $\alpha$  by protein kinase GCN2 mediates gene-specific translational control of *GCN4* in yeast. *Cell* **68**, 585-596 (1992).
- 217 Bushman, J. L., Foiani, M., Cigan, A. M., Paddon, C. J. & Hinnebusch, A. G. Guanine nucleotide exchange factor for eIF-2 in yeast: genetic and biochemical



- analysis of interactions between essential subunits GCD2, GCD6 and GCD7 and regulatory subunit GCN3. *Mol Cell Biol* **13**, 4618-4631 (1993).
- 218 Moehle, C. M. & Hinnebusch, A. G. Association of RAP1 binding sites with stringent control of ribosomal protein gene transcription in *Saccharomyces cerevisiae*. *Mol Cell Biol* **11**, 2723-2735 (1991).
- 219 Pritchard, L., Corne, D., Kell, D., Rowland, J. & Winson, M. A general model of error-prone PCR. *Journal of theoretical biology* **234**, 497-509, doi:10.1016/j.jtbi.2004.12.005 (2005).
- 220 Williams, N. P., Hinnebusch, A. G. & Donahue, T. F. Mutations in the structural genes for eukaryotic initiation factors 2 $\alpha$  and 2 $\beta$  of *Saccharomyces cerevisiae* disrupt translational control of *GCN4* mRNA. *Proc Natl Acad Sci USA* **86**, 7515-7519 (1989).
- 221 Dong, J. *et al.* Genetic identification of yeast 18S rRNA residues required for efficient recruitment of initiator tRNA(Met) and AUG selection. *Genes & development* **22**, 2242-2255 (2008).
- 222 Harashima, S. & Hinnebusch, A. G. Multiple *GCD* genes required for repression of *GCN4*, a transcriptional activator of amino acid biosynthetic genes in *Saccharomyces cerevisiae*. *Mol Cell Biol* **6**, 3990-3998 (1986).
- 223 Dorris, D. R., Erickson, F. L. & Hannig, E. M. Mutations in *GCD11*, the structural gene for eIF-2g in yeast, alter translational regulation of *GCN4* and the selection of the start site for protein synthesis. *EMBO J* **14**, 2239-2249 (1995).
- 224 Anand, B., Majumdar, S. & Prakash, B. Structural basis unifying diverse GTP hydrolysis mechanisms. *Biochemistry* **52**, 1122-1130, doi:10.1021/bi3014054 (2013).
- 225 Sprang, S. R. GAP into the breach. *Science* **277**, 329-330 (1997).
- 226 Geneious created by Biomatters v. 6.1.
- 227 Consortium, T. U. Update on activities at the Universal Protein Resource (UniProt) in 2013. *Nucleic Acids Res* **41**, D43-47, doi:10.1093/nar/gks1068 (2013).
- 228 Nanda, J. S. *et al.* eIF1 controls multiple steps in start codon recognition during eukaryotic translation initiation. *J Mol Biol* **394**, 268-285 (2009).
- 229 Gietz, R. D. & Sugino, A. New yeast-*Escherichia coli* shuttle vectors constructed with in vitro mutagenized yeast genes lacking six-base pair restriction sites. *Gene* **74**, 527-534 (1988).
- 230 Parent, S. A., Fenimore, C. M. & Bostian, K. A. Vector systems for the expression, analysis and cloning of DNA sequences in *S. cerevisiae*. *Yeast* **1**, 83-138 (1985).
- 231 Christianson, T. W., Sikorski, R. S., Dante, M., Shero, J. H. & Hieter, P. Multifunctional yeast high-copy-number shuttle vectors. *Gene* **110**, 119-122 (1992).
- 232 Hinnebusch, A. G. A hierarchy of *trans*-acting factors modulate translation of an activator of amino acid biosynthetic genes in *Saccharomyces cerevisiae*. *Mol Cell Biol* **5**, 2349-2360 (1985).
- 233 Grant, C. M., Miller, P. F. & Hinnebusch, A. G. Requirements for intercistronic distance and level of eIF-2 activity in reinitiation on *GCN4* mRNA varies with the downstream cistron. *Mol Cell Biol* **14**, 2616-2628 (1994).

- 234 Martin-Marcos, P., Cheung, Y. N. & Hinnebusch, A. G. Functional elements in initiation factors 1, 1A and 2 $\beta$  discriminate against poor AUG context and non-AUG start codons. *Mol Cell Biol* (2011).
- 235 Alone, P. V., Cao, C. & Dever, T. E. Translation initiation factor 2 $\gamma$  mutant alters start codon selection independent of Met-tRNA binding. *Mol Cell Biol* **28**, 6877-6888 (2008).
- 236 Schmeing, T. M. *et al.* The crystal structure of the ribosome bound to EF-Tu and aminoacyl-tRNA. *Science* **326**, 688-694, doi:10.1126/science.1179700 (2009).
- 237 Goldstein, A. L. & McCusker, J. H. Three new dominant drug resistance cassettes for gene disruption in *Saccharomyces cerevisiae*. *Yeast* **15**, 1541-1553 (1999).
- 238 Acker, M. G., Kolitz, S. E., Mitchell, S. F., Nanda, J. S. & Lorsch, J. R. Reconstitution of yeast translation initiation. *Methods Enzymol* **430**, 111-145 (2007).
- 239 Muir, T. W., Sondhi, D. & Cole, P. A. Expressed protein ligation: a general method for protein engineering. *Proc Natl Acad Sci U S A* **95**, 6705-6710 (1998).
- 240 Algire, M. A. *et al.* Development and characterization of a reconstituted yeast translation initiation system. *RNA* **8**, 382-397 (2002).
- 241 Kapp, L. D., Kolitz, S. E. & Lorsch, J. R. Yeast initiator tRNA identity elements cooperate to influence multiple steps of translation initiation. *RNA* **12**, 751-764, doi:10.1261/rna.2263906 (2006).
- 242 Hershey, J. W. B. & Merrick, W. C. in *Translational Control of Gene Expression* (eds N. Sonenberg, J. W. B. Hershey, & M. B. Mathews) 33-88 (Cold Spring Harbor Laboratory Press, 2000).
- 243 Maag, D. & Lorsch, J. R. Communication between eukaryotic translation initiation factors 1 and 1A on the yeast small ribosomal subunit. *J Mol Biol* **330**, 917-924 (2003).
- 244 Hashimoto, N. N., Carnevalli, L. S. & Castilho, B. A. Translation initiation at non-AUG codons mediated by weakened association of eukaryotic initiation factor (eIF) 2 subunits. *Biochem. J.* **367**, 359-368 (2002).
- 245 Agirrezabala, X. *et al.* Structural insights into cognate versus near-cognate discrimination during decoding. *EMBO J* **30**, 1497-1507, doi:10.1038/emboj.2011.58 (2011).
- 246 Cochella, L. & Green, R. Fidelity in protein synthesis. *Current biology : CB* **15**, R536-540, doi:10.1016/j.cub.2005.07.018 (2005).
- 247 Ogle, J. M., Murphy, F. V., Tarry, M. J. & Ramakrishnan, V. Selection of tRNA by the ribosome requires a transition from an open to a closed form. *Cell* **111**, 721-732 (2002).
- 248 Pape, T., Wintermeyer, W. & Rodnina, M. Induced fit in initial selection and proofreading of aminoacyl-tRNA on the ribosome. *EMBO J* **18**, 3800-3807, doi:10.1093/emboj/18.13.3800 (1999).
- 249 Zaher, H. S. & Green, R. Fidelity at the molecular level: lessons from protein synthesis. *Cell* **136**, 746-762, doi:10.1016/j.cell.2009.01.036 (2009).
- 250 Xia, T. *et al.* Thermodynamic parameters for an expanded nearest-neighbor model for formation of RNA duplexes with Watson-Crick base pairs. *Biochemistry* **37**, 14719-14735, doi:10.1021/bi9809425 (1998).

## CURRICULUM VITAE

---

### Education

---

- Ph.D. in Biology
    - Johns Hopkins University, 2013
    - Dissertation Title: Establishing the Fidelity of Start Codon Recognition: Role of Eukaryotic Initiation Factor 2
  - B.S. in Molecular and Cellular Biology
    - University of Illinois at Urbana-Champaign, 2006
    - Area of emphasis: Microbiology
    - Minor: Chemistry
- 

### Professional Experience

---

- Doctoral Research Scientist May 2010—Oct 2013
  - Laboratory of Gene Regulation and Development, National Institute of Child Health and Human Development
  - Employed a wide range of techniques, such as biochemistry, genetics, and molecular biology, to provide a comprehensive analysis of the dissertation project
  - Performed a battery of in vivo and in vitro assays to examine the function of eukaryotic Initiation Factor 2 (eIF2), which is an essential factor for protein synthesis
  - Identified a new structural element in eIF2 that is essential for establishing the fidelity of protein synthesis
- Teaching Assistance Jan 2008—May 2008 and Jan 2009—May 2009
  - Cell Biology Laboratory course at the Johns Hopkins University
  - Supervised undergraduate students through planning, executing, and troubleshooting multiple projects
- Graduate Student Aug 2007—Apr 2010
  - Laboratory of Biochemistry and Molecular Biology, National Cancer Institute
  - Employed a variety of genetic and cell biology techniques to elucidate the function of nuclear organization in the maintenance of genome stability in *Schizosaccharomyces pombe*
- Post-baccalaureate Research Fellow Jan 2007—Jul 2007
  - Laboratory of Molecular Biology, National Cancer Institute
  - Applied genetic and biochemical methods to study the regulation of Leu-aminopeptidase protein in *Pseudomonas aeruginosa* pathogenicity
- Undergraduate Researcher Jun 2005—Dec 2006
  - Department of Microbiology, University of Illinois at Urban-Champaign
  - Generated a large-scale library of random mutations in *Salmonella enterica* serovar *typhimurium* genome to identify factors involved in the pathogenicity of SodCI protein
  - Designed a fluorescence-based assay to monitor the export of SodCI, which is essential for its function in the pathogenicity of *Salmonella*

- Undergraduate Researcher May 2004—Jun 2006
  - Department of Cell and Developmental Biology, University of Illinois at Urban-Champaign
  - Examined the consequences of nuclear organization on gene expression
  - Designed programs for automated fluorescence microscopy using the ISee Imaging System
  - Created programs in C++ and Matlab for the processing of live microscopy images

---

### **Leadership Positions and Experience**

---

- National Institutes of Health Entrepreneur and Commercialization Club Steering Committee Aug 2013—Present
- Graduate Student Research Symposium Planning Committee 2012—2013
- Johns Hopkins-National Institutes of Health Graduate Program Representative 2011—2012
- Responsible for the maintenance and repair of sophisticated laboratory equipment
- Analyzed markets, interacted with company representatives, and negotiated the best price for the best available product in multiple occasions

---

### **Peer-reviewed Publications**

---

- Yan Hu, Igor Kireev, Matt Plutz, [Nazanin Ashourian](#), and Andrew S. Belmont J. Cell Biol. 2009 Large-scale chromatin structure of inducible genes: transcription on a condensed, linear template

---

### **Honors and Awards**

---

- Helen Hays Undergraduate Research Award, 2006
- Clark Undergraduate Research Excellence Award, 2005
- Phi Eta Sigma National Honor Society
- Paul Franke Scholarship, 2004-2006
- University of Illinois Dean's List, 2005-2006
- Willard, A. C. Memorial Scholarship, 2004-2005
- Illinois Scholar, 2002-2003

---

### **Other Qualifications**

---

- Proficient in the PyMOL software for the analysis of protein structures
- Programming in Java and C++
- Experience with Matlab and ISEE Imaging System

---

### **Meetings and Presentations**

---

- Ribosomes Conference, Poster presentation, July 2013
- National Institute of Child Health and Human Development Fellows Retreat, Poster presentation, May 2013
- Johns Hopkins University, Department of Cell, Molecular, Developmental Biology and Biophysics, Seminar, May 2013
- Program in Cellular Regulation and Metabolism, National Institute of Child Health and Human Development, Seminar, February 2013
- Ninth Annual NIH Graduate Student Symposium, Poster presentation, January 2013

- Protein Synthesis and Translational Control, Cold Spring Harbor Conference Series, Poster presentation, September 2012
- Graduate Student Forum at National Institute of Child Health and Human Development Intramural Scientific Retreat, Seminar (invited), May 2012
- Program in Cellular Regulation and Metabolism, National Institute of Child Health and Human Development, Seminar May 2012
- Johns Hopkins University-National Institutes of Health Graduate Partnership Program, Seminar, May 2012
- Protein Synthesis and Translational Control, EMBO Conference Series, Poster presentation, September 2011
- Program in Cellular Regulation and Metabolism, National Institute of Child Health and Human Development, Seminar May 2011
- Johns Hopkins University-National Institutes of Health Graduate Partnership Program, Seminar, April 2011